Non-modal Partial Melting of Metasedimentary Pendants in the Southern Sierra Nevada and Implications for the Deep Origin of Within-pluton Isotopic Heterogeneity

Thesis by

Lingsen Zeng

In Partial Fulfillment of the Requirements

for the Degree of

Doctor of Philosophy

California Institute of Technology

Pasadena, California

Defended on September 15, 2003

Acknowledgment

Every rock speaks for itself, and every geomorphic feature speaks for itself too. The best achievement is to learn, appreciate, and enjoy the beauty and essence of geology for the past five years. Pursuing a PhD degree at Caltech is proved to be a great personal journey. It is great to get to know those great scientists and personalities, but also learn from fellow students.

I would like to thank my advisor, Jason Saleeby. To me, he is more a friend than an advisor. His door always is open to me and he listens to my research plans and half-baked ideas. I greatly appreciate his support, friendship, advice, and patience.

I want to thank Hugh Taylor for serving as my academic advisor and for his encouragement. Thanks to James Chen for his timely help whenever I had questions or troubles when I was working in the radiogenic isotope lab. Thanks to Brian Wernicke and Kenneth Farley for their support of my PhD qualification research. Thanks also to John Eiler, George Rossman, Peter Wyllie, Paul Asimow, Leon Silver, Gerald Wasserburg, Kerry Sieh, Ed Stolper, and other faculty members in the GPS Division for encouragement and sharing ideas. Thanks to Mihai Ducea and Cin-Ty Lee for their friendship. I am grateful to Zhiqing Xu, Haibing Li and Jingsui Yang who are at the Institute of Geology, Chinese Academy of Geological Sciences, for continuously to share the progresse made in China. Thanks to Jim O'Donnel and Susan Leising who make the library a lovely working place. Thanks to Lindsey M. Hedges for her assistance in sample and photo preparation. Thanks to Francis Alberade and Janne Blichert-Toft for their sharing ideas with regard to the mantle and crustal geochemistry, when they were at Caltech as visiting scholars. Thanks Terry Gennaro for his friendship and assistance that greatly facilitated every field trip I have taken. Thanks to all the secretaries working in the GPS Division for their efforts to make things work smoothly.

Thanks to all fellow graduate students and postdocs in the GPS Division who make seemingly dull graduate study enjoyable. Thanks especially to Zhengrong Wang, Edwin Schauble, Ji Chen, Sidao Ni, Xianglei Huang, Kaiwen Xia, Liz Johnson, Julie O'Leary, Er Tan, Bruce Hsu, Yongqin Jiao, Zhimei Yan, Shing-Lin Wang, Ying Tan, The-Ru Song, Danny Natawidjaja, Chi Ma, Hiroto Kimura, Heping Liu, Joe Akins for their friendship.

I would like to thanks my wife, Jing Liu, for her love, her push, and her encouragement, and my daughter, Carisa Zeng, for her enrichment of my daily and family life.

Abstract

Results from field mapping, structural analysis, major and trace element geochemistry, and radiogenic isotopic data from the Goat Ranch migmatite complex on the south shore of Lake Isabella, southern Sierra Nevada, California, are presented to (1) determine the major and trace element, Sr and Nd isotopic compositions of anatectic melts from pelitic sources; (2) investigate the structural and metamorphic responses of the Isabella pendant to the emplacement of the Goat Ranch pluton at ~100 Ma; and (3) evaluate the magnitude of assimilation of metasediment-derived melts by the Goat Ranch pluton at a mid-crustal level. Nd and Sr isotopic compositions were measured on the non-migmatitic distal wallrocks, leucosomes, migmatites, traverses into the Goat Ranch pluton, leucogranite dikes, and samples from the Rabbit Island, Heal Peak, and Bob Rabbit plutons. Major and trace element analyses were performed on selected samples of the leucosomes, migmatites and metapelites. Major and trace element analyses in addition to field and petrographic data demonstrate that leucosomes are products from partial melting of the pelitic protolith host. These data show that (1) contamination of Goat Ranch intrusion is restricted to the immediate proximity to migmatitic wallrocks. Isotopic heterogeneity of the Goat Ranch intrusion is not related to assimilation at or near the level of exposure, but from a deeper source; (2) as compared to the metapelites, leucosomes have higher Sr and lower Sm concentrations and lower Rb/Sr ratios. Sr and Nd isotope compositions of leucosomes, migmatites and metapelites suggesting a disequilibrium partial melting of the metapelite protolith; (3) based on their Sr, Nd and other trace element characteristics, two groups of leucosomes have been identified. Group A leucosomes show distinct positive Eu anomalies, relatively high Rb, Pb, Ba and K_2O contents, and low Rb/Sr ratios. Group B leucosomes have negative Eu anomalies, relatively low Rb, Pb, Ba and K_2O contents, and low Rb/Sr ratios as well; (4) the leucogranite dikes also can be subdivided into Group A (high $^{87}Sr/^{86}Sr(T)$ and low $\varepsilon_{Nd}(T)$), and Group B (low $^{87}Sr/^{86}Sr(T)$ and high $\varepsilon_{Nd}(T)$); (5) H_2O-fluxed melting of quartz + plagioclase with minor involvement of muscovite melting dominated the leucosome production; (6) Group A leucogranite dikes resulted from partial melting of the lower pelite, and Group B dikes from partial melting of the upper pelite; and (7) the Bob Rabbit pluton represents an extreme end-member case that was derived completely from melting of the upper pelite or its equivalent in depth in the I-SCR (strongly contaminated and reduced I-type pluton) zone. Strain analysis shows that progressive partial melting resulted in the loading framework transition in the upper pelite unit from LBF structure (the stronger phase forms a load-bearing framework) to IWL structure (the weaker phase forms an interconnected weak matrix) with proximity to the pluton. The presence of melts has greatly affected the strain partitioning within the migmatite zone.

By incorporating accessory phase dissolution kinetics into non-modal partial melting of metasedimentary sources, theoretical modeling shows that non-modal partial melting of a pelitic source results in melts following two paths in ε_{Nd}-$^{87}Sr/^{86}Sr$ ratio space. Path 1 represents those partial melting reactions that favor muscovite/biotite dehydration and apatite but not monazite dissolution, leading to melts with elevated Rb/Sr, $^{87}Sr/^{86}Sr$, Sm/Nd, and ε_{Nd} values. In contrast, Path 2 represents those partial melting reactions in which muscovite/biotite dehydration plays an insignificant role, and favor monazite over apatite dissolution, and lead to melts with lower Rb/Sr, $^{87}Sr/^{86}Sr$, Sm/Nd, and ε_{Nd} values than their sources.

Table of Contents

List of Tables

Chapter 2

Chapter 3

Chapter 5

Chapter 6

List of Figures

Chapter 1

Chapter 2

Chapter 3

Chapter 4

Chapter 5

Chapter 6

Chapter 1

Granitic batholith, crustal anatexis, and migmatite:

Introduction and thesis overview

The Sierra Nevada batholith is one of the best studied composite batholiths in the world. It represents the type example of Cordilleran-type composite batholithic belts formed in Mesozoic time as a continental arc. Arc environments (island or continental arc) are believed to be the important loci for the generation of new continental crust. Therefore, geochemical and petrologic studies on the Sierra Nevada batholith have greatly advanced our understanding of the mechanisms for the formation, growth, and differentiation of continental crust. Compared with other granitic batholiths, the Sierra Nevada batholith has its own salient features, including (1) an oblique crustal section exposure with the emplacement pressure gradually increasing from ~2 to ~10 kb toward its southern end; (2) deeply incised canyons, highly exhumed plateau surface and excellent exposure, and (3) well-preserved pre-batholithic metasedimentary framework rocks. These features offer excellent opportunities to (1) determine the extent of within-pluton elemental or isotopic heterogeneities; (2) study depth-dependent batholith emplacement mechanisms (diapirism vs. diking); (3) examine the metamorphic and structural responses of the metamorphic pendants to the emplacement of plutons at different crustal levels; and (4) evaluate the magnitude of crustal contaminations.

In general, the source regimes for a large granitic batholith that formed in an arc environment consist of the convecting mantle, sub-arc lithospheric mantle, subducting oceanic crust, lower crust of the , and overriding plate, possibly the mid- to upper crust. The isotopic compositions of Sr, Nd, Pb and O in batholithic rocks are sensitive indicators of the source materials and the type of crust into which they intruded. Knowledge of the geochemical characteristics and relative contributions of each component to batholiths is essential to formulate petrogenetic models. Previous studies have shown that the Sierra Nevada batholith can be subdivided into the Eastern and Western zones by the initial $^{87}Sr/^{86}Sr$ (Sr(i)) = 0.706 line (Kistler and Peterman, 1973; Kistler, 1990), a fundamental boundary that separated two distinct pre-batholithic lithosphere domains (oceanic versus continental). This boundary was also confirmed later by Nd, Pb and O geochemical studies of the batholithic rocks (DePaolo, 1981; Chen and Tilton, 1991; Saleeby et al., 1987; Masi et al., 1981; Pickett and Saleeby, 1994). Based on whole-rock chemistry, mineralogy, and mineral chemistry of the batholithic rocks, Ague and Brimhall (1987 and 1988a & b) have divided the Sierra Nevada batholith into I-WC (weakly contaminated I-type), I-SCR (strongly contaminated and reduced I-type), I-MC (moderately contaminated I-type), and I-SC (strongly contaminated I-type) belts from west to east, except for some seemingly out-of-place I-WC plutons. These studies have stressed the importance of fundamental differences in the pre-batholith lithospheric structures between the eastern and western Sierra Nevada in generating their distinct isotopic signatures. The I-SCR plutons are particularly interesting because they are confined to a narrow northwest-trending belt within the western zone of the Sierra Nevada batholith, and at exposure levels they are intruded into only the pre-batholithic metasedimentary pendants. The I-SCR plutons are metaluminous to strongly peraluminous granites containing Fe-rich biotite with $\log(X_{Mg}/X_{Fe}) < -0.21$ (Ague and Brimhall, 1988a). They interpreted such granites to have resulted from contamination of I-type granites with highly reduced sediments or metasediments represented by the metasedimentary pendants. Such plutons offer the best opportunities to put constraints on the maximum crustal contributions from the mid- to shallow-crustal levels to the Sierra Nevada batholith. A number of detailed radiogenic isotopic studies on large-scale composite granitic intrusives including the Tuolumne intrusive suite (Kistler et al., 1986), Bear Valley intrusive suite (Saleeby et al., 1987), and Tehachapi Mountains (Pickett and Saleeby, 1994) have demonstrated their commonly high-degree Sr and Nd isotopic heterogeneities. As an end-member source component, Clemens-Knot (1992) identified a depleted mantle component for the early Cretaceous mafic intrusions of the southwestern Sierran Foothills. In contrast, an enriched sub-arc lithospheric mantle with radiogenic Sr and nonradiogenic Nd isotopic compositions has also been proposed as a key source regime for some granitic plutons (e.g., the 90 Ma old Lamarck intrusive suite) in the eastern Sierra (Coleman et al., 1992; Coleman et al., 1998). The crustal components are much more complicated not only because of large compositional differences between the lower crust and upper crust, but also because crustally derived melts have a complicated trace element and radiogenic isotopic geochemistry. Nevertheless, all the models for the generation of granitic batholiths have called for various degrees of crustal involvement. The relative importance of mantle wedge, pre-existing continental crust, or subducting oceanic slab components in the formation of granitic batholiths still remains an outstanding question. For example, based on the Sr-Nd isotopic systematics of the Sierra Nevada and Peninsular batholiths, DePaolo (1981) suggested that batholithic rocks have ~50% contributions from pre-existing continental crust. Ducea (2002) proposed zero net continental crust formation in the major episode of mid-Cretaceous Sierran arc magmatism; i.e., that the Sierra Nevada batholith is purely crust derived via recycling of pre-batholithic continental crust. In contrast, Coleman et al. (1992) and Coleman et al., (1998) suggested rapid growth of juvenile continental crust by melting an enriched sub-arc lithospheric mantle in the late Cretaceous. In their point of view, such batholiths have zero crustal component. These are virtually the same geochemical data sets have been used to argue for both zero net crustal growth, and essentially 100% crustal growth! Recent Sr and Nd isotopic studies of the mantle xenoliths (Beard and Glazner, 1995; Zeng et al., 2001) also suggested an enriched lithospheric mantle underlying the Sierra Nevada batholith, but it is not clear whether it represents the pre-batholith or post-batholith lithospheric mantle.

The Sierra Nevada and other Cordilleran batholiths have characteristic and systematic geographic variations of isotopic ratios (Sr, Nd, Pb and O), trace and some major elements, all of which have been attributed to variation in such source components (Kistler and Paterman, 1973; DePaolo, 1981; Farmer and DePaolo, 1983; Solomon and Taylor, 1986; Ague and Brimhall, 1988; Silver and Chappell, 1988; Kistler, 1990; Chen and Tilton, 1991; Pichett and Saleeby, 1994). The interpretations of such isotopic patterns fall into two fundamentally different schools: (1) the isotopic heterogeneities reflect mainly the deep-crustal and/or upper-mantle source regions from which the batholith were generated (Kistler and Paterman, 1973; Silver and Chappell, 1988; Hildreth and Moorbath, 1988; Ducea and Saleeby, 1998; Chen and Tilton, 1991), and (2) the isotopic heterogeneities are derived primarily from fractionation, crystallization and assimilation of heterogeneous mid- to upper-crustal rocks in shallow- to mid-crustal magma chambers (DePaolo, 1981; Saleeby, 1990; Clemens-Knott, 1992). Most of these models assumed an equilibrium assimilation of crust materials in the form of either bulk materials or melts derived from such sources. In these models, crustally derived melts are assumed to be in equilibrium with their sources and thus truly represent their sources such that the metasedimentary framework rocks can be classified as one of the end-members, irrespective of the form of assimilation. But recent experimental and field observations have demonstrated that crustal anatexis is commonly non-modal in nature (e.g., Vielzeuf and Holloway, 1988; Patino Douce and Harris, 1998; Zeng et al, Chapter 3, 5 & 6), and the melts produced by such a partial melting process are frequently in either Sr or Nd isotopic disequilibrium with their sources (e.g., Knesel and Davidson, 2002; Ayers and Harris, 1997). These advances have questioned the faithfulness of the crustally derived melts as representative of their sources. If crustal contamination of a granitic batholith occurred mainly as assimilation of metasediment-derived melts, then knowledge of elemental and isotopic characteristics of such melts is necessary for determining the magnitude of crustal contributions, especially in the mid- to shallow-crustal levels. A number of observations have shown that (1) the southern Sierra Nevada batholith is characterized by its unique and uniformly high δO^{18} values (Masi et al., 1981; Lackey et al., in press); (2) south of the Lake Isabella region in exposures from ~4 to ~9 kb, pelitic and psammitic wallrock units are preferentially melted out of the pendants leaving quartzite-marble-calc-silicate and local biotite-garnet-sillimanite/kyanite refractory pendants and enclaves (Saleeby et al., 1987; Saleeby, 1990; Pickett and Saleeby, 1993); and (3) the Goat Ranch pluton-migmatite complex represents the best remnant of an anatectic complex which has not lost its structural integrity. Thus, this is an idea area to explore the regionally important process of metasediment wallrock anatexis and its potential geochemical impact on the Sierra Nevada batholith. This thesis concentrates on the best developed of these migmatite complexes in the Isabella pendant in the Lake Isabella area of the southern Sierra Nevada.

Migmatites as a crustal anatexis system

Migmatite complexes occur commonly in high-grade metamorphic framework rocks associated with large-scale granitic batholiths. They provide a natural laboratory to examine and address a number of important questions with regard to magmatism, high-grade metamorphism and deformation. Unlike leucogranite bodies or granitic batholiths, the melts and their sources in migmatite complexes can be unambiguously identified. Since most migmatite complexes appear to have formed in major episodes of an orogenesis, they provide a window to examine the interplay among deformation, magmatism and high-T metamorphism. By studying migmatitic and high-grade associated metamorphic pendant rocks that are in direct contact with the invading batholithic rocks which promoted the partial melting, we can evaluate the importance of shallow- to mid-crustal level assimilation of metasedimentary rocks if we know the geochemical and isotopic compositions of melts derived from such sources. Leucosomes represent the anatectic melts from a metasedimentary source, they provide an excellent opportunity to (1) test experimentally determined partial melting reactions; (2) characterize the geochemical and isotopic nature of anatectic melts; (3) evaluate equilibrium vs. disequilibrium melting models; and (4) examine the role of accessory minerals in shaping the trace element and radiogenic isotopic geochemistry of the anatectic melts.

Migmatites as partially molten rocks

Migmatites consist of leucosomes, melanosomes and mesosomes. Leucosomes represent the in situ (limited migration) melts from mesosomes and melanosomes are the residues from which the leucosomes are extracted. Migmatites occur in many high-grade metamorphic terrains and generally represent low melt-fraction rocks. Therefore, they provide a good opportunity to study how low-degree partial melting affects the strain partitioning between the newly formed melt and the solid residue, and the bulk mechanical properties of the rock undergoing partial melting. These observations are essential to (1) relate characteristic microstructures to specific melt fractions and strain rates, and thereby obtain diagnostic microstructural criteria with which to identify synmagmatic deformation in naturally deformed rocks; (2) differentiate microstructures of strained partially molten aggregates from those of static melting aggregates; (3) draw broader implications for the rheology of melting vs. crystallizing rocks; (4) determine the extent that mechanical anisotropies of rocks affect melt segregation; (5) examine how the strength of a partially-molten aggregate varies as a function of melt contents; and (6) determine the processes that control the transition from porous intergranular flow to channellized flow in partially molten aggregates.

Thesis Overview

The study area of this thesis (Fig. 1) is located slightly to the east of the regional $Sr_i = 0.706$ line, an important boundary that divides the Sierra Nevada batholith into the eastern and western zone, and also within the belt of I-SCR plutons (strongly contaminated and reduced I-type) as defined by Ague and Brimhall (1988a). My thesis research consisted of (1) detailed fieldwork consisting of geologic mapping, structural analysis, field petrography and sample collection (Appendix: Plate 1 and Table 1); (2) petrography; (3) radiogenic isotopic studies (Sr and Nd); (4) sample preparation for major, trace element and stable isotope analyses; and (5) data integration and synthesis. Below I present an overview of the main chapters of my thesis.

Chapter 2 is focused on the Rb-Sr and Sm-Nd radiogenic isotopic geochemistry of the Goat Ranch pluton which triggered migmatization in adjacent pelites of the Isabella pendant, and of leucosomes, migmatites, and the upper pelite protolith unit of the pendant. By integrating the data from this study with previous results, they show that (1) both the Goat Ranch pluton and the upper pelite unit are isotopically heterogeneous; (2) the isotopic heterogeneity of the Goat Ranch pluton was derived from a deeper source than the observation level; and (3) assimilation of melt products from the metasedimentary framework rocks at the level of observation is minimal.

Chapter 3 is focused on the major and trace element, and radiogenic isotopic geochemistry of anatectic melts from the upper pelite unit of the Isabella pendant. Geochemical data on the leucosomes, migmatites and metapelites suggest that partial melting of metapelite is non-modal and dominated by H_2O-fluxed melting of quartz + plagioclase assemblage with minor involvement of muscovite dehydration melting. The leucosomes can be subdivided into two groups. Group A leucosomes with positive Eu anomalies have higher Sm/Nd, Rb/Sr, and $^{87}Sr/^{86}Sr(T)$ (T = 100 Ma), $\varepsilon_{Nd}(T)$, K_2O and P_2O_5 than those of Group B. Group A leucosomes have $\varepsilon_{Nd}(T)$ values significantly higher than those of the migmatites and metapelites, suggesting Nd isotopic disequilibrium. Breakdown of quartz and plagioclase with minor contributions from muscovite resulted in low Rb/Sr ratios characterizing both Group A and Group B leucosomes. Accessory phases such as rutile group minerals are shown to be responsible for the low V, Na, and Ta concentrations in the leucosomes as compared to those in the metapelites. These observations call for caution to be taken in evaluating the potential mid- to shallow-crustal contributions to granitic batholiths, for anatectic melts as potential contaminants do not carry geochemical tracers that represent their sources faithfully.

Chapter 4 deals with the effect of progressive partial melting on the strain partitioning and transition from highly- to non-migmatitic rocks within the upper pelite unit of the Isabella pendant. Field and petrographic observations demonstrate that (1) within the proximity of the Goat Ranch pluton, the upper pelite unit has experienced a relatively high extent of partial melting which resulted in the formation of interconnected melt network and migmatite zone, and (2) with distance away from the pluton, partial melting has been increasingly inhibited and reduced, and as a result melts occurred as isolated pockets. Strain analysis suggests that melts had mechanical behavior similar to metamud-rich layers in pebble conglomerates from adjacent quartzite strata. The presence of melt greatly affects the strain partitioning and the bulk rheologic properties of a partially molten rock as well as rheologic contrasts with nonmigmatitic protolith domains. With increasing distance away from the Goat Ranch pluton, decreasing extent of partial melting resulted in the loading framework transition from the IWL (interconnected weak layer) structure to LBF (load bearing framework) structure.

Chapter 5 is a study concentrated on the origin of the leucogranite dikes that intrude into the Isabella pendant. These leucogranite dikes are similar to and located within the belt of I-SCR plutons of Ague and Brimhall (1987). The Sr and Nd isotopic data of these leucogranite dikes as well as the lower and upper pelite units of the Isabella pendant provide a framework for discussing the origin of some of the I-SCR plutons, and the maximum extent of crustal contamination at this level of observation.

Chapter 6 represents an attempt to incorporate accessory mineral dissolution kinetics into crustal anatectic models to explore the effects of accessory mineral dissolution and non-modal partial melting in the Rb-Sr and Sm-Nd isotopic systematics of anatectic melts. This chapter is a theoretical treatment of the subject that was in part stimulated by the subjects of Chapters 3 and 5.

Figure 1 Generalized geologic map of the Lake Isabella area, southern Sierra Nevada, California (after Ross, 1986; Saleeby and Busby, 1993; Saleeby and Zeng, in prep.). The inset box indicates the detailed mapping area of this thesis.

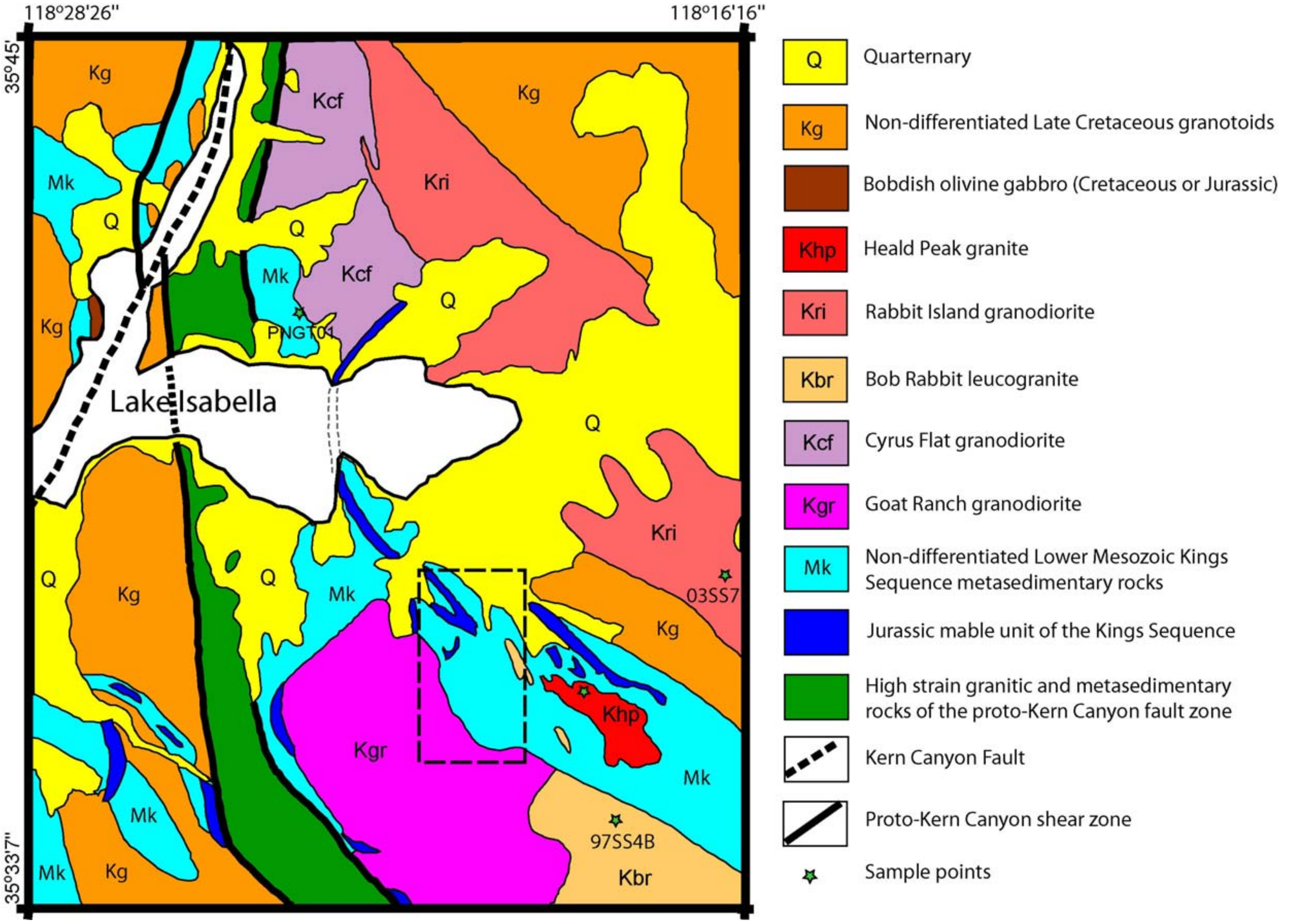
118°28'26"
118°16'16"
35°45'
35°33'7"
Lake Isabella
Kg
Kcf
Kri
Mk
Q
Kgr
Khp
Kbr
PNGT01
03SS7
97SS4B
Q Quarternary
Kg Non-differentiated Late Cretaceous granotoids
Bobdish olivine gabbro (Cretaceous or Jurassic)
Khp Heald Peak granite
Kri Rabbit Island granodiorite
Kbr Bob Rabbit leucogranite
Kcf Cyrus Flat granodiorite
Kgr Goat Ranch granodiorite
Mk Non-differentiated Lower Mesozoic Kings Sequence metasedimentary rocks
Jurassic mable unit of the Kings Sequence
High strain granitic and metasedimentary rocks of the proto-Kern Canyon fault zone
Kern Canyon Fault
Proto-Kern Canyon shear zone
Sample points

Chapter 2

The origin of within-pluton isotopic heterogeneities in the southern Sierra Nevada batholith: Constraints from Sr and Nd isotopes

Lingsen Zeng and Jason B. Saleeby

Division of Geological and Planetary Sciences, California Institute of Technology,
Pasadena, CA 91125

Mihai N. Ducea
Department of Geological Sciences, University of Arizona, Tucson, AZ 85721

Abstract

The extent to which pre-existing continental crustal components have been introduced into granitic magmas of the Sierra Navada batholith (SNB) as melted sediments within source and/or ascent domains has been the focus of much attention. In order to test the potential importance of this process at relatively deep crustal levels (3-5 kb), we have performed a detailed study of one of the best developed migmatite complexes of the metasedimentary framework of the southern Sierra Navada batholith, and on the immediately adjacent 100 Ma Goat Ranch granodioritic intrusion, which triggered partial melting in a 50 to ~500 m wide zone in the adjacent psammitic-pelitic rocks. Nd and Sr isotopic ratios were measured on non-migmatitic distal wallrocks, leucosomes from the migmatites; and on traverses into the Goat Ranch granodioritic intrusion away from contacts with the migmatites. We also analyzed a suite of enclaves within the Goat Ranch granodioritic intrusion which yielded bulk compositions of andesite and which have mineralogically equilibrated with the host Goat Ranch granodioritic intrusion. The

initial $^{87}Sr/^{86}Sr$ of Goat Ranch granodioritic intrusion and enclaves range from 0.7061 to 0.7071, and ε_{Nd}(100 Ma) from -1.1 to -6.5. Leucosomes have initial $^{87}Sr/^{86}Sr$ from 0.7124 to 0.7247, and ε_{Nd} from -6.0 to -11.0 while nonmigmatitic metapelites yield a similar range. Contamination of Goat Ranch granodioritic intrusion, as seen by large shifts in initial $^{87}Sr/^{86}Sr$ and ε_{Nd} values, is restricted to immediate proximity to the migmatitic wall rocks. Isotopic heterogeneity of the Goat Ranch granodioritic intrusion is, however, not related to assimilation at or near the level of exposure, a similar conclusion reached for 100 Ma (ca. 8kb) Sierra Nevada batholith rocks located further south in an oblique crustal section. Isotopic variation patterns in 10-20 kb level Sierra Nevada batholith and lower crustal residue assemblages carried as xenoliths in Neogene volcanic rocks further to the north lie along the same trend as the Goat Ranch granodioritic intrusion data, and suggest that the Goat Ranch granodioritic intrusion heterogeneity is inherited from such a source. Leucosomes in the migmatite complex appear to have crystallized nearly in place after segregation as partial melts. This, as well as the limitation in their ability to contaminate the Goat Ranch granodioritic intrusion, appears to have been energy limited. Enclaves in the Goat Ranch granodiorite strongly resemble remnants of disrupted commingled mafic dikes observed elsewhere in the southern Sierra Nevada batholith. We therefore propose that the deep-level source components partly represented by the lower crust and the uppermost lithospheric mantle exert first-order control on batholith isotopic geochemistry.

Introduction

Young granitic batholiths along the entire western margin of the Americas and the southeast coast of China represent the best Phanerzoic analogues to the average upper-crustal composition in Archean cratons (Martin, 1994). Observations made generally from mid- to upper-crustal level exposures of such batholiths on the Earth's surface as well as experimental studies of plausible source materials (e.g., Clemens and Vielzeuf, 1987) and of liquid line of decent of arc magmas (e.g., Wyllie, 1984) are used to formulate and test petrogenetic models of continental arc magmatism. However, these observations can not uniquely answer a number of first-order questions with regard to the origin of large granitic batholiths such as the Sierra Nevada batholith, the best studied Cordilleran-type batholith. The relative importance of mantle wedge, pre-existing continental crust, or subducting oceanic slab components in the formation of granitic batholiths still remains an outstanding question. The Sierra Nevada and other batholiths have characteristic and systematic geographic variations of isotopic ratios (Sr, Nd, Pb and O), trace and some major elements which have been attributed to variation in such source components (Kistler and Paterman, 1973, 1978; Silver and Taylor, 1978; DePaolo, 1981; Farmer and DePaolo, 1983; Solomon and Taylor, 1986; Ague and Brimhall, 1988a; Silver and Chappell, 1988; Kistler, 1990; Chen and Tilton, 1991; Pickett and Saleeby, 1994). The interpretations of such isotopic patterns fall into two fundamentally different schools: (1) the isotopic heterogeneities reflect mainly the deep-crustal and/or upper-mantle source regions from which the batholith was generated (Kistler and Paterman, 1973, 1978; Silver and Chappell, 1988; Hildreth and Moorbath, 1988; Ducea and Saleeby, 1998c), and (2) the isotopic heterogeneities are derived primarily from fractionation, crystallization and assimilation of heterogeneous mid- to upper-crustal rocks in shallow- to mid-crustal magma (DePaolo, 1981; Saleeby, 1990; Clemens-Knott, 1992). In support of the second school of thought, for example, Halliday (1983) demonstrated the contamination of mid- to high-crustal level granitic plutons of Scotland by incorporation of country-rock-derived melts. By studying migmatitic, high-grade metamorphic pendant rocks that are in direct contact with the invading batholithic rocks which promoted the partial melting, we can evaluate the importance of shallow- to mid-crustal level assimilation of metasedimentary rocks, one of classic geologic problems in batholithic granite-bearing and high-grade metamorphic terranes (Sederholm, 1967).

In the Lake Isabella area of the southern Sierra Nevada, a well-preserved pendant composed of continental margin metasedimentary rocks is engulfed in granodiorite plutons emplaced during the late Cretaceous, over a relatively short time span (~2 My). Excellent exposures, a well-defined migmatite complex, and a coherent protolith stratigraphic sequence for the pendant provide an unparalleled opportunity to characterize the geochemical and isotopic compositions of the invading plutons and pre-existing continental crustal rocks, and to further constrain the relative importance of each component in the formation of the batholith. In this paper, we present new detailed Sr and Nd isotopic data from this igneous and high-grade metamorphic complex. These data are used in conjunction with regional published isotopic data of the batholith to evaluate the extent of the anatectic contributions from metasedimentary pendant rocks in the formation of the Sierra Nevada batholith. Specifically, we have examined the geochemical relationships between the partial-melting products of the pendant represented by leucosomes in an extensive migmatitic metapelite unit, and the adjacent

Goat Ranch granodiorite. We will address: (1) what is the extent of mixing between metasedimentary-derived melts and batholithic magmas; and (2) does this process have a significant effect in generating within-pluton isotopic heterogeneities at the observed crustal level?

Geologic Setting

☐ Geologic background

We have specifically focused on the Goat Ranch granodiorite intrusion. This pluton has particularly well-defined relation with the partly migmatitic pendant rocks. The Goat Ranch pluton covers an area of ~80 km^2 and maps out as a circular body with roughly concordant contacts with its ductily-deformed wallrocks. It consists of a uniform medium-grained hornblende-biotite granodirotite. The Goat Ranch pluton is located within the belt of the I-SCR (strongly contaminated-reduced I-type) plutons which was defined by Ague and Brimhall (1987, 1988a and 1988b) based on the compositional data of plutonic biotites, whole-rock geochemistry, and mineral assemblages. The pressures at which the present exposure of the Sierra Nevada batholith was emplaced gradually increase southward from 2 kb to ~9 kb (Pickett and Saleeby, 1993; Ague, 1997). The Goat Ranch pluton was emplaced at a pressure within the range of 3-5 kb (Dixon, 1995). This lies in the medial range of pressures over which the Sierra Nevada batholith was emplaced, with pressure as low as 1-2 kb occurring to the north and as high as 8-9 kb to the south (Ague and Brimhall, 1988b; Saleeby, 1990; Pickett and Saleeby, 1993; Ague, 1997).

The metasedimentary framework rocks of the southern Sierra Nevada region consist of high-grade quartz-rich clastic and calcareous continental margin sedimentary protoliths with subordinate mafic metavolcanic layers. These rocks which are parts of the Isabella pendant have been designated as the Kings sequence by Saleeby and Busby (1993). Despite the high-grade metamorphism, some of the high-grade schists actually preserved Middle Triassic and Late Triassic-Early Jurassic shallow water fauna. Pelitic and subordinate psammitic units of the Kings metasedimentary sequence are common in the metamorphic pendants near the Lake Isabella area. These pelite-psammite units (referred to below as pelite units) have experienced extensive high-grade metamorphism and local migmatization in the southern Sierra region in response to the intrusion of large batholithic plutons during the mid-Cretaceous (Saleeby and Busby-Spera, 1986). A geologic map of the detailed study area within the Isabella pendant is shown in Figure 1. The structure is characterized by a steeply-SE plunging isoclinal anticline as indicated by facing data and fossil ages (Saleeby and Zeng, in prep.) with older and younger pelite units situated in core and envelope positions of the fold, respectively. The migmatite zone has a well-preserved and well-defined metamorphic gradient through the upper pelite unit.

The upper metapelite unit consists of andalusite/sillimanite, biotite, quartz, k-feldspar, muscovite and plagioclase. Except for the migmatite leucosomes, the metamorphic texture of this metapelite unit is penetratively schistose and/or gneissose, reflecting a high degree of plastic strain during plutonism and metamorphism. The leucosomes mainly consist of quartz, k-feldspar and plagioclase, and have a granoblastic texture. In contrast, the melanosomes mainly consist of sillimanite and biotite with an insignificant amount of quartz and K-feldspar. On microscopic and hand-specimen scales, leucosomes and melanosomes form alternating layers of millimeter to centimeter thick, typical of migmatites. The leucosomes can be morphologically divided into (1) concordant (stromatitic) and pervasive network leucosomes (Fig. 2a); (2) discordant dikes and pockets of pegmatites and aplites; and (3) agmatitic and randomly distributed distinct leucosomes of varied sizes. The thicknesses of the leucosomes vary from centimeter to millimeter. These leucosomes are shown to represent partial melting product of metasedimentary rocks that failed to be highly mobilized and extracted from the host unit (Zeng et al., Chapter 3). In areas outside the migmatite zone, well-preserved bedding features indicate the protolith was a relatively thin bedded immature turbidite sequence of roughly greywacke composition with subordinate mafic volcanic layers.

The Goat Ranch granodiorite is composed of plagioclase in slightly greater abundance than K-feldspar, quartz, biotite, minor hornblende, and trace amounts of zircon, rutile and apatite. Enclaves are sparsely distributed within the Goat Ranch granodiorite intrusion. These enclaves mainly consist of plagioclase, hornblende, biotite, quartz, with minor K-feldspar, and trace amounts of zircon and apatite. The grain sizes of constituent minerals of these enclaves are much finer than those of host granodiorites. Based on petrographic observations, the enclaves appear to have mineralogically equilibrated with the host granodiorite. Major element geochemistry data on the granodiorites and enclaves show that enclaves have higher MgO, Al_2O_3, CaO, and FeO* content than those in the granodiorites, but both have similar Na_2O and K_2O content (Zeng and Saleeby, in prep.). The major element compositions of the enclaves are andesitic.

Data and interpretation

We have conducted Sr and Nd whole rock isotopic studies in order to characterize the isotopic compositions of pelitic and psammitic members of the metapelite unit, as well as leucosomes, finely layered migmatites, and granodiorites, and to examine the isotopic homogeneity of the granodiorite and metapelite. The sample preparation techniques and analytical procedures used for the Rb-Sr and Sm-Nd isotopic analyses are those described by Pickett and Saleeby (1994) and Ducea and Saleeby (1998a & c). The analytical results are given in Table 1. Calculations of initial Sr and Nd ratios were based on a 100±2 Ma zircon age measured on the Goat Ranch pluton, as well as a series of syn-deformational and syn-metamorphic felsic dikes which cut the high-grade pendant rocks (Saleeby and Zeng, in prep.).

Sr and Nd isotopic composition data of the granodiorites and mafic enclaves show extreme heterogeneity (Fig. 3). $^{87}Sr/^{86}Sr(T)$ (where T =100Ma) values of the Goat Ranch granodiorite range from 0.7061 to 0.7071, and $\varepsilon_{Nd}(T)$ from -1.1 to -6.5. The enclaves have a similar range. The leucosomes have $^{87}Sr/^{86}Sr(T)$ ratios ranging from 0.7124 to 0.7247, similar to those of the non-migmatitic metapelites that preserved protolith features, but have $\varepsilon_{Nd}(T)$ values ranging from -6.0 to -11.0, much wider than that of the metapelites. The $^{87}Sr/^{86}Sr(T)$ and $\varepsilon_{Nd}(T)$ values for the finely layered migmatites overlap with those of metapelite. In these finely layered migmatites, leucosomes and melanosomes occur at mineral grain scales prohibiting their complete separation for analysis. In Figure 4a and b, the Nd and Sr isotopic compositions for both granodiorites and associated enclaves are plotted against their distance away from the contact between the Goat Ranch pluton and the upper pelite unit. Sr and Nd isotopic compositions of the granodiorites show a larger degree of heterogeneity and do not correlated with their distances from the contact. This suggests that the variations in both Sr and Nd isotopic compositions of granodiorites were not derived from assimilation of the metasediments-derived melts, but from a deeper source. This further suggests that interaction between the pendant rocks and granitic batholith at this crustal level is limited to the areas proximal to the intrusion contact. As discussed below, this is in contrast to the contamination processes that occurred at lower crustal levels. The observed large degrees of Sr and Nd isotopic heterogeneity in the Goat Ranch pluton with a span of five ε_{Nd} units, are comparable with those from the Tuolumne Intrusive Suite, whose $\varepsilon_{Nd}(T)$ values span seven units (Kistler et al., 1986; Coleman and Glazner, 1998), and the Fine Gold Intrusive Suite, whose $\varepsilon_{Nd}(T)$ values span six units (Truschel, 1996).

Figure 3a is an $\varepsilon_{Nd}(T) \sim {}^{87}Sr/{}^{86}Sr(T)$ plot of our data on the Goat Ranch granodiorite, and the adjacent migmatite complex. Figure 3b shows these data compiled along with other available data from the Sierra Nevada batholith. The most distinct feature shown in Figure 3b is the negative correlation between initial $\varepsilon_{Nd}(T)$ and ${}^{87}Sr/{}^{86}Sr(T)$ for the rocks from the southern Sierra Nevada, which is common to rocks from continental margin granitic batholiths (DePaolo, 1981; McCulloch and Chappell, 1982). The relatively large variations in the initial ratios of ${}^{87}Sr/{}^{86}Sr$ compared to $\varepsilon_{Nd}(T)$ of the metasedimentary rocks is consistent with the fact that Rb/Sr are much more easily fractionated by common crustal processes such as weathering, melting and metamorphism, while Sm and Nd are more resistant to disturbance by these processes (Goldstein, 1988). The high degree of heterogeneity shown in the Sr and Nd isotopic compositions of both the metasedimentary rocks and leucosomes (Figure 3b) suggests that some of the features seen in the Sr-Nd systematics of granitoids worldwide may arise from a common source by assimilation of anatectic melts from non-modal partial melting of metasedimentary wallrocks (Zeng et al., Chapter 3), but not from contributions from the lower and upper crust, respectively (DePaolo, 1981).

It has been shown that one of the common source components for most of the Earth's granitic batholiths is similar to that of island arc with an ε_{Nd}= +8 (DePaolo, 1980; Allegre and Ben Otman, 1981). Therefore, to evaluate the importance of the crustal contribution, it is necessary to have some knowledge of the nature of depleted mantle source for the formation of the Sierra Nevada batholith. The batholith data array defines an overall trend which extends from the center of the island arc field far into the range of values characteristic of old continental crust (Figure 3b). This is consistent with the source of the batholith as a mixture of a mantle source component similar to island arcs and recycled continental crustal components. There are two ways to evaluate the isotope characteristics of the depleted mantle source. On one hand, one can examine mafic intrusives or extrusives of the same age as the batholitic rocks which had experienced little or minor crustal contamination, such as the mafic rocks examined by Clemens-Knott(1992) along the western Sierra, or Session et al. (2000) along the eastern Sierra. The other approach is to examine data from mantle xenoliths brought to the surface by post-batholithic basaltic volcanism, and for which age and petrographic data suggest a cogenetic relationship with the overlying batholith (Ducea and Saleeby, 1996 and 1998c; Mukhopadhyay and Manton, 1994). Based on such isotopic data and on the regional relations of the pre-batholithic metamorphic framework it can be argued that these mafic batholithic assemblages were not only derived from least modified depleted mantle, but they also ascended and even emplaced into tectonically accreted depleted mantle (oceanic lithosphere) domains. In contrast, mafic batholithic intrusive complexes of the eastern Sierra that were generated, ascended and emplaced into the North American Proterozoic continental lithosphere domain yield $\varepsilon_{Nd}(T)$ values that range from -2.91 to -5.63, and $^{87}Sr/^{86}Sr(T)$ values from 0.70619 to 0.70679 (Coleman, et al., 1992). Since we do not have good constraints on the isotopic characteristics of pre-batholithic subcontinental lithospheric mantle that potentially affected the isotopic compositions of the batholith, we first evaluate whether the observed isotopic heterogeneity could be derived from contamination by assimilation of mid-level metasedimentary rocks. Studies carried out by Clemens-Knott (1992) have shown that the least contaminated mafic rocks from the western Sierra Nevada batholith have rather uniform initial ε_{Nd} values ranging from +4.2 to +6.1, and $^{87}Sr/^{86}Sr$ of 0.70338 to 0.70408. We take the most primitive values: WKB94: Sr=258.1ppm, $^{87}Sr/^{86}Sr(T) = 0.70354$; Nd = 6.2ppm, $\varepsilon_{Nd}(T)=+6.1$, representing the Nd and Sr isotopic compositions of the upper depleted mantle source at the formation of Sierra Nevada batholith. If the depleted mantle source is rather uniform, then the observed Sr and Nd isotopic heterogeneities of the Goat Ranch granodiorite should be derived either from the pre-existing mid- and shallow-level crustal rocks, or from the lower crust and the uppermost lithospheric mantle.

❑ Evaluating the crustal contribution

Previous studies of the Sierra Nevada batholith, based on geologic, petrologic and geochemical data, have proposed a number of models to explain the observed petrologic and geochemical features, especially on the Sr, Nd, Pb and O isotopic heterogeneities. Mainly based on Sr isotopic studies of the batholith, several of the earlier models proposed that batholith generation was a result of (1) partial melting in a thick prism of crustal rocks marginal to the continent (Bateman and Eaton, 1967); (2) partial melting of the lower crust and upper mantle with assimilation of the upper crustal rocks (Hamilton and Myers, 1967; Kistler et. al , 1971); (3) partial melting of a subducted slab of oceanic crust and trapped sediments (Dickinson, 1970); and (4) partial melting in a zone that laterally transects the upper mantle and the lower crust (Kistler and Peterman, 1973). In a regional study of batholithic Nd and Sr isotopes, DePaolo (1981) noted that most of samples scatted along a trajectory extending from the mantle array to a low ε_{Nd}-high Sr end-member typical of North American cratonic basement, but with an added correlation of higher $\delta^{18}O$ toward the basement contaminated samples. DePaolo (1981) interpreted these data to suggest that assimilated craton-derived metasedimentary material constituted the main continental component within well-mixed and fractionated magmatic systems. All of these hypotheses have called for various degrees of crustal components in the formation of the batholith, and to a great extent these are not mutually exclusive. The question lies in whether the observed isotopic heterogeneities of the batholith mainly derived from the heterogeneous mantle source, deep continental crust or pre-batholith shallow continental crust. The extent to which each of these has or has not contributed to the batholith's material budget has important implications for the evolution of continental crust over geologic history.

The decoupling of Sr from Nd isotopic geochemistry in the continental crust during crustal differentiation either by crustal anatexis, metamorphism or other reworking processes (Goldstein, 1988) makes the Rb-Sr isotopic system a useful tool to unravel the relative contributions of different reservoirs to the formation of granitic batholiths. Almost all granitic batholiths around the Earth bear a crustal signature that was acquired either at deep levels where silicic magmas are produced by high-degree melting of the lower crust during the underplating of mafic magma at the base of the continental crust, or at mid- to shallow-crustal levels during magma ascent and assimilation of wallrocks. It is widely held that in response to the underplating of hot basaltic magma, lower continental crust will undergo partial melting (Bergantz, 1988; Huppert and Sparks, 1988), which might consume most of the energy provided by the relatively hot mantle-derived mafic magma. Because the amount of energy available for a crustal column within a magmatic arc is finite, the AFC (Assimilation-Fractionation-Crystallization) processes (Depaolo, 1981; Taylor, 1981) at mid- to shallow-crustal levels may be limited by the amount of energy available. Therefore, AFC may play a limited role in modifying the isotopic compositions of the newly emplaced granitoid intrusions at mid- to shallow-crustal levels.

The crustal components contributed to the Sierra Nevada batholith are much more complicated because of the high and relative mobility of Rb and Sr and the resulting variations in Sr isotopic compositions of the crustal rocks at different crustal levels. However, the vertical variations in Sr isotopic compositions of crustal rocks provide us an opportunity to differentiate the relative amount of contribution from the lower crust and upper crust to the batholith, respectively. Figure 5a shows that Goat Ranch granodiorites and enclaves have rather uniform initial $^{87}Sr/^{86}Sr$ isotopic compositions regardless of Sr concentrations, while leucosomes and metapelites have a wider range of initial $^{87}Sr/^{86}Sr$ values and Sr concentrations. The granodiorites and mafic enclaves define a vector pointing to a different source from the pelites and migmatites of this study (Fig. 5a). However, the feature seen in Figure 5a does not show up in the initial $^{143}Nd/^{144}Nd$

versus 100/Nd diagram (Fig. 5b). If partial melting products (leucosome) from the metapelite were extracted and well mixed into the adjacent Goat Ranch granodiorite, it is conceivable that the granodiorites should exhibit highly heterogeneous Sr isotopic compositions to an extent comparable to that of the leucosomes and metapelites. This is opposite to what we observed in Sr isotopic compositions of the Goat Ranch granodiorites and enclaves. This indicates that partial melting of metapelite and mobilization of melt products had minor effects on the isotopic compositions of the Goat Ranch granodiotite even though intensive migmatization in the metapelite unit occurred as a result of the emplacement of the Goat Ranch pluton.

In an extensive study of late Cenozoic volcanic rock-hosted lower crustal/upper mantle xenoliths, Ducea and Saleeby (1996a, 1998a, b, c) resolved a thick (~50 km) garnet-rich mafic to ultramafic keel to the batholith, which mineralogically resembles eclogite facies rocks. Isotopic, trace element and Sm/Nd-Rb/Sr isochron age data show this keel to be petrogenetically linked to the overlying batholith as an accumulation of residues produced by dehydration melting of deep crust-upper mantle mafic to intermediate composition assemblages (Wolf and Wyllie, 1994). They found that the average isotopic compositions of garnet pyroxenite residues are strikingly similar to those of the batholith which host the xenolith-bearing volcanic centers. Based on age constraints and the similarities in isotopic compositions, the garnet pyroxenite xenoliths were interpreted to be the mafic residues from a partial melting event at the mantle-lower crust boundary which generated silicic melt that formed the Sierra Nevada batholith (Ducea and Saleeby, 1998c). The Garnet pyroxenite xenolith data define a nearly vertical array in the Sr-Nd systematics diagram (Fig. 3b), suggesting a lower crustal signature.

The Nd, Sr and Pb isotopic studies on the deep-level (~7 to 9 kb) Cretaceous intrusive rocks from the Tehachapi Mountains, to the south of this study area, also suggest that the source components responsible for the Sierra Nevada batholith involved a mixture between depleted mantle derived magma and pre-existing lower continental crust in part represented by deep-level metasedimentary pendants (Pickett and Saleeby, 1994). The data presented here, together with those from Ducea and Saleeby (1998c), and Pickett and Saleeby (1994) strongly suggest that Sr and Nd isotopic heterogeneities within the Goat Ranch granodiorite intrusion are derived from deep-level crustal sources, with an insignificant contribution from the partially melted metasedimentary rocks at the observed level of exposure.

We conceive of AFC as an energy-limited process (Ghiorso and Kelemen, 1987; Spera and Bohrson, 2001; Thompson et al., 2002) at mid- to upper crustal levels (Fig. 6). At deeper crustal levels, there is much more energy available and thus lower crustal anatexis powered by the underplating of hot mantle-derived mafic magma is more efficient. Melting, mixing and fractionation at deep crustal levels will generate predominant geochemical signatures that will not be easily overprinted by energy-limited AFC processes occurring at mid- to shallow crustal levels

Conclusions

We have presented Sr and Nd isotopic data on the best known example of a mid-crustal level (4-5 kb) syn-batholithic migmatite complex derived from continental clastic sediments as well as the batholithic pluton which drove the partial melting. The detailed Nd and Sr isotopic data on the non-migmatitic distal wallrocks (sillimanite grade), leucosomes from the migmatites, and on traverses into the Goat Ranch pluton away from contacts with the migmatites demonstrate that (1) the Goat Ranch granodiorite pluton has heterogeneous Sr and Nd isotopic compositions, which is partly overlapping with Sr and Nd isotopic compositions of the garnet pyroxenite xenoliths which represent the deep crust-upper mantle residues related to high-volume batholith magma production; (2) the metapelites and their leucosomes have a wide range of Sr isotopic compositions which vary much more than the range observed in the pluton, but show a similar range of Nd isotopic ratios as does the pluton; (3) the observed within-pluton isotopic heterogeneities of the Goat Ranch granodiorite were derived from deep-level source regimes which may extend deeper than 7-9 kb; (4) the extent of assimilation of metasediment-derived melt at shallow- to mid-crustal level is low enough to be insignificant.

Since the Mesozoic batholithic rocks reflect the same source variability as the mafic rocks and mantle xenoliths, we propose that the deep-level source components partly represented by the lower crust and the uppermost lithospheric mantle exert first-order control on batholith isotope geochemistry. If mid- and shallow-level contamination of large granitic batholiths by assimilation of metasedimentary pendant-derived melts is limited in general, then the isotopic characteristics of a granitic batholith may provide a useful tool to constrain the isotopic geochemistry of the deep basement.

Figure 1 Geologic map of the study area located to the south of Lake Isabella, southern Sierra Nevada, California.

Figure 1

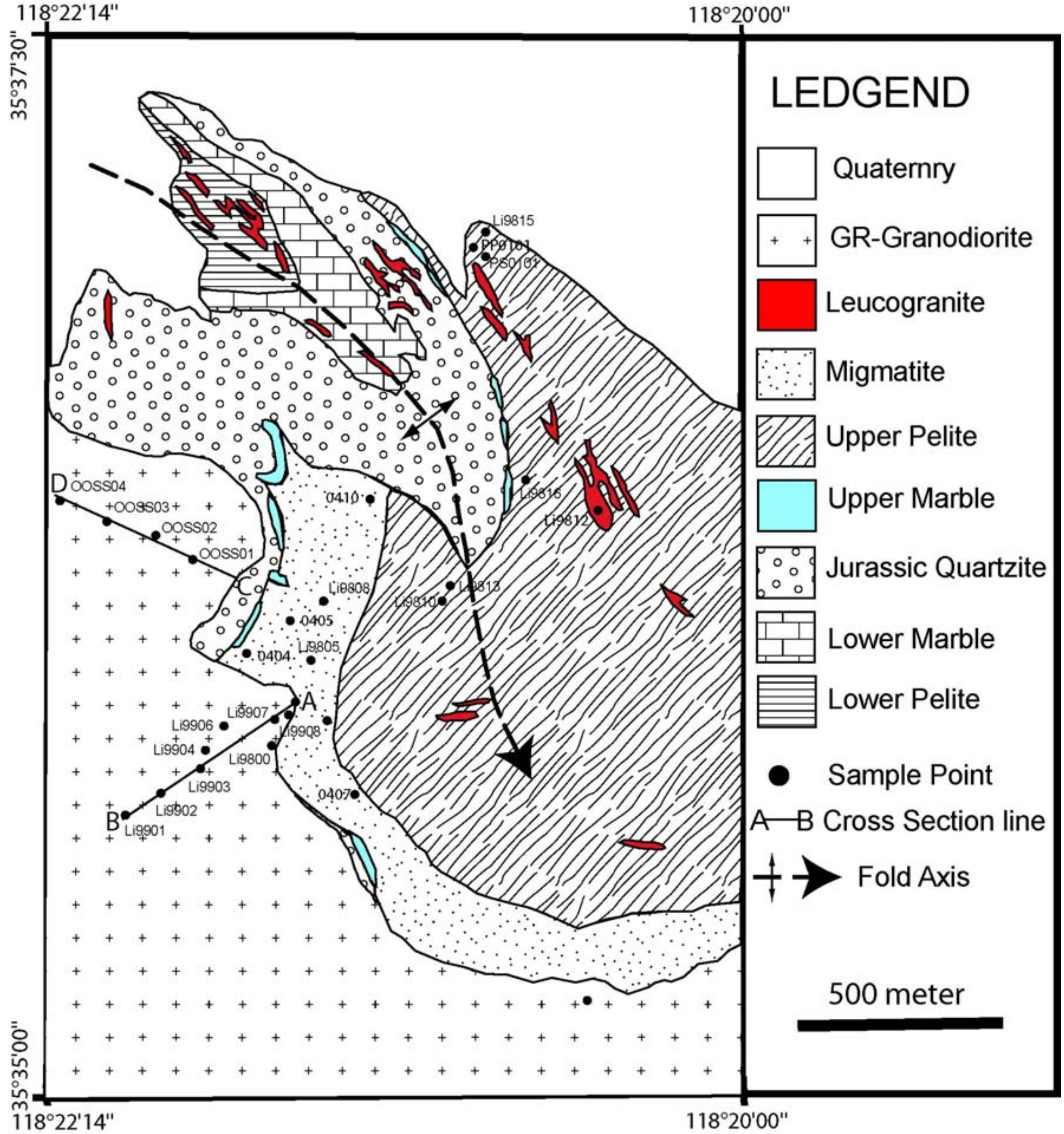
118°22'14"
118°20'00"
35°37'30"
35°35'00"
118°22'14"
118°20'00"
LEDGEND
Quaternry
GR-Granodiorite
Leucogranite
Migmatite
Upper Pelite
Upper Marble
Jurassic Quartzite
Lower Marble
Lower Pelite
Sample Point
A—B Cross Section line
Fold Axis
500 meter
Li9815
PP0101
PS0101
Li9816
Li9812
Li9813
Li9810
0410
Li9808
0405
Li9805
0404
0407
D
OOSS04
OOSS03
OOSS02
OOSS01
C
A
B
Li9907
Li9906
Li9908
Li9904
Li9800
Li9903
Li9902
Li9901

Figure 2 Photos show the typical structures and textures of migmatites (a) typical outcrop scale anastomosing (network) structure, note marking pen for sacle; (b) microscopic scale layer structure of migmatites defined by alternate layers of leucosome and melanosome.

Figure 2a


'89 5 21

(b)

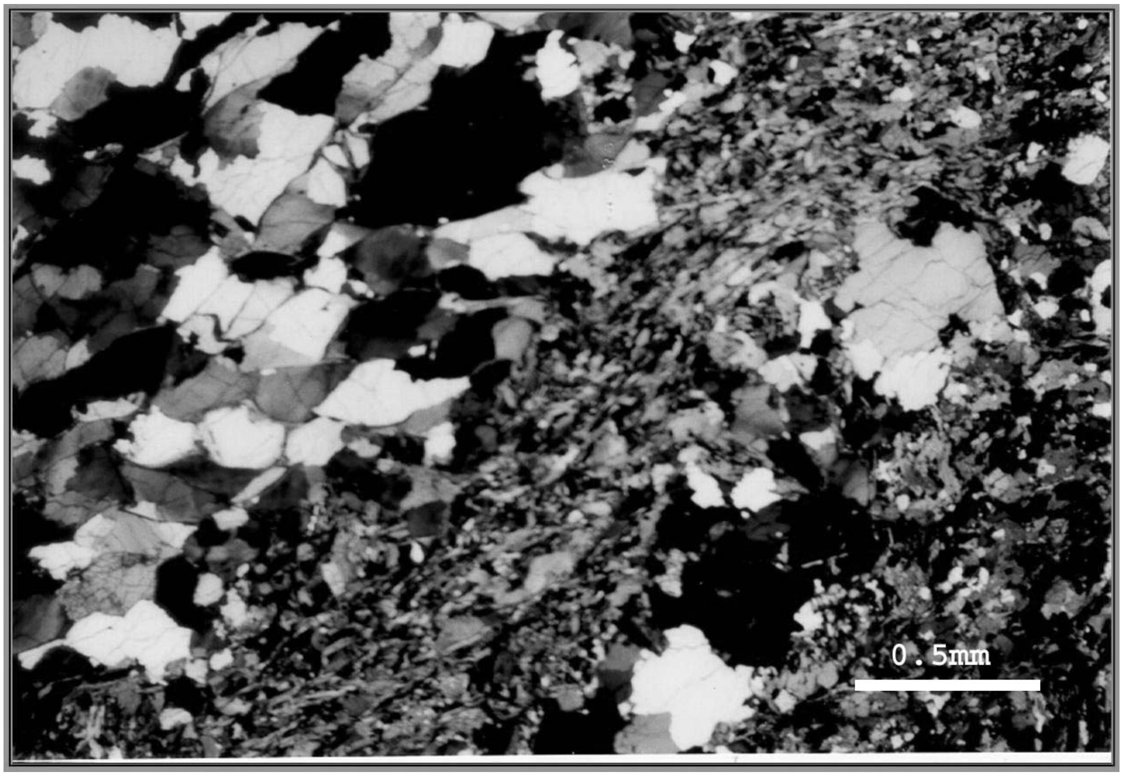

Figure 3 (a) Sr-Nd systematics of rocks from the Goat Ranch granodiorites and enclaves showing that (1) enclaves have a similar isotopic composition to their hosted granodiorites and (2) high magnitude of isotopic heterogeneities of the Goat Ranch granodiorite intrusion. The symbol sizes are larger than the analytical errors. The Nd and Sr measurements were corrected for mass fractionation by normalization to ^{146}Nd/^{142}Nd = 0.63615, and ^{86}Sr/^{88}Sr = 0.1194. External precisions during this period of measurement for Sr and Nd isotopic compositions are ±0.000016 (n=16), and ± 0.000019 (n=16) respectively. ^{87}Sr/^{86}Sr for the NBS987 standard is 0.710252, and ^{143}Nd/^{144}Nd for La Jolla Nd standard 0.511859. (b) Plot of ^{87}Sr/^{86}Sr (at 100 Ma) versus ε_{Nd} (at 100 Ma) of the granitic rocks, metasedimentary framework rocks, pyroxenite xenoliths, and mafic intrusions from the central and southern Sierra Nevada Batholith. The data set defines a trend extending from the depleted mantle domain into the Sierra Nevada batholith domain. The Sr and Nd isotopic compositions of the Goat Ranch granodiorites and enclaves are heterogeneous, they together with the garnet pyroxenite suggest a vertical array pointing toward the cryptic lower crustal or upper mantle domain. Data sources: Amphibolite data are from Zeng et al (in preparation), CK(92)-Clement-Knott(1992), PS(94)-Pickett & Saleeby (1994), Pyroxenite(98)-Ducea(1998). Other background data are taken from DePaolo(1981) and Allegre & Ben Othman(1981). The mixing lines are calculated by taking WKB94: Sr=258.1 ppm, ^{87}Sr/^{86}Sr(T) = 0.70354; Nd = 6 .2 ppm, ε_{Nd}(T)=+6.10, representing the Nd and Sr isotopic compositions of the upper depleted mantle source, and 0410L: Sr=263.7 ppm, ^{87}Sr/^{86}Sr(T) = 0.72465; Nd = 27.0 ppm, ε_{Nd}(T)=-6.98, and Li98/15: Sr= 143.7 ppm, ^{87}Sr/^{86}Sr(T) = 0.71249; Nd = 47.7 ppm, ε_{Nd}(T)= -11.31 as end-members for the crustal sources. ε_{Nd}(T) is calculated at T= 100 Ma using the equation:

$$\varepsilon_{Nd}(t) = \left[\frac{({}^{143}Nd/{}^{144}Nd)_{sample}(t)}{({}^{143}Nd/{}^{144}Nd)_{CHUR}(t)} - 1 \right] \times 10^4$$

with $({}^{143}Nd/{}^{144}Nd)_{CHUR}(0) = 0.512635$ and $({}^{147}Sm/{}^{144}Nd)_{CHUR}(0) = 0.1966$. t is time.

Figure 3a

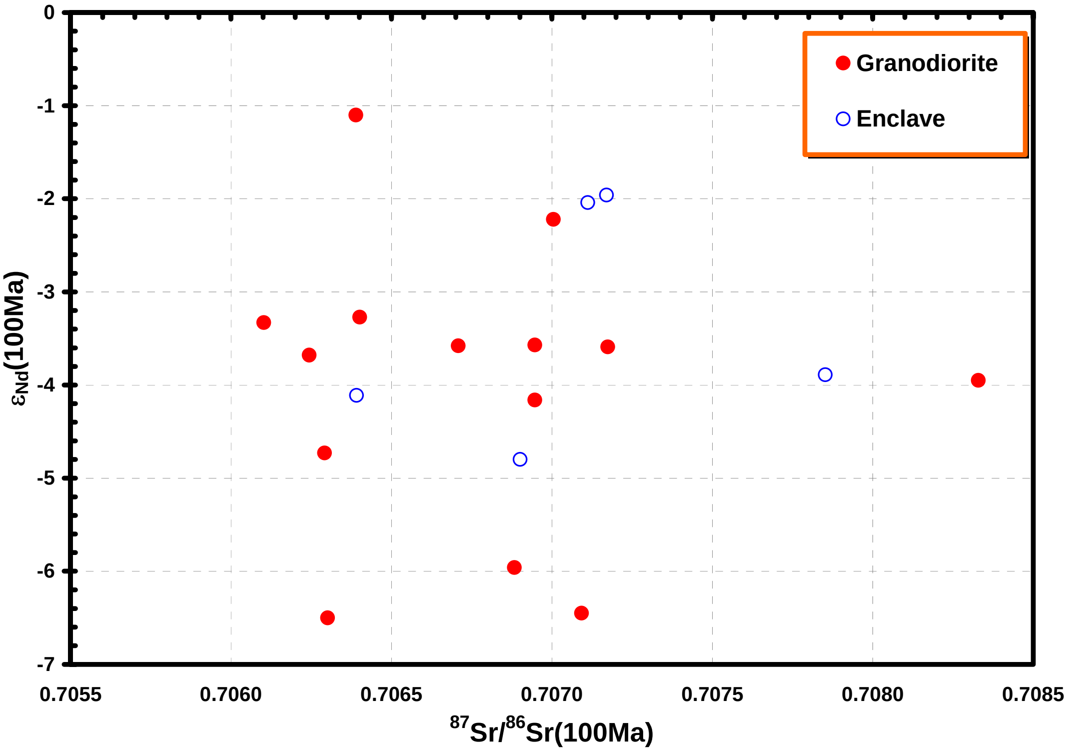

Figure 3b

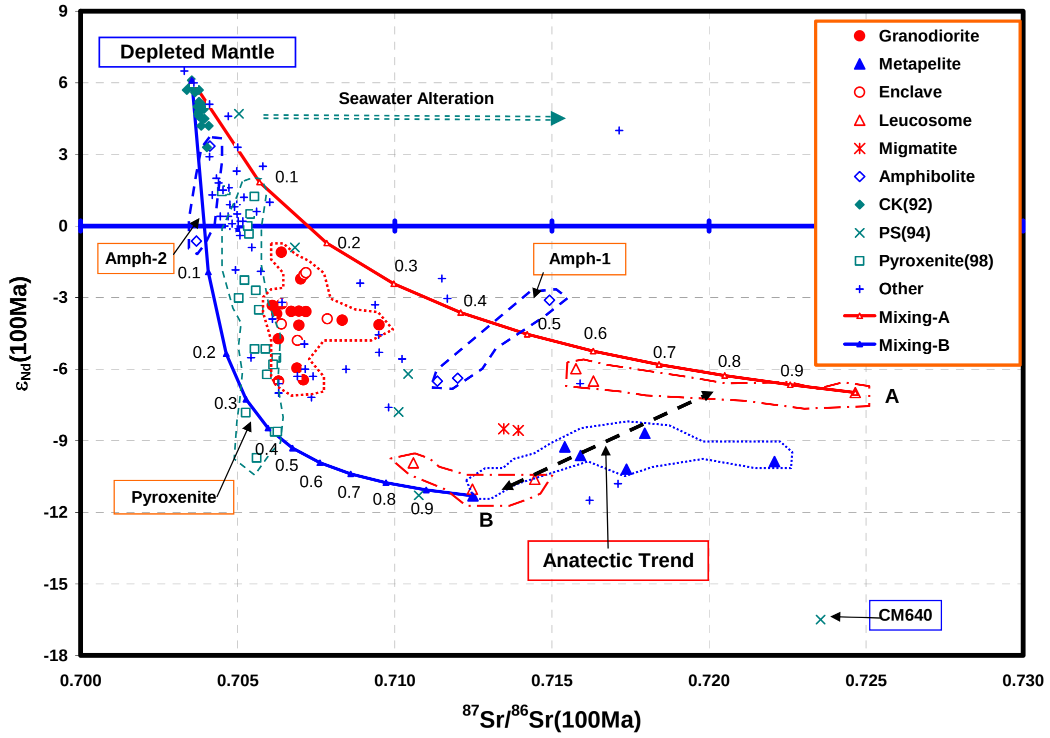

Figure 4 Sr and Nd isotopic compositions of the granodiorites and associated enclaves plotted against their distance away from the contact between the Goat Ranch granodiorite pluton and the upper metapelite unit. The symbol sizes are larger than the analytical errors. Plots of (a) and (b) correspond to cross-section line A-B and line C-D in Figure 1, respectively. In diagram (a), Sr isotopic compositions both of the granodiorite and enclave have greater variations than their Nd isotopic compositions. Both diagram a and b show roughly that Nd and Sr isotopic compositions of the granodiorites are negatively correlated. The higher is $\varepsilon_{Nd}(T)$ value, the lower is the $^{87}Sr/^{86}Sr(T)$ ratio.

Figure 4a

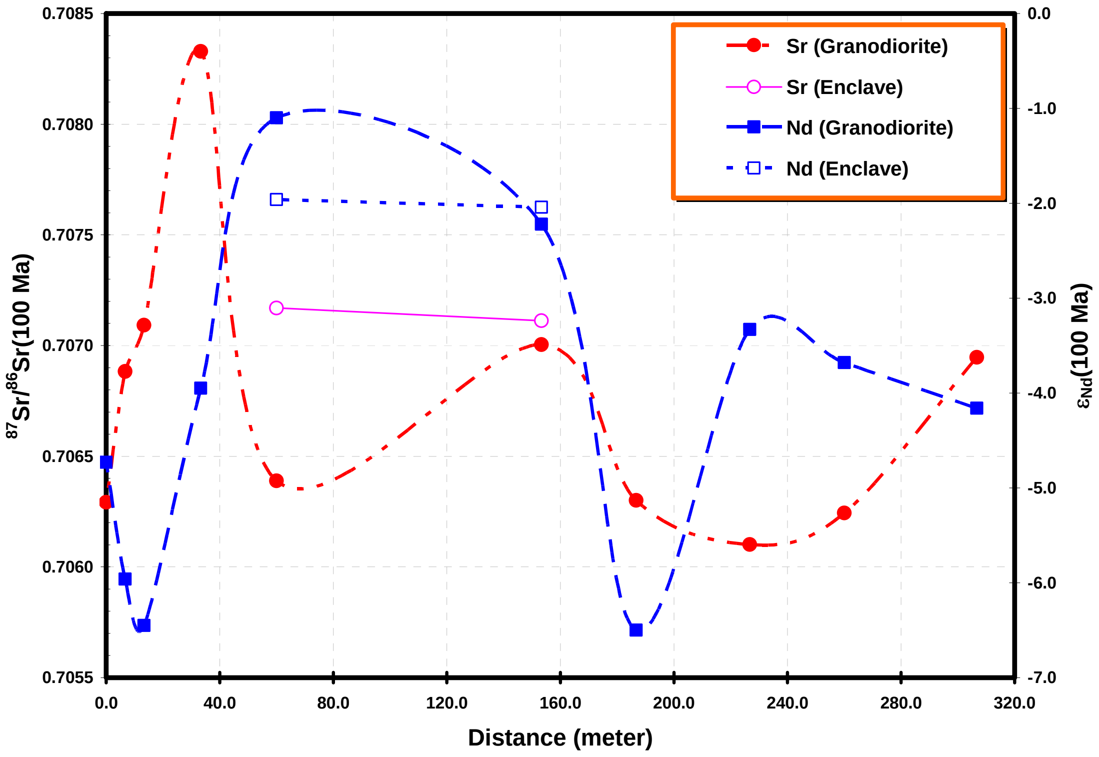

Figure 4b

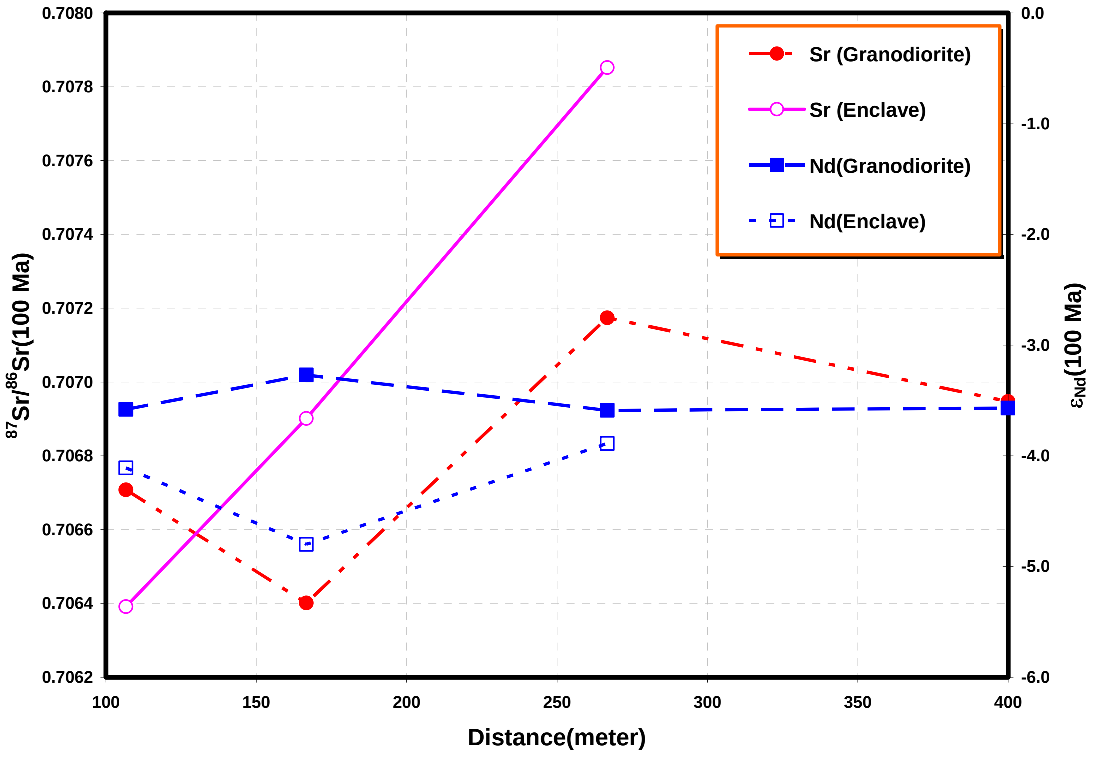

Figure 5 (a) Plot of measured $^{87}Sr/^{86}Sr$ versus 1000/Sr, and (b) Plot of measured $^{143}Nd/^{144}Nd$ versus 100/Nd. The symbol sizes are larger than the analytical errors. The granodiorites and enclaves have relatively uniform Sr isotopic composition as compared to the wide spreading of Sr isotopic compositions of the metapelites and leucosomes.

Figure 5a

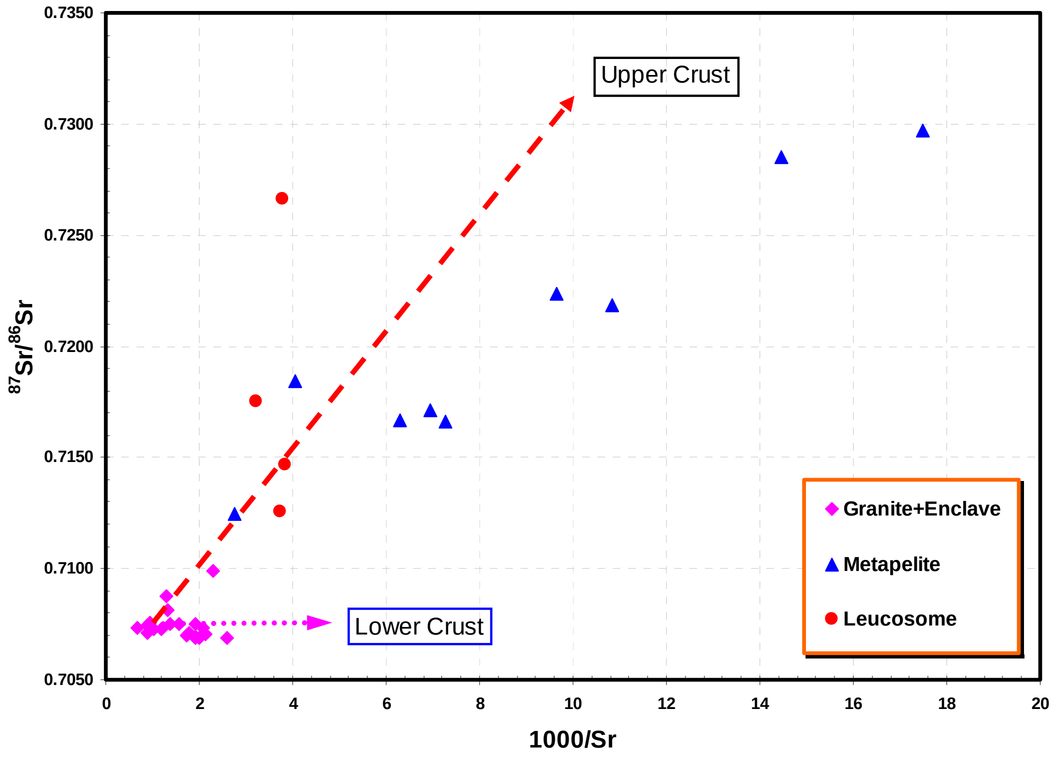

Figure 5b

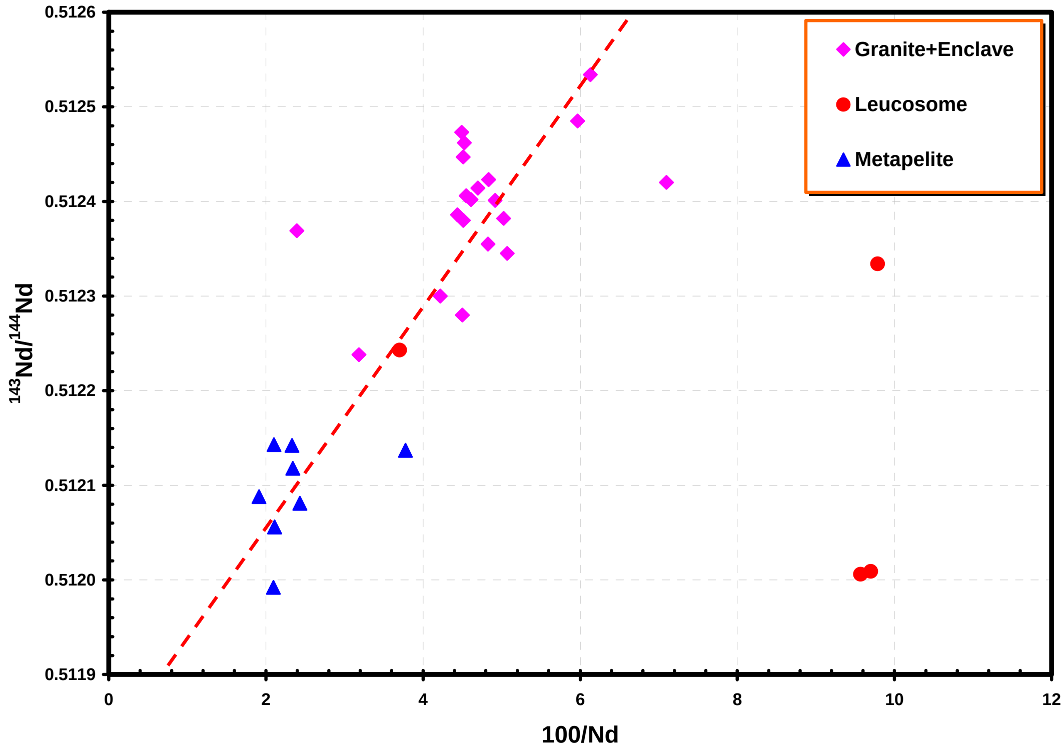

Figure 6 Model involving two-stage partial melting to form a granitic batholith. We conceive AFC as an energy-limited process. At deeper level, there is much more energy available, and partial melting of lower crust powered by the underplating of mantle-derived mafic magma is relatively efficient. Melting, mixing and fractionation at deep crustal levels will generate the predominant geochemical signatures that will not be easily overprinted by AFC processes occurring at mid- to shallow levels. Partial melting at the lowermost crustal level would produce dense mafic residues such as garnet pyroxenites. Due to extensive exchange or mixing of a depleted mantle component with a lower crustal source, the garnet pyroxenite would bear a lower crustal or deeper source signature which is similar to that of the Goat Ranch pluton.

Figure 6

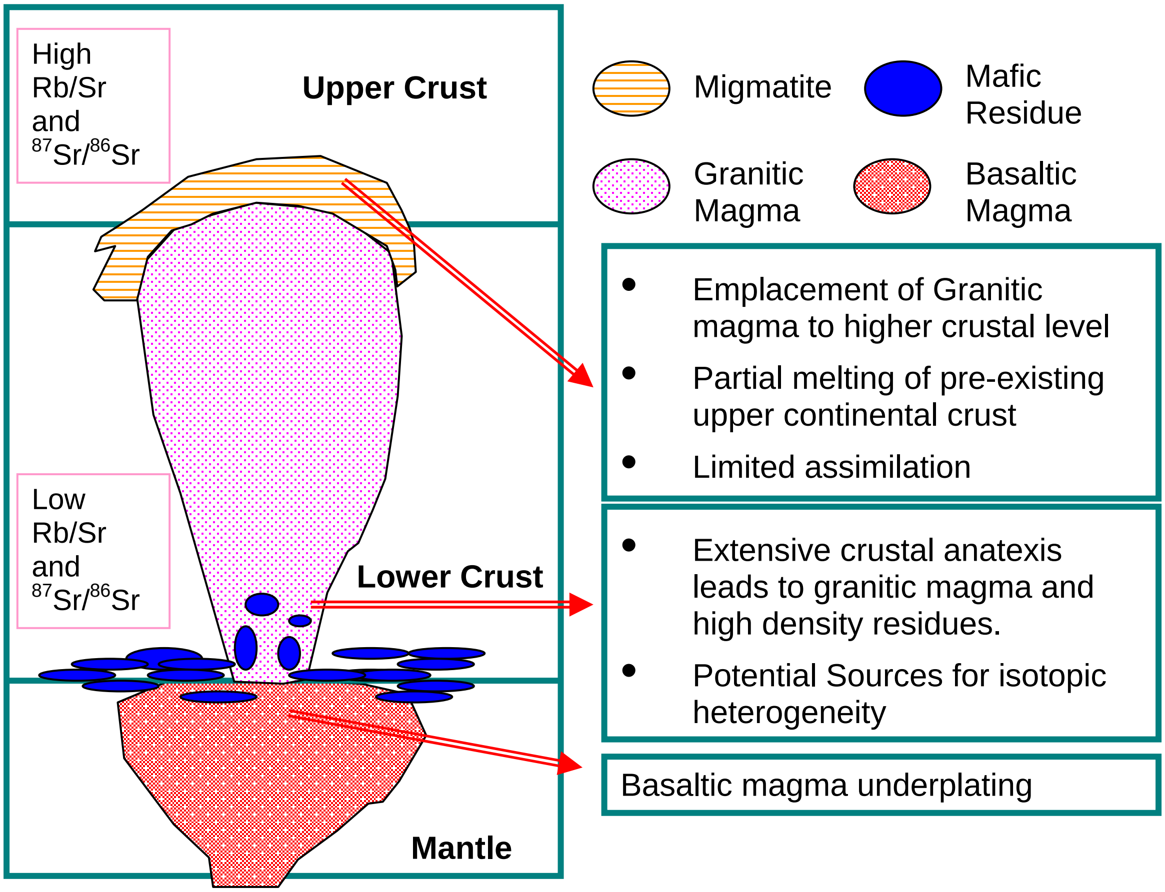

- Emplacement of Granitic magma to higher crustal level
- Partial melting of pre-existing upper continental crust
- Limited assimilation

- Extensive crustal anatexis leads to granitic magma and high density residues.
- Potential Sources for isotopic heterogeneity

Basaltic magma underplating

Table 1. Whole rock Rb-Sr and Sm-Nd isotopic compositions of the granodiorites, enclaves, metapelites, migmatites and leucosomes from the Lake Isabella area, southern Sierra Nevada, California

Sample	Rock-Type	Rb(ppm)	Sr(ppm)	^{87}Rb/^{86}Sr	^{87}Sr/^{86}Sr	^{87}Sr/^{86}Sr(100)	Sm(ppm)	Nd(ppm)	^{147}Sm/^{144}Nd	^{143}Nd/^{144}Nd	ε_{Nd}(100)
OOSS01-X	Enclave	85.23	580.05	0.42248	0.706992	0.706391	4.98	22.53	0.133622	0.512386	-4.11
OOSS01-G	Granodiorite	73	478.9	0.438306	0.707331	0.706708	4.47	21.98	0.122906	0.512406	-3.58
OOSS02-X	Enclave	59.34	1137.65	0.149982	0.707114	0.706901	4.79	20.72	0.13962	0.512355	-4.8
OOSS02-G	Granodiorite	66.94	518.75	0.371008	0.706928	0.706401	4.24	20.68	0.123956	0.512423	-3.27
OOSS03-X	Enclave	49.11	757.75	0.186378	0.708117	0.707852	4.66	20.34	0.138356	0.512401	-3.89
OOSS03-G	Granodiorite	74.57	1118.1	0.191788	0.707447	0.707174	4.75	21.28	0.135072	0.512414	-3.59
OOSS04-G	Granodiorite	77.28	963.19	0.230694	0.707274	0.706947	4.15	21.69	0.115767	0.512402	-3.57
Li9901	Granodiorite	70.96	519.09	0.393092	0.707505	0.706947	4.69	22.16	0.128097	0.51238	-4.16
Li9902	Granodiorite	79.83	521.13	0.440434	0.70687	0.706244	7.05	22.17	0.192363	0.512447	-3.68
Li9903	Granodiorite	75.64	384.14	0.566158	0.706907	0.706102	2.9	14.09	0.12432	0.51242	-3.33
Li9904	Granodiorite	68.39	501.58	0.392039	0.706858	0.706301	7.41	23.7	0.189132	0.5123	-6.5
Li9906a	Enclave	67.79	718.55	0.271285	0.707498	0.707112	3.86	22.26	0.104675	0.512473	-2.04
Li9906b	Granodiorite	74.27	633.54	0.337074	0.707484	0.707005	3.73	22.1	0.101966	0.512462	-2.22
Li9907a	Enclave	107.94	1057.64	0.293469	0.707587	0.70717	3.24	16.76	0.116689	0.512485	-1.96
Li9907b	Granodiorite	100.23	564.46	0.510586	0.707115	0.706389	3.36	16.31	0.124706	0.512534	-1.1
Li9908	Granodiorite	79.16	839.58	0.27111	0.707269	0.706883	4.25	22.22	0.115721	0.51228	-5.96
Li9909	Granodiorite	88.46	471.24	0.538731	0.707059	0.706292	3.87	19.72	0.118777	0.512345	-4.73
Li9800	Granodiorite	78.0	774.6	0.289761	0.708741	0.708329	3.75	19.9	0.1142497	0.512382	-3.95
Li9802	Granodiorite	85.2	1502.1	0.163123	0.707324	0.707092	4.74	31.39	0.0913344	0.512238	-6.45
Li9812	Granodiorite	41.4	434.1	0.274138	0.709892	0.709502	7.54	41.77	0.109149	0.512369	-4.14
PP0101	Metapelite	175.65	103.56	4.8844	0.722352	0.715412	8.96	42.66	0.1270	0.512118	-9.26
PS0101	Metapelite	108.39	69.21	4.5123	0.728495	0.722083	8.06	41.11	0.1185	0.512081	-9.87
Li9805	Migmatite	123.31	158.54	2.2375	0.716645	0.713465	8.37	47.52	0.1064	0.512143	-8.5
Li9808	Migmatite	90.80	137.32	1.9022	0.716636	0.713932	7.83	42.89	0.1103	0.512142	-8.57
Li9810	Metapelite	153.10	247.20	1.7831	0.718446	0.715912	9.51	52.30	0.1100	0.512088	-9.62
Li9813	Metapelite	88.00	92.30	2.7484	0.721861	0.717956	4.89	26.48	0.1171	0.512137	-8.69
Li9815	Metapelite	163.70	143.70	3.2790	0.717148	0.712489	7.48	47.72	0.0947	0.511992	-11.31
Li9816	Metapelite	172.10	57.20	8.6757	0.729700	0.717372	8.20	47.39	0.1046	0.512056	-10.19
L0404	Leucosome	12.34	267.17	0.1394	0.712585	0.712397	1.63	10.45	0.0939	0.512006	-11.03
L0405	Leucosome	15.46	260.32	0.1709	0.714695	0.714452	3.08	27.69	0.0670	0.512009	-10.62
L0407	Leucosome	134.58	311.01	1.2469	0.717532	0.715761	3.39	10.22	0.1996	0.512334	-5.98
L0410	Leucosome	126.13	263.71	1.3780	0.726609	0.724651	6.26	27.01	0.1395	0.512243	-6.98

Chapter 3

Non-modal crustal anatexis during the formation of migmatite at the southern Sierra Nevada, California

Lingsen Zeng   Jason B. Saleeby

Division of Geological and Planetary Sciences, California Institute of Technology, Pasadena, CA 91125

Mihai Ducea

Department of Geological Sciences, University of Arizona, Tucson, AZ 85721

Abstract

We provide data on the geochemical and isotopic consequences of non-modal partial melting of a thick Jurassic pelite unit at mid-crustal levels which produced a migmatite complex in conjunction with the intrusion of part of the southern Sierra Nevada Batholith at ca. 100 Ma. Field relations suggest that this pelitic migmatite formed and then abruptly solidified prior to substantial mobilization and escape of its melt products. Hence this area yields insights into potential mid-crustal level contributions of crustal components into Cordilleran-type batholiths. Major and trace element data in addition to field and petrographic data, demonstrate that leucosomes are products from partial melting of the pelitic protolith host. Compared with the metapelites, leucosomes have higher Sr and lower Sm concentrations and lower Rb/Sr ratios. The initial $^{87}Sr/^{86}Sr$ ratios of leucosomes range from 0.7124 to 0.7247, and are similar to those of the metapelite protoliths (0.7125 to 0.7221). However, the leucosomes have a much wider range of initial ε_{Nd} values which range from -6.0 to -11.0, as compared to -8.7 to -11.3 for the metapelites. Sr and Nd isotopic compositions of the leucosomes, migmatites and metapelites suggest a disequilibrium partial

melting of the metapelite protolith. Based on their Sr, Nd and other trace element characteristics, two groups of leucosomes have been identified. Group A leucosomes show distinct positive Eu anomalies, relatively high Rb, Pb, Ba and K_2O contents, and low Rb/Sr ratios (0.15<Rb/Sr<1.0). Group B leucosomes have negative Eu anomalies, relatively low Rb, Pb, Ba and K_2O contents, and low Rb/Sr ratios (<0.15) as well. Finely laminated migmatites as well as the metapelite protoliths also show negative Eu anomalies. The low Rb concentrations and Rb/Sr ratios of the Group B leucosomes together suggest that partial melting was non-modal and dominated by water-saturated or H_2O-fluxed melting of quartz + plagioclase assemblage with the minor involvement of muscovite melting. Breakdown of quartz and plagioclase with minor contributions from muscovite resulted in low Rb/Sr ratios characterizing both Group A and Group B leucosomes. In contrast, Group A leucosomes have greater contributions from K-feldspar, which is suggested by (1) their relatively high K concentrations, (2) positive Eu anomalies, and (3) their Pb and Ba concentrations as correlated with their K_2O contents. It is also shown that accessory minerals have played a critical role in regulating the partitioning of key trace elements such as Sm, Nd, Nb, and V between melt products and residues during migmatization.

The various degrees of parent/daughter fractionations in the Rb-Sr and Sm-Nd isotopic systems as a consequence of non-modal crustal anatexis would render melt products with distinct isotopic signatures which could profoundly influence the products of subsequent mixing events. This is not only important for geochemical patterns of intracrustal differentiation, but also a potentially important process in generating crustal-scale as well as individual pluton-scale isotopic heterogeneities.

Introduction

The origin of geochemical and isotopic heterogeneities of large granitic batholiths is a fundamental question with regard to granitoid petrogenesis and the evolution of continental crust (Fyfe, 1973; Sawyer, 1998). Heterogeneity in the initial radiogenic isotopic compositions of granitic plutons is commonly attributed to heterogeneities inherited from source regimes and preserved due to incomplete mixing of the derivative magma. However, contamination of granitic magmas by assimilation of anatectic melts of wallrocks during ascent could also profoundly affect the geochemical and isotopic character of the final products. The role of crustal anatexis at various crustal levels in generating geochemical and isotopic heterogeneities is poorly understood. Thus, characterization of the geochemical and isotopic nature of anatectic melts in high-grade metamorphic terrains would help to better understand the sources of such heterogeneity and their potential magnitude.

Recent experimental and field observations (Vielzeuf and Holloway, 1988; Le Breton and Thompson, 1988; Rushmer, 1991; Puziewicz and Johannes, 1990; Inger and Harris, 1993; Gardien et al., 1995; Harris et al., 1995; Tommasini and Davies, 1997; Knesel and Davidson, 2002 and references therein) have shown that partial melting at crustal levels is commonly non-modal and disequilibrium in terms of the isotopic compositions of melting products. Disequilibrium melting refers to any melting event where the liquid phase was not in chemical equilibrium with the residue prior to melt extraction. Non-modal melting is the melting process where the proportion of reactant phases in the source is different from their proportions entering the melt. Because of the predominance of relatively complicated non-equilibrium mineral assemblages and the lower temperatures that characterize continental crust, crustal anatexis in response to thermal or chemical perturbations is more complex than melting in the mantle. Following a given temperature trajectory and for mica-bearing metasedimentary rocks, muscovite dehydration melting precedes biotite dehydration melting (e.g., Patiño-Douce and Harris, 1998). In contrast to muscovite dehydration melting, biotite dehydration melting is more complex because it is continuous over a wide range of temperatures. The temperature at which this reaction occurs depends on the composition of biotite (Mg/Fe ratio, Ti and F concentration) and the bulk Al content of source rocks (Le Breton and Thompson, 1988; Vielzeuf and Montel, 1994; Patiño-Douce and Beard, 1996; Stevens el al., 1997; Nabelek and Bartlett, 2000).

In this paper, we report the results of a detailed field and geochemical study of a well-developed migmatite zone in the Isabella pendant of the southern Sierra Nevada batholith in California. This migmatite zone is of particular interest because it represents a single prograde metamorphic sequence from greenshist facies metasediments to migmatites that lie in direct contact with the ca. 100 Ma Goat Ranch granodiorite pluton of the composite batholith. Field relations suggest that this pelitic migmatite zone formed and then abruptly solidified prior to substantial mobilization and escape of its melting products. Hence this area yields important insights into potential mid-crustal level contributions of crustal components into Cordilleran-type batholiths. In this paper, we intend to address (1) the geochemical nature of the melting products from the metapelite, (2) the magnitude of isotopic heterogeneity produced by such crustal anatexis, (3) elemental and isotopic fractionations associated with the formation of the migmatites, and (4) implications for the intracrustal differentiation and isotopic heterogeneities within Cordilleran-type batholiths. The nomenclature used in this paper follows that of Johannes (1988). Leucosome is the leucogranitic layer formed during migmatization, and the melanosome is the selvage between the leucosome and mesosome. Mesosome has intermediate color between the leucosome and melanosome in a migmatite and differentiates into leucosome and melanosome during migmatization. The rock undergoing migmatization is called the parent rock which in the non-migmatitic far field is also referred to as the protolith.

Geologic setting

Metamorphic rocks of the Isabella pendant consist of a stratified sequence of pelitic and psammitic schist and gneiss, quartzite, marble and calc-silicate rock. This sequence of stratified rocks constitutes one of the best preserved sections through the early Mesozoic Kings sequence which constitutes a distinct family of pendants that runs for over 250 km along the axis of the southern Sierra Nevada batholith (Saleeby and Busby, 1993). The entire pendant reached amphibolite facies conditions during the emplacement and engulfment of the late Cretaceous plutons. U/Pb zircon ages indicate the emplacement of these plutons in the 100±2 Ma time interval (Saleeby and Zeng, in prep).

A geologic map of the area that was studied in detail within the Isabella pendant is shown in Figure 1. The structure is characterized by a steeply-SE plunging isoclinal anticline with pelite units situated in core and envelope positions of the fold. Metamorphic fabrics associated with the fold are L-S with the linear element parallel to steeply-plunging fold axes. Finite strain studies on deformed pebble conglomerate in the quartzite unit indicate a stretch factor up to ~1000% along the steep lineations. Homoaxial deformation in satellite dikes from the Goat Ranch intrusion and leucosomes of the migmatitic pelite, as well as peak metamorphic textures indicate that the isoclinal folding and L-S fabric development occurred during pluton emplacement.

The upper pelite unit (J-pelite) which envelopes the large fold and is in contact with the Goat Ranch intrusion has an apparent stratigraphic thickness in excess of 1 km. Remnants of primary structures in the lowest metamorphic grade areas suggest a protolith of thin bedded compositionally immature turbidites. The protolith was remarkably homogenous in lithologic composition and in primary structure. Except for subordinate psammitic layers, the notable lithologic variation through the entire unit results from a metamorphic gradient which roughly extends normal to the axial surface of the large fold and into the proximal contact zone with the Goat Ranch intrusion. Based on the mineral assemblages, we can define metamorphic zones with proximity to the Goat Ranch granodiorite. The zones (Fig. 1) consist of (1) distal biotite-andalusite schist, (2) biotite-andalusite co-existing with sillimanite-microcline schist with incipient granitic leucosomes, (3) biotite-sillimanite-microcline schist with local granitic leucosomes, and (4) sillimanite-microcline schist with significant or extensive leucosomes.

High-grade pelites and migmatites

Migmatitic metamorphic zones occur at several localities that are closely related to batholithic contacts within the Kings Sequence pelites of the Lake Isabella region. The migmatite zone shown in Figure 1 is the most extensive of these and can be related to a very well-defined metamorphic gradient through the upper pelite unit (J-pelite). This pelite unit has a relatively uniform and stratigraphically thick protolith sequence, and its transition from its migmatite zone into the xenolithic marginal phase of the Goat Ranch intrusion is well exposed. This area was originally studied by Best and Weiss (1964) who designated the rocks as “hornfelses,” therefore envisioning metamorphism and migmatization as pluton emplacement-related. Except for granoblastic textures in the migmatite leucosomes, the metamorphic textures are penetratively schistose and/or gneissose and reflect a high degree of plastic strain during plutonism and metamorphism (Saleeby and Busby, 1993). Swarms of felsic dikes that are distinct from the migmatitic leucosomes cut each stratigraphic unit of the pendant, and exhibit high ductile strain features that are co-axial with the isoclinal folding event, and which developed during their intrusion. These dikes also yield U/Pb zircon ages in the 100±2 Ma range (Saleeby and Zeng, in prep), which along with the meso- and map-scale relations between the migmatite and Goat Ranch pluton indicate that migmatization and high magnitude strain resulted from batholith emplacement. The leucosomes that developed during migmatization can be morphologically divided into: (1) concordant (stromatitic) and pervasive network leucosomes (Fig. 2a and b), (2) discordant dikes and pockets of pegmatites and aplites (Fig. 2d), and (3) agmatitic and randomly distributed leucosome patches of various sizes which appear to represent the gathering of quartzo-feldspathic segregations into larger, granitic- or pegmatitic tubes and dikes. There are also very finely laminated migmatites which have stromatitic or pervasive network structures such as shown in Figure 2a. Such finely laminated migmatitic textures and structures pervade much of the matrix of the migmatite complex including the residue-rich domains from which larger-scale leucosomes have segregated. Finely laminated migmatites occur in two field setting: (1) large (10's m^2) domains with no apparent segregation of thickened (≥cm scale) leucosomes; and (2) domains where such thickened leucosomes lie within a host of the finely laminated migmatites. True melanosomes, or pure residue layers, are restricted to sub-millimeter scale lamina of predominately biotite with subordinate sillimanite, felsic minerals, opaque minerals, and rare garnet. The extremely fine scale with typical one to two mineral grain thicknesses prohibits the pure separation and analysis of such melanosomes. We return to this problem below.

Non-migmatitic pelitic metapelite in the Zone 1 (Fig. 1) consists of andalusite biotite, quartz, plagioclase, K-feldspar, muscovite (<5%) and minor sillimanite. The leucosomes associated with the finely laminated migmatite mainly consist of quartz, K-feldspar and plagioclase, and have a granoblastic texture. Generally, quartz, plagioclase and K-feldspar in the leucosomes are substantially coarser than those in the mesosomes or melanosomes. In thin section, some of the leucosomes have trace amounts of apatite located at the boundaries of quartz and plagioclase, which suggests relatively high levels of P_2O_5 in such leucosomes. In contrast, the melanosome mainly consist of biotite (up to 60%) and sillimanite with subordinate quartz, plagioclase and K-feldspar. Garnets co-existing with biotites are rarely found within the migmatite zone. They are found in only two localities that are in proximity to the Goat Ranch pluton throughout the entire study area.

The pressures at which the presently exposed Sierra Nevada batholith was emplaced gradually increase southward from 2 kb at latitude $37^{o}45'$N, to ~9 kb at the extreme southern end of the batholith (Ague and Brimhall, 1987; Pickett and Saleeby, 1993; Ague, 1997). In this studied area, the Goat Ranch pluton was emplaced at a pressure between 3 and 5 kb (Dixon, 1995) and at a temperature of ~700^{o}C (Elan, 1985). The presence of andalusite coexisting with biotite in the upper pelitic unit suggests temperature as low as ~450^{o}C at 1.5 km way from the Goat Ranch intrusion. Elan (1985) has studied the P-T conditions of thermal metamorphism of the Isabella pendant that is in direct contact with the Cyrus Flat pluton in the north shore area of the Isabella pendant ~5 km north of the study area. His results show that the temperature at the contact between the Isabella pendant and Cyrus Flat pluton was about 730^{o}C, declining to ~430-475^{o}C at the margin of the aureole ~2 km from the contact, and the Cyrus Flat pluton was emplaced at a pressure about 3 kb. Because of the structural continuity throughout the entire Isabella pendant, similarity in metamorphic assemblages of the metasedimentary rocks studied by Elan (1985) to those of this study area, and the same age of the Goat Ranch and Cyrus Flat plutons (Saleeby and Zeng, in prep.), the P-T conditions determined by Elan (1985) appear to be applicable to the study area. Thermobarometric studies by Pickett and Saleeby (1993) carried out on a small metasedimentary pendant to the south of the study area have yield peak metamorphic conditions of 10.8 kb and 788 ^{o}C. Because the metasedimentary rocks in the present study were located at a much higher crustal level than those studied by Pickett and Saleeby (1993), thermal conditions resolved by these workers is taken as an upper bound for the Goat Ranch granodiorite and its proximal thermal aureole.

The common occurrence of leucogranite dikes with primary tourmalines and skarn deposits within calcareous units suggests intensive hydrothermal activity during high-grade metamorphism and the formation of the migmatite complex. Such hydrothermal fluids, circulating through the calcareous units, could play an important role in modifying the trace element compositions (i.e., Sr) of the pelites during their high-grade metamorphism and localized partial melting. The implied elevated fluid activity might have lowered the solidus and promoted partial melting of quartz + plagioclase assemblage, while inhibited muscovite dehydration melting (Patiño-Douce and Harris, 1998).

Analytical techniques

We have carried out major, trace element and Sr-Nd isotopic analysis on a suite of leucosomes and their proximal hosts, finely laminated migmatites and metapelites from the Isabella pendant. Migmatites containing thickened leucosomes (≥cm-scale) were selected for separation of leucosomes for major, trace and Sr-Nd isotopic analysis. We refer to such migmatite after extraction of the thickened leucosomes as proximal host for leucosomes. Bulk-rock major and trace element concentrations were obtained by X-ray fluorescence at the Department of Geology, Washington State University. Procedures and reproducibility are reported in Johnson et al. (1999). Bulk-rock major and trace element data are listed in Table 1. We have conducted Sr and Nd bulk-rock isotopic studies to characterize the isotopic compositions and test for homogeneity versus heterogeneity of the metapelites, leucosomes, proximal hosts and finely laminated migmatites. The analytical techniques are described in Pickett and Saleeby (1994) and Ducea and Saleeby (1998a and b). The Nd and Sr measurements were corrected for mass fractionation by normalization to $^{146}Nd/^{142}Nd$ = 0.63615, and $^{86}Sr/^{88}Sr$ = 0.1194. External precisions during this period of measurement for Sr and Nd isotopic compositions are ±0.000016 (n=18), and ± 0.000019 (n=18), respectively. $^{87}Sr/^{86}Sr$ for the NBS987 standard is 0.710252 and $^{143}Nd/^{144}Nd$ for La Jolla Nd standard 0.5118587. The analytical results are given in Table 2. Initial Sr and Nd ratios were corrected back to 100 Ma which is the emplacement age of the Goat Ranch and adjacent plutons, and the timing of peak metamorphism and deformation of the Isabella pendant (Saleeby and Zeng, in prep.). In the following sections, the symbol sizes in all the plots are larger than the analytical errors.

Major and trace element geochemistry

Major and trace element data are listed in Table 1. Metapelites, migmatites (including the proximal host for leucosome and the finely laminated migmatite) and leucosomes can be distinguished in their major element compositions. The metapelites have higher Al_2O_3, TiO_2, FeO and MgO, but lower MnO and CaO contents than those in the migmatites and leucosomes. In general, the leucosomes have higher SiO_2 contents than both the migmatites and metapelites. Selected major element variations for the leucosomes, migmatites and metapelites are illustrated in Figure 3. The metapelites have limited ranges of SiO_2 from 63.01 to 64.95, as compared to relatively greater variations of SiO2 contents in the migmatites. Leucosomes have lower FeO+MgO/Al_2O_3 ratios (<0.2743) than those of both the migmatites and metapelites (>0.2788). As shown in Figure 3, Al_2O_3, TiO_2, MgO and FeO are negatively correlated with SiO_2 in the metapelites, migmatites and leucosomes, which suggests that their major element geochemistry is dominantly controlled by constituent phases involved in the partial melting. Preferentially melting of quartz and plagioclase assemblage out of a pelitic source will lead to elevated SiO_2 but decreased FeO contents in the leucosome (Fig. 3c). Due to limited volume of leucosomes extracted for analyses, the complimentary proximal host samples have similar major element compositions to those of the finely laminated migmatites (Fig. 3a, b and c). Both the proximal hosts and migmatites have lower Al_2O_3 contents than those in the metapelites. This may be due to protolith variations towards psammitic compositions expressed mineralogically by a non-uniform distribution of sillimanites. Based on their K_2O contents (Fig. 3d), the leucosomes can be subdivided into two groups: high-K Group A and low-K Group B. Group A has K_2O contents ranging from 3.68 to 4.59 wt%, while Group B has much lower K_2O content from 0.36 to 0.49 wt%. We have calculated CIPW norm of those leucosomes with major element geochemistry data and plotted them on an Ab-An-Or ternary diagram (Fig. 4). We plotted our data in the 10 kb field, even though the leucosomes represent metapelite-derived melts generated at a pressure of 3-4 kb. This diagram (Fig. 4) also shows the composition data of melts from experimental partial melting of muscovite schist (MS) and muscovite-biotite schist (MBS) under both water-present and water-absent conditions at 10 kb and 6kb, respectively (Patiño-Douce and Harris, 1998). It is interesting to find that Group A leucosomes are of granitic composition and Group B leucosomes of trondhjemitic composition, which suggests that Group B leucosomes may have formed from H_2O-fluxed melting reaction at significant lower temperatures than Group A leucosomes.

Metapelites, leucosomes and migmatites can be distinguished in their trace element compositions as well. The leucosomes have the lowest Ni, Cr, Sc, V, Nb, Zn and La concentrations, as compared to those in both the migmatites and metapelites (Table 1). The metapelites have higher Rb/Sr ratios ranging from 0.62 to 3.01, than those of the leucosomes (<0.50). Ba and Rb concentrations in the leucosomes are positively correlated with their K_2O (wt%) contents (Fig. 5e and 5f). Nb and V concentrations are positively correlated with TiO_2 contents of leucosomes, migmatites and metapelites (Fig. 6). The leucosomes have lower Nb (<13 ppm) and V (<64 ppm) concentrations than those of the migmatites and metapelites which are greater than 15 ppm and 64 ppm, respectively. Trace element data on the leucosomes fall into two groups: Group A leucosomes have higher Rb, Ba and Pb concentrations, and higher Rb/Sr ratios than those of Group B (Fig. 5). In a spider diagram (Fig. 7), all samples show LREE enrichment characteristics. Except for two leucosomes which have positive Eu anomalies, most samples show consistent negative Eu anomalies. We return to the interpretation of these data following the presentation of the radiogenic isotopic data.

Sr and Nd isotopic geochemistry

Radiogenic isotopic data for Sr and Nd are given for metapelites, migmatites and leucosomes in Table 2. Figure 8 shows the isotopic compositions of samples analyzed on an ε_{Nd}(T) versus $^{87}Sr/^{86}Sr$(T) diagram. A value of 100 Ma was assigned for T in order to evaluate the radiogenic isotopic composition at the time of migmatization (Zeng, 2003; Saleeby and Zeng, in prep.) Rb and Sr concentrations in the leucosomes range from 12.3 to 134.6 ppm, and 260.3 to 675.1 ppm, respectively. Metapelites have Rb and Sr concentrations ranging from 88.0 to 175.7 ppm, and 57.2 to 247.2 ppm, respectively. Migmatites (including the proximal hosts for thickened leucosome samples) have Rb and Sr concentrations ranging from 90.8 to 168.2 ppm, and 137.3 to 471.1 ppm, respectively. Some of the proximal host samples have high Sr concentrations of up to 471 ppm. This may be due to concentration of Sr rich minerals (e.g., plagioclase or K-feldspar) in the leucosomes lamina. Compared with the metapelites, the leucosomes have low Rb/Sr ratios. Sm and Nd concentrations in the leucosomes range from 1.6 to 6.3 ppm, and 10.2 to 27.7 ppm, respectively. The metapelites have Sm and Nd concentrations ranging from 4.9 to 9.5 ppm, and 26.5 to 52.3 ppm, respectively. The migmatites have Sm and Nd concentrations ranging from 5.6 to 8.4 ppm, and 21.1 to 47.5 ppm, respectively. Based on their Rb concentrations, Rb/Sr and Sm/Nd ratios, the leucosomes can be subdivided into Group A and Group B as well. Group A has high Rb concentrations (>100 ppm), Rb/Sr (>0.15) and Sm/Nd (>0.20) ratios. In contrast, Group B has low Rb concentrations (<20 ppm), low Rb/Sr (<0.10) and Sm/Nd (<0.20) ratios. Both Group A and Group B leucosomes have Rb/Sr ratios less than 1.0.

The leucosomes have a much wider range of $\varepsilon_{Nd}(T)$ values than the migmatites and metapelites, but they have a similar range of initial $^{87}Sr/^{86}Sr$ ratios. The initial $^{87}Sr/^{86}Sr$ ratios of leucosomes range from 0.7124 to 0.7247, similar to those of the metapelite protoliths (0.7125 to 0.7221). However, the leucosomes have initial ε_{Nd} values ranging from -6.0 to -11.0, as compared to -8.7 to -11.3 for the metapelites, which implies that partial melting was disequilibrium with respect to the Sm-Nd isotope system. As shown in Figure 8, Group A leucosomes have higher initial ε_{Nd} values (>-7.0) and $^{87}Sr/^{86}Sr$ ratios (>0.7145) than those of Group B leucosomes. Because of the number of Sr-Nd radiogenic isotopic analyses for the metapelites (n=6) is greater than that of major and trace element analyses (n=3), the size of Sr-Nd covariation field for the metapelite is larger than that for major and trace element data. This suggests that major and trace element data may not truly represent the range of major and trace element heterogeneities in the upper pelite unit.

In summary, two groups of leucosomes have been identified based on their trace element, Sr-Nd isotopic and major element geochemical characteristics: (1) Group A leucosomes, including samples of L0406, L0407 and L0410, have higher initial ε_{Nd} values (>-7.0) than the migmatites and metapelite protoliths (<-8.5), positive Eu anomalies, high Pb, Ba, Rb, and K_2O contents, high $^{87}Sr/^{86}Sr$ ratios (>0.7145), and are of granitic composition; and in contrast, (2) Group B leucosomes including samples of L0404 and L0405, have similar initial ε_{Nd} values to those of the migmatites and metapelites, negative Eu anomalies, low Pb, Ba, Rb, and K_2O contents, low $^{87}Sr/^{86}Sr$ (<0.7145) ratios and are of trondhjemitic composition. Finally, as shown in Figure 10a, there is a relative enrichment of Sr in the migmatites (Fig. 10a) as compared to the metapelite protolith. This suggests that the pelitic sources were metasomatised by Sr-enriched fluids during migmatization. Such fluids may be derived from fluids circulating through the stratigraphically adjacent marble units, because the marble has relatively high Sr (up to 380 ppm) but extremely low Rb (~1 ppm) concentrations (Table 2). Field relations also support this interpretation in that the marble unit that lies stratigraphically adjacent to the upper pelite is discontinuous and highly lenticular as shown in Figure 1 by apparent happenstance. The marble is very well developed within the proximal migmatite zone, but is quite discontinuous throughout much of the lower grade zones.

Data interpretation and discussion

Before we proceed to data interpretation, we will briefly discuss the possible melting reactions under the attendant P-T conditions during the emplacement of the southern Sierra Nevada Batholith at ~100 Ma. Disequilibrium melting refers to any melting process in which the liquid phase is not in chemical equilibrium with its residual prior to melt extraction. In disequilibrium melting, the concentration of a given element in the melt depends on its concentration in the minerals of the initial solid and on the mineral proportions which dissolve into the melt (Allegre and Minster, 1978). Non-modal melting is a melting process where the proportions of reactant phases in the source are different from their proportions entering the melt

1. Common melting reactions and their characteristics

Aluminous schists and gneisses are generally considered to be likely sources for peraluminous granitic melts (Wyllie, 1979; Vielzeuf and Holloway, 1988; Le Breton and Thompson, 1988; Rushmer, 1991; Vielzeuf and Montel, 1994; Patiño-Douce and Beard, 1995 & 1996; Thompson, 1996; Patiño-Douce and Harris, 1998; Knesel and Davidson, 2002; Whittington and Treloar, 2002). For pelitic and quartzo-feldspathic rocks, the melting reactions that produce granitic melts are listed as following (Fig. 9):

1. Water-saturated melting reaction

   $Qtz + Ab + Or + H_2O \rightarrow Melt$

2. Water-saturated melting reaction

   $Qtz + Kfs + Als + H_2O \rightarrow Melt$

3. H_2O-fluxed melting of muscovite

   $Mus + Pl + Qtz + H_2O \rightarrow Melt$

4. Fluid-absent muscovite dehydration melting

   $Mus + Pl + Qtz \rightarrow Als + Kfs + Melt \pm Bt$

5. Fluid-absent biotite dehydration melting after exhaustion of muscovite

   $Bt + Pl + Als + Qtz \rightarrow Grt + Kfs + melt$

where Qtz, Ab, Or, Kfs, Als, Pl, Mus, Bt, and Grt are quartz, albite, orthoclase, K-feldspar, aluminosilicate, plagioclase, muscovite, biotite and garnet, respectively. The mineral abbreviations are after Kretz (1983). For these melting reactions, muscovite dehydration melting reactions occur at much lower temperatures (<750^{o}C) as contrasted with ~825 to 900 ^{o}C for biotite dehydration melting, and results in a lower degree of partial melting due to the water contents of the melt being buffered by the muscovite dehydration melting (Le Breton and Thompson, 1988). Under the same P-T conditions and for the same protolith, influx of water has interesting effects on melting behavior. In partial melting without free water, water is liberated by incongruent breakdown of hydrous minerals such as muscovite and biotite. Such a melting reaction is referred to as dehydration partial melting. Water-saturated and water-fluxed partial melting reactions are melting processes with excess water. Water and fluid are used interchangeably in the following discussions. Increasing water activity depresses the plagioclase + quartz solidus more strongly than it depresses the stability of micas which limits or excludes the participation of muscovite in both water-saturated and water-fluxed melting reactions. However, the onset of fluid-present melting will result in a reduced water activity in the protolith, and thus drive the melting toward reactions with increasing proportions of hydrous minerals as in reaction 3, 4, and 5, except in geologically improbable case of a huge water reservoir accessible continuously to the protolith during melting. These interesting but complex features of crustal anatexis lead to the complicated melt products and geochemistry commonly observed in migmatite zones. Modeling of complex melting reactions in pelitic protoliths, and the geochemical consequences of incongruent dehydration melting of muscovite and biotite in metapelites has been explored by Harris and Inger (1992), Inger and Harris (1993) and Harris et al. (1995). They showed that three melting reactions (reaction 3, 4 and 5) that involve different degrees of hydrous minerals have a distinctive restite mineralogy that controls the trace-element distribution between the sources and melts. Depending on the P-T conditions, water activity (α_{H2O}) and protolith mineral assemblages, these reactions would control both the volume of melt produced and the mineralogy of the restites. These reactions in turn control the trace-element and radiogenic isotopic compositions of the resultant melt. The variations in radiogenic isotopic compositions of the melts result from different isotopic compositions in the various phases that undergo non-modal partial melting. In terms of the mass proportions of muscovite relative to plagioclase entering the melts, reaction 3 has a muscovite/plagioclase ratio of 0.6, which is significantly less than the value of 3.1

for reaction 4 (Patiño-Douce and Harris, 1998). Taking the Rb-Sr system as an example, because muscovite and biotite are the principal hosts of Rb, and plagioclase and K-feldspar for Sr, the differences in muscovite/plagioclase ratios between reaction 3 and 4 result in distinctive Rb/Sr ratios and Sr isotopic compositions of the melts produced by reaction 3 from those by reaction 4. Note that under water-saturated conditions, partial melting is dominated by melting of quartz + feldspar (reaction 1 and 2) and muscovite or biotite is excluded from such partial melting reactions even though there are abundant micas in a pelitic source. Consequently, both reaction 1 and 2 result in melts having low Rb/Sr and $^{87}Sr/^{86}Sr$ ratios. For the temperature range under consideration, one of the reactions (reaction 1 through 4) predominates in the melt production. Moreover, these partial melting processes not only modify the orthoclase/albite ratio by varying proportions of plagioclase entering the melt and by K-feldspar forming as a residual phase, they also influence the contents of Ba, Na and Pb, as well as the ratios of Rb/Sr, K_2O/Na_2O, and Sm/Nd in the melt by varying proportions of muscovite and biotite with respect to plagioclase and K-feldspar consumed during partial melting (Inger and Harris, 1993; Guillot, 1993). Based on the petrographic and geochemical data, the potential major phases that were involved in the partial melting of the Isabella pendant upper pelite unit are muscovite, biotite, K-feldspar, quartz, plagioclase and aluminosilicate (principally sillimanite). Muscovite, biotite and feldspars are the dominant phases that would regulate the partitioning of Rb, Sr, Ba, Pb and K between the melt and residue. Therefore, these element concentrations of the leucosomes would be good indices for the melting processes during the formation of migmatite in this area.

2. Incongruent melting of muscovite

Below we interpret the trace element and isotopic data for the leucosomes and migmatites in the context of non-modal melting of muscovite. In contrast to Sr, Rb is more compatible with biotite than muscovite and feldspar (Peucat, 1986; Henderson, 1982; Nash and Crecraft, 1985) such that (1) biotite is characterized by the highest Rb/Sr ratio and relatively high time integrated $^{87}Sr/^{86}Sr$ ratio due to radioactive decay of ^{87}Rb; (2) muscovite has the intermediate Rb/Sr and $^{87}Sr/^{86}Sr$ ratios; and (3) feldspar (plagioclase and K-feldspar) has the lowest Rb/Sr and $^{87}Sr/^{86}Sr$ ratios, as compared to the bulk-rock values. The P-T conditions of migmatization that were outlined above indicate temperatures below that of biotite dehydration partial melting which occurs generally in the range of 825 to 900°C under fluid-absent conditions (Clemens and Vielzeuf, 1987; Patiño-Douce and Johnston, 1991). High modal content of biotite which is typically in excess of 60% in the melanosomes of the migmatites also suggests that biotite was not involved significantly in partial melt production, or it occurred as a product of the fluid-absent muscovite dehydration melting (reaction 4). However, this would give rise to very low Rb concentrations and unradiogenic Sr isotopic compositions in the leucosomes as compared to their sources, which is not evident in the data. The rarity of garnet coexisting with biotite and K-feldspar, even at localities of highest temperatures in the proximity of the Goat Ranch pluton, also suggests that fluid-absent biotite dehydration melting did not play a significant role in generating the migmatite zone. Based on the trace element and Rb-Sr isotopic data of the leucosomes, we suggest that most of the leucosomes were derived from partial melting of quartz + plagioclase assemblages and/or muscovite dehydration melting under either fluid-present or fluid-absent conditions. An important feature shown in the Rb-Sr isotopic systematics (Fig. 10b) of the leucosomes is that their initial $^{87}Sr/^{86}Sr$ ratios are positively correlated to their Rb/Sr ratios. This relation indicates that those leucosomes with relatively elevated Rb/Sr ratios resulted from increasing proportions of muscovite over plagioclase entering the melt. The control of initial $^{87}Sr/^{86}Sr$ of anatectic melts by the relative proportions of muscovite over plagioclase entering the melt has been observed experimentally by Knesel and Davidson (2002). One leucosome sample from the study area (L0410) stands out from the rest by its highest Rb/Sr and initial $^{87}Sr/^{86}Sr$ ratios (Fig. 10b). We suggest that this marks the fluid-absent muscovite dehydration melting in the production of that particular leucosome layer. Group A leucosomes have high Rb concentrations that overlap with those in the metapelites, and higher Rb/Sr ratios than Group B leucosomes, which suggests a greater proportion of muscovite entering the Group A melts. Group B leucosomes have lower Rb concentrations than the metapelites by about an order of magnitude. This is evidence against these leucosomes being generated from either fluid-absent muscovite or biotite dehydration melting, since both melting reactions generally result in melts with Rb/Sr ratios greater than 1.0. Group A leucosomes might be derived either from fluid-absent muscovite dehydration melting with biotite in the restite, or from H_2O-fluxed incongruent melting of muscovite. Group B leucosomes may in contrast be derived from H_2O-fluxed incongruent melting of muscovite or water-saturated melting of quartz and plagioclase assemblage. This interpretation is consistent with the inferences drawn based on the major element compositions of the leucosomes (Fig. 4).

3. K-feldspar signature

The significant role of K-feldspar in the partial melting of metapelites was reported to have given rise to positive Eu anomalies of the respective leucosomes (McDermott, et al., 1996; Harris et al., 1986). Figure 5a shows that positive Eu anomalies of Group A leucosomes are associated with their high K_2O contents. For crustal rocks, K-feldspar is the major phase that hosts Pb. The positive correlation between Pb and K_2O in the Group A leucosomes, migmatites and metapelite protoliths

(Fig. 5c) also suggests that positive Eu anomalies of Group A leucosomes arise from either the melting or entrainment of K-feldspars. Ba is commonly in trace or minor amounts in feldspars. Alkali feldspars commonly have Ba concentrations ranging from 1000 to 10000 ppm, significantly higher than those of plagioclases. Fluid-absent conditions favor residual K-feldspar, but at higher temperatures or increasing water activities, K-feldspar will melt in greater proportions (McDermott, et al., 1996). This is marked by a decrease in the Rb/Sr ratio and increase in Ba content of a melt which also characterizes the trace element geochemistry of the Group A leucosomes (Fig. 5e). The Ba concentrations of Group A leucosomes are higher than those of both migmatites and metapelites by a factor of three (Table 1).

Given the possibility that Sr metasomatism occurred during the partial melting of the metapelite, such metasomatism will lower the Rb/Sr ratios not only in the migmatites but also in the leucosomes to various extents (Fig. 5b). Group A leucosomes may have been derived from muscovite dehydration melting reaction in which K-feldspar was also assimilated into the melt. Such assimilation would produce melts having low Rb/Sr ratios, positive Eu anomalies, and elevated Sr, Ba, Pb and K contents. In contrast, Group B leucosomes might represent the melting products from a K-feldspar-limiting H_2O-fluxed muscovite melting or melting of quartz + plagioclase assemblages which results in melts having low Rb/Sr ratio, negative Eu anomalies, and decreased Pb, Ba and K concentrations (Fig. 5).

4. The role of accessory phases

Previous studies have shown that accessory minerals such as zircon, apatite, ilmenite and monazite play a critical rock in controlling the distribution of trace elements such as Zr, Hf, Sm, Nd, U, Th, Nb and Pb between melt products and residues (Hogan and Sinha, 1991; Rapp and Watson, 1986; Ayers and Harris, 1997, Bea et al., 1994; Zeng et al., 2003). Rutile group minerals (e.g., ilmenite) are the predominant host for Ti as well as a variety of trace elements such as Nb, Ta and V. Therefore, if ilmenite stayed as a residue during partial melting, the resultant leucosomes should have lower concentrations of Ti, Nb, Ta and V than the residue as well as the protolith. Figure 6 shows that: (1) both Nb and V concentrations in the leucosomes, migmatites and metapelites are positively correlated with their TiO_2 (wt%) contents; (2) the leucosomes have lower concentrations of Nb (<13 ppm) and V (< 64 ppm), and TiO_2 contents than those in the metapelites and migmatites. This suggests that ilmenite behaved as a residual phase during partial melting, and is consistent with the relatively high concentration of opaque minerals observed in melanosome lamina.

Geochemical observations and theoretical modeling have shown that dissolution of apatite may play an important role in shaping the Nd isotopic systematics of anatectic melts (Ayers and Harris, 1997; Zeng et al., 2003). The observation that elevated $\varepsilon_{Nd}(T)$ values of the leucosomes correspond to elevated P_2O_5 contents suggests that the Nd isotopic compositions of the leucosomes are strongly affected by the dissolution of apatite (Fig. 11). Group A leucosomes have substantially higher $\varepsilon_{Nd}(T)$ values and P_2O_5 contents than those of Group B, reflecting a greater apatite component and possibly higher temperature of melting. Increased dissolution of apatite into melt phases requires higher temperature conditions because water has little effect in the dissolution of apatite (Harrison and Watson, 1984). The inference of higher temperature conditions for the formation of Group A leucosomes is in accordance with the conclusion drawn based on the correlations among K_2O, Pb and Ba contents, and positive Eu anomalies as discussed in the previous section. The dissolution behavior of apatite may also strongly influence the Nd isotopic systematics of melt products (Zeng et al., 2003). For example, contrasted to monazite, apatite usually has higher Sm/Nd ratio and thus high time-integrated ε_{Nd} values relative to those of the bulk-rock (Ayers and Harris, 1997). Dissolution or entrainment of apatite into the melt will elevate both the Sm/Nd ratio and ε_{Nd} value of the melt. The large variations in Sm/Nd ratios of the leucosomes from 0.11 to 0.33, and elevated $\varepsilon_{Nd}(T)$ values as compared to their sources suggest the important role of accessory minerals playing in fractionation Sm from Nd and developing Nd isotopic disequilibrium during crustal anatexis.

Conclusions

We have performed major and trace element, and radiogenic isotopic studies on a suite of leucosomes, their complementary proximal hosts, migmatites, and metapelites. We found that the leucosomes fall into two groups: (1) Group A leucosomes have higher initial ε_{Nd} values (>-7.0) than the migmatites and metapelites (<-8.5), positive Eu anomalies, high Pb, Ba, Rb, and K_2O contents, high $^{87}Sr/^{86}Sr$ ratios (>0.7145), and are of granitic composition; and in contrast, (2) Group B leucosomes have similar initial ε_{Nd} values to those of the migmatites and metapelites, negative Eu anomalies, low Pb, Ba, Rb, and K_2O contents, low $^{87}Sr/^{86}Sr$ ratios (<0.7145) and are of trondhjemitic composition. These data can be modeled as a result of non-modal partial melting of the pelite protolith. Given the relatively low temperatures of the metamorphic reactions at the level of exposure and observation, and low contents of muscovite and plagioclase, and high contents of K-feldspar in the pelitic protolith, Group B leucosomes may represent melts from fluid-present partial melting reactions of quartz + feldspar assemblages (reaction 1 and 2) or H_2O-fluxed melting of muscovite (reaction 3). Intensive concurrent hydrothermal activity as evidenced by skarn deposits in the stratigraphically adjacent marble unit as well as pegmatitic dikes may have limited the role of fluid-absent muscovite dehydration melting in the production of leucosomes, even though the major and trace element, and radiogenic isotopic data suggest that some of Group A leucosomes may have formed from such a reaction.

In summary, we demonstrate that during the formation of the migmatite zone in the Isabella pendant (1) the leucosomes were partial melting products from pelitic sources which had been metasomatised by Sr-enriched fluids as suggested by the high Sr concentrations of migmatites relative to those of the metapelites; (2) trace element and radiogenic isotope geochemistry data suggest that crustal anatexis could generate a spectrum of leucogranitic melts with various major, trace element and radiogenic isotopic compositions; (3) Sm and Nd isotopic compositions of the leucosomes suggest the disequilibrium nature of non-modal crustal anatexis and small degrees of parent/daughter fractionation by accessory phases during partial melting; (4) both leucosomes and metapelites have a high degree of isotopic heterogeneity; and (5) trace minerals such as ilmenite play a dominant role in controlling the redistribution of key trace elements such as Nb, V, and Ta between the melt products and solid residue.

Field, geochemical and isotopic data from this study suggest that formation of a migmatite zone within the pre-existing metaclastic country rocks in response to thermal perturbations induced by the impingement of hot silicic magma is a potentially important mechanism to help differentiate the continental crustal into more silicic upper crust and corresponding mafic parts. If melts generated by non-modal crustal anatexis could segregate and migrate to shallower levels of the crust, it will efficiently redistribute heat-generating (U, Th, and K), LILE and LREE elements into the shallow crust. The various degrees of parent/daughter fractionation of both the Rb-Sr and Sm-Nd systems as a consequence of non-modal crustal anatexis would render distinct isotopic reservoirs that could profoundly influence the products of subsequent mixing events. This is not only critical for intracrustal differentiation, but also potentially an important process in generating crustal isotopic heterogeneities. Because some of granitic batholiths acquire their crustal signatures by wallrock-derived melt contamination, complicated Sr and Nd isotopic compositions of crustally derived melts requires extreme care in interpreting batholithic Sr and Nd systematics.

Figure 1 Geologic map of the Isabella pendant at the south Lake Isabella area and adjacent Goat Ranch granodiorite intrusion showing the distribution of migmatitic zone and tentative metamorphic zonation within the upper pelite unit.

Figure 1

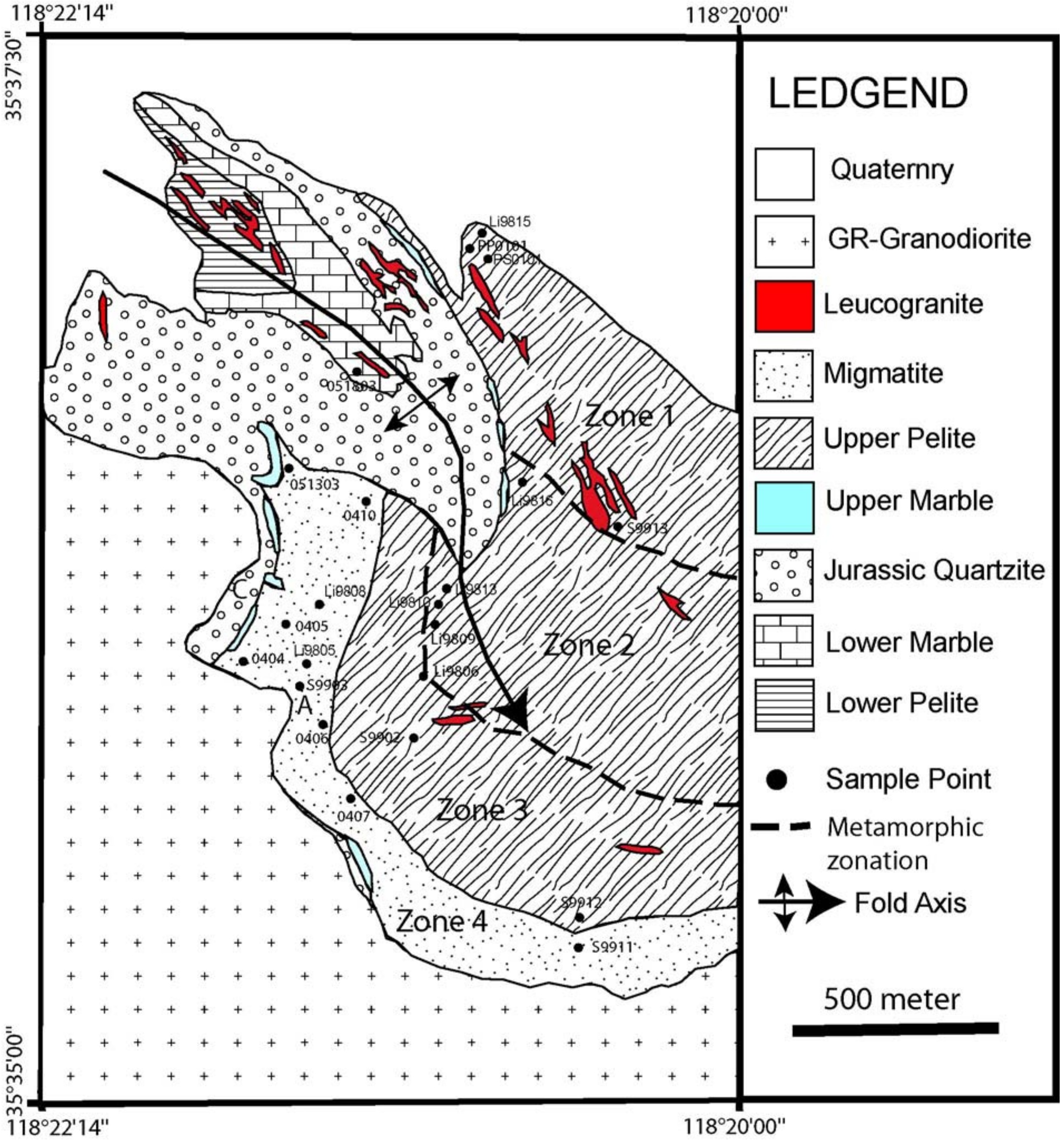
118°22'14"
118°20'00"
35°37'30"
35°35'00"
118°22'14"
118°20'00"
LEDGEND
Quaternry
GR-Granodiorite
Leucogranite
Migmatite
Upper Pelite
Upper Marble
Jurassic Quartzite
Lower Marble
Lower Pelite
Sample Point
Metamorphic zonation
Fold Axis
500 meter
Li9815
PP0101
PS0101
051803
Zone 1
Li9816
S9913
051303
0410
C
Li9808
Li9810
Li9813
0405
Li9809
Zone 2
0404
Li9805
S9903
Li9806
A
0406
S9902
Zone 3
0407
S9912
Zone 4
S9911

Figure 2 Photos showing the structures of the migmatites showing (1) photomicrograph of stromatitic structure, (2) field photography of anastomose structure, (3) field photograph of chaotic structure, and (4) field photograph of melt pockets along the fracture zone.

Figure 2(a)

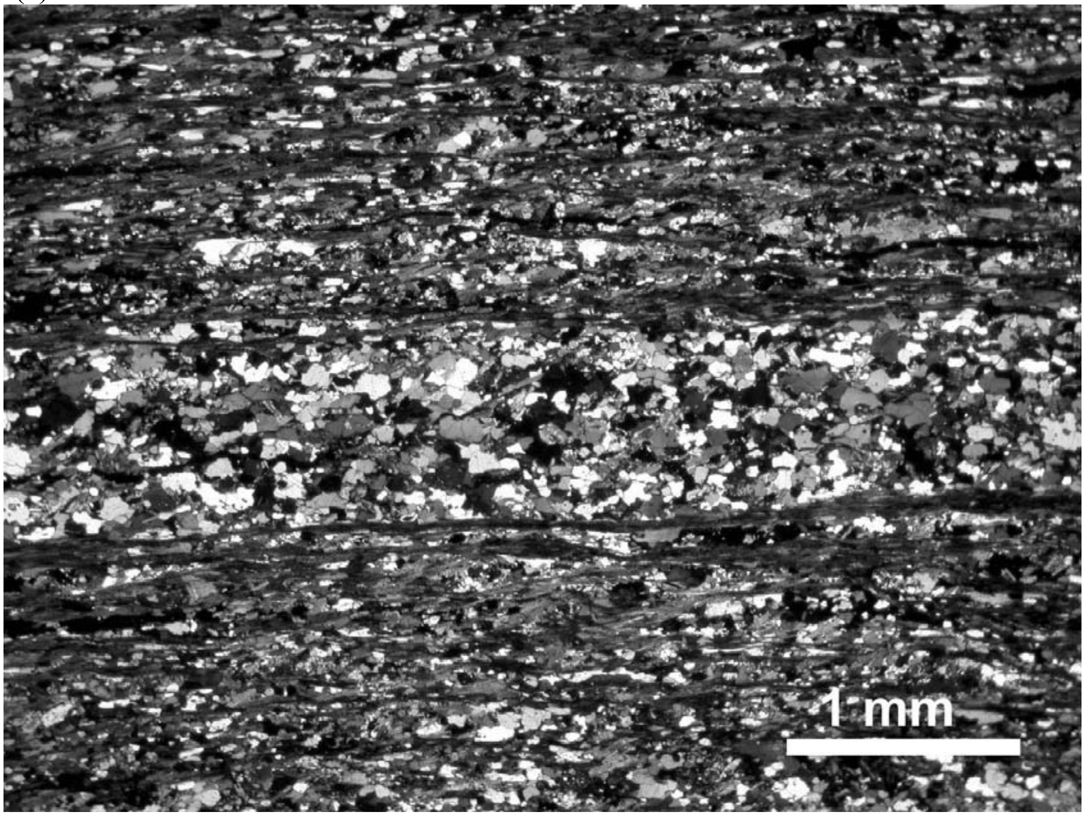

(b)

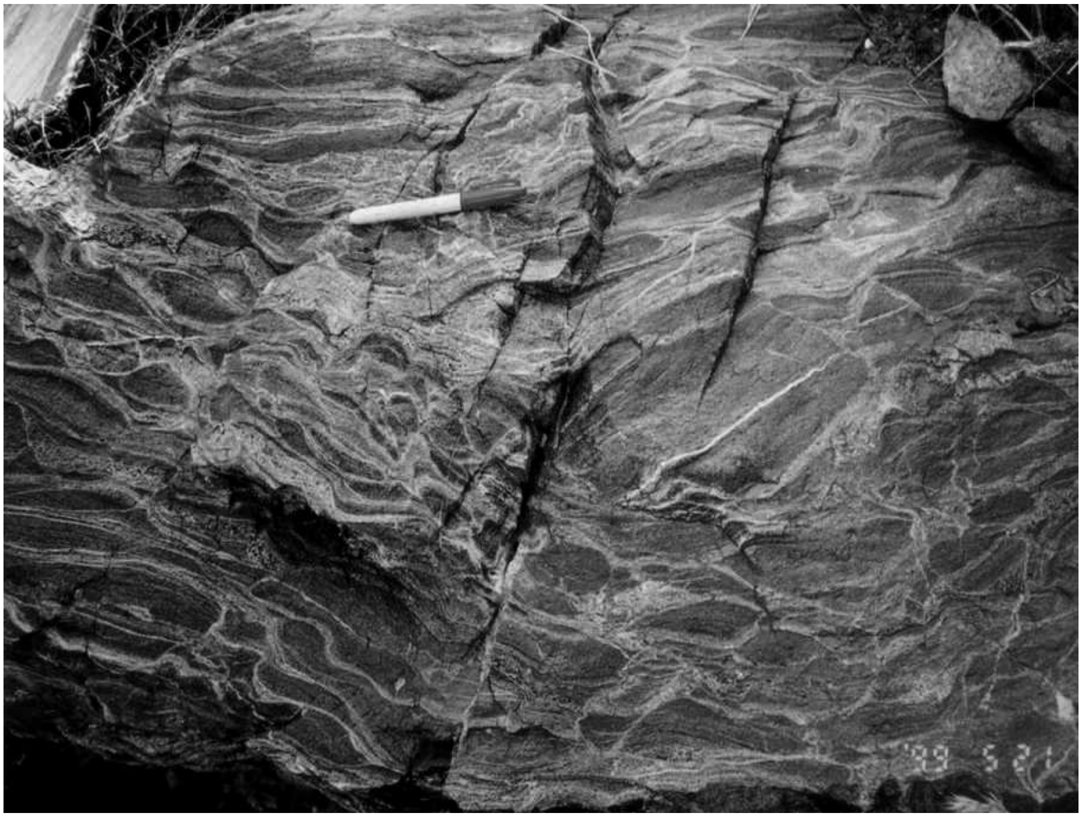

(c)

(d)

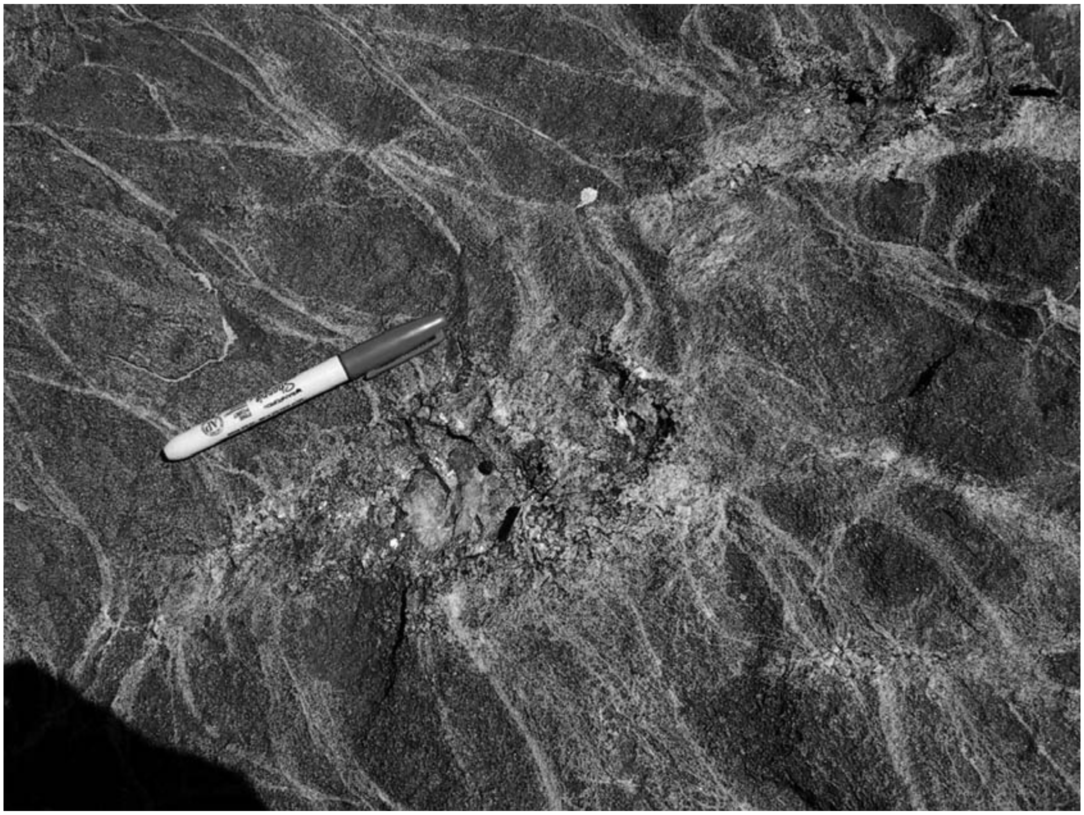

Figure 3 Selected major element oxides versus SiO_2 diagram for selected leucosomes, migmatites (including proximal host for leucosome and migmatite) and metapelites. Diagrams showing the relationships between (a) Al_2O_3, (b) TiO_2, (c) FeO and (d) K_2O with SiO_2 (wt %). The term "proximal host for leucosome" is referred to the material after the separation of relatively large size of leucosomes from a finely laminated migmatite. The leucosomes separated for Sr and Nd isotopic analysis are 0.5 cm to 1 cm thick. The term "migmatite" is applied to finely laminated migmatites without removal of any leucosomes.

Figure 3 (a)

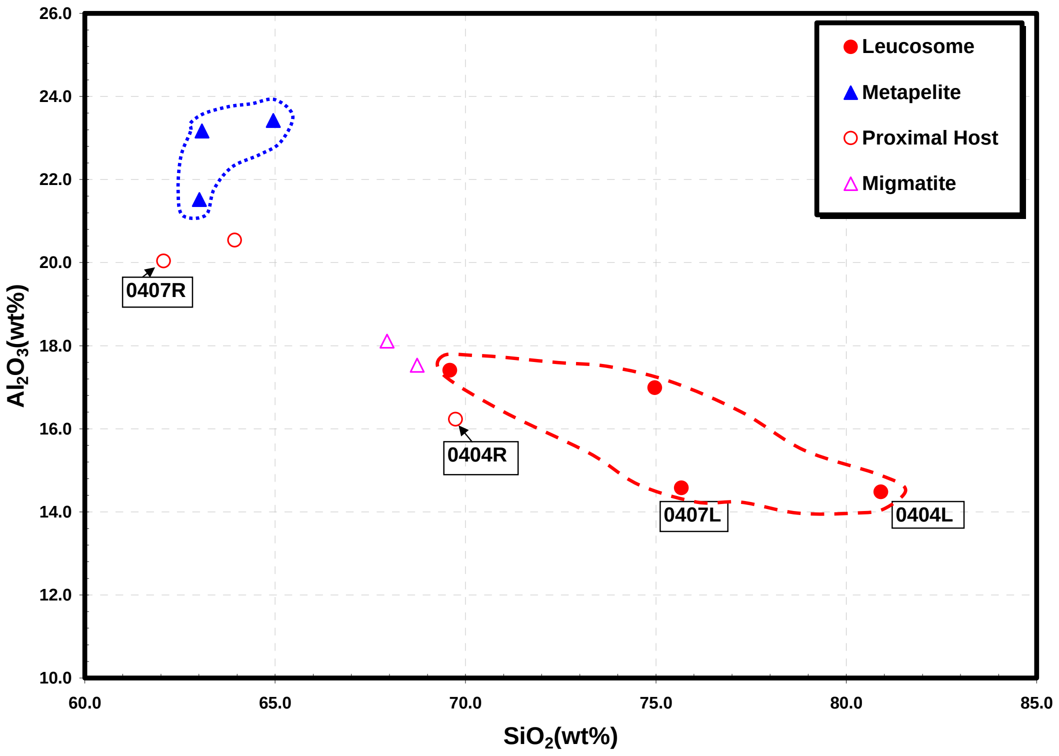

26.0
24.0
22.0
20.0
18.0
16.0
14.0
12.0
10.0
Al_2O_3(wt%)
60.0
65.0
70.0
75.0
80.0
85.0
SiO_2(wt%)
● Leucosome
▲ Metapelite
○ Proximal Host
△ Migmatite
0407R
0404R
0407L
0404L

(b)

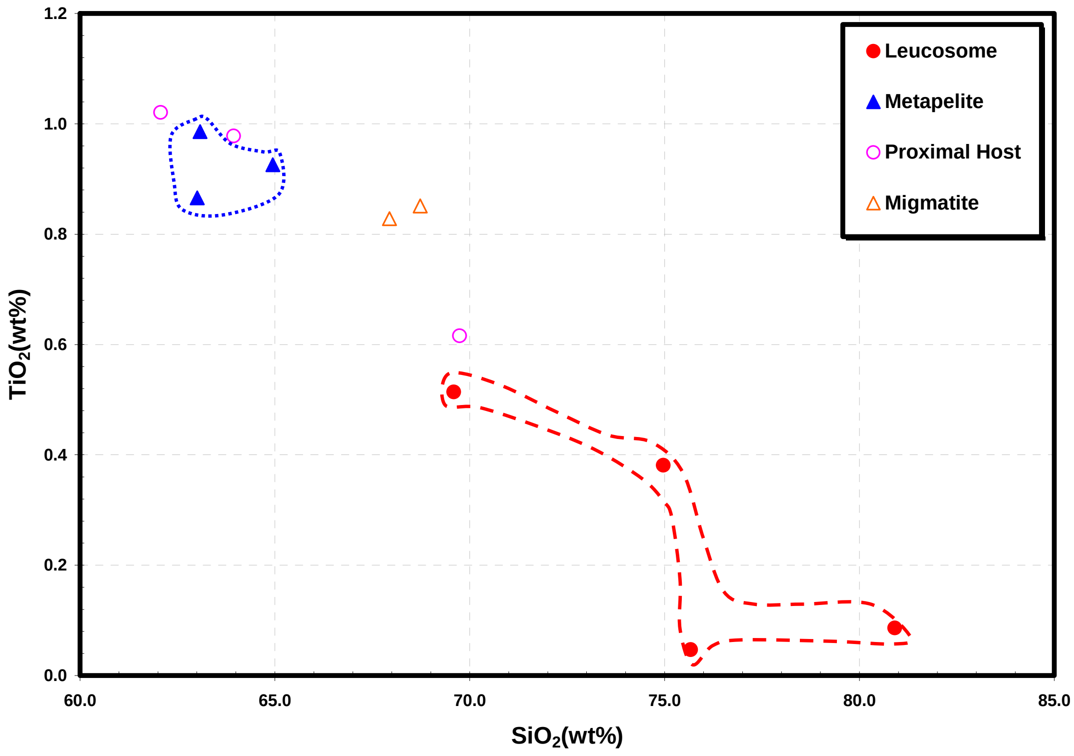

1.2
1.0
0.8
0.6
0.4
0.2
0.0
TiO_2(wt%)
60.0
65.0
70.0
75.0
80.0
85.0
SiO_2(wt%)
● Leucosome
▲ Metapelite
○ Proximal Host
△ Migmatite

(c)

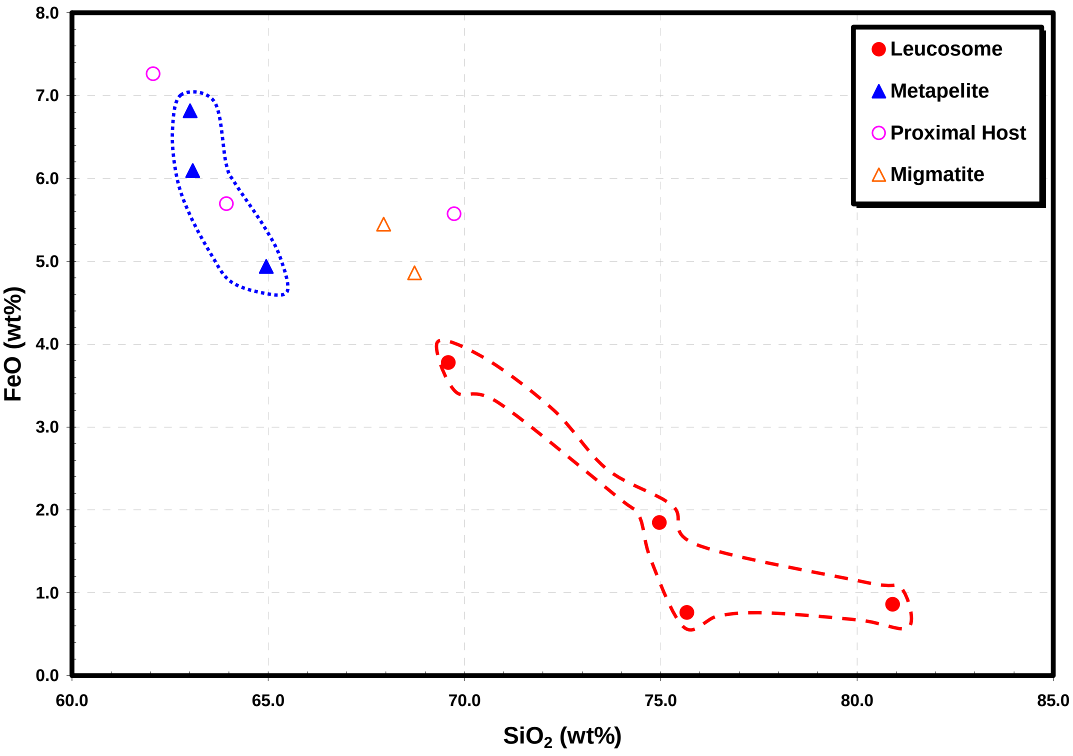

8.0
7.0
6.0
5.0
4.0
3.0
2.0
1.0
0.0
FeO (wt%)
60.0
65.0
70.0
75.0
80.0
85.0
SiO_2 (wt%)
● Leucosome
▲ Metapelite
○ Proximal Host
△ Migmatite

(d)

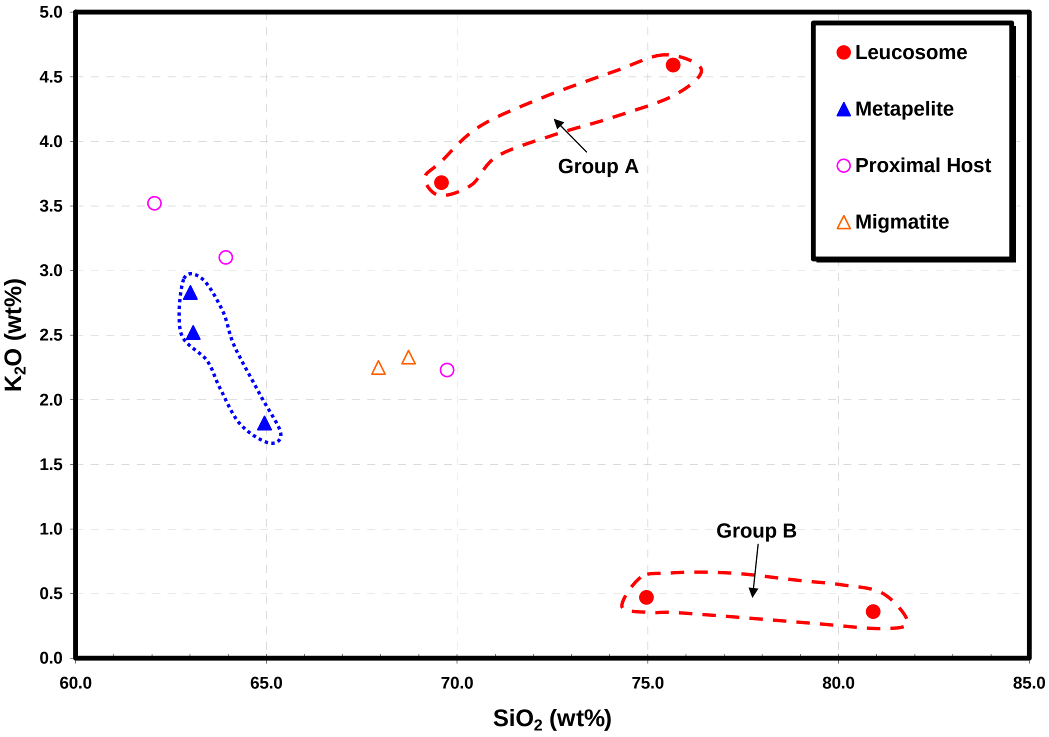

5.0
4.5
4.0
3.5
3.0
2.5
2.0
1.5
1.0
0.5
0.0
K_2O (wt%)
60.0
65.0
70.0
75.0
80.0
85.0
SiO_2 (wt%)
Group A
Group B
● Leucosome
▲ Metapelite
○ Proximal Host
△ Migmatite

Figure 4 Normative albite (Ab)-anorthite (An)-orthoclase (Or) contents of the leucosomes compared with experimentally generated melt compositions (after Patino Douce and Harris, 1998). Two leucosomes are plotted within the trondhjemite field, and the others in the granite field. The Ab-An-Or classification for silicic rocks is after Barker (1979).

Figure 4

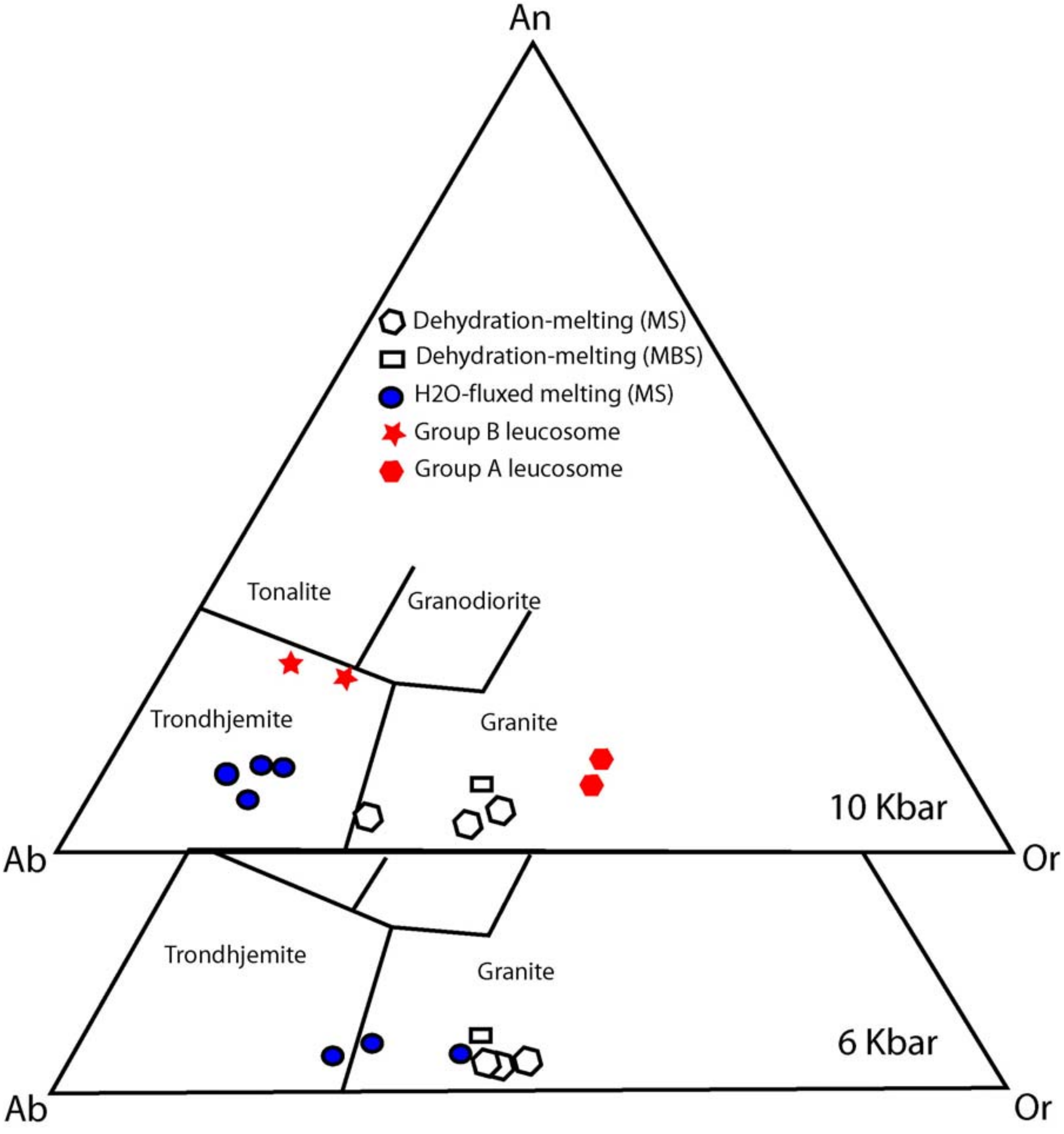
An
Dehydration-melting (MS)
Dehydration-melting (MBS)
H2O-fluxed melting (MS)
Group B leucosome
Group A leucosome
Tonalite
Granodiorite
Trondhjemite
Granite
10 Kbar
Ab
Or
Trondhjemite
Granite
6 Kbar
Ab
Or

Figure 5 Covariation diagrams showing the relationships between (a) Eu anomaly and K_2O (wt %), (b) Eu anomaly and Rb/Sr ratio, (c) Pb and K_2O (wt %), (d) Pb and Ba, (e) Ba and K_2O (wt %), and (f) Ba and Rb for the leucosomes, migmatites and metapelites. These diagrams show that positive Eu anomalies of leucosomes were arisen from the increasing contribution of K-feldspar to the melt.

Figure 5 (a)

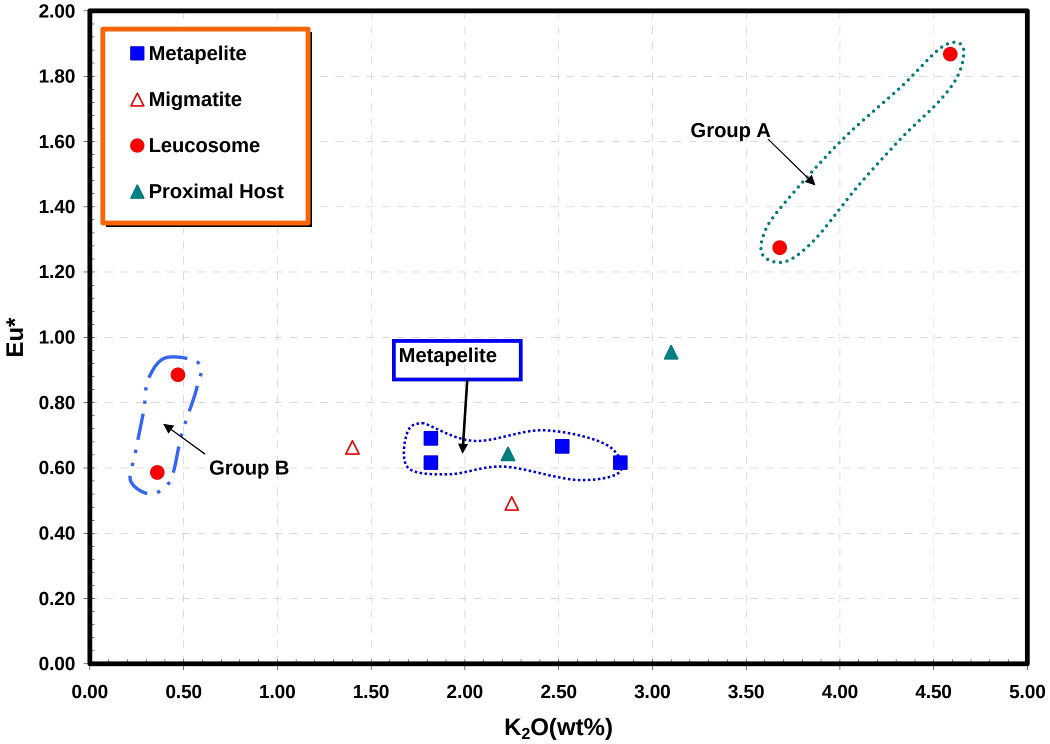

■ Metapelite
△ Migmatite
● Leucosome
▲ Proximal Host
Group A
Group B
Metapelite
Eu*
K$_2$O(wt%)
2.00
1.80
1.60
1.40
1.20
1.00
0.80
0.60
0.40
0.20
0.00
0.00
0.50
1.00
1.50
2.00
2.50
3.00
3.50
4.00
4.50
5.00

(b)

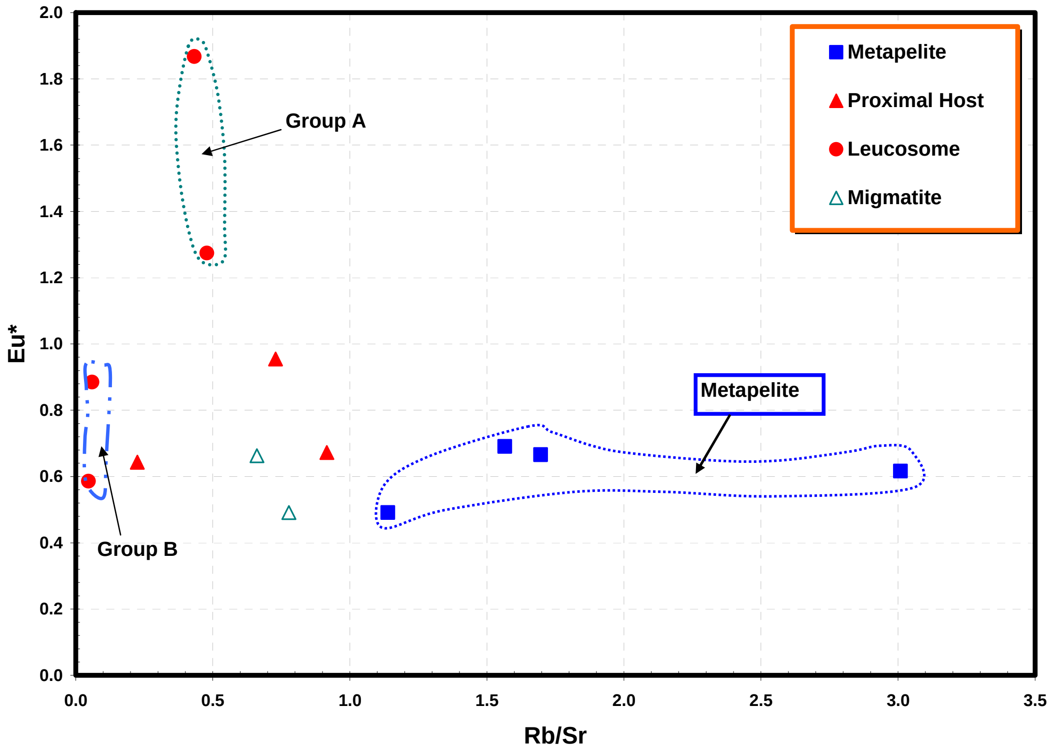

■ Metapelite
▲ Proximal Host
● Leucosome
△ Migmatite
Group A
Group B
Metapelite
Eu*
Rb/Sr
2.0
1.8
1.6
1.4
1.2
1.0
0.8
0.6
0.4
0.2
0.0
0.0
0.5
1.0
1.5
2.0
2.5
3.0
3.5

(c)

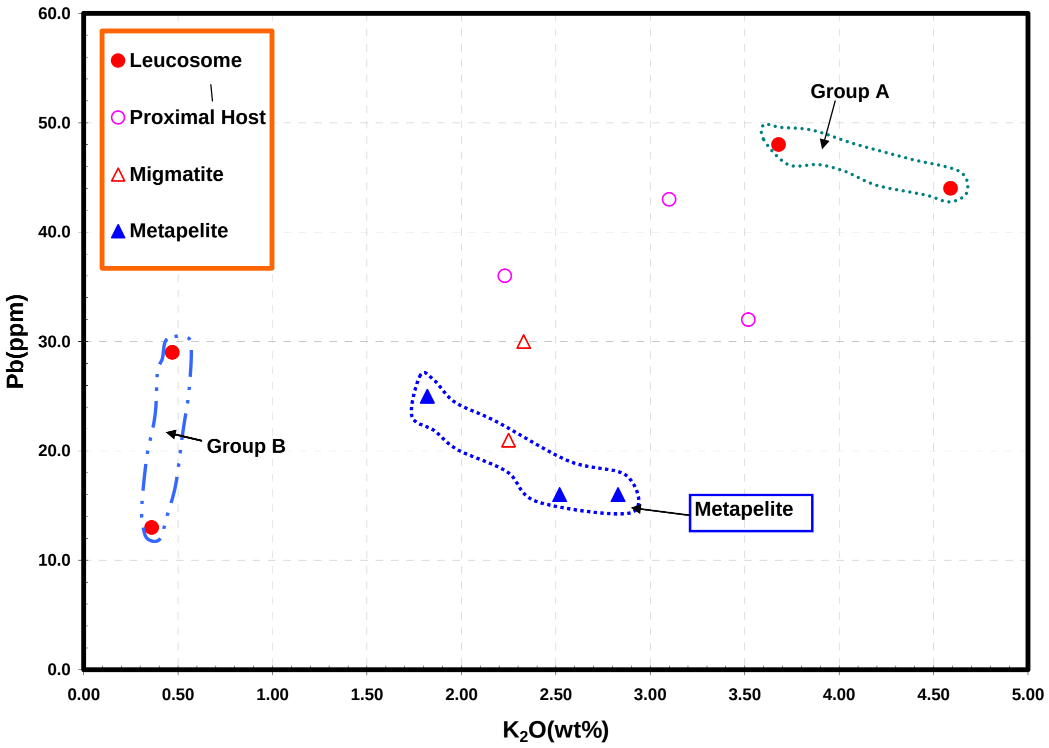

60.0
50.0
40.0
30.0
20.0
10.0
0.0
Pb(ppm)
0.00
0.50
1.00
1.50
2.00
2.50
3.00
3.50
4.00
4.50
5.00
K$_2$O(wt%)
● Leucosome
○ Proximal Host
△ Migmatite
▲ Metapelite
Group A
Group B
Metapelite

(d)

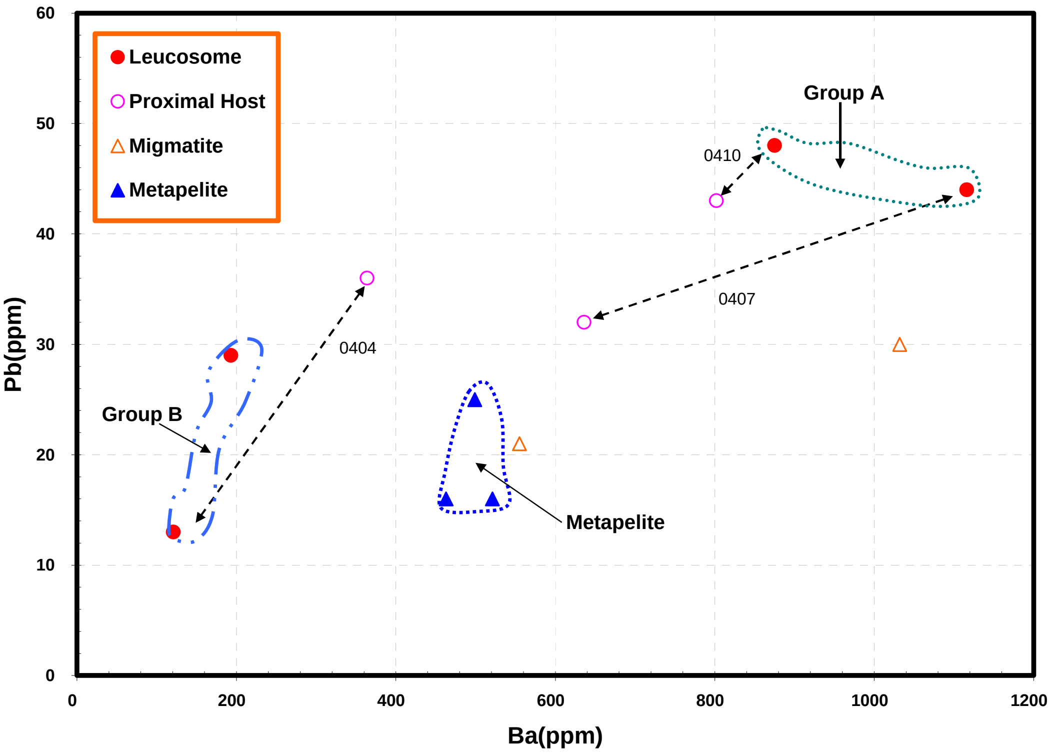

60
50
40
30
20
10
0
Pb(ppm)
0
200
400
600
800
1000
1200
Ba(ppm)
● Leucosome
○ Proximal Host
△ Migmatite
▲ Metapelite
Group A
0410
0407
0404
Group B
Metapelite

(e)

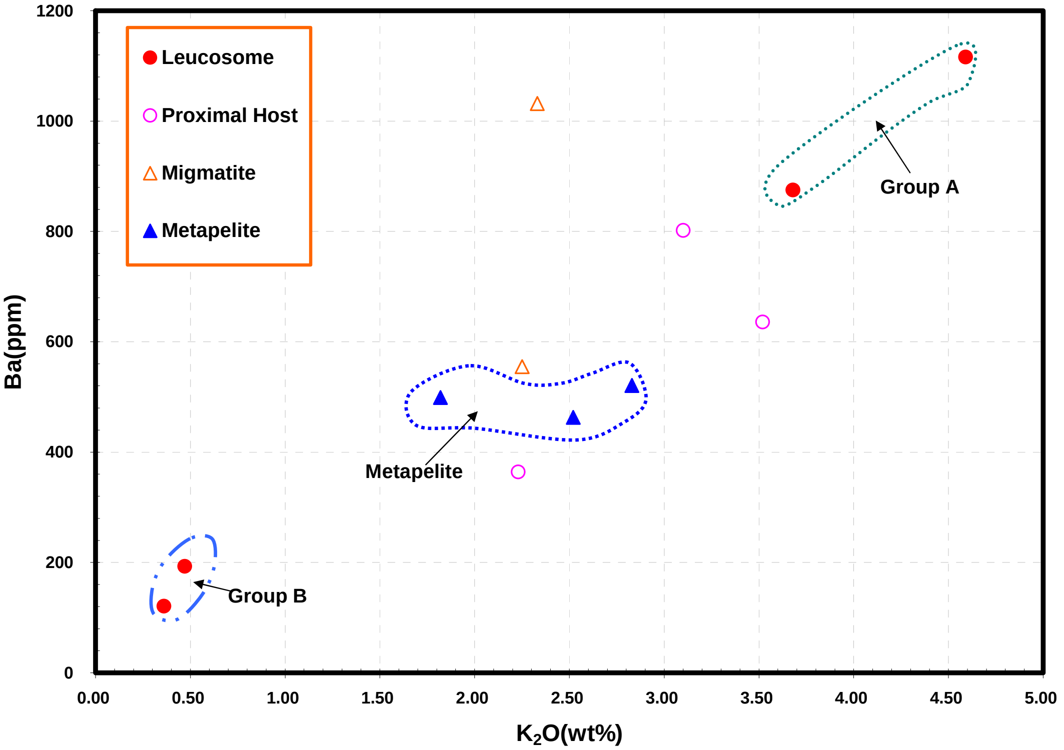
● Leucosome
○ Proximal Host
△ Migmatite
▲ Metapelite
Group A
Metapelite
Group B
Ba(ppm)
K$_2$O(wt%)
0
200
400
600
800
1000
1200
0.00
0.50
1.00
1.50
2.00
2.50
3.00
3.50
4.00
4.50
5.00

(f)

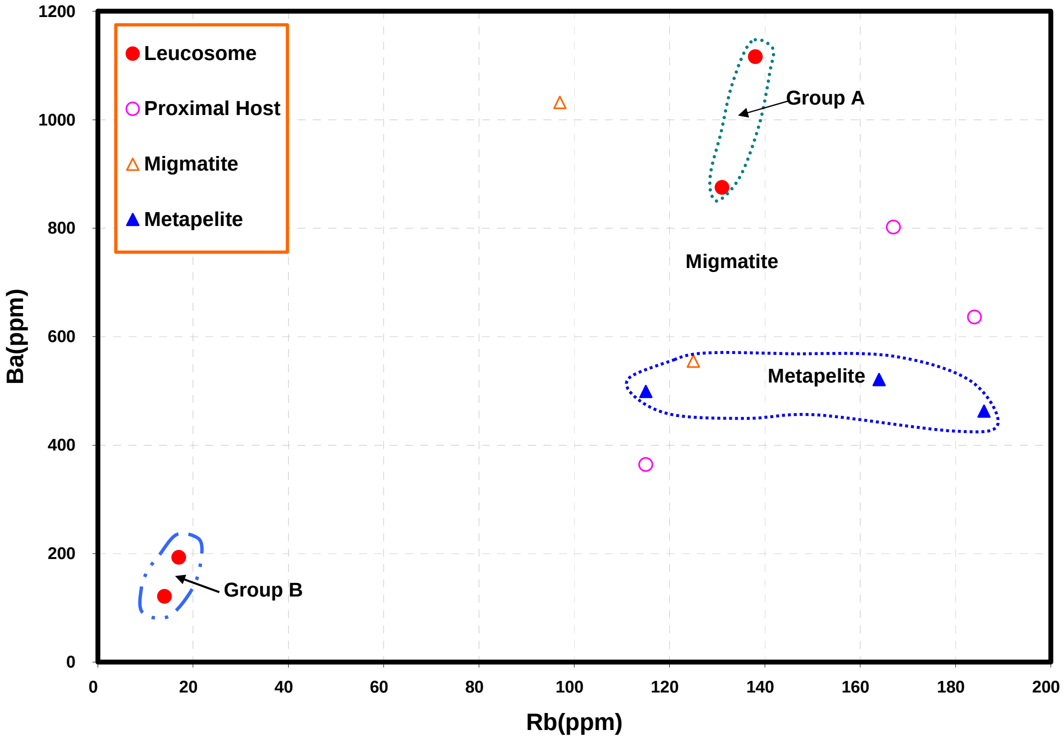
● Leucosome
○ Proximal Host
△ Migmatite
▲ Metapelite
Group A
Migmatite
Metapelite
Group B
Ba(ppm)
Rb(ppm)
0
200
400
600
800
1000
1200
0
20
40
60
80
100
120
140
160
180
200

Figure 6 Plots of (a) Nb versus TiO_2 (wt %). (b) Nb over V. These plots show that both Nb and V in the leucosomes, migmatites and metapelites are negatively correlated with the contents of Ti, suggesting that illmenite stayed as a residue phase during the partial melting of the upper pelite protolith.

Figure 6(a)

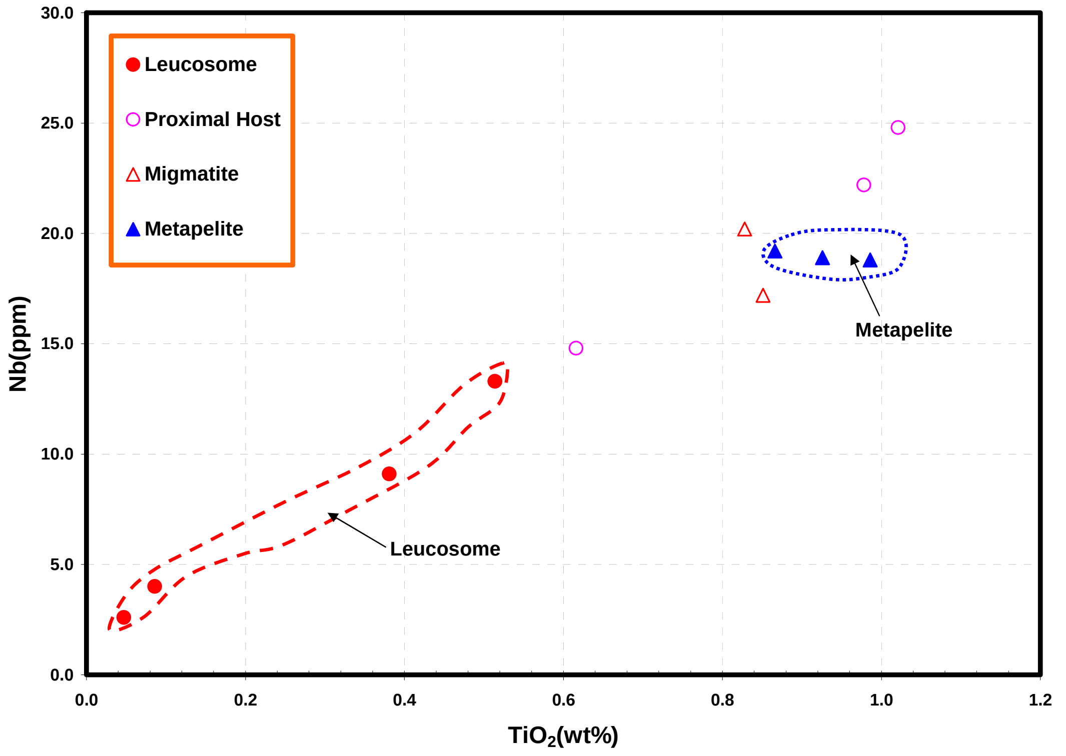
30.0
25.0
20.0
15.0
10.0
5.0
0.0
Nb(ppm)
0.0
0.2
0.4
0.6
0.8
1.0
1.2
TiO_2(wt%)
● Leucosome
○ Proximal Host
△ Migmatite
▲ Metapelite
Metapelite
Leucosome

(b)

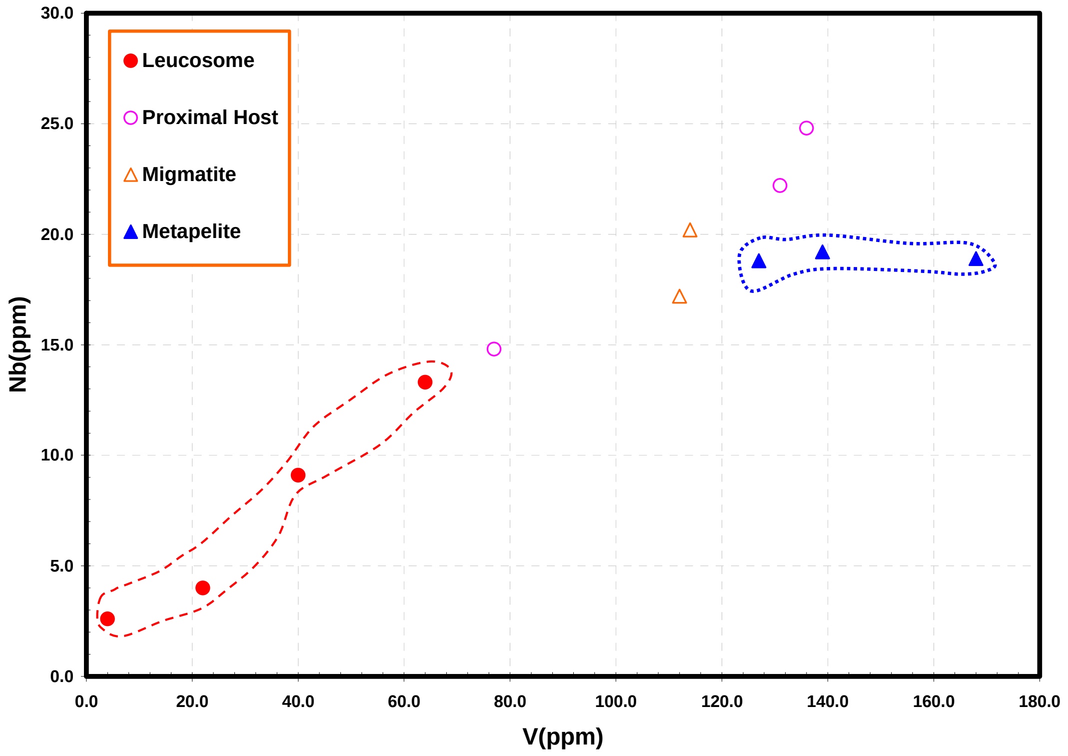
30.0
25.0
20.0
15.0
10.0
5.0
0.0
Nb(ppm)
0.0
20.0
40.0
60.0
80.0
100.0
120.0
140.0
160.0
180.0
V(ppm)
● Leucosome
○ Proximal Host
△ Migmatite
▲ Metapelite

Figure 7 REE spider diagram showing the REE characteristics of the leucosomes, migmatites and metapelites. REE are normalized to the primitive mantle (PM) (Sun and McDonough, 1989). Except for two leucosomes which have distinct positive Eu anomalies, all the rest samples have consistently negative Eu anomalies. Rare element data are from Zeng and Saleeby (In preparation)

Figure 7

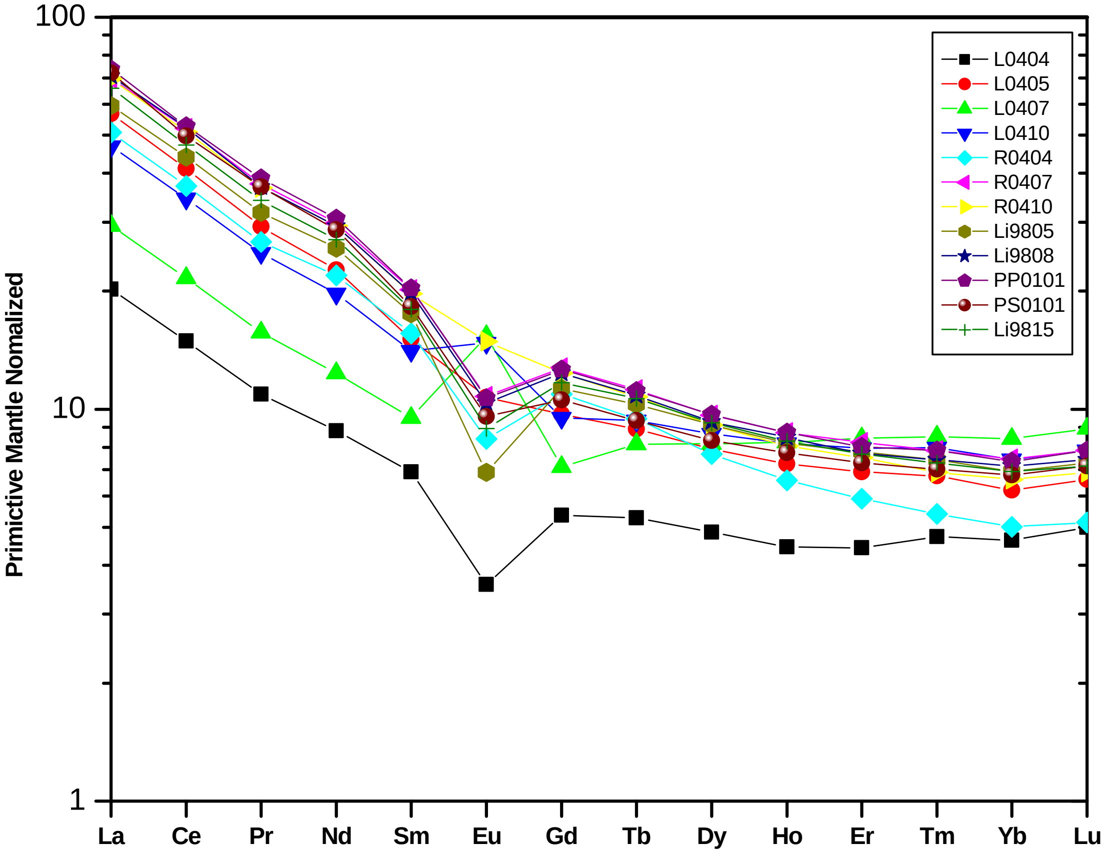
100
10
1
Primictive Mantle Nomalized
La
Ce
Pr
Nd
Sm
Eu
Gd
Tb
Dy
Ho
Er
Tm
Yb
Lu
L0404
L0405
L0407
L0410
R0404
R0407
R0410
Li9805
Li9808
PP0101
PS0101
Li9815

Figure 8 Nd-Sr radiogenic isotopic systematics of the metapelite protoliths, migmatites and leucosomes. The diagram shows that the leucosomes have a much wider range of initial ε_{Nd} values than the metapelite protoliths, but they have similar ranges of initial Sr isotopic ratios, suggesting that melts that formed the Group A leucosomes are in Nd isotopic disequilibrium with respect to their protoliths.

Figure 8

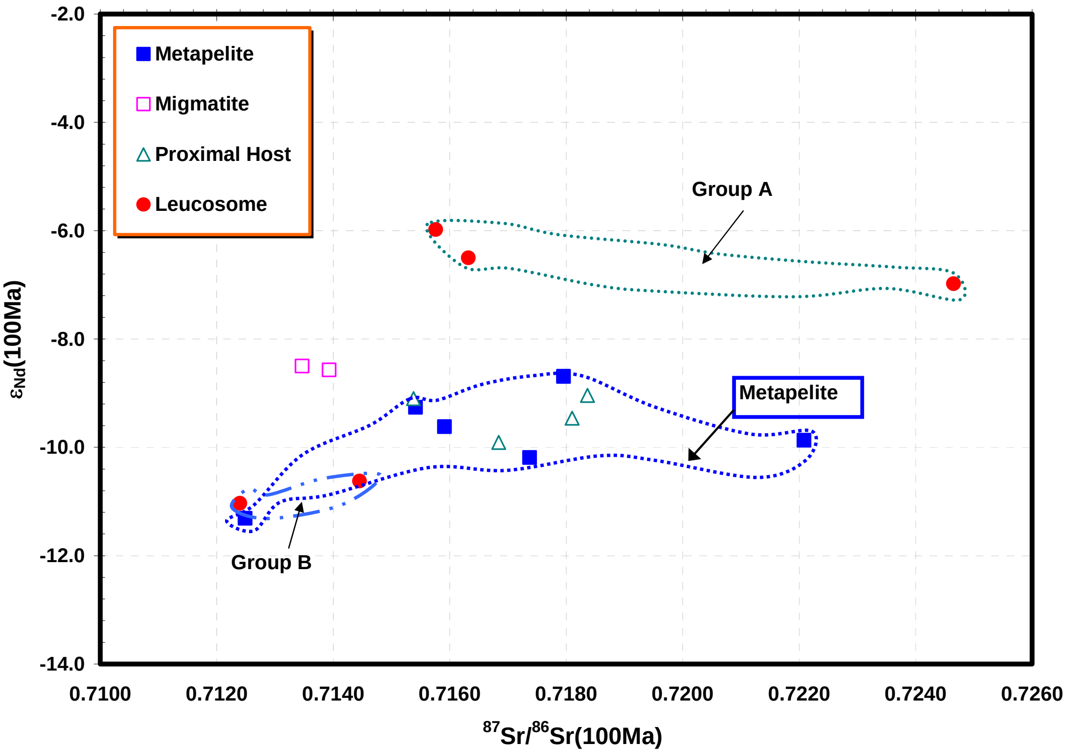

-2.0
-4.0
-6.0
-8.0
-10.0
-12.0
-14.0
ε_{Nd}(100Ma)
0.7100
0.7120
0.7140
0.7160
0.7180
0.7200
0.7220
0.7240
0.7260
^{87}Sr/^{86}Sr(100Ma)
■ Metapelite
□ Migmatite
△ Proximal Host
● Leucosome
Group A
Metapelite
Group B

Figure 9 P-T diagram showing experimentally determined solidus for experimentally determined melting reactions for a metasedimentary source (after Whittington and Treloar, 2002). Water-saturated melting reaction Qtz + Ab + Or + H_2O = M from Ebadi and Johannes (1991). Calculated locus of water-saturated melting reaction Qtz + Kfs + Als + H_2O = M from Johannes and Holtz (1996). Dehydration melting reactions Qtz + Ms + Pl = Kfs + Sil + Bt+ M (natural system) for muscovite-biotite schist (MBS) and muscovite schist (MS) from Patiño Douce and Harris (1998). Biotite dehydration melting reaction (1) Bt + Pl+ Qtz = Opx + Grt + Kfs + M (natural system) from Vielzeuf and Montel (1994), (2) and (4) Bt + Pl + Qtz = Opx + M (natural system) from Patiño Douce and Beard (1995), and (3) Phl + Qtz = En + M (MASH system) from Vielzeuf and Clemens (1992). M=melt, Qtz=Quartz, Ab=albite, Or=orthoclase, Kfs=K-feldspar, Als=aluminosilicate, Ms=muscovite, Pl=plagioclase, Sil=sillimanite, Bt=biotite, Opx=orthopyroxene, Grt=garnet, Phl=phologopite, En=enstatite. Ilm=illmenite, Cpx=clinopyroxene, L=melt, V=vapor or water. Mineral abbreviations are after Kretz (1983).

Figure 9

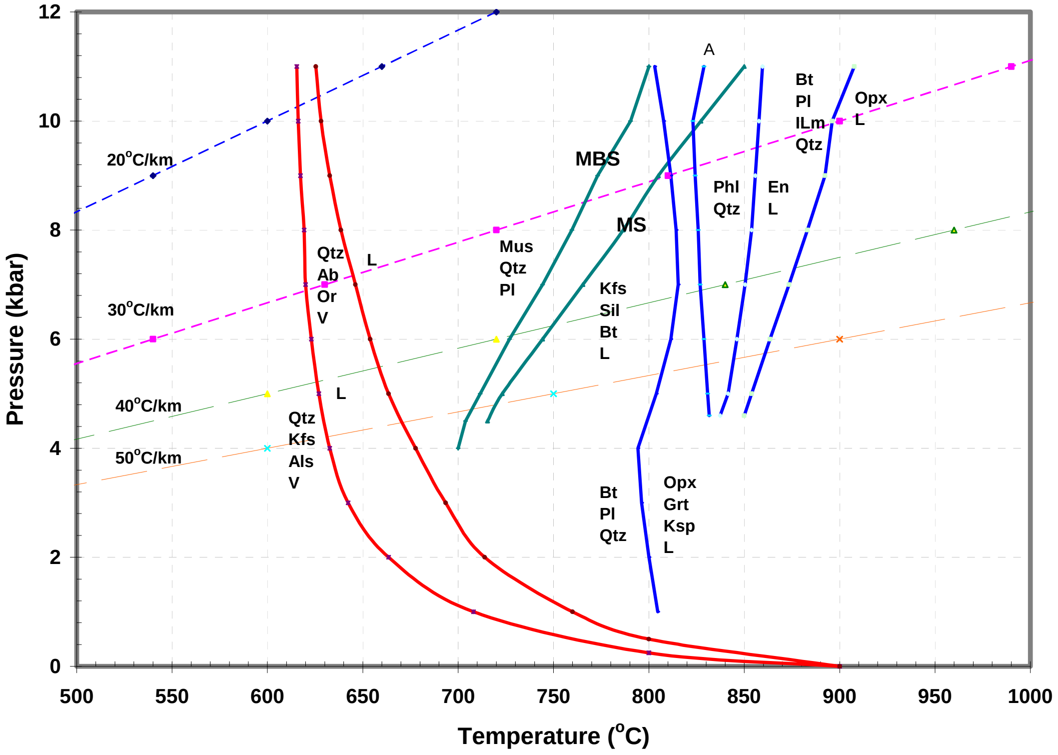
Pressure (kbar)
Temperature (°C)
0
2
4
6
8
10
12
500
550
600
650
700
750
800
850
900
950
1000
20°C/km
30°C/km
40°C/km
50°C/km
Qtz
Ab
Or
V
L
L
Qtz
Kfs
Als
V
MBS
MS
Mus
Qtz
Pl
Kfs
Sil
Bt
L
A
Bt
Pl
ILm
Qtz
Opx
L
Phl
Qtz
En
L
Bt
Pl
Qtz
Opx
Grt
Ksp
L

Figure 10 (a) Sr isotopic compositions of the metapelites, migmatites (proximal host and finely laminated migmatite) and leucosomes showing the higher Sr concentrations in the leucosomes than those in the pelite protoliths. For comparison, it also shows the Sr isotopic compositions of the Goat Ranch granodiorite and enclave samples. The Goat Ranch data are from Zeng et al. (Chapter 2). (b) The initial $^{87}Sr/^{86}Sr$ ratios of the metapelites, migmatites and leucosomes are plotted against their respective Rb/Sr ratios. It shows that initial $^{87}Sr/^{86}Sr$ ratios of the leucosomes roughly increase with their Rb/Sr ratios, suggesting an increasing proportion of muscovite relative to plagioclase entering the melt.

Figure 10

(a)

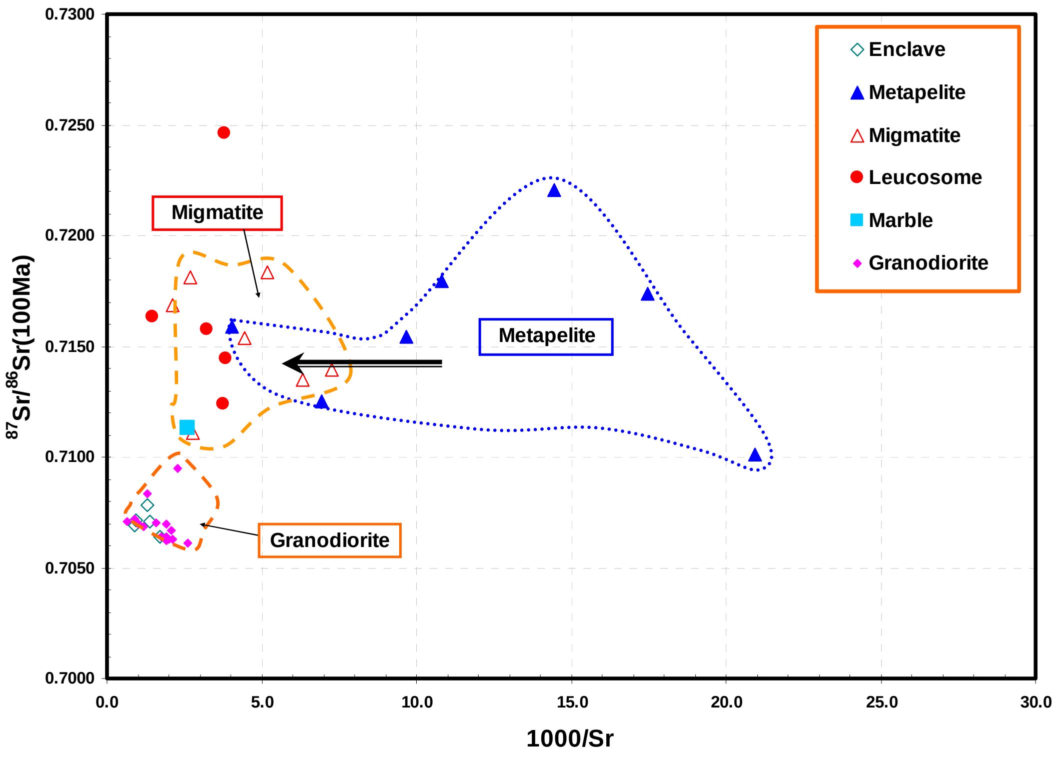

0.7300
0.7250
0.7200
0.7150
0.7100
0.7050
0.7000
$^{87}Sr/^{86}Sr(100Ma)$
0.0
5.0
10.0
15.0
20.0
25.0
30.0
1000/Sr
◇ Enclave
▲ Metapelite
△ Migmatite
● Leucosome
■ Marble
◆ Granodiorite
Migmatite
Metapelite
Granodiorite

(b)

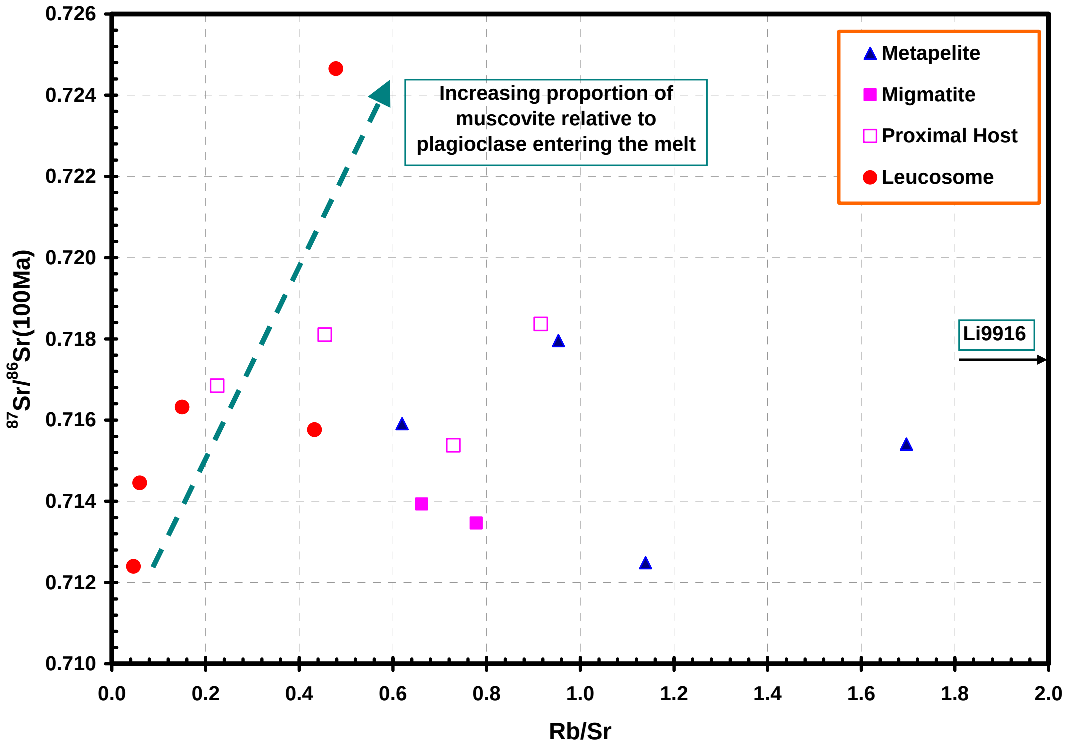

0.726
0.724
0.722
0.720
0.718
0.716
0.714
0.712
0.710
$^{87}Sr/^{86}Sr(100Ma)$
0.0
0.2
0.4
0.6
0.8
1.0
1.2
1.4
1.6
1.8
2.0
Rb/Sr
Increasing proportion of muscovite relative to plagioclase entering the melt
▲ Metapelite
■ Migmatite
□ Proximal Host
● Leucosome
Li9916

Figure 11 (a) Nd isotopic compositions of the metapelites, migmatites and leucosomes plotted against Nd concentrations. Melts from the pelitic source have lower Nd concentrations and wider initial ε_{Nd} values than their sources. (b) Plot of the initial ε_{Nd} values of the metapelites, migmatites, and leucosomes versus their respective P_2O_5 content (wt%). Group A leucosomes have higher initial ε_{Nd} values than their sources. In contrast, Group B leucosomes have similar initial ε_{Nd} values to their sources. The correlation of the initial ε_{Nd} values of the leucosomes with their P_2O_5 content (wt%) suggests that those high initial ε_{Nd} values may be due to increasing dissolution of apatite during melting.

Figure 11

(a)

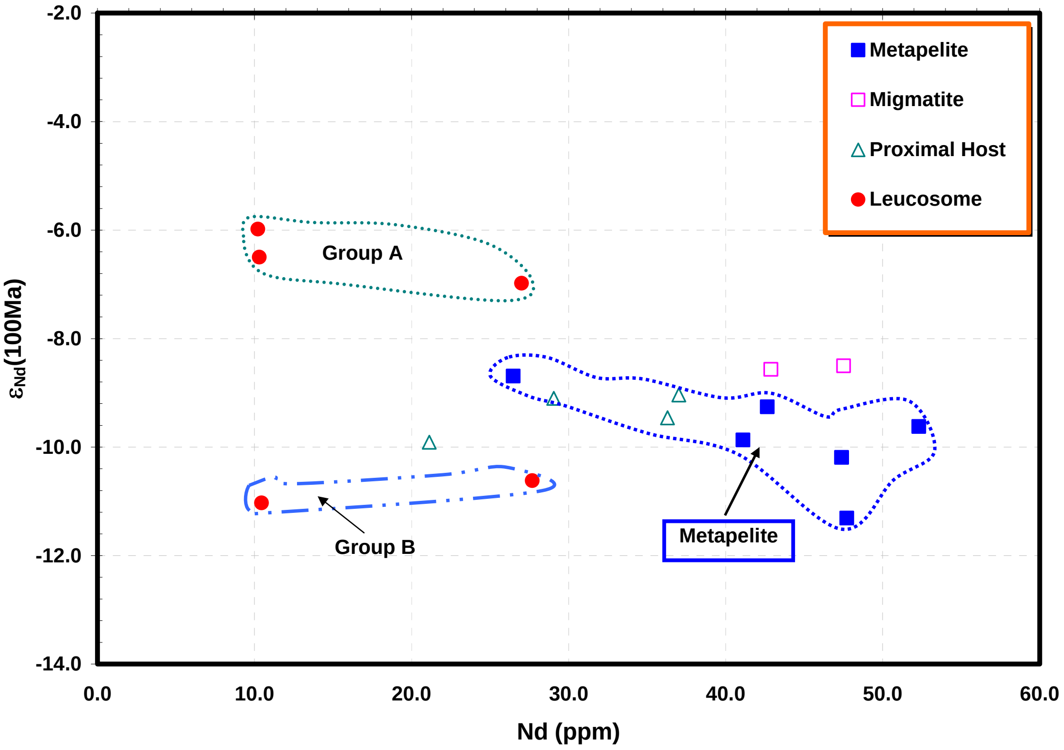
-2.0
-4.0
-6.0
-8.0
-10.0
-12.0
-14.0
ε_{Nd}(100Ma)
0.0
10.0
20.0
30.0
40.0
50.0
60.0
Nd (ppm)
■ Metapelite
□ Migmatite
△ Proximal Host
● Leucosome
Group A
Group B
Metapelite

(b)

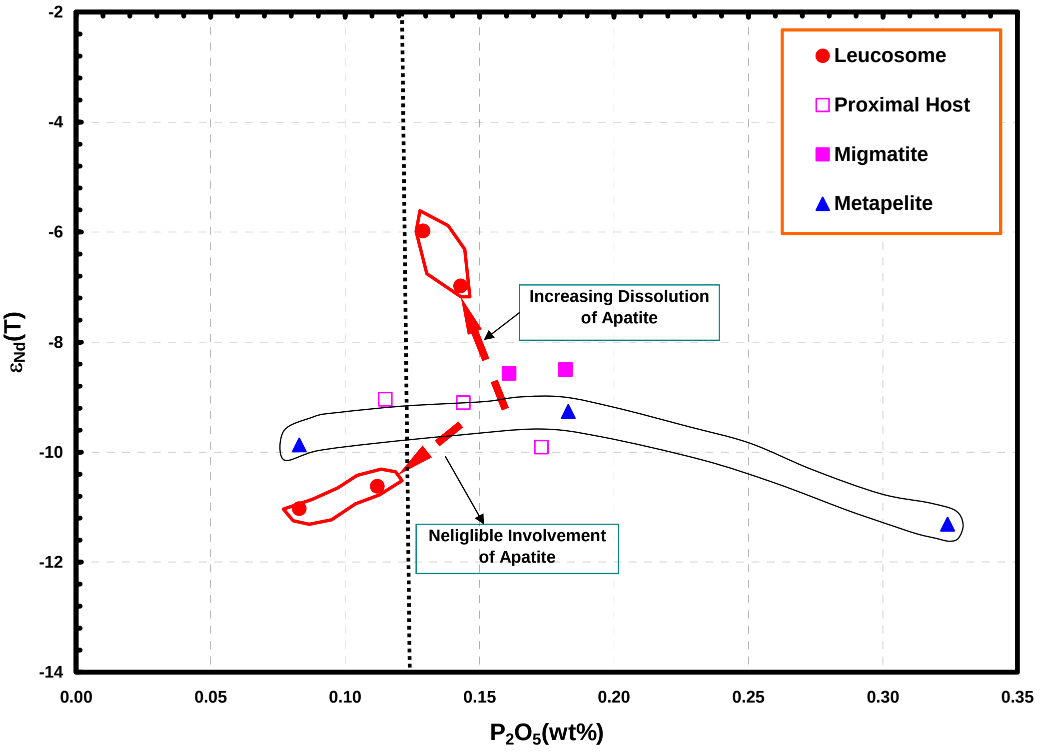
-2
-4
-6
-8
-10
-12
-14
ε_{Nd}(T)
0.00
0.05
0.10
0.15
0.20
0.25
0.30
0.35
P_2O_5(wt%)
● Leucosome
□ Proximal Host
■ Migmatite
▲ Metapelite
Increasing Dissolution of Apatite
Neliglible Involvement of Apatite

Table 1 Major and trace element analytical results for selected samples of the metapelite, migmatite and leucosomes

Sample	L0404	L0405	L0407	L0410	R0404	R0407	R0410	Li9805	Li9808	PP0101	PS0101	Li9815
	Leucosome	Leucosome	Leucosome	Leucosome	Proximal host	Proximal host	Proximal host	Migmatite	Migmatite	Pelite	Pelite	Pelite
SiO2	80.91	74.97	75.67	69.59	69.74	62.07	63.94	67.94	68.73	63.08	64.95	63.01
Al2O3	14.48	16.99	14.58	17.41	16.23	20.04	20.54	18.11	17.53	23.17	23.42	21.52
TiO2	0.09	0.38	0.05	0.51	0.62	1.02	0.98	0.83	0.85	0.99	0.93	0.87
FeO	0.86	1.85	0.76	3.78	5.57	7.26	5.70	5.45	4.86	6.10	4.94	6.82
MnO	0.03	0.05	0.01	0.07	0.08	0.11	0.08	0.08	0.14	0.05	0.03	0.04
CaO	0.54	1.64	0.95	0.61	1.03	0.76	0.64	0.76	0.70	0.25	0.22	0.25
MgO	0.18	0.54	0.14	1.00	1.36	2.16	1.49	1.82	1.40	1.64	1.59	2.09
K2O	0.36	0.47	4.59	3.68	2.23	3.52	3.10	2.25	2.33	2.52	1.82	2.83
Na2O	0.72	2.06	2.13	1.89	1.42	1.47	1.74	0.90	1.19	0.84	0.54	0.39
P2O5	0.08	0.11	0.13	0.14	0.17	0.12	0.14	0.18	0.16	0.18	0.08	0.32
Total	98.25	99.06	99.01	98.68	98.45	98.53	98.35	98.31	97.90	98.81	98.52	98.14
Ni	13	14	8	22	22	38	35	35	35	35	41	33
Cr	11	17	3	41	46	92	88	76	77	106	123	93
Sc	2	4	0	14	14	29	26	27	11	23	21	20
V	22	40	4	64	77	136	131	114	112	127	168	139
Ba	121	193	1116	875	364	636	802	555	1032	463	499	521
Rb	14	17	138	131	115	184	167	125	97	186	115	164
Sr	229	269	302	230	426	186	215	156	148	102	65	119
Zr	69	188	82	116	179	227	193	225	254	190	166	167
Y	21	33	35	36	28	41	38	35	37	37	33	35
Nb	4	9	3	13	15	25	22	20	17	19	19	19
Ga	18	20	15	18	16	26	26	21	22	26	28	25
Cu	4	0	1	0	27	0	0	0	11	12	0	8
Zn	8	21	6	49	67	94	77	85	75	74	80	111
Pb	13	29	44	48	36	32	43	21	30	16	25	16
La	8	18	17	41	42	50	55	57	41	48	59	60
Ce	24	88	34	73	73	91	77	78	91	89	84	88
Th	5	18	12	17	15	18	16	16	19	17	16	14

Table 2 Nd and Sr isotopic compositions of the metapelite protoliths, migmatites and leucosomes

Sample	Rock-Type	Rb(ppm)	Sr(ppm)	^{87}Rb/^{86}Sr	^{87}Sr/^{86}Sr	^{87}Sr/^{86}Sr(100)	Sm(ppm)	Nd(ppm)	^{147}Sm/^{144}Nd	^{143}Nd/^{144}Nd	ε_{Nd}(100)[2]	Eu/Eu*[1]
PP0101	Metapelite	175.65	103.56	4.8844	0.722352	0.715412	8.96	42.66	0.1270	0.512118	-9.26	0.6656
PS0101	Metapelite	108.39	69.21	4.5123	0.728495	0.722083	8.06	41.11	0.1185	0.512081	-9.87	0.6907
Li9805	migmatite	123.31	158.54	2.2375	0.716645	0.713465	8.37	47.52	0.1064	0.512143	-8.5	
Li9808	migmatite	90.80	137.32	1.9022	0.716636	0.713932	7.83	42.89	0.1103	0.512142	-8.57	0.6628
Li9810	Metapelite	153.10	247.20	1.7831	0.718446	0.715912	9.51	52.30	0.1100	0.512088	-9.62	
Li9813	Metapelite	88.00	92.30	2.7484	0.721861	0.717956	4.89	26.48	0.1171	0.512137	-8.69	
Li9815	Metapelite	163.70	143.70	3.2790	0.717148	0.712489	7.48	47.72	0.0947	0.511992	-11.31	0.4912
Li9816	Metapelite	172.10	57.20	8.6757	0.729700	0.717372	8.20	47.39	0.1046	0.512056	-10.19	0.6163
R0410	PH	163.63	224.41	2.0987	0.718356	0.715378	5.84	29.05	0.1216	0.512123	-9.1	0.6724
R0406	PH	168.18	370.00	1.3086	0.719961	0.718101	7.55	36.30	0.1257	0.512107	-9.46	0.9544
R0407	PH	177.11	193.36	2.6375	0.722111	0.718364	5.63	37.02	0.0919	0.512106	-9.04	
R0404	PH	105.81	471.06	0.6464	0.717761	0.716843	6.83	21.13	0.1955	0.512129	-9.91	0.6433
L0404	Leucosome	12.34	267.17	0.1394	0.712585	0.712397	1.63	10.45	0.0939	0.512006	-11.03	0.5862
L0405	Leucosome	15.46	260.32	0.1709	0.714695	0.714452	3.08	27.69	0.0670	0.512009	-10.62	0.8849
L0406	Leucosome	101.26	675.07	0.4286	0.716931	0.716322	2.99	10.31	0.1745	0.512291	-6.5	
L0407	Leucosome	134.58	311.01	1.2469	0.717532	0.715761	3.39	10.22	0.1996	0.512334	-5.98	1.8676
L0410	Leucosome	126.13	263.71	1.3780	0.726609	0.724651	6.26	27.01	0.1395	0.512243	-6.98	1.2746
051803	Marble	1.02	383.32	0.0077	0.711327	0.711317	0.05	0.26	0.1216	0.512417	-3.35	

1. Eu anomaly is calculated by $Eu/Eu^{*} = \frac{Eu_N}{\sqrt{Sm_N \times Gd_N}}$, where Eu_N, Sm_n and Gd_N are normalized to primitive mantle (Sun and McDonough, 1989). Rare earth element data are from Zeng and Saleeby (In preparation). PH = Proximal host for leucosome.
2. Calculated at t = 100 Ma using the equation $\varepsilon_{Nd}(t) = \left[\frac{(^{143}Nd/^{144}Nd)_{sample}(t)}{(^{143}Nd/^{144}Nd)_{CHUR}(t)} - 1\right] \times 10^4$, and $(^{143}Nd/^{144}Nd)_{CHUR}(0) = 0.512635$ and $(^{147}Sm/^{144}Nd)_{CHUR}(0) = 0.1966$.

Chapter 4

Progressive melting of metasedimentary wallrocks and its effects on the strain partitioning: An example from the southern Sierra Nevada batholith, California

Lingsen Zeng and Jason B. Saleeby

Division of Geological and Planetary Sciences, California Institute of Technology,
Pasadena, CA 91125

Abstract

The upper metapelite unit of the Jurassic-Triassic Kings Sequence preserved as a metamorphic pendant in the southern Sierra Nevada batholith (SNB) underwent partial melting in response to the emplacement of the mid-Cretaceous Goat Ranch granodiorite pluton. Partial melting and in situ segregation of leucogranitic melt led to the formation of migmatites proximal to the granodiorite. Field observations show that the migmatites have heterogeneous structural geometries due to progressive partial melting commensurate with high magnitude finite strain. Thus, these patterns may yield important insights into how partial melting contributes to strength contrasts and strain partitioning in metasedimentary rocks developed under high-grade conditions. Adjacent to the pluton, leucosomes form an interconnecting network with solid residues left as segregated and deformed lentoids. With distance away from the pluton, leucosomes become progressively more isolated and ultimately occur as isolated pockets in the metapelite. This transition in the structural styles of the migmatite reflect decrease extents of partial melting away from the pluton, and suggest that loading framework for the migmatite changed from LBF structure (the stronger phase forms a load-bearing

framework that contains pockets of the weaker phase) to IWL structure (the weaker phase forms an interconnected weak matrix or layers separating boudins or clasts of the stronger phase) with proximity to the pluton. Strain studies of the adjacent massive quartzite and marble units indicate steeply-plunging high magnitude stretch fabrics with elongation factors in excess of 1000%. Metamorphic mineral fabrics and structural relations of the Goat Ranch pluton as well as dikes within the pendant rocks suggest deformation and migmatization as a result of the diapiric emplacement of the Goat Ranch pluton (Saleeby and Zeng, in prep.). In contrast to the quartzites and marbles, the strain recorded by solid residues within the migmatite only suggests 200% to 300% stretching factors, which are similar to the strain recorded by deformed pebble conglomerate interbedded with and enclosed by pelitic material. The similarities appear to be due to the melt within the metapelite absorbing a greater component of deformation, just as the pelitic matrix did in the pebble conglomerates. The presence of melt within such a deforming material is likely to (1) result in a marked strength contrast between melts and solid residues, and (2) affect the strain partitioning such that melt will accommodate more strain due to its low strength than the solid residue, given the same stress. The formation of relatively weak migmatitic zone in the proximity of the invading pluton might facilitate deformation of the pendant and help intensify the downward return flow of metasedimentary pendants and pumping higher level crustal material to deeper levels during the formation of large-scale granitic batholiths.

Introduction

Knowledge of the mechanical properties of partially molten rocks is critical for understanding strain and material transport patterns in pluton-metamorphic terrains as well as for constraining and testing theoretical and numerical modeling of a number of tectonic processes involving crustal anatexis (Hollister, 1986; Hardy, 1994; Sawyer, 1994; Vanderhaeghe and Teyssier, 2001). For example, crustal anatexis at the lower continental crust level greatly reduces crustal strength and its capability to support the overlying crustal load, and may eventually lead to the collapse of an over-thickened continental crust (Hollister, 1986; Davidson et al., 1994). Experimental studies have shown that the strengths of solids and melts differ by several orders of magnitude (Shaw, 1965; Bottinga and Weill, 1972; Shaw, 1980). Rocks with less than 10% melt have peak differential strengths on the order of 100 MPa which is significantly higher than that of completely molten silicates with values of 1-100 kPa or less (Renner et al., 2000). Therefore, the mechanical behavior of rocks is expected to change from linearly elastic to elastic-plastic, and to viscous during progressive heating and crustal anatexis. Migmatites occurring in many high-grade metamorphic terrains generally represent products from various degrees of partial melting. Such migmatites provide a good opportunity to study how low-degree partial melting affects strain partitioning between the newly formed melt and the solid residue, and the bulk mechanical properties of rocks undergoing partial melting. In high-grade metamorphic terrains, partial melting and localized deformation of rocks are commonly interrelated. Field observations show that partial melts represented by leucosomes in migmatitic terrains commonly mimic original layering, but also form as interconnected network structures or are concentrated in shear zones, boudin necks, tensile cracks or axial planes of minor folds (Brown et al., 1995; Brown, 1994). As pointed out by Brown (1997), the rheological changes that accompany progressive melting and the effect of these changes on deformation mechanisms remains an outstanding question in structural and metamorphic geology.

During the emplacement of the Sierra Nevada batholith at its mid- to deep crustal levels, the introduction of hot felsic magma into the immediate proximity of metasedimentary pendants has induced partial melting and formation of migmatitic zones within the less refractory units of the metasediments proximal to the plutons. The appearance of melt within the initially solid pendant rock is expected to induce dramatic changes in the mechanical properties and mechanisms that accommodate syn-magmatic strain. In the Lake Isabella area of the southern Sierra Nevada, a well-preserved pendant composed of continental margin metasedimentary rocks is engulfed in granodiorite plutons emplaced over a relatively short time span (~2Ma). The metasedimentary pendant consists of the mid-Triassic to lower Jurassic Kings Sequence (Saleeby, 1990; Saleeby and Busby, 1993; Saleeby and Zeng, in prep). It possesses a well-defined stratigraphy characterized by a layered metabasalt of possible pre-Mesozoic age overlain by the lower Mesozoic section progression upwards from a lower pelitic unit to thick carbonate, quartzite, and finally the upper pelite ± psammite unit, the focus of this study. Excellent exposures, a well-defined migmatite complex in the upper pelite unit, and a coherent protolith stratigraphic sequence, together with well developed thermal gradient across the upper pelite unit away from its contact with the Goat Ranch pluton provides an excellent opportunity to study how the loading framework changes with increasing extent of partial melting. Another asset of this study area arises from the fact that lithological variations within the adjacent quartzite unit provides a good calibration for the strength changes in the upper pelite unit as a result from progressive partial melting. Thus this study area may provide important insights to the question proposed by Brown (1997) that were pointed out above. In this paper, we will first discuss the structure of the migmatite complex, and then demonstrate that during progressive melting of the upper pelite: (1) competence contrasts developed within the relatively homogeneous protolith sequence; (2) how the loading framework and its mechanical properties changed with increasing melt fraction; and (3) discuss how this may have effected the return flow and downward transport of the metasedimentary roof pendant as it was dynamically linked to the emplacement of the Goat Ranch pluton.

Geologic setting

This study is focused on a migmatite zone located in the south shore area of the Lake Isabella. This migmatite zone is of particular interest because it represents a single prograde metamorphic sequence from greenschist facies metasediments to migmatites that lie in direct contact with the Goat Ranch granodiorite pluton. The Goat Ranch pluton covers an area of ~80 km^2 and maps out as a circular body with roughly concordant contacts with its ductily deformed wallrocks. It consists of a uniform medium-grained hornblende-biotite granodiorite. The Goat Ranch granodiorite is composed of plagioclase in slightly greater abundance than K-feldspar, biotite, quartz, minor hornblende, and trace amounts of zircon, rutile and apatite. Metamorphic rocks of the Isabella pendant consist of a stratified sequence of pelitic and psammitic schist and gneiss, quartzite, marble and calc-silicate rock. This sequence constitutes one of the best preserved sections through the early Mesozoic Kings sequence which occurs as a distinct family of pendants that runs for over 250 km along the axis of the southern Sierra Nevada batholith (Saleeby and

Busby, 1993). The entire Isabella pendant reached amphibolite facies conditions during the emplacement and engulfment by a number of ~100 Ma plutons. The pressures at which the central and southern Sierra Nevada batholith were emplaced gradually increase southward from ~2 kb to 10 kb (Pickett and Saleeby, 1993; Ague, 1997). In this study area, the Goat Ranch pluton was emplaced at pressures within the range of 4-5 kb (Dixon, 1995). A detailed thermobarometric study within the aureole of a large composite pluton (Cyrus Flat pluton) of 100±2 Ma age in the north shore area of the Lake Isabella yields pressures of 3 ± 0.5 kb and temperature of ~700°C (Elan, 1986). The deformation and metamorphism in the Isabella pendant as a result of the intrusion of the Cyrus Flat pluton in the north shore area are similar to those in the south shore area induced by the Goat Ranch pluton. The similar ages of the Goat Ranch and Cyrus Flat plutons (Saleeby and Zeng, in prep.) suggest that the entire Isabella pendant was brought to its maximum grade of metamorphism at ~100 Ma in 3 to 5 kb conditions. The presence of andalusite coexisting with biotite and k-feldspar in the upper pelitic unit at maximum observed distances from both the Goat Ranch pluton and Cyrus Flat plutons suggests a temperature as low as ~450°C in the far field. The occurrence of diopside and wollastonite in the calc-silicate rocks in both the north and south shore of the Lake Isabella, the same age of the Goat Ranch and Cyrus Flat plutons, and structural continuity of the Isabella pendant throughout the southern Sierra Nevada batholith indicate that the temperature achieved as this structural level during the emplacement of the Goat Ranch granodiorite is likely to have been ~ 700 °C.

The tremendous flux of Cretaceous magma into virtually all crustal levels of the Sierra Nevada batholith and its metamorphic framework rendered regional metamorphic conditions of amphibolite grade from pressures of ~ 2 to ~ 8 kb (Bateman et al., 1963; Saleeby, 1990; Pickett and Saleeby, 1993). Further thermal perturbation superimposed on the above conditions along the inner contact aureoles of plutons at ~ 3 kb and greater depths promoted conditions conducive to partial melting of labile lithologies within the metasedimentary pendants. Such conditions are well preserved along the aureole of the Goat Ranch granodiorite where it intruded the upper pelite unit. In contrast, the quartzite and marble units resisted partial melting as a result of their highly siliceous and calcareous bulk compositions, having constituted highly refractory assemblages.

Structure and metamorphism

A generalized geologic map of the study area within the Isabella pendant is shown in Figure 1. The structure is characterized by a steeply-SE plunging isoclinal anticline with pelite units situated in its core and envelope positions. Metamorphic fabrics associated with the fold are L-S with linear elements parallel to steeply-plunging fold axis. Figure 2 shows the typical fold geometry in the marble, quartzite and pelite units, which mimic the large-scale fold shown in Figure 1 and occurring regionally in other similar pendants. Finite strain studies on deformed pebble conglomerate (Fig. 3) in the quartzite unit indicate a stretch factor at least locally in excess of ~1000% along the steep-plunging lineations (Fig. 5a and b). Homoaxial deformation in satellite dikes of the Goat Ranch pluton and leucosomes of the migmatitic pelite, as well as peak metamorphic textures, for example, large garnet porphyroblasts in the lower pelite unite that were formed at ~100 Ma Sm-Nd garnet-whole rock age (Saleeby and Zeng, in prep.) indicate that the isoclinal folding and L-S fabric development occurred during ~100 Ma pluton emplacement.

The upper pelite unit (J-pelite) forms the envelope of a large fold and is in contact with the Goat Ranch intrusion for ~ 4 km curvilinear trace. The upper pelite has an apparent stratigraphic thickness in excess of 1 km. Remnants of primary structures in the lowest metamorphic grade areas suggest a protolith of thin bedded compositionally immature turbidites. Many of the thin sandy beds are psammitic to quartzo-feldspathic in composition, but their intervening lamellae as well as the bulk of the unit are Al-excess pelites. The unit is remarkably homogenous in composition. The only notable lithologic variation results from a metamorphic gradient which roughly extends at right angles across the axial surface of the large fold and into the proximal contact zone with the Goat Ranch intrusion.

Based on the mineral assemblages and extent of migmatization, metamorphic and structural zones may be defined as a function of from the contact between the pelite and Goat Ranch granodiorite. Before proceeding to the discussion of the structural and metamorphic zonations in the upper metapelite unit, we discuss the nomenclature adopted in the study (after Johannes, 1988). Leucosome refers to the leucogranitic layer formed during partial melting, melanosome refers to the selvage between the leucosome and mesosome, mesosome refers to the mesocratic layers in a migmatite suite. It is darker than the leucosomes but lighter than the melanosomes, and of metamorphic appearance (schist or gneiss). Interlayered leucosome, mesosome and melanosome are collectively referred to as migmatite. Migmatization and partial melting to form migmatite are used here interchangeably. The rock prior to migmatization is called the parent rock. The metamorphic zonations within the upper pelite unit (Fig. 1) consists of (1) distal biotite-andalusite and/or sillimanite schist without leucosomes (Zone 1); (2) biotite-andalusite co-existing with sillimanite-microcline schist with incipient leucogranitic leucosomes occurring as isolated pockets (Zone 2); (3) biotite-sillimanite-microcline schist with local leucogranitic leucosomes, showing weakly interconnected or layered structure (Zone 3); and (4) sillimanite-microcline schist, gneiss and granofels with extensive leucosomes that formed well-developed interconnected network structure (Zone 4). Nonmigmatized Zone 1 rocks (Fig. 1) consist of andalusite and/or sillimanite, biotite, quartz, k-feldspar, muscovite (<5%) and minor plagioclase. Typical leucosomes in Zone 4 mainly consist of quartz, k-feldspar and plagioclase, and have a granoblastic texture and coarser grain sizes than the immediately adjacent melanosome and mesosome. In contrast, melanosomes mainly consists of sillimanite and biotite with minor to trace amount of quartz and K-feldspar. The presence of quartz and K-feldspar within the melanosomes suggests incomplete segregation of leucogranitic melt from its parent rock either due to its high viscosity (Clements and Petford, 1999; McKenzie, 1987) or unfavorable stress condition (Brown, 1995). Locally in Zone 4, there are garnets co-existing with biotite in the melanosomes.

The metamorphic zonation patterns of the upper pelite unit suggest that the thermal gradient within the upper pelite unit resulted from heating by the Goat Ranch pluton. Progressive partial melting of the upper pelite with greater proximity to its contact with the Goat Ranch pluton resulted in progressively greater fractions of leucosome formed with proximity to the pluton. Based on the amounts and structures of leucosomes, they can be morphologically (Fig. 4) divided into (1) no leucosome in Zone 1; (2)

discordant dikes and isolated pockets of pegmatites and aplites in Zone 2; (3) agmatic and randomly distributed distinct leucosomes of various sizes which appear to gather the quartzo-feldspathic segregations into larger, granite- or pegmatite-like tubes and dikes in Zone 3; and (3) concordant (stromatitic) and pervasive network leucosomes in Zone 4. In Zone 4, leucosomes of millimeter to centimeter thickness form interconnected networks that surround the elongated or lentoid-shaped melanosome + mesosome (referred to as solid residue or solid block). The solid blocks with sizes varying from centimeters to tens of centimeters are either sub-parallel or oblique at low angles (20 to 30 degree) to the foliations of the migmatite (Fig. 4a). In Zone 2, isolated pockets of leucosomes are found not only on hand specimen scale but also on microscopic scale (Fig. 4b). Such leucosomes occur as lentoids distributed discontinuously in a solid dominant matrix.

Theoretical framework

Before we discuss the field relations and their implications for the effects of partial melting on strain partitioning, we will first briefly review background theory on the rheology of composite materials. It is a common practice to extrapolate experimentally determined single phase rheologic properties to the analysis of the mechanical properties of the crust and mantle, even though geologists would acknowledge that most of the rocks are multiple-phase aggregates (Rosenberg, 2001; Zhao and Ji, 1997; Handy, 1994). For simplicity, most multi-phase systems can be characterized by strong and weak phases based on the competence or strength of the constituent minerals (Treagus, 2002). On a microscopic scale, the physical properties of partially molten rocks depend on the grain-scale distribution of melt. Whether the melts are distributed along the grain boundaries and form an interconnected network, or as isolated pockets in a region surrounded by grains strongly affects the bulk mechanical properties of partial molten rocks. On a mesoscopic scale, the presence of melt within an otherwise completely solid rock would be expected to have profound effects on the mechanical properties of the rock under deformation conditions. The establishment of competence or strength contrasts within a rock by the presence of partial melts will affect the strain partitioning and thus its deformation pattern.

The rheology of composite materials is intimately related to their structures. In naturally and experimentally deformed multiple-phase aggregates, most of the meso-structures observed can be described in general terms by two basic types: (1) the stronger phase forms a load-bearing framework (LBF structure) that contains pockets of the weaker phase; and (2) the weaker phase forms an interconnected weak matrix or layers separating boudins or clasts of the stronger phase (IWL structure, interconnected weak layers) (Handy, 1990 & 1994). The gross rheological properties of very low melt fraction rocks will be dominated by the mechanical properties of the grains in contact, regardless of the viscosity of any small fraction of the intergranular melt. The response of such a system to deformation will therefore be similar to that of sub-solidus rocks, with brittle behavior at high strain rates and ductile at low strain rates, and effective shear viscosity on the order of 10^{18} Pa s. As the proportion of partial melt increases, the strength and effective viscosity decrease (Arzi, 1978; Van Der Molen and Paterson, 1979). The strength falls rapidly when displacive movement can take place in the melt phase between grains.

Dynamic viscosity is a measure of internal friction in moving fluids that arises as a consequence of molecular collisions. It is expressed as a constant of proportionality (η) between the shear strain rate ($\dot{\varepsilon}$) and shear stress (τ) such that

$$\tau = \eta \dot{\varepsilon} \qquad (1)$$

where η is the dynamic viscosity. Such a fluid is said to be Newtonian. For a two-phase composite material, its bulk mechanical strength S can be estimated by assuming either equal strain or equal stress in the two phases. By assuming homogeneous strain in the mixture, the upper bound S_u, also called the Voigt bound, is defined by

$$S_u = xS_w + (1-x)\ S_s \qquad (2)$$

By assuming homogeneous stress in the two phases, the lower bound S_L, also called the Reuss bound, is defined by

$$S_L = 1/\{x/S_w + (1-x)/S_s\} \qquad (3)$$

where S_w and S_s are the strength of the weak and strong phases, respectively, and x is the fraction of weak phase in the composite material (Zhao and Ji, 1997; Hill, 1965; Vigneresse et al., 1996; Treagus, 2002). The same principles can be applied to a viscous composite material or mixture; its bulk viscosity will be bounded by expression 2 and 3 in a similar fashion. Assume homogeneous stress in the mixture, then

$$\sigma = \eta_w \dot{\varepsilon}_w = \eta_s \dot{\varepsilon}_s = \eta \dot{\varepsilon} \qquad (4)$$

where η, η_w, and η_s are the bulk viscosity, viscosity of the weak and strong phase, respectively. The bulk viscosity of the composite material is determined by replacing S_L by η_L in Equation 3, then

$$\eta_L = 1/\{x/\eta_w + (1-x)/\eta_s\} \qquad (5)$$

Assume homogeneous strain within the mixture, then

$$\varepsilon = \varepsilon_S = \varepsilon_W \quad (6)$$

where ε , ε_S, and ε_W are the bulk strain, strain in the weak and strong phase, respectively. The bulk viscosity of the mixture under this condition is given by replacing S_U by η_U in Equation 2, then:

$$\eta_u = x\eta_w + (1\text{-}x)\ \eta_s \quad (7)$$

By using Shaw's viscosity model for silicic melts (Shaw, 1972) and temperature estimate of 700°C, the viscosities of the melts are calculated based on the major element composition data of the leucosomes (Zeng, et al., 2003, Chapter 3). The viscosities of the melts represented by the leucosomes are in a range from 10^{10} to 10^{12} Pa s. Using Equations 5 and 7, the lower and upper bounds of the viscosity of the migmatite are estimated by assuming the viscosities of the melt (η_w) and the solid (η_s) are 10^{11} and 10^{15} Pa s (Lisle et al., 1983), respectively. It should be noted that the viscosity of a rock in natural conditions is always between the lower and the upper bounds. For a homogeneous stress condition that corresponds to the lower bound (η_L), the presence of small fractions of melt will greatly affect the bulk viscosity of the composite material. The bulk strength of the migmatite will fall rapidly with increasing degrees of partial melting due to the large contrast in strength of the melt phase and the solid residue (Fig. 5).

Structural expression of competence contrast

Strained pebble conglomerates within the quartzite unit that is adjacent to the upper pelite unit provide a natural calibration for the competence contrast established in the migmatite zone as a result of partial melting. In the quartzite unit, pebble conglomerates which have not experienced partial melting, deformation is dominated by high stretching factors with a ratio exceeding 1000% (Saleeby and Zeng, in prep.). High stretching strain induced by the emplacement of the Goat Ranch granodiorite pluton is represented by the highly stretched quartz pebbles with the quartzite, and tight passive folds in the metapelite, quartzite, as well as marble units.

For a given strained rock, the stretching lineation is defined by minerals or mineral aggregates that are aligned preferentially parallel to the orientation of maximum stretching strain. The Z axis, parallel to the stretching lineation, is the direction of maximum finite stretch, the Y axis is the direction of intermediate finite stretch, and the X axis is the direction of minimum finite stretch. We refer to the XZ section as the surface that contains the stretching lineation (L), and XY section as the surface perpendicular to the stretching lineation (L). Given a constant applied stress, the accommodating strain should be inversely correlated to viscosity as shown in equation 1. It is difficult to measure the finite strain of leucosomes in the either the XZ or XY surface due to their high mobility which included syn-deformation melt migration and solidus to subsolidus plastic deformation. As a proxy for an estimate of the minimum finite strain in the migmatites, we measured aspect ratios of residual blocks which include melanosome and mesosome. Therefore, we only make a comparison of the strain observed along the XY surface in the migmatite with that of pebble conglomerates. Deformed pebbles in pebble conglomerate are excellent strain markers for structural analysis (Lisle et al., 1983; Treagus and Treagus, 2002; Treagus, 2002). In the study area, a semi-continuous layer of pebble conglomerate matrixed by meta-mud and meta-silt is interbedded with massive and thick-bedded quartzite. Pebbles mainly consisting of quartz are usually ten times more viscous than muddy or silty matrix material (Lisle et al., 1983). The pebble conglomerate has a typical IWL structure in which pebbles behave as strong phases and metamud-rich layers form a weak interconnected network. Finite strain studies of the pebble conglomerate offer a constraint on the minimum strain in the quartzite unit. The continuity of the structural geometry throughout the entire section of the Isabella pendant affords an opportunity to apply these minimum strain estimates to the entire pendant. For the pebble conglomerate, in both the XZ and XY section, we have carefully examined the geometry of deformed pebbles and the orientation of the stretching lineations, and measure their axial ratios. In a XZ section, the ratio of the maximum stretch over minimum stretch is referred as R_{xz}, and in a XY section as R_{xy}. The same approach is applied to measure R_{xy} for solid residues in the migmatites in Zone 4 of the upper pelite unit. The results are shown in Figure 6 and 7 for the pebble conglomerate and migmatite, respectively.

Strain recorded in the deformed pebble conglomerate shows that (1) parallel to the XZ section, pebbles record stretching factor as high as 4000% with an average of 800% to 1000%, and (2) but in XY section, pebbles have stretching factor ranging from 200% to 500% and an average of 300% (Fig. 6). Petrographic observations show that metamud-rich layers have distinctive deformation features from those of strong pebbles, and consist of fine quartz, K-feldspar, plagioclase and muscovite. Metamud-rich layers show strong grain size reduction, formation of subgrain boundaries and strong preferred orientations in quartz aggregates, typical of mylonitic structure. In contrast, pebbles show only weak internal deformation, and quartz within the pebbles have coarser grain size by an order of magnitude than those in the metaclay layers. The highly deformed metamud-rich matrix behaved as weak phases that facilitated strain partitioning and localization. The competence contrast between the pebbles and the metamud-rich matrix depends not only on their relative strengths but also their relative sizes. Stretch factors recorded in the pebble conglomerate vary widely from ~4.0 to ~40.0 along the XZ surface, and from ~1.0 to ~7.0 in the XY surface. Such variations may suggest that larger pebbles embedded within the metamud-rich layers strengthen the medium and result in less strain accommodated by pebbles.

The aspect ratios of the solid residue in the migmatitic pelite are on the average 300% (Fig. 7a & b) which is similar to the strain inferred from the deformation of the pebble conglomerates along the XY section (Fig. 6c & d). We suggest that the leucogranitic melts represented by leucosomes behaved rheologically similar to the weak metamud-rich matrix in the pebble conglomerate. The appearance of melt is likely to affect the strain partitioning such that melt will accommodate more strain due to its low strength than the solid residue, given the same stress, as well as reduce the bulk viscosity. Assuming the viscosities of the melt (leucosome) and the solid (melanosome + mesosome) are 10^{11} and 10^{15} Pa s, respectively, 10% of melts presented in the migmatite could reduce its bulk viscosity from 10^{15} to as little as 10^{12} Pa s (Fig. 5). This is consistent with inferences drawn from experimental and field observations on partially molten rocks (e.g., Dell'Angello and Tullis, 1988; Brown, 1994; Rosenberg and Riller, 2000; Rosenberg, 2001).

Loading framework transition in the upper pelite unit

The presence of melt within the upper pelite unit due to the emplacement of the Goat Ranch granodiorite changed the rheological properties of the pelite such that there was strong strain partitioning between solid residue and melt phases. The transition from purely solid deformation to melt-enhanced deformation can be demonstrated by comparing the strain variations of metapelite with those rocks strained without melt presence.

The mechanisms and characteristic length-scales over which anatectic melts can be mobilized depend strongly on melt fraction due to the high viscosities of silicic melts (Patiño Douce and Johnston, 1991). The melt productivity depends on temperature, pressure, bulk compositions, and amount of water available during partial melting. Under given P-T conditions, the amount of melt that can be generated is determined by the water content and the mineral compositions of the source rock. Due to the general non-modal character of crustal anatexis, the proportions of quartz, plagioclase, K-feldspar, muscovite, biotite and aluminosilicate are key parameters that control the melting reactions. For the P-T conditions of this field area during the emplacement of Goat Ranch pluton, relevant partial melting would proceed via the reactions: (1) Quartz + Plagioclase + H_2O → Melt ($\Delta V<0$); (2) Muscovite + Plagioclase + Quartz + H_2O → Melt ($\Delta V<0$), and with minor role played by (3) Muscovite + Aluminosilicate + Quartz → Melt + Sillimanite + K-feldspar ± Biotite ($\Delta V>0$). These experimentally determined melting reactions for metasedimentary sources are after Whittington and Treloar (2002) and references therein. The relative importance of these reactions in the study area are defined by the major and trace element, and radiogenic isotope geochemistry of the respective leucosomes (Zeng et al., Chapter 3). The sign of volume change of anatectic melting (ΔV)

would strongly affect the segregation and migration of melt produced (Brown, 1994 & 1997; Brown et al., 1995; Rushmer, 2001). For fluid-absent dehydration partial melting of muscovite with high positive volume changes ($\Delta V>0$), it will induce rapid pore pressure development during early stage of partial melting (Rushmer, 2001), which will lower effective normal stress and promote melt-enhanced embrittlement and fracture of the surroundings (Wickman, 1987; Davidson et al., 1994). This would facilitate melt segregation, escape, and accumulation at sites of low relative stress. This is likely to account for some of the structures in Zone 4 and Zone 3. Such structures include (1) gathering and thickening of leucosomes at the necking area of the solid residues in Zone 4 and (2) segregation and accumulation of leucosomes along the tensile fractures in Zone 3. In contrast, for fluid-present partial melting with negative volume changes ($\Delta V<0$) and without applied differential stress, melts tend to retain and segregate in situ. But continuous melting of quartz + plagioclase assemblages at a proper temperature condition will lead to gradual buildup of melts and allow melt-dominant deformation (Murrell, 1985; Brown et al., 1995). If such a pervasive partial melting produces a high enough fraction of melts, the melts will inevitably form interconnected networks such as in Zone 4. Such a melt-dominant rheology leads to partitioning of strain into weak highly strained domains (melts), leaving weakly strained domains of solid residues (Bell 1985; Handy et al., 2001). As discussed above, this deformation pattern is similar to the strain pattern in the pebble conglomerates. At lower temperatures than those represented in Zone 4 and 3, neither fluxed-melting of quartz + plagioclase assemblage nor muscovite dehydration melting is favored to generate a large amount of melt, instead limited and small melt fractions (a few percent) are generated. Such melts tend to stay in situ and form as isolated pockets such as in Zone 2.

Figure 8 shows (a) a cross section; (b) simple thermal structure calculation for the thermal gradient; (c) melt fraction; and (d) structure transitions across the metapelite complex. Field observations indicate that melt fractions of less than 4% are typical of Zone 2, 5 to 9% of Zone 3, and 10 to ~15% of Zone 4. The thermobarometric constraints are discussed above. Due to relatively low temperatures and low contents of muscovite in the upper pelite unit, the maximum degree of partial melting is unlikely to exceed 15%, which is typical for partial melting reactions (1) and (2) and as discussed in Stevens et al. (1997), and Vielzeuf and Holloway (1988). With distance away from Goat Ranch pluton, extent of partial melting decreases rapidly as temperature drops (Fig. 8c). As a result, leucosomes form an interconnecting network close to the contact, while solid residues occur as segregated and deformed lentoids. With increasing distance away from the contact, leucosomes become progressively isolated and finally occur as isolated pockets in the metapelite host. This transition in structural styles of the migmatite suggest that loading framework for the migmatite changed from IWL structure to LBF structure with decreasing extent of partial melting (Fig. 8d).

Summary and conclusions

We have presented field observations on the characteristics of high-strain ductile deformation of the best known example of a mid-crustal level (3-5 kb) syn-batholithic migmatite complex in the metasedimentary framework pendants of the Sierra Nevada batholith. Such high-strain ductile deformation pervades the subject pendant, but is intensified and entails partial melting of labile pelite-psammite along the inner aureole of the ca. 100 Ma Goat Ranch granodiorite pluton. Deformations both in the pebble conglomerates from the refractory quartzite and the migmatite zone demonstrate that: (1) leucogranitic melt generated by the anatexis of the upper pelite unit played a similar role rheologically to the metamud-rich layers within the pebble conglomerate; (2) the presence of melt within the metapelite enhanced the deformation of the migmatite zone proximal to the Goat Ranch pluton; and (3) loading framework of the metapelite changed from LBF to IWL with increasing melt fraction across the upper pelite unit.

Both theory and observational data discussed above indicate that the presence of melt will greatly modify not only the bulk strength of a given system, but also the strain partitioning within the partially molten rocks. This is most readily seen in the relationship between viscosity and melt fraction (Fig. 5). Under the conditions of partial melting of a pelitic source, the presence of leucogranitic melt would greatly affect the deformation pattern of the wall rocks surrounding a granitic pluton. Regional observations indicate that at progressively deeper levels southward from the Isabella pendant (~ 4 to 9 kb) labile pelitic-psammitic units were melted out of the respective pendants, leaving quartzite, marble and local sillimanite-kyanite schist as refractory pendants and enclaves (Saleeby et al., 1987; Saleeby, 1990; Pickett and Saleeby, 1993). The relationships that we discuss above suggest profound domain weakening induced by such selective migmatization. Such weakening is suggested to profoundly affect the deformation of mid- to lower crust metasedimentary pendants and to facilitate the vertical transport and return of higher crustal rocks to the deeper level. Regional relations discussed in Saleeby (1990) and Saleeby and Zeng (in prep.) indicate strong downward or return flow components of transportation in the southern Sierra pendants during voluminous batholith emplacement. Migmatization, as described above, and progressively higher degrees of melting in labile lithologies southward at deeper crustal levels in effect help lubricate the return flow process as well as partition the attendant strain.

Figure 1 Geologic map of the Goat Ranch area. All the tight isoclinal folds are characterized by SE-steeply plunging fold axes that are parallel to the stretching lineations, which suggest the material flowed in and out of the map view.

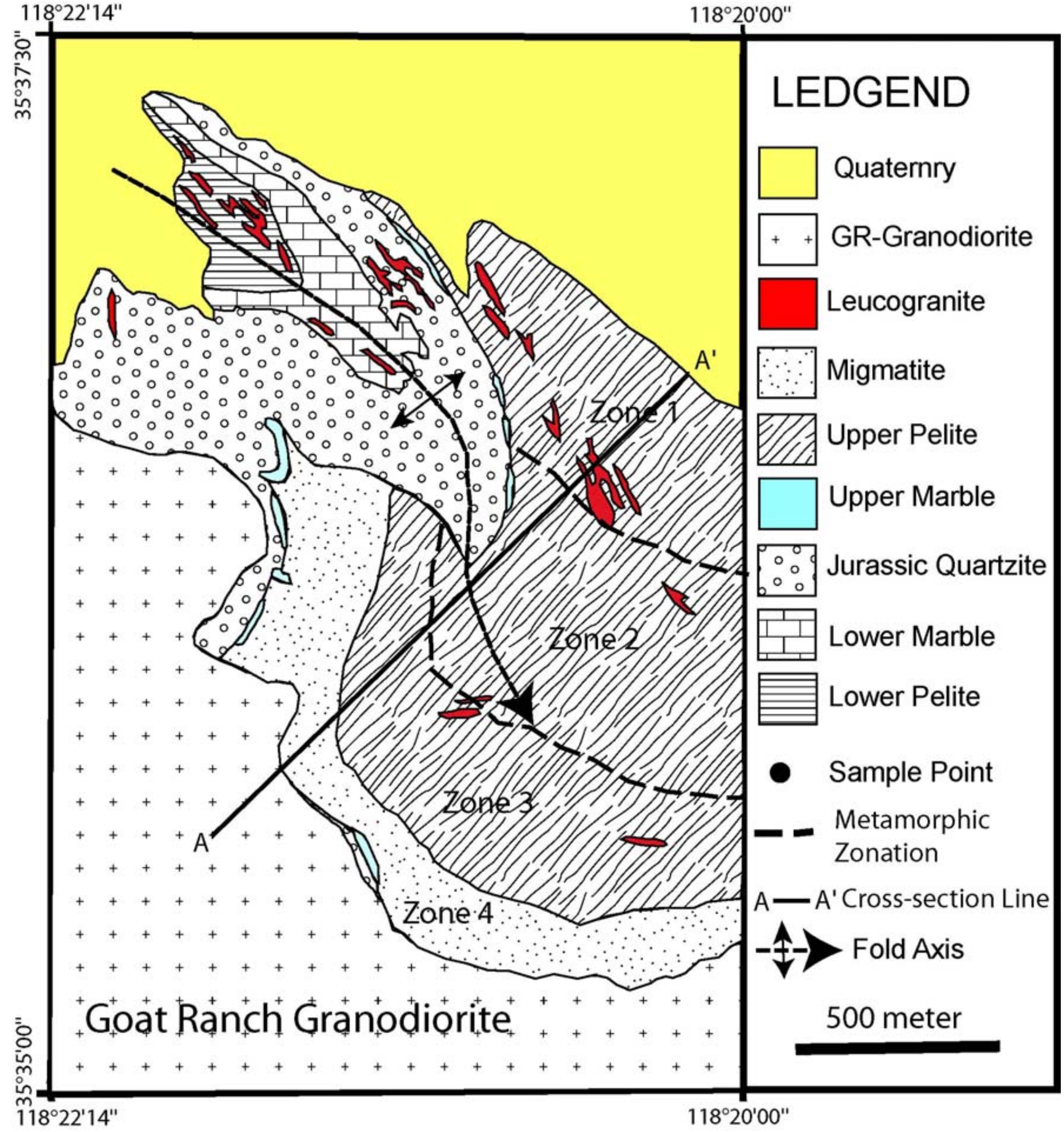
118°22'14"
118°20'00"
35°37'30"
35°35'00"
118°22'14"
118°20'00"
LEDGEND
Quaternry
GR-Granodiorite
Leucogranite
Migmatite
Upper Pelite
Upper Marble
Jurassic Quartzite
Lower Marble
Lower Pelite
Sample Point
Metamorphic Zonation
A — A' Cross-section Line
Fold Axis
500 meter
A'
Zone 1
Zone 2
Zone 3
Zone 4
A
Goat Ranch Granodiorite

Figure 2 Photo showing the typical fold geometry observed in the Jurassic marble unit. The fold axis is parallel to the stretching lineation (L) which is typically steep to the SE, but in this photo is near vertical, parallel to the hammer handle. Folds in the marble, quartzite, and the pelite units have similar geometry as the structure shown in this photo not only on hand specimen scale but on map scale as well.

Figure 3 Photographs showing (a) deformed pebble conglomerate in the section subparallel to the stretching lineation in the quartzite unit; (b) deformed pebble conglomerate in the XY section perpendicular to the stretching lineation.


(a)
(b)

Figure 4 Photos showing typical migmatite structures: (A) interconnected network structure (Zone 4). Thin leucosomes form interconnected network surrounding the relatively rigid lentoid shaped melanosome + mesosome blocks; (B) isolated melt pocket (Zone 2); (C) layer structure (Zone 3 & 4); (D) leucosomes appear to gather the quartzo-feldspathic segregation into larger, granite- or pegmatite-like dikes along the tensile fractures (Zone 3 and 4).

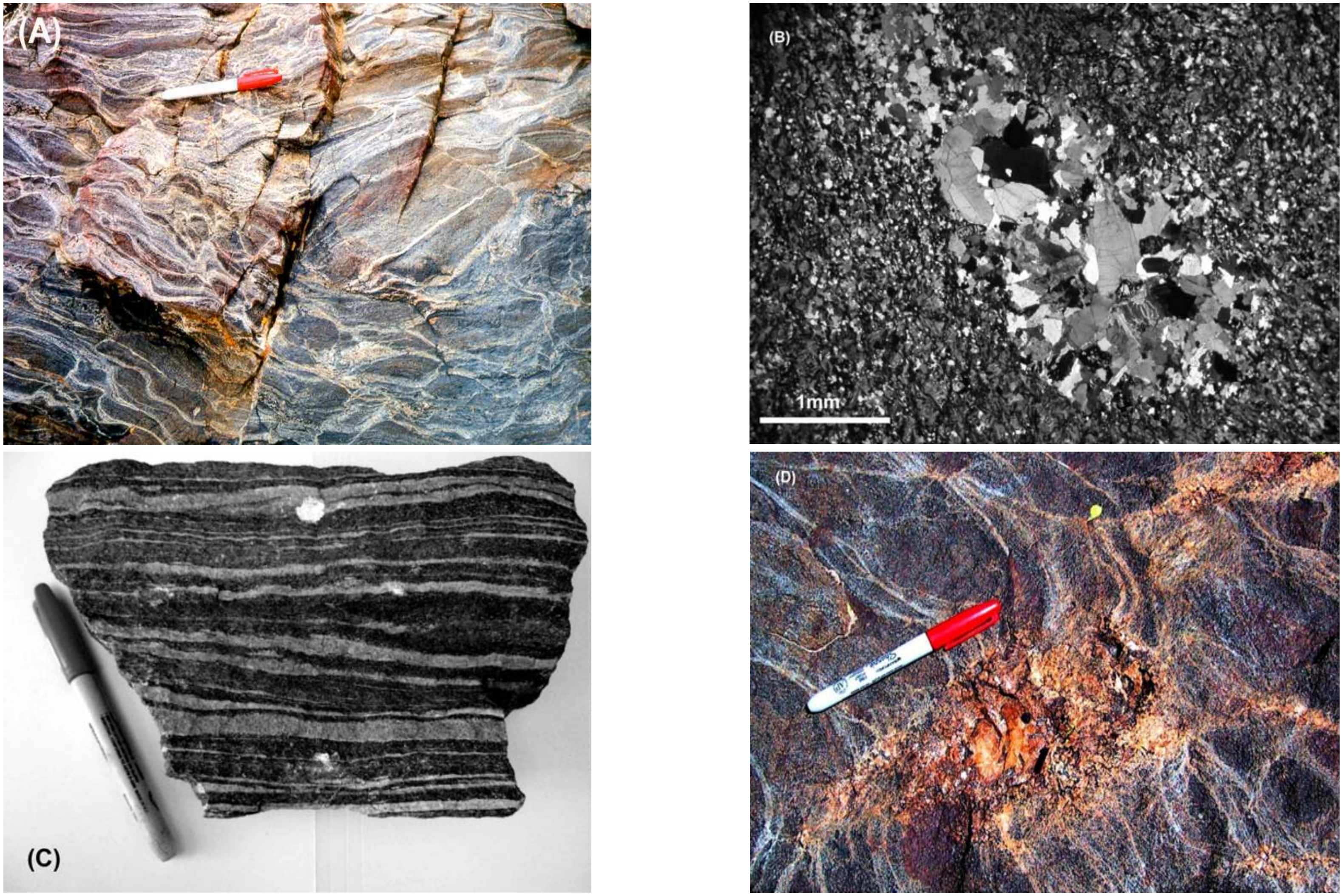
(A)
(B)
1mm
(C)
(D)

Figure 5 The rheology of a partially molten rock as a function of melt fraction. η_U and η_L represent the upper and lower bound of the rheology of a partially molten rock. They are calculated by Equations 7 and 5, assume the viscosities of the melt (η_w) and the solid (η_s) are 10^{11} and 10^{15} Pa s, respectively. For a homogeneous stress condition that corresponds to the lower bound (η_L), the presence of small fractions of melt will greatly affect the bulk viscosity of the composite material. The viscosity of the melt is estimated based on Shaw's model (Shaw, 1972) and the major element geochemistry data of the leucosomes (Zeng et al., 2003)

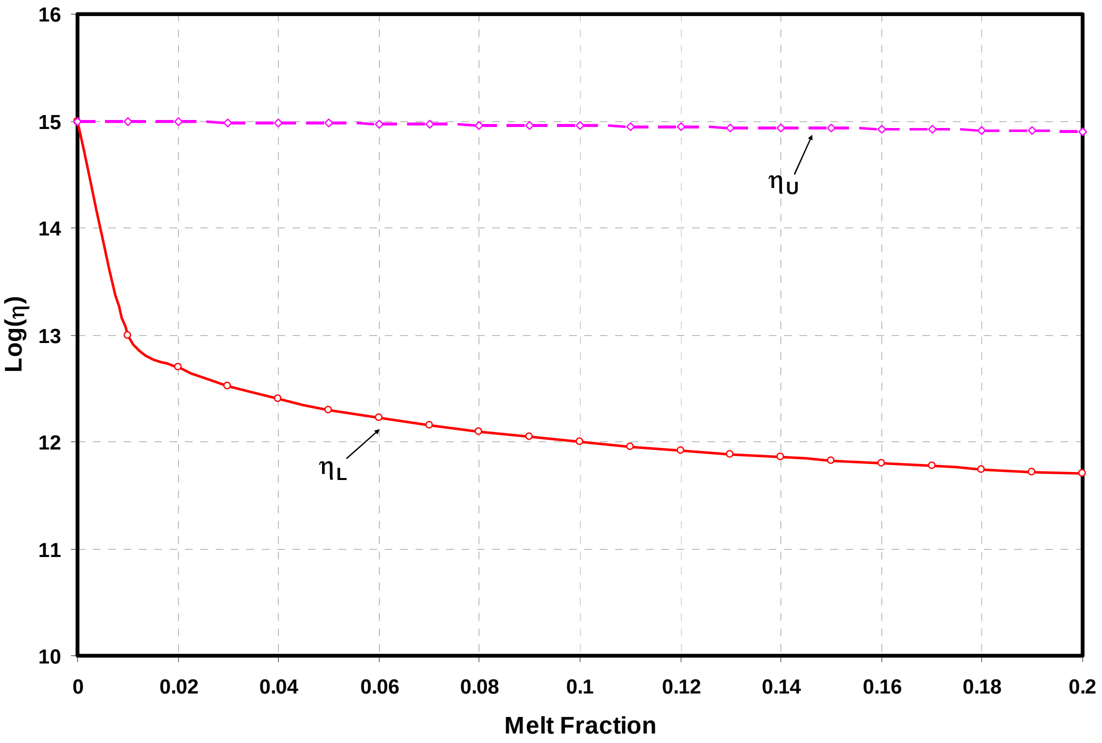
16
15
14
13
12
11
10
Log(η)
0
0.02
0.04
0.06
0.08
0.1
0.12
0.14
0.16
0.18
0.2
Melt Fraction
ηU
ηL

Figure 6 Results from field measurement of deformed pebble conglomerates in the quartzite unit. (a) The widths of stretched pebbles plotted against their lengths showing the stretching factors along the XZ section. (b) Histogram showing that along the stretching lineation most of the deformed pebbles recorded stretching strain about 600% to 1000%, but maybe as high as 4000%. (c) Measurement conducted along the XY section showing stretching strain along XY direction ranging from 100% to >600%, but averaging at 300% as shown in histogram plot (d).

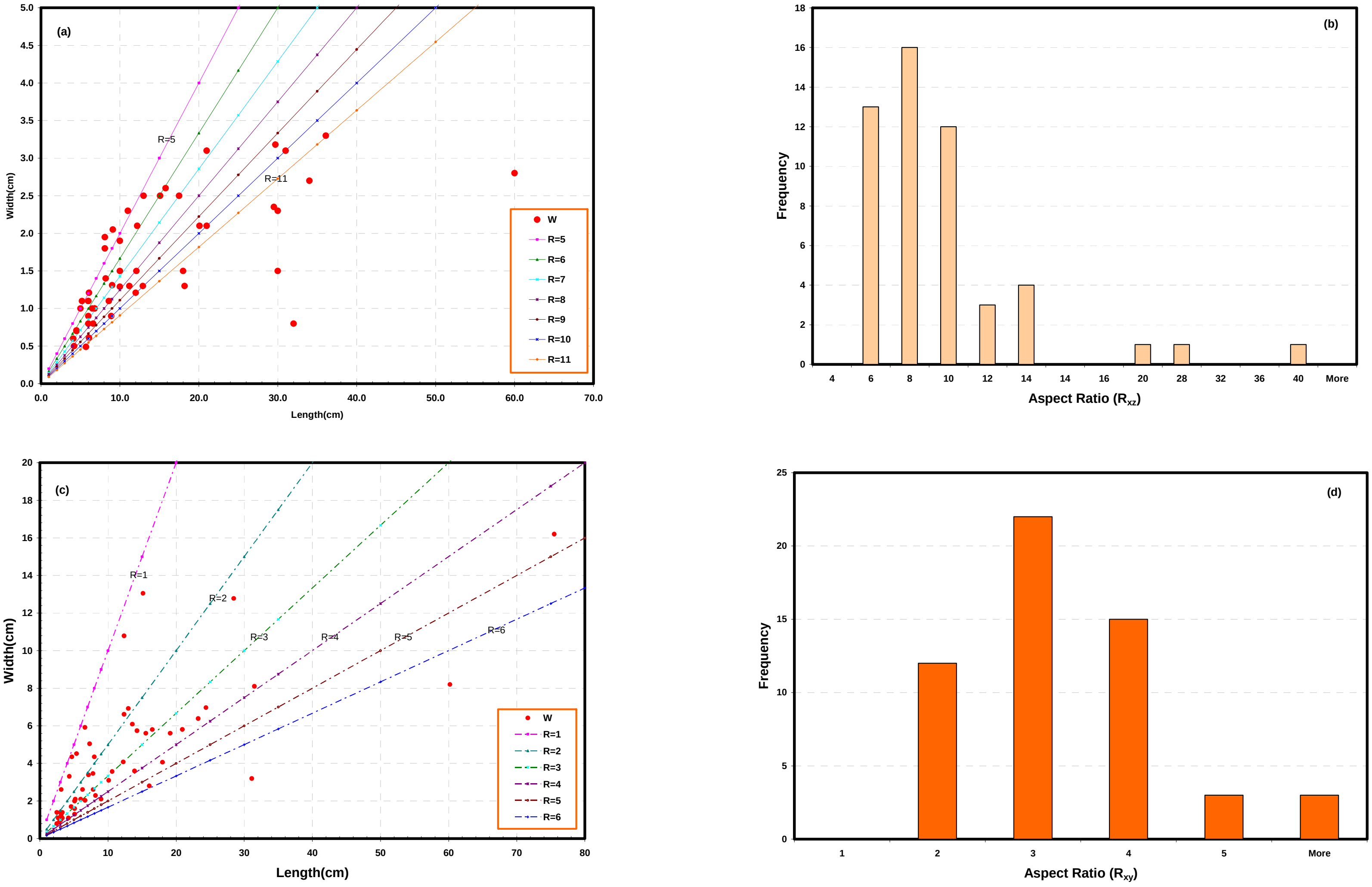
(a)
Width(cm)
Length(cm)
0.0
0.5
1.0
1.5
2.0
2.5
3.0
3.5
4.0
4.5
5.0
0.0
10.0
20.0
30.0
40.0
50.0
60.0
70.0
R=5
R=11
W
R=5
R=6
R=7
R=8
R=9
R=10
R=11
(b)
Frequency
Aspect Ratio (R_{xz})
0
2
4
6
8
10
12
14
16
18
4
6
8
10
12
14
14
16
20
28
32
36
40
More
(c)
Width(cm)
Length(cm)
0
2
4
6
8
10
12
14
16
18
20
0
10
20
30
40
50
60
70
80
R=1
R=2
R=3
R=4
R=5
R=6
W
R=1
R=2
R=3
R=4
R=5
R=6
(d)
Frequency
Aspect Ratio (R_{xy})
0
5
10
15
20
25
1
2
3
4
5
More

Figure 7 Results from field measurement of deformed migmatites in the upper pelite unit. (A) Widths of stretched melanosomes + mesosome plotted against their lengths showing the stretching factors along the XY section. (b) Histogram showing that in the XY section, most of the stretched melanosome + mesosome recorded stretching strain about 100% to 500%, with an average of 300%.

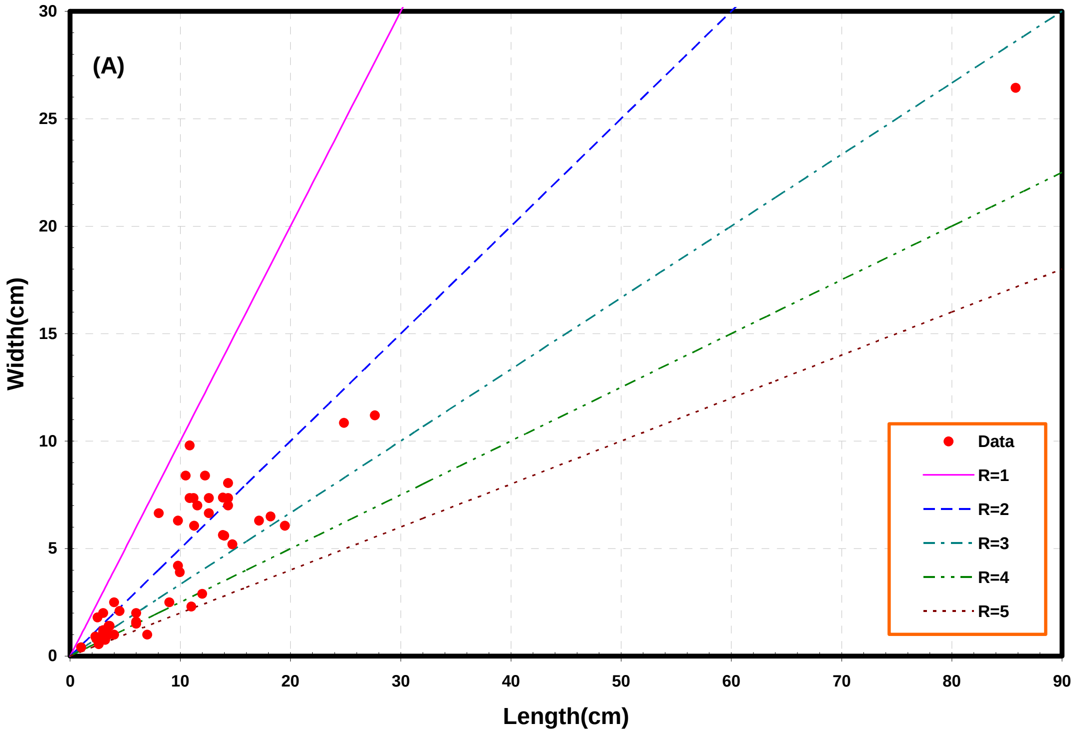
(A)
Width(cm)
Length(cm)
0
5
10
15
20
25
30
0
10
20
30
40
50
60
70
80
90
● Data
R=1
R=2
R=3
R=4
R=5

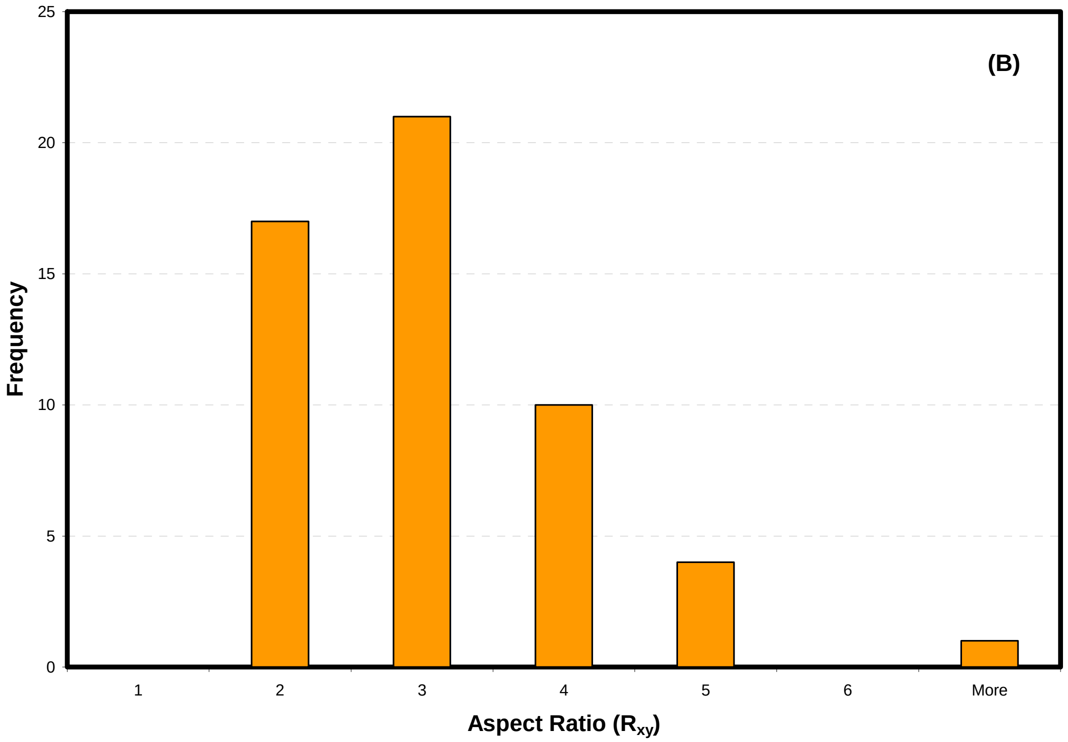
(B)
Frequency
Aspect Ratio (R_{xy})
0
5
10
15
20
25
1
2
3
4
5
6
More

Figure 8 (a) Simplified cross section across the metapelite complex showing the metamorphic zonations and respective structure zonations. (b) Calculated thermal gradient due to invasion of the Goat Ranch pluton, assuming the granitic magma temperature was ~800°C, and the far-field temperature of the pelite unit was about 450°C as suggested by the presence of andalusite in Zone 1. (c) Schematic diagram showing the increasing partial melting in the upper pelite unit with decreasing distance from the contact of the upper pelite unit and the Goat Ranch pluton. (d) Diagram showing the loading framework transition from the IWL structure (the weaker phase forms an interconnected weak matrix or layers separating boudins or clasts of the stronger phase) to the LBF structure (the stronger phase forms a load-bearing framework that contains pockets of the weaker phase) to with decreasing extent of partial melting.

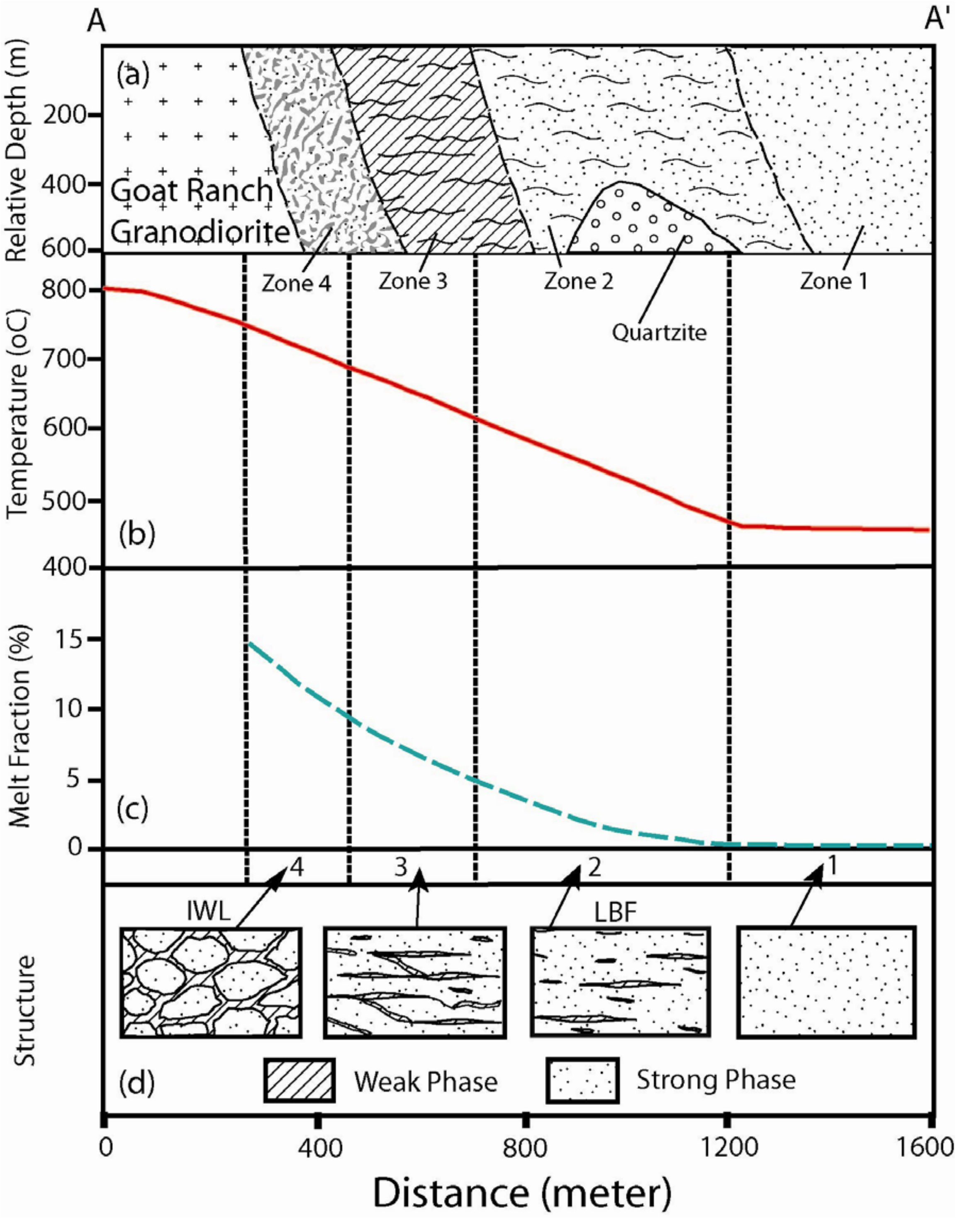
A
A'
(a)
Relative Depth (m)
200
400
600
Goat Ranch Granodiorite
Zone 4
Zone 3
Zone 2
Zone 1
Quartzite
Temperature (oC)
800
700
600
500
400
(b)
Melt Fraction (%)
15
10
5
0
(c)
4
3
2
1
IWL
LBF
Structure
(d)
Weak Phase
Strong Phase
0
400
800
1200
1600
Distance (meter)

Chapter 5

Partial melting of pelitic sources and the origin of leucogranite dikes in the Isabella pendant, southern Sierra Nevada, California

Lingsen Zeng and Jason B. Saleeby

Division of Geological and Planetary Sciences, California Institute of Technology,
Pasadena, CA 91125

Abstract

Crustal anatexis plays an important role in granitoid petrogenesis for it not only renders an important component for batholiths, but also acts as a potentially important contaminant during the ascent and emplacement of granitic magmas. Knowledge of the geochemical and isotopic nature of melts produced by crustal anatexis is thus required to better understand various components for granitic batholiths. In the major phases of Sierra Nevada arc magmatism between ~115 and 85 Ma, partial melting of metasedimentary pendants was widespread at relatively deep crustal levels. We have conducted a detailed Rb-Sr and Sm-Nd isotopic study on a suite of ~100 Ma leucogranite dikes which are hosted by the metasedimentary Isabella pendant, and samples from the bounding Rabbit Island, Rob Rabbit, and Heald Peak plutons. In order to assess potential metasedimentary component within these granitoids, we also analyzed samples from the metapelite units of the Kings Sequence which constitutes the Isabella pendant. The leucogranite dikes have $\varepsilon_{Nd}(T)$ (T=100 Ma) values ranging from -7.44 to -19.40, and $^{87}Sr/^{86}Sr(T)$ ratios from 0.70769 to 0.73974. The lower Mesozoic Kings sequence in the Isabella pendants is bounded stratigraphically by the lower (Triassic?) and upper (lower

to mid-Jurassic) pelite units. Each of them has distinctive Sr and Nd isotopic compositions. The lower pelite unit has $\varepsilon_{Nd}(T)$ values and $^{87}Sr/^{86}Sr(T)$ ratios ranging from -17.03 to -19.15, and 0.72674 to 0.75550, respectively. In contrast, the upper pelite unit has $\varepsilon_{Nd}(T)$ values and $^{87}Sr/^{86}Sr(T)$ ratios ranging from -8.50 to -11.31 and 0.71249 to 0.72208, respectively. Leucogranite dikes pervade the pendant cutting both pelite units as well as intervening quartzite and marble units. Based on their $^{87}Sr/^{86}Sr(T)$ and $\varepsilon_{Nd}(T)$ values, the leucogranite dikes can be subdivided into two groups. Group A leucogranite dikes have $^{87}Sr/^{86}Sr(T)$ and $\varepsilon_{Nd}(T)$ greater than 0.7300 and less than -12.0, while Group B dikes have $^{87}Sr/^{86}Sr(T)$ and $\varepsilon_{Nd}(T)$ less than 0.7300 and greater than -12.0, respectively. Both the lower and upper pelite units have Rb/Sr ratios ranging from 0.10 to 2.82. Six out of nine leucogranite dikes analyzed have Rb/Sr ratios greater than 2.0, contrasting with in situ leucosomes within the upper pelite which have Rb/Sr ratios less than 1.0. The leucogranite dikes having high Rb/Sr ratios (>2.0) reflect significant contributions from muscovite breakdown during the formation of such dikes. The higher the Rb/Sr ratio, the greater amount of muscovite must have entered the melt. Four leucogranite dikes have Rb/Sr>5.0 and $^{87}Sr/^{86}Sr(T)>0.7200$, suggestive of a derivation from a mica-rich source, possibly the Lower pelite. Based on similarities in Sr and Nd isotopic compositions of the different groups of leucogranite dikes and pelite units, we interpret Group A leucogranite to have been derived from the lower pelite unit and Group B from the upper pelite unit, respectively. The leucogranite dikes have Sm and Nd concentrations about an order of magnitude lower than those in the pelite units, and have higher Sm/Nd ratios (up to 0.45) than those in the pelite units. This suggests relative enrichments of Sm over Nd during partial melting, which also has been observed in situ leucosomes within the upper pelite. Sm/Nd ratios of the leucogranite dikes do not correlate with their Rb/Sr ratios, implying that the factors that control the Sm-Nd isotopic systematics during crustal anatexis are not the same as those that control the Rb-Sr isotopic systematics. A similar pattern is observed in the in situ leucosomes of the Upper pelite unit (Chapter 3). This observation demonstrates the decoupling of the Rb-Sr from Sm-Nd isotopic system during crustal anatexis due to difference in the melting/dissolution behavior of major rock-forming phases and accessory phases.

The Goat Ranch pluton has been shown to have been responsible for the partial melting of part of the upper pelite unit along its entire contact aurole (Chapter 2). The Isabella pendant is also cut by the Rabbit Island, Bob Rabbit and Heald peak plutons, but such migmatization in proximal wallrocks is not observed. It is interesting that in contrast to the Goat Ranch pluton, the Rabbit Island, Bob Rabbit and Heald peak plutons have high Rb/Sr ratios which suggest that they have higher amounts of crustal components than the Goat Ranch pluton. The Bob Rabbit pluton has the highest Rb/Sr, $^{87}Sr/^{86}Sr(T)$ but lowest $\varepsilon_{Nd}(T)$ among these four plutons. Its Sr and Nd isotopic compositions overlap with those of the upper pelite, which suggests that it might be derived completely from melting of the upper pelite or its equivalent in depth. Structural studies (Chapter 4; Saleeby and Zeng, in prep.) indicate tremendous amounts of vertical strain and differential transport within the Isabella pendant and its invading leucogranite dikes during the emplacement of the bounding plutons. Such transport patterns may explain why the leucogranite dikes, and the high-sediment component plutons cannot be readily correlated with the immediate hosting pendant rocks in terms of their geochemical tracers.

Introduction

Anatexis is commonly observed in high-grade metamorphic terrains, and considered as an important process to remobilize and redistribute heat-producing elements (e.g. U, Th and K), and rare-earth elements within the continental crust. Crustal anatexis in general involves a series of complicated fluid-present and fluid-absent melting reactions which can potentially fractionate parent-daughter elements of radiogenic isotopic systems, particularly Rb from Sr and Sm from Nd, as well as produce melts that are not in isotopic equilibrium with their protoliths (Whittington and Treloar, 2002; Knesel and Davidson, 2002; Ayres and Harris, 1997; Harris and Inger, 1992; Tommasini and Davies, 1997; Hammouda et al., 1996; Zeng et al., Chapter 3). In different tectonic settings, crustal anatexis may occur as a result of one or a combination of the following processes: (1) thermal effects induced by underthrusting of heat-producing element enriched continental crust in a collision zone (e.g., Himalaya) (Harrison et al., 1998; Inger and Harris, 1992; Patiño Douce et al., 1990); (2) thermal perturbations due to invasion of basaltic magma systems from a greater depth (Bergantz, 1989; Huppert and Sparks, 1988); (3) fluid-driven fluxed melting (Patiño Douce and Harris, 1998); and (4) decompression melting (Harris et al., 1994; Patiño Douce and Harris, 1998) in a rapidly exhumed high-grade metamorphic terrain.

In continental arc environments, the intrusion of batholiths into deep- to mid-crustal levels may also lead to anatexis in metasedimentary wall rocks. The degree of melt production of this type of anatexis is limited by the P-T conditions and the bulk and mineral compositions of the metasedimentary wall rocks. In this study, we present geochemical data on the crustal anatexis in labile protolith units of the metasedimentary pendants which underwent high-grade metamorphism and high-magnitude plastic strain during the emplacement of the mid-Cretaceous part of the southern Sierra Nevada batholith. During the major episode of Mesozoic Sierra Nevada batholith formation, spanning from ~125 to ~85 Ma (Evernden and Kistler, 1972; Chen and Moore, 1982; Saleeby et al., 1987), the invading plutons triggered widespread partial melting of metasedimentary pendants and formation of migmatitic complexes in the southern deeper level exposures of the batholith (Saleeby et al., 1987; Pickett and Saleeby, 1994; Zeng et al., 2003, Chapter 2 and 3). During their ascent, granitic batholiths are likely to partially assimilate wallrocks by incorporating wallrock-derived melts. Since melts derived from such metasedimentary sources bear distinctive geochemical and isotopic characteristics, they are potentially important contaminants in terms of rendering distinctive geochemical signatures. Knowledge of the isotopic characteristics of metasediment-derived melts is crucial to evaluate potential components and their relative contributions to individual granitic plutons as well as the composite batholith. To characterize the isotopic geochemistry of metasediment-derived melts, we have carried out a detailed Rb-Sr and Sm-Nd isotopic study on a suite of ~100 Ma leucogranite dikes which pervade the Isabella metasedimentary pendant; and samples from the Rabbit Island, Rob Rabbit, and Heald Peak plutons which bound the pendant; and metapelite units of the Kings Sequence which constitute the Isabella pendant. We intend to resolve (1) the isotopic characteristics of melts derived from metasedimentary protoliths; (2) the relationship between in situ leucosomes and cross-cutting leucogranite dikes; (3) the magnitude of parent-daughter fractionation (e.g., Sm from Nd); and (4) implications for the crustal contamination of granitic batholiths. We will first discuss isotopic compositions of two contrasting potential sources for the leucogranites, consisting of ca. 100 Ma granite-granodiorite plutons and pelite units of the hosting pendant. Secondly, we will present the Rb-Sr and Sm-Nd isotopic data for leucogranite dikes with integration of in situ leucosome data to illustrate the geochemical and isotopic consequences of non-modal partial melting of metasediments. Finally, we will interpret the data in terms of broader implications for the effects of elemental fractionation on the development of crustal geochemical heterogeneities.

Geologic setting and petrography

Figure 1 is a generalized geologic map of part of the Isabella pendant and its bounding plutons. In Chapter 2, we define the Goat Ranch pluton and the immediately adjacent Goat Ranch migmatite complex in the Isabella pendant. This igneous and high-grade metamorphic complex is located within the belt of the I-SCR plutons (strongly contaminated and reduced I-type) defined by Ague and Brimhall (1987 &1988). The metasedimentary framework rocks of the Isabella pendant consist of high-grade derivatives of quartz-rich clastic, muddy and calcareous, continental margin-type sedimentary assemblages with subordinate metavolcanic rocks (Saleeby, 1990; Saleeby and Busby, 1993). These are the southernmost known rocks of the Lower Mesozoic Kings Sequence, which forms a regional belt of wallrock pendants in the southern axial Sierra Nevada region. In the Goat Ranch area, south of the Lake Isabella, the Isabella pendant consists of Lower Triassic (?) psammitic-pelitic schist (lower pelite unit), Middle to Upper Triassic massive marble, Lower Jurassic thin and thick-bedded quartzite, metachert and quartz pebble-conglomerate, Lower Jurassic marble lenses, and Lower to

Middle Jurassic psammitic-pelitic schists (upper pelite unit). The metamorphic wallrocks of this region exhibit extreme syn-batholithic transposition into steep constrictional shape fabrics and map- to meso-scale sheath folds (Saleeby, 1990; Zeng and Saleeby, 2003a; Saleeby and Zeng, in prep). Due to such high strain, the stratigraphic thicknesses of the units that constitute the Isabella pendant are poorly constrained. The lower and upper pelite units have similar lithologic compositions and textures. Both metapelite units consist of andalusite/sillimanite, biotite, K-feldspar, quartz, muscovite and plagioclase. Except for the migmatite leucosomes in the upper pelite unit, the metamorphic texture of the metapelite units is penetratively schistose and/or gneissoise, reflecting a high degree of plastic strain during plutonism and metamorphism. They contain mafic metavolcanic lenses consisting of basaltic materials that were metamorphosed to thin amphibolite layers or lenses. In the proximity of the Goat Ranch granodiorite pluton, textures of the upper pelite unit are gneissic with well-developed migmatitic fabrics expressed by a structurally complex array of quartz-feldspar leucosomes and biotite-rich melanosomes, Many of these features are suggestive of the in situ production of partial melts and limited migration (Zeng et al., Chapter 3).

The Isabella pendant is intruded by a number of tourmaline-bearing leucogranite dikes. Leucogranite dikes of 0.5 meter to several meters thick were intruded into the lower and upper pelite and quartzite units, and locally in the Triassic marble unit of the Isabella pendant. They both cross-cut and are variably transposed with the foliation of the metapelites (Saleeby and Zeng, in prep.). They exhibit textures ranging from hypidiomorphic granular and pegmatitic with various degrees of plastic deformation to strongly mylonitic. Mesoscopic relations as well as U/Pb zircon data indicate that the high-strain fabrics developed at solidus to hot sub-solidus conditions (Saleeby and Zeng, in prep). Sample descriptions for which geochemical data are presented here are given in Table 1. All the leucogranite dikes analyzed in this study have a significant amount of tourmaline ranging from ~5 to ~15%. Field observations show that leucogranite dikes have similar mineral compositions to some of relatively thick leucosomes that gathered along the extension fractures in the upper pelite unit. U/Pb zircon ages on several of these leucogranite dikes (Saleeby and Zeng, in prep) indicate that they formed coeval with the adjacent Goat Ranch pluton which drove the partial melting in the upper pelite unit resulting in the formation of its migmatite zone.

The Bob Rabbit pluton mainly consists of quartz (~45%), K-feldspar (~40%), plagioclase (~6%), biotite (<5%) and muscovite (<2%), and oxides. Quartz aggregates show undulated extinction and weakly preferred orientation, suggesting it may have undergone syn-magmatism plastic deformation. The Bob Rabbit pluton occurs as a stock-like body bounding the Isabella pendant with a relatively sharp contact. The mineral composition of the Bob Rabbit pluton is similar to that of the leucogranite dikes. The Heald Peak pluton has quartz (~30%), K-feldspar (~40%), plagioclase (~25%), biotite (2%), muscovite (1%) and oxides. The Rabbit Island pluton consists of quartz (~35%), plagioclase (~35%), K-feldspar (~17%), biotite (~10%), mucovite (1%), and oxides (2%). All the samples from these plutons have trace amount of apatite and zircon which dominantly reside as inclusions within K-feldspar, plagioclase and quartz. The Goat Ranch granodiorite is composed of plagioclase, biotite, quartz, K-feldspar, minor amount of hornblende, and trace amount of zircon, rutile and apatite.

Sr and Nd isotopic compositions

We have conducted Sr and Nd bulk rock isotopic studies in order to characterize the isotopic compositions of the leucogranite dikes, and samples from the Rabbit Island, Rob Rabbit, and Heald Peak plutons, and the Lower pelite units. Radiogenic isotopic data from this study are integrated with data of the upper pelite unit and its leucosomes as well as the Goat Ranch pluton (Chapters 2 and 3) to assess the origin of the leucogranite dikes and adjacent leucogranite-like plutons. The analytical results are given in Table 2 and summarized in a series of plots (Fig 2 through 5). In all of the plots, symbol sizes are much larger than the analytical errors. The sample preparation techniques and analytical procedures used for the Rb-Sr and Sm-Nd isotopic analyses are those described by Pickett and Saleeby (1994) and Ducea and Saleeby (1998a & b). Calculations of initial Sr and Nd ratios were base on 100±2 Ma zircon ages measured on the Goat Ranch pluton, as well as several of the leucogranite dikes. In addition to the proximal thermal effects of the Goat Ranch intrusion, as manifested by the upper pelite migmatitic aureole, the entire Isabella pendant was under high-grade conditions at ca. 100 Ma. This is evident to the north of the study area where the lower pelite unit likewise has a migmatitic aureole where garnets in melanosomes yield ca. 100 Ma Sm-Nd ages adjacent to the Cyrus Flat pluton which yields a 100±3 Ma zircon age (Saleeby and Zeng, in prep). Likewise, the Rabbit Island intrusion has imparted a high-grade aureole along the eastern margin of the Isabella pendant at 100±2 Ma (Saleeby and Zeng, in prep.). In the internal areas of the Isabella pendant, it is impossible to distinguish the aureole of the Goat Ranch, Cyrus Flat and Rabbit Island intrusions.

The leucogranite dikes have Sm and Nd concentrations ranging from 0.5 to 3.4 ppm, and 1.6 to 19.0 ppm, respectively. The lower pelites have Sm and Nd concentrations ranging from 5.5 to 22.7 ppm, and 33.0 to 90.3 ppm, while Sm and Nd concentrations in the upper pelites range from 4.9 to 12.1, and 26.5 to 67.0 ppm, respectively. The leucogranites have Rb and Sr concentrations ranging from 61.0 to 329.4 ppm, and 11.2 to 339.8 ppm, respectively. The lower pelites have Rb and Sr concentrations ranging from 32.7 to 320.6 ppm, and 51.0 to 331.0 ppm. Rb and Sr concentrations in the upper pelites range from 74.9 to 273.8, and 47.8 to 254.7 ppm, respectively. The leucogranite dikes have $\varepsilon_{Nd}(T)$ ranging from -7.44 to -19.40, and $^{87}Sr/^{86}Sr(T)$ from 0.7077 to 0.7397. The lower pelites have $\varepsilon_{Nd}(T)$ and $^{87}Sr/^{86}Sr(T)$ ranging from -17.03 to -19.15, and 0.7267 to 0.7555, respectively. The upper pelite unit has $^{87}Sr/^{86}Sr(T)$ and $\varepsilon_{Nd}(T)$ ranging from 0.7125 to 0.7221, and -8.50 to -11.31, respectively. The Goat Ranch granodiorite has $^{87}Sr/^{86}Sr(T)$ ranging from 0.7061 to 0.7071, and $\varepsilon_{Nd}(T)$ from -1.1 to -6.5, with a average $^{87}Sr/^{86}Sr(T)$ and $\varepsilon_{Nd}(T)$ of 0.7070 and -4.01, respectively. As compared to that of the Goat Ranch pluton, the Rabbit Island, Rob Rabbit and Heald Peak plutons have higher Rb/Sr ratio up to 5.5. Among these plutons, the Bob Rabbit has highest $^{87}Sr/^{86}Sr(T)$ (0.7133) but lowest $\varepsilon_{Nd}(T)$ (-10.03), the Heald Peak has the lowest $^{87}Sr/^{86}Sr(T)$ (0.7059) but highest $\varepsilon_{Nd}(T)$ (-6.92), and the Rabbit Island has the intermediate values.

In summary, both Sm and Nd concentrations in the leucogranite dikes are about an order of magnitude lower than those in the upper and lower pelite units. The low concentrations of Sm and Nd in the dikes suggest that they may be LREE depleted. With regard to Sr and Nd isotopic compositions, the lower pelite is distinctive from the upper pelite (Fig. 2 & 3). The lower pelite distinguishes itself from the upper pelite by its more radiogenic Sr ($^{87}Sr/^{86}Sr(T) > 0.7200$) and nonradiogenic Nd ($\varepsilon_{Nd}(T) < -12.0$) isotopic compositions, which provides a basis to discuss the origin of these leucogranite dikes and the implications for the formation of plutons within the I-SCR zone. Based on their $^{87}Sr/^{86}Sr(T)$ and $\varepsilon_{Nd}(T)$ values, the leucogranite dikes can be subdivided into two groups. Group A leucogranites have $^{87}Sr/^{86}Sr(T)$ and $\varepsilon_{Nd}(T)$ values greater than 0.7300 and less than -12.0, respectively, while $^{87}Sr/^{86}Sr(T)$ and $\varepsilon_{Nd}(T)$ values of Group B leucogranites are less than 0.7300 and greater than -12.0, respectively. As shown in the Table 1, Group A and Group B leucogranite dikes are not associated with any particular stratigraphic units in this study area.

Discussion: Origin of leucogranite dikes

Leucogranite dikes are widespread in the Isabella pendant. Likely sources are the last fractionated magmas from the adjacent batholith or from the anatexis of metasedimentary units at a deeper level. It has been suggested that metasedimentary pendant-derived partial melts might be an important component for the Sierra Nevada batholith (DePaolo, 1980 & 1981; Saleeby et al., 1987; Allegre and Ben Othman, 1980; Hildreth and Moorbath, 1988, Ague and Brimhall, 1988). Thus if the leucogranite dikes that are so well developed in the Isabella pendant were derived from such a metasedimentary source, they may furnish insights into the geochemical and isotopic characteristics of such a potential component and provide constraints on the manner in which such a component may be introduced into the batholith. In the following section, we use Sr and Nd isotopic data as well as elemental concentration data to constrain the possible origin of the dikes.

Batholith derivation

Previous studies mainly based on field observations have suggested that these leucogranite dikes might represent magma bodies fractionated from the nearby intrusions (Saleeby, 1990). The Goat Ranch granodiorite has $^{87}Sr/^{86}Sr(T)$ ratios ranging from 0.7061 to 0.7071, and $\varepsilon_{Nd}(T)$ values from -1.1 to -6.5 (Zeng, et al., Chapter 2). The average Rb-Sr and Sm-Nd isotopic compositions of the Goat Ranch pluton are Rb = 73.9 ppm, Sr = 686.4 ppm, Rb/Sr = 0.1077, $^{87}Sr/^{86}Sr(T)$ = 0.7070, Sm = 4.7 ppm, Nd = 22.6 ppm, Sm/Nd = 0.2099, and $\varepsilon_{Nd}(T)$ = -4.01 (Table 2). To evaluate whether the leucogranite dikes were derived from a magma source similar to the Goat Ranch pluton, we have done simple end-member mixing calculations as shown in Figure 2. Except for sample 051203-LG which we will discuss in detail in the following section, simple mixing calculations show that it is unlikely that leucogranite dikes were derived directly from the magma that produced the Goat Ranch granodiorite (Fig. 2).

Leucogranite dike sample 051203-LG was emplaced into the lower pelite unit. It has the lowest $^{87}Sr/^{86}Sr(T)$ ratio of 0.70769, and relatively high $\varepsilon_{Nd}(T)$ value of -7.94, as compared to the other leucogranite dikes. Its Sr and Nd isotopic compositions are similar to those of the Goat Ranch, Rabbit Island, and Heald Peak plutons. This dike may have been derived directly from the Goat Ranch granodiorite with only ~10% contamination by its lower pelite host (Fig. 2). But its Sr and Nd concentrations are too low to reconcile with simple mixing of a Goat Ranch granodioritic melt with melts derived from the lower pelite. Sr and Nd concentrations in this dike are 38.1 and 3.4 ppm, respectively, which are much lower than 686 and 23 ppm of average Sr and Nd concentrations of the Goat Ranch pluton, 234.7 and 20.6 ppm of the Rabbit Island, as well as those of the lower and upper pelite unit (Table 2). The possibility that this dike can be produced by the mixing of magmas from either the Goat Ranch or the Rabbit Island pluton with bulk melts from the upper or the lower pelite unit can thus be ruled out. Moreover, this dike has high Rb/Sr ratio of 3.37, similar to that of the Heald Peak (Table 2), which may suggest that it has likely been derived from the same magma source that formed the Heald Peak pluton. However, the lower Sr concentration of this particular dike by a factor of three than that of the Heald Peak pluton requires another source component with a much lower Sr concentration but a higher $^{87}Sr/^{86}Sr(T)$ ratio. Only a component with high Rb/Sr ratio, similar to the melts derived from muscovite or biotite dehydration melting of either the lower or the upper pelite can satisfy this requirement. Simple mixing calculations by taking the Heald Peak as well as those leucogranite dikes with Sr concentration lower than 38.0 ppm as end-members indicate that this dike can be generated by mixing 15 to 25 % of magmas from the Heald Peak with 85 to 75% melts from either the upper pelite or the lower pelite units. Even for this dike having such a low $^{87}Sr/^{86}Sr(T)$ ratio, high fractions of metasediment-derived melts are required for its generation.

Anatexis of metasedimentary pendants

If the leucogranite dikes of the Isabella pendant were not derived from magma sources similar to the Goat Ranch, Rabbit Island or Heald Peak plutons, then both the lower and upper pelite units or their equivalents at depth, may be the potential sources, given their relatively high fertility. Both the lower and upper pelite units contain

Proterozoic continental material, as shown by Nd model ages and U/Pb zircon data (Saleeby et al., 1987; Pickett and Saleeby, 1994). The Sample CM640 analyzed by Pickett and Saleeby (1994) is collected from a King Sequence-like metasedimentary pendant to the south of this study area, and has $^{87}Sr/^{86}Sr(T)$ and $\varepsilon_{Nd}(T)$ of 0.72355 and -16.5, respectively, which are similar to those of the Lower pelite unit from this study. Though both pelite units have similar lithologic compositions, the differences in their ages and amounts of recycled continental basement materials lead to their distinctive Sr and Nd isotopic compositions (Fig. 2 and 3). Thus, melts derived from these two pelite units would have similar lithologic compositions but would bear distinctive Sr and Nd isotopic compositions.

In contrast to the leucosomes of the upper pelite unit which have Rb/Sr ratios less than 1.0, six out of nine leucogranite dikes analyzed have Rb/Sr ratios greater than 2.0 (Fig. 4a). The other three leucogranite dikes have Rb/Sr ratios less than 1.0, which are similar to the leucosomes within the Upper pelite unit. The lower pelite unit has Rb/Sr ratios between 0.10 and 2.82. The upper pelite unit has Rb/Sr ratios ranging from 0.36 to 3.01. The wide range of Rb/Sr ratios for the metapelites indicates: (1) a non-uniform distribution of primary Rb and Sr bearing phases (muscovite + biotite vs. plagioclase + K-feldspar); (2) variations in protolith lithology (pelite vs. psammite); or (3) different degrees of volcanic inputs. Two types of partial melting reactions are relevant to the formation of the leucogranite dikes in the study area: (1) H_2O-fluxing partial melting and (2) muscovite or biotite dehydration partial melting of muscovite bearing metapelites, which is also suggested by the major and trace element, and Sr and Nd isotopic geochemistry data of the leucosomes (Zeng et al., Chapter 3). Each melting reaction generates melts with distinctive Rb and Sr geochemical signatures. In general, H_2O-fluxing partial melting results in melts of low Rb but high Sr concentrations, and relatively low Rb/Sr and initial $^{87}Sr/^{86}Sr$ ratios. In contrast, muscovite or biotite dehydration partial melting produces melts of high Rb but low Sr concentrations, and thus high Rb/Sr and initial $^{87}Sr/^{86}Sr$ ratios (Harris and Inger, 1992; Knesel and Davidson, 2002), due to the higher proportion of Rb-bearing phases relative to Sr-bearing phases entering a melt. For a metasedimentary rock that contains muscovite, biotite, quartz, K-feldspar, plagioclase, and aluminosilicate, muscovite and biotite are the dominant hosts of Rb, and have Rb/Sr ratios greater than 1.0. For fluid-absent melting of a metapelite source that involves either muscovite or biotite dehydration reaction, melts generally will have Rb/Sr ratios in the range of 3.0 to 6.0 (Harris and Inger, 1992). This suggests that leucogranite dikes with high Rb/Sr ratios (>2.0) have significant contributions from muscovite/biotite dehydration melting (Fig. 3b). The higher the Rb/Sr ratio, the higher the amount of muscovite or biotite involved. Four leucogranite dikes (TPLG01, 1027LG01, 1027LG02, and 1027LG03) have high Rb/Sr (>5.0) and $^{87}Sr/^{86}Sr(T)$ (>0.720), also suggestive of a derivation from a mica-rich source. Field and petrographic observations show that: (1) both pelite units have large amounts of biotite (>35%); (2) biotite occurs as a residue phase during muscovite dehydration partial melting during the formation of leucosomes; and (3) garnet is generally absent in the metapelite (except for sample PNGT01) and the migmatite complex. The sample PNGT01 was collected from the Lower pelite unit near its contact with the Cyrus Flat pluton. In this particular location, abundant garnets occur both in the lower pelite and the Cyrus Flat pluton within the immediate proximity of the contact. Because garnet is a common residue phase of biotite dehydration melting under either fluid-present or fluid-absent conditions (Vielzeuf and Holloway, 1988; Clemens and Vielzeuf, 1987; Spear et al., 1999; Patiño Douce and Harris, 1998), the absence of garnet suggests that biotite dehydration melting reaction played an insignificant role during anatexis of the Isabella pendant. We, therefore, suggest that muscovite dehydration partial melting of either the lower or upper pelite unit resulted in the leucogranite dikes with high Rb/Sr ratios (>2.0). In this case, the Rb/Sr ratio also can be an indicative of degree of melting. The leucogranite dikes with Rb/Sr ratios less than 1.0 might have formed from similar melting reactions (H_2O-fluxing partial melting of quartz + plagioclase assemblage) as the leucosomes in the migmatite zone of the upper pelite unit. The leucosomes are interpreted to have formed from partial melting of the upper pelite without significant muscovite breakdown (Zeng, et al., Chapter 3).

Group A leucogranite dikes have wide range of $\varepsilon_{Nd}(T)$ values from -12.9 to -19.4 and limited variations in $^{87}Sr/^{86}Sr(T)$ ratios ranging from 0.73056 to 0.73974. Because they have much more radiogenic Sr isotopic compositions than those of the upper pelite (<0.7200) (Fig. 2 and 3), the most likely source is the lower pelite or its equivalents at a greater depth. Group B leucogranite dikes have similar range of $^{87}Sr/^{86}Sr(T)$ and $\varepsilon_{Nd}(T)$ to those of the upper pelite and its derivative-leucosomes (Fig. 2 and 3), and thus may be produced by partial melting of the upper pelite.

Leucogranite dike sample 051303LG which intruded the upper pelite unit has lower $\varepsilon_{Nd}(T)$ (-15.67) and higher $^{87}Sr/^{86}Sr(T)$ (0.7391), as compared to the host pelite having $\varepsilon_{Nd}(T) > -11.31$ and $^{87}Sr/^{86}Sr(T) < 0.7221$, respectively. This suggests that this particular leucogranite dike could not be derived from partial melting of its upper pelite host. The most reasonable source would be the lower pelite unit. Those dikes within the upper pelite unit and having higher $\varepsilon_{Nd}(T)$ values than -12.0 may have been derived from the partial melting of the upper pelite unit with only limited migration. These dikes have similar Nd and Sr isotopic compositions to the in situ leucosomes derived from melting of the upper pelite.

These leucogranite dikes contain high amount of tourmaline (Table 1), which indicates that they are Boron-rich or –saturated. Generally, Boron is strongly partitioned into the fluid phases during water-rock interactions such that extensive leaching and redistribution of B is likely at temperatures >150°C (Leeman and Sisson, 1996; Henry and Dutrow, 1996). Dehydration reactions can strongly lead to B loss in metamorphic rocks and thus greatly elevate B concentrations in the metasediment-derived melts. High contents of tourmaline (up to ~15%) in these leucogranite dikes are also consistent with derivation from dehydration partial melting of mica-rich metapelites.

The sample analyzed from the Bob Rabbit pluton has Rb/Sr = 5.5, $^{87}Sr/^{86}Sr(T)$ = 0.7133, Sm/Nd = 0.27, and $\varepsilon_{Nd}(T)$ = -10.06. As compared to other rock types analyzed in this study, it has: (1) Sr and Nd isotopic compositions similar to the upper pelite (Fig. 3); (2) a high Rb/Sr ratio, similar to those leucogranite dikes with high Rb/Sr ratios (Fig. 4); and (3) a Sm/Nd ratio similar to those of leucogranite dikes and the Group A leucosomes (Fig. 5). These observations suggest that the Bob Rabbit pluton represents a relatively large-scale plutonic body formed by anatexis of metasedimentary sources. This finding also suggests that within the belt of the I-SCR plutons degrees of crustal contaminations vary from pluton to pluton. For example, the Goat Ranch pluton has minor contaminations by the nearly Isabella pendant rocks (Zeng et al., Chapter 2), whereas the Bob Rabbit pluton may have 100% crustal contributions.

The Sm/Nd and Rb/Sr as well as the Nd and Sr isotopic data on the leucogranite dikes as well as the migmatite complex reveal a melting reaction controlled decoupling of these systems. The leucogranite dikes have Sm/Nd ratios ranging from 0.22 to 0.45. The lower pelite has Sm/Nd ratios ranging from 0.17 to 0.25, with an average value of 0.20, while the upper pelite has limited variations in Sm/Nd ratios ranging from 0.16 to 0.19, with an average value of 0.18. This value is close to the average Sm/Nd ratio of 0.17 for the upper continental crust (Taylor and McLennan, 1985). The leucogranite dikes, except for sample 1154b, have higher Sm/Nd ratios (up to 0.45) than their hypothetical source rocks (the upper and lower pelite), suggesting relative Sm enrichments over Nd during partial melting (Fig. 5a). This feature also has been observed in the leucosomes (Fig. 5b). Sm/Nd ratios of the leucogranite dikes do not correlate with their Rb/Sr ratios, implying that the factors that control the geochemical behavior of the Sm-Nd isotopic system during crustal anatexis are different from those for the Rb-Sr system. The Rb-Sr isotopic systematics in the metapelite-derived melts is controlled by major rock-forming phases (muscovite + biotite vs. plagioclase + K-feldspar) involved in melting reactions. The Rb/Sr ratios of the melts are indices of the extent of muscovite/biotite involvement in partial melting. In contrast**,** the Sm and Nd budget of the melt and residue in a non-modal crustal anatexis are dominated by dissolution of accessory minerals such as apatite and monazite, due to their high concentrations of Sm and Nd. Therefore, it is quite possible that the Sm-Nd and Rb-Sr isotopic systems are decoupled in a crustal anatexis event. The magnitude of the decoupling depends on (1) extent of partial melting, (2) amount of accessory minerals entrained as restites, (3) rate of melt segregation (Watt and Harley, 1993; Sawyer, 1991; Watt et al., 1996).

In summary, all the dikes in this study area were derived from non-modal partial melting of either the lower pelite or the upper pelite unit or their equivalents at greater depths. The Bob Rabbit pluton represents a large-scale magma body derived from a similar source. The leucogranite dikes can be subdivided into two groups based on the Sr and Nd isotopic compositions. However, Group A and Group B leucogranite dikes do not correlated with any particular stratigraphic units of the Isabella pendant, which suggest significant vertical transport under high magnitude of strain during emplacement of those bounding plutons. The structural setting of the Bob Rabbit pluton as a stock-like body bounding the Isabella pendant with a relatively sharp contact indicates the melting of a pelite source and the ascent of its melt from a distinctly deeper crustal level than that of the Isabella pendant pelite units and its migmatite zone. Considering the high degree of vertical strain that the Isabella pendant as well as its in situ leucosomes and more mobile leucogranite dikes underwent during the emplacement of the adjacent plutons (Chapter 4; Saleeby and Zeng, in prep.), the Bob Rabbit pluton could have been derived from the upper pelite unit where it was deformed at a deeper structural level relative to the modern exposure level.

Conclusions

We have presented Sr and Nd isotopic composition data for samples from the Rabbit Island, Heald Peak and Bob Rabbit plutons, and a suite of leucogranite dikes, metapelites, and in situ leucosomes from the migmatitic pelite of the Lake Isabella pendant. These data show that:

1. Leucogranite dikes have ε_{Nd}(T) values ranging from -7.44 to -19.40, and ^{87}Sr/^{86}Sr(T) ratios from 0.70769 to 0.73974.
2. The lower pelite unit has distinctive Sr and Nd isotopic compositions from the upper pelite unit. The Lower pelite unite has ε_{Nd}(T) values and ^{87}Sr/^{86}Sr(T) ratios ranging from -17.03 to -19.15, and 0.72674 to 0.75550, respectively. In comparison, the upper pelites have ^{87}Sr/^{86}Sr(T) and ε_{Nd}(T) ranging from 0.7125 to 0.7221, and -8.50 to -11.31, respectively.
3. Based on their ^{87}Sr/^{86}Sr(T) and ε_{Nd}(T) values, the leucogranite dikes can be subdivided into two groups. Group A has ^{87}Sr/^{86}Sr(T) and ε_{Nd}(T) values greater than 0.7300 and less than -12.0, while Group B has ^{87}Sr/^{86}Sr(T) and ε_{Nd}(T) values less than 0.7300 and greater than -12.0, respectively.
4. Based on their similarities in Sr and Nd isotopic compositions, we interpret Group A leucogranite dikes to have been derived from the lower pelite, while Group B dikes from the upper pelite unit.
5. Both Sm and Nd concentrations in the leucogranite dikes are approximately an order of magnitude lower than those in the upper pelite and lower pelite. The leucogranite dikes, except for sample 1154b, have higher Sm/Nd ratios (up to 0.45) than their hypothetical source rocks (the upper and lower pelite units), suggesting relative Sm enrichments over Nd during partial melting.
6. Fractionation of Sm from Nd by dissolution of accessory phases during crustal anatexis may result in the decoupling of this system from the Rb-Sr isotopic system. Decoupling of the Rb-Sr from the Sm-Nd isotopic system has profound

consequences on the Sr-Nd systematics of those granitic batholiths with significant crustal components.

7. The Bob Rabbit pluton represents an extreme case of crustal derived leucogranite plutons within the belt of the I-SCR plutons. Degrees of mid- to shallow-level crustal contamination within this particular zone may vary pluton from pluton. Some may have negligible contributions from nearby metasedimentary wallrocks, the others may have high magnitude of contributions from wallrock-derived melts.
8. The structural setting of the Bob Rabbit pluton as a stock-like body bounding the Isabella pendant with a relatively sharp contact indicates the melting of a pelite source and the ascent of its melt from a distinctly deeper crustal level than that of the Isabella pendant pelite units and its migmatite zone. Considering the high degree of vertical strain that the Isabella pendant as well as its in situ leucosomes and more mobile leucogranite dikes underwent during the emplacement of the adjacent plutons (Zeng and Saleeby, Chapter 4; Saleeby and Zeng, in prep.), the Bob Rabbit pluton could have been derived from the upper pelite unit when it was deformed at a deeper structural level relative to the modern exposure level.

Table 1. Leucogranite dike sample descriptions.

Sample	**Host-unit**	**Mineralogy**	**Petrography Notes**
1027LG01	Quartzite	Q+Pl+Kf+Tur+Mus+Il+Ep	~10-15% tourmaline uniformly distribute as small needle-like crystals
1027LG02	Quartzite	Q+Kf+Pl+Mus+Tur	Tourmaline locally concentrated as small pockets
1027LG03	Quartzite	Q+Kf+Pl+Mus+Tur+il+ep	Coarse quartz and K-feldspar, Tourmaline up to 8%. Grain size up to 0.5 cm and occur as clusters.
TPLG-01	Lower Pelite	Q+Pl+Kf+Mus+Tur+Il	~10% Tourmaline uniformly distribute as tiny crystals
TPLG-02	Lower Pelite	Q+ Kf +Pl+Tur+Mus	Up to ~`10% Tourmaline non-uniformly distribute as clusters
051101LG	Upper pelite	Q+Kf+Pl+Mus+Tur	Tourmaline less than 3%
051203LG	Lower Pelite	Q+ Kf +Pl+ Mus+Tur	About 5% tourmaline
051303LG	Upper pelite	Q+Pl+Kf+Tur+Mus+Gt	About 5% tourmaline non-uniformly distribute as clusters
1154b	Upper pelite	Q+Kf+Pl+Mus+Tur	About 6% tourmaline

Q: quartz, Kf: K-feldspar, Pl: plagioclase, Mus: muscovite, Tur: tourmaline, Ilm: Illmenite, Ep: Epidote, Gt: Garnet.

Table 2. Rb-Sr and Sm-Nd isotopic compositions of leucogranite dikes, the Rabbit Island, Rob Rabbit and Heald Peak plutons, lower pelite and upper pelite units, and leucosomes in the upper pelite unit from the Lake Isabella area, southern Sierra Nevada, California.

Sample	Rock-type	Rb(ppm)	Sr(ppm)	^{87}Rb/^{86}Sr	^{87}Sr/^{86}Sr	^{87}Sr/^{86}Sr(T)	Sm(ppm)	Nd(ppm)	^{147}Sm/^{144}Nd	^{143}Nd/^{144}Nd	ε_{Nd}(T)	Source
TPLG01	Leucogranite	145.71	23.99	17.5263	0.744997	0.720092	0.54	1.72	0.1892	0.512252	-7.44	1
TPLG02	Leucogranite	61.00	143.08	1.2295	0.736268	0.734521	1.30	4.66	0.1685	0.511796	-16.08	1
1027LG01	Leucogranite	329.40	11.16	86.1400	0.862150	0.739743	0.96	2.12	0.2736	0.512027	-12.90	1
1027LG02	Leucogranite	206.77	33.99	17.5810	0.759798	0.734816	0.78	2.23	0.2108	0.511653	-19.40	1
1027LG03	Leucogranite	195.21	38.60	14.6045	0.751313	0.730560	0.71	1.66	0.2574	0.511858	-15.99	1
051101-LG	Leucogranite	119.34	339.76	1.0105	0.712313	0.710878	1.92	8.54	0.1357	0.512174	-8.28	1
051203-LG	Leucogranite	128.38	38.05	9.7150	0.721493	0.707688	0.96	3.40	0.1700	0.512214	-7.94	1
051303-LG	Leucogranite	140.44	56.86	7.1316	0.749217	0.739083	0.48	1.61	0.1805	0.511824	-15.67	1
1154b	Leucogranite	125.66	152.46	2.3719	0.715235	0.711864	3.38	18.96	0.1079	0.512189	-7.63	1
051203-P	T-pelite	142.17	76.55	5.3635	0.751938	0.744316	5.49	32.96	0.1006	0.511702	-17.03	1
PNGt01	T-pelite	32.65	331.03	0.2846	0.745982	0.745577	22.74	90.31	0.1522	0.511723	-17.29	1
TP01	T-pelite	320.62	122.63	7.5404	0.737455	0.726740	9.56	49.96	0.1156	0.511603	-19.15	1
TP02	T-pelite	144.00	51.02	8.1629	0.767095	0.755495	12.08	67.03	0.1089	0.511686	-17.45	1
Li98/5	J-pelite	74.90	190.10	1.1334	0.716645	0.715034	8.37	47.52	0.1064	0.512143	-8.50	1
Li98/8	J-pelite	90.80	254.70	1.0255	0.716636	0.715178	7.83	42.89	0.1103	0.512142	-8.57	2
Li98/10-11	J-pelite	153.10	247.20	1.7831	0.718446	0.715912	9.51	52.30	0.1100	0.512088	-9.62	2
Li98/13	J-pelite	88.00	92.30	2.7484	0.721861	0.717956	4.89	26.48	0.1171	0.512137	-8.69	2
Li98/15	J-pelite	163.70	143.70	3.2790	0.717148	0.712489	7.48	47.72	0.0947	0.511992	-11.31	2
Li98/16	J-pelite	172.10	57.20	8.6757	0.729700	0.717372	8.20	47.39	0.1046	0.512056	-10.19	2
PP0101	J-pelite	175.65	103.56	4.8844	0.722352	0.715412	8.96	42.66	0.1270	0.512118	-9.26	2
PS0101	J-pelite	108.39	69.21	4.5123	0.728495	0.722083	8.06	41.11	0.1185	0.512081	-9.87	2
L0404	Leucosome	12.34	267.17	0.1394	0.712585	0.712397	1.63	10.45	0.0939	0.512006	-11.03	2
L0405	Leucosome	15.46	260.32	0.1709	0.714695	0.714452	3.08	27.69	0.0670	0.512009	-10.62	2
L0406	Leucosome	101.26	675.07	0.4286	0.716931	0.716322	2.99	10.31	0.1745	0.512291	-6.50	2
L0407	Leucosome	134.58	311.01	1.2469	0.717532	0.715761	3.39	10.22	0.1996	0.512334	-5.98	2
L0410	Leucosome	126.13	263.71	1.3780	0.726609	0.724651	6.26	27.01	0.1395	0.512243	-6.98	2
L0408	Leucosome	12.40	441.53	0.0848	0.710725	0.710588	3.26	12.98	0.1517	0.512100	-9.93	1
Goat Ranch	Granodiorite	73.90	686.39	0.3497	0.707508	0.707011	4.72	22.59	0.1279	0.512388	-4.01	3
97SS4B	Bob Rabbit	255.79	46.87	15.7365	0.735649	0.713287	3.63	13.71	0.1603	0.512098	-10.06	1
00SS5	Heald Peak	283.56	120.76	6.7571	0.715523	0.705921	0.82	16.14	0.0307	0.512175	-6.92	1
03SS7	Rabit Island	146.48	234.71	1.7952	0.710738	0.708187	2.64	20.55	0.0777	0.512186	-7.29	1

1. Data sources: 1- this study; 2- Zeng et al. (2003a); 3- Zeng et al. (2003b). T-pelite = lower Pelite, J-pelite = upper pelite.
2. The average Sr and Nd isotopic compositions of the Goat Ranch granodiorite is calculated based on the data of Zeng et al. (2003b).
3. The Nd and Sr measurements were corrected for mass fractionation by normalization to ^{146}Nd/^{142}Nd = 0.63615, and ^{86}Sr/^{88}Sr = 0.1194. External precisions during this period of measurement for Sr and Nd isotopic compositions are ±0.000013 (n=25), and ± 0.000017(n=25), respectively. ^{87}Sr/^{86}Sr for the NBS987 standard is 0.710252, and ^{143}Nd/^{144}Nd for La Jolla Nd standard 0.511859.
4. ε_{Nd}(T) is Calculated at T= 100 Ma using the equation:

   $$\varepsilon_{Nd}(t) = \left[\frac{({}^{143}Nd/{}^{144}Nd)_{sample}(t)}{({}^{143}Nd/{}^{144}Nd)_{CHUR}(t)} - 1 \right] \times 10^4$$

   and $({}^{143}Nd/{}^{144}Nd)_{CHUR}(0) = 0.512635$ and $({}^{147}Sm/{}^{144}Nd)_{CHUR}(0) = 0.1966$.

Figure 1 Generalized geologic map of the Lake Isabella area, southern Sierra Nevada, California. It shows the location of the leucogranite dike samples, samples from the Rabbit Island (Kri), Heald Peak (Khp), and Bob Rabbit (Kbr) plutons, and the lower pelite unit.

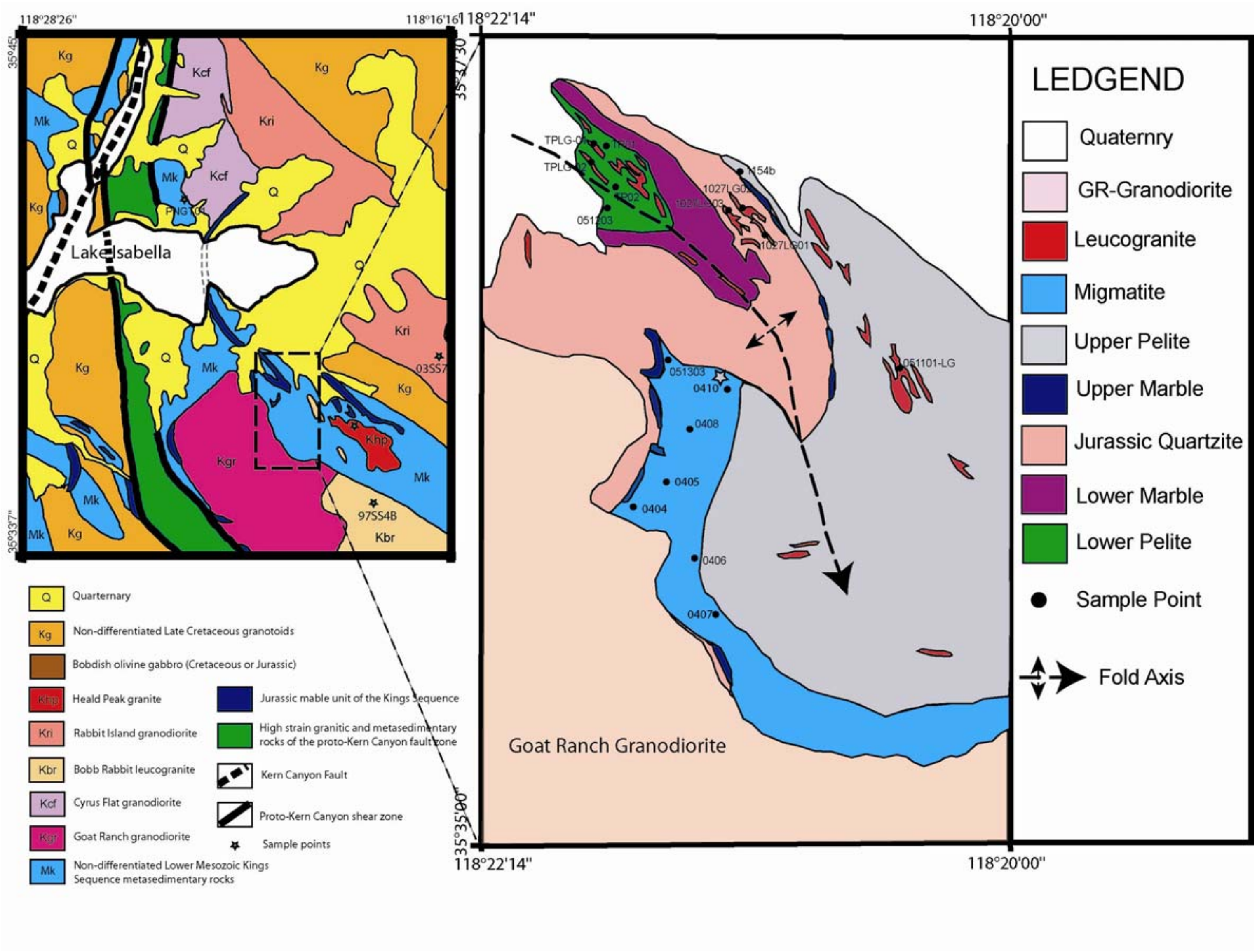
118°28'26"
118°16'16"
35°45'
35°33'7"
Kg
Kcf
Kri
Mk
Q
PNGT06
Lake Isabella
Kri
03SS7
Kg
Khp
Kgr
Mk
97SS4B
Kbr
Q Quarternary
Kg Non-differentiated Late Cretaceous granotoids
Bobdish olivine gabbro (Cretaceous or Jurassic)
Khp Heald Peak granite
Kri Rabbit Island granodiorite
Kbr Bobb Rabbit leucogranite
Kcf Cyrus Flat granodiorite
Kgr Goat Ranch granodiorite
Mk Non-differentiated Lower Mesozoic Kings Sequence metasedimentary rocks
Jurassic mable unit of the Kings Sequence
High strain granitic and metasedimentary rocks of the proto-Kern Canyon fault zone
Kern Canyon Fault
Proto-Kern Canyon shear zone
Sample points
118°22'14"
118°20'00"
35°37'30"
35°35'00"
TPLG-01
TP01
TPLG-02
TP02
051203
1154b
1027LG02
1027LG03
1027LG01
051101-LG
051303
0410
0408
0405
0404
0406
0407
Goat Ranch Granodiorite
LEDGEND
Quaternry
GR-Granodiorite
Leucogranite
Migmatite
Upper Pelite
Upper Marble
Jurassic Quartzite
Lower Marble
Lower Pelite
Sample Point
Fold Axis

Figure 2 Sr-Nd systematics plot showing Sr and Nd isotopic compositions of the leucogranite dikes, lower and upper pelite units, leucosomes within the upper pelite, , and samples from nearby plutons, together with the average Sr and Nd compositions of the Goat Ranch pluton. Leucogranites can be subdivided into two groups. Group A leucogranites have $^{87}Sr/^{86}Sr(T)$ and $\varepsilon_{Nd}(T)$ values greater than 0.7300 and less than -12.0, while $^{87}Sr/^{86}Sr(T)$ and $\varepsilon_{Nd}(T)$ values of Group B leucogranites are less than 0.7300 and greater than -12.0, respectively. Taking the Goat Ranch granodiorite as a common end member, the other end members chosen for simple mixing calculation of A, B, C, and D are sample TP01, TP02, Li98/15 and Li98/13, respectively. These mixing calculations suggest that most of the leucogranite dikes can not be produced by simply direct mixing of melts from a similar source to the Goat Ranch pluton with contaminants from either the lower pelite or the upper pelite. Instead, their Nd and Sr isotopic characteristics suggest that they are principally melts from the pelite units or equivalents located at greater depths. The leucosome and part of the upper pelite data are from Zeng et al (2003b and c). The symbol sizes are much larger than the analytical errors. T=100 Ma.

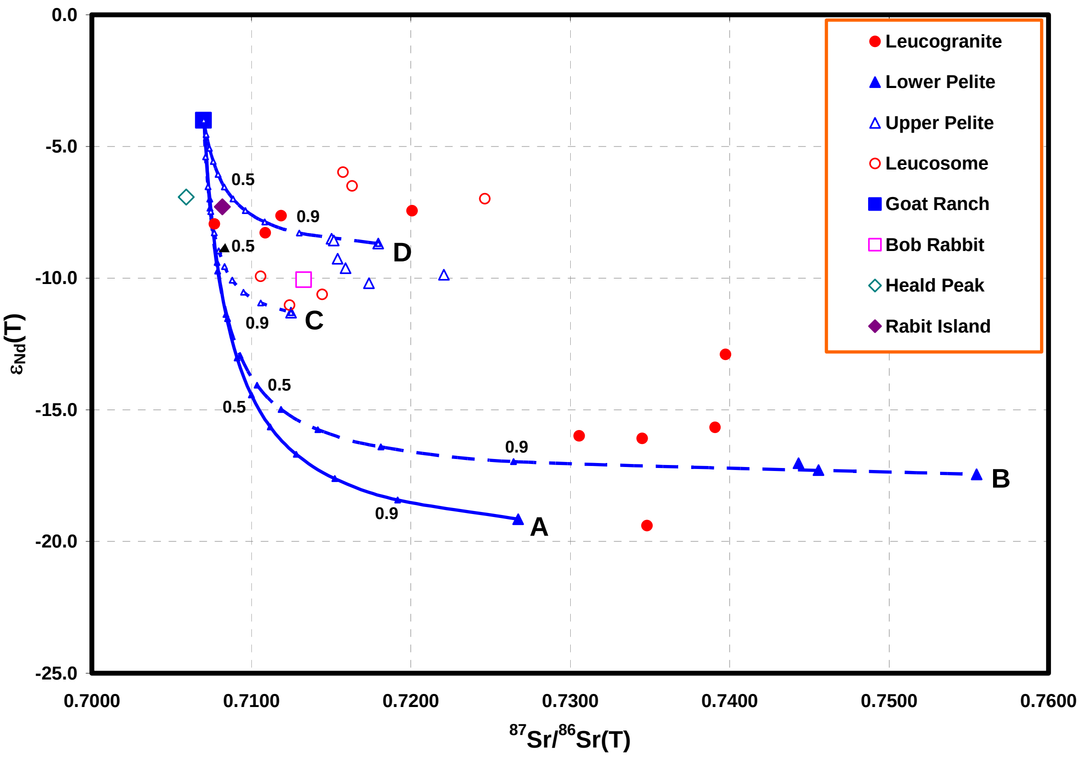

0.0
-5.0
-10.0
-15.0
-20.0
-25.0
0.7000
0.7100
0.7200
0.7300
0.7400
0.7500
0.7600
^{87}Sr/^{86}Sr(T)
ε_{Nd}(T)
● Leucogranite
▲ Lower Pelite
△ Upper Pelite
○ Leucosome
■ Goat Ranch
□ Bob Rabbit
◇ Heald Peak
◆ Rabit Island
0.5
0.9
D
0.5
0.9
C
0.5
0.5
0.9
B
0.9
A

Figure 3 Diagrams showing the range of (A) Sr and (B) Nd initial isotopic compositions for each group of rock types discussed in this study. LG-A: Group A leucogranite dikes; LG-B: Group B leucogranite dikes; TP: lower pelite unit; JP: upper pelite unit; LS-A: Group A leucosomes; LS-B: Group B leucosomes; GRg: Goat Ranch granodiorite; RI: Rabbit Island granodiorite; HP: Heald Peak pluton; BR: Bob Rabbit pluton. T = 100 Ma.

Figure 3A

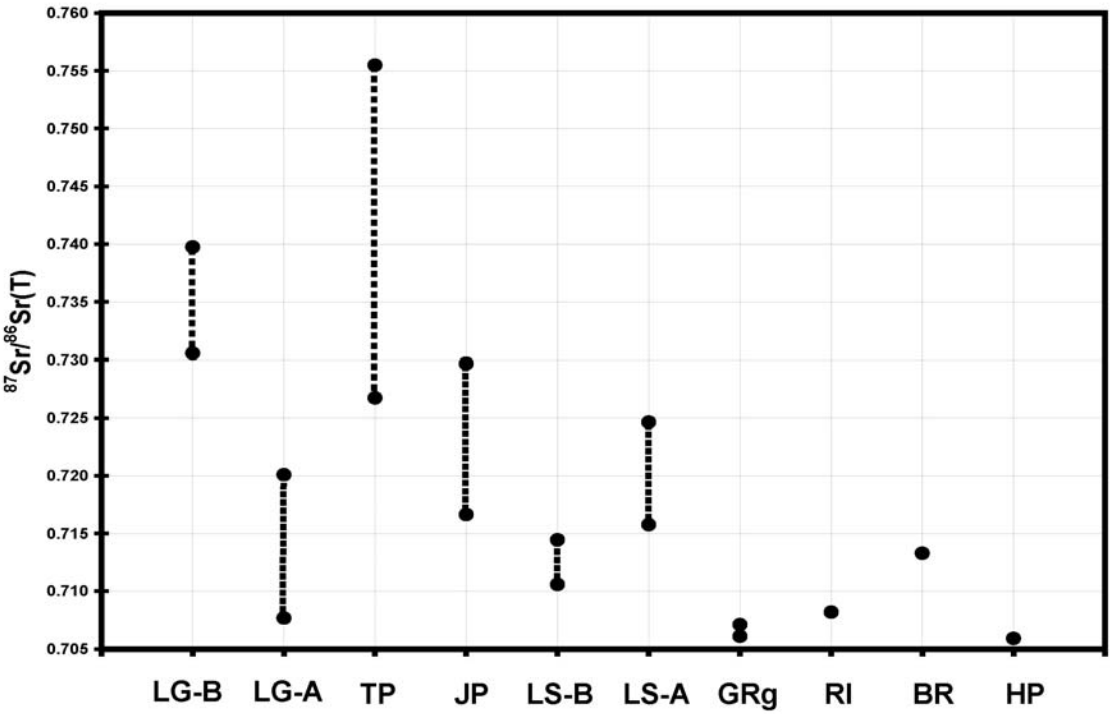

Figure 3B

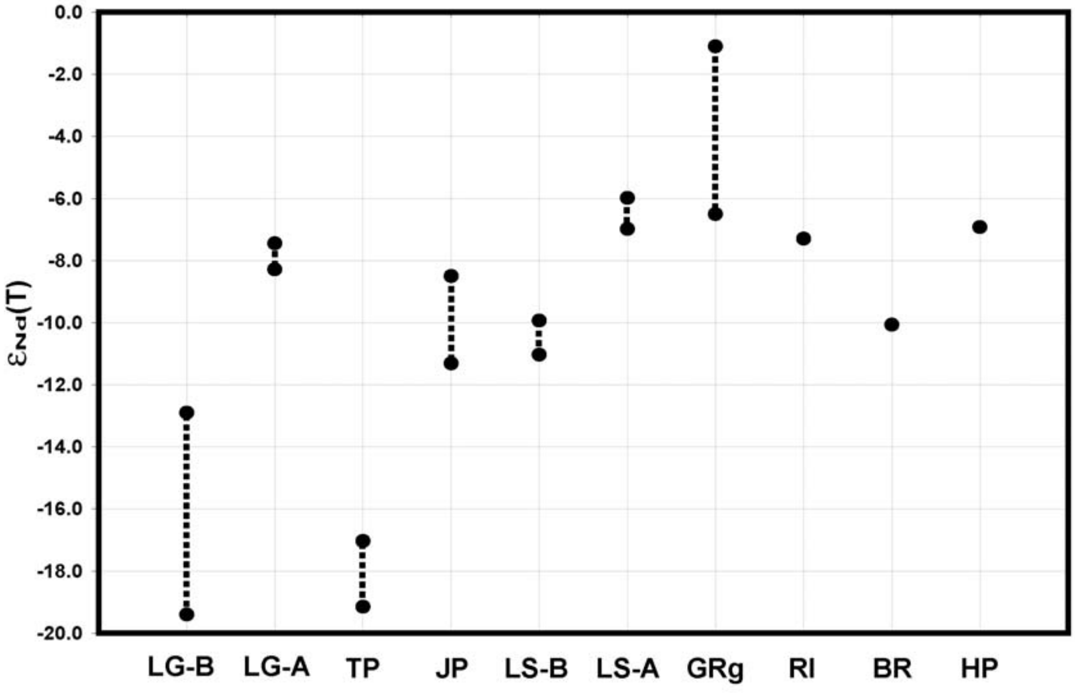

Figure 4 (A) Plot of Sr concentrations in the leucogranite dikes and leucosomes against their Rb concentrations. All the leucosomes have Rb/Sr ratios less than 1.0. Except for two leucogranite dikes that have Rb/Sr ratios less than 1.0, the others have Rb/Sr ratios greater than 2.0. For leucogranite dikes with Rb/Sr ratio greater than 5.0, they were derived from muscovite dehydration melting of a source similar to that of the lower pelite or the upper pelite. (B) Plot of initial $^{87}Sr/^{86}Sr$ ratios of the leucogranite dikes, leucosomes, the lower pelites and upper pelites against their Rb/Sr ratios. For leucogranite dikes with $^{87}Sr/^{86}Sr(T)$ >0.7300, they might be derived from various degrees of partial melting of the lower pelite, while those having $^{87}Sr/^{86}Sr(T)$ less than 0.7300, they might form from upper pelite-derived melts. The symbol sizes are larger than the analytical errors in these plots. T=100 Ma.

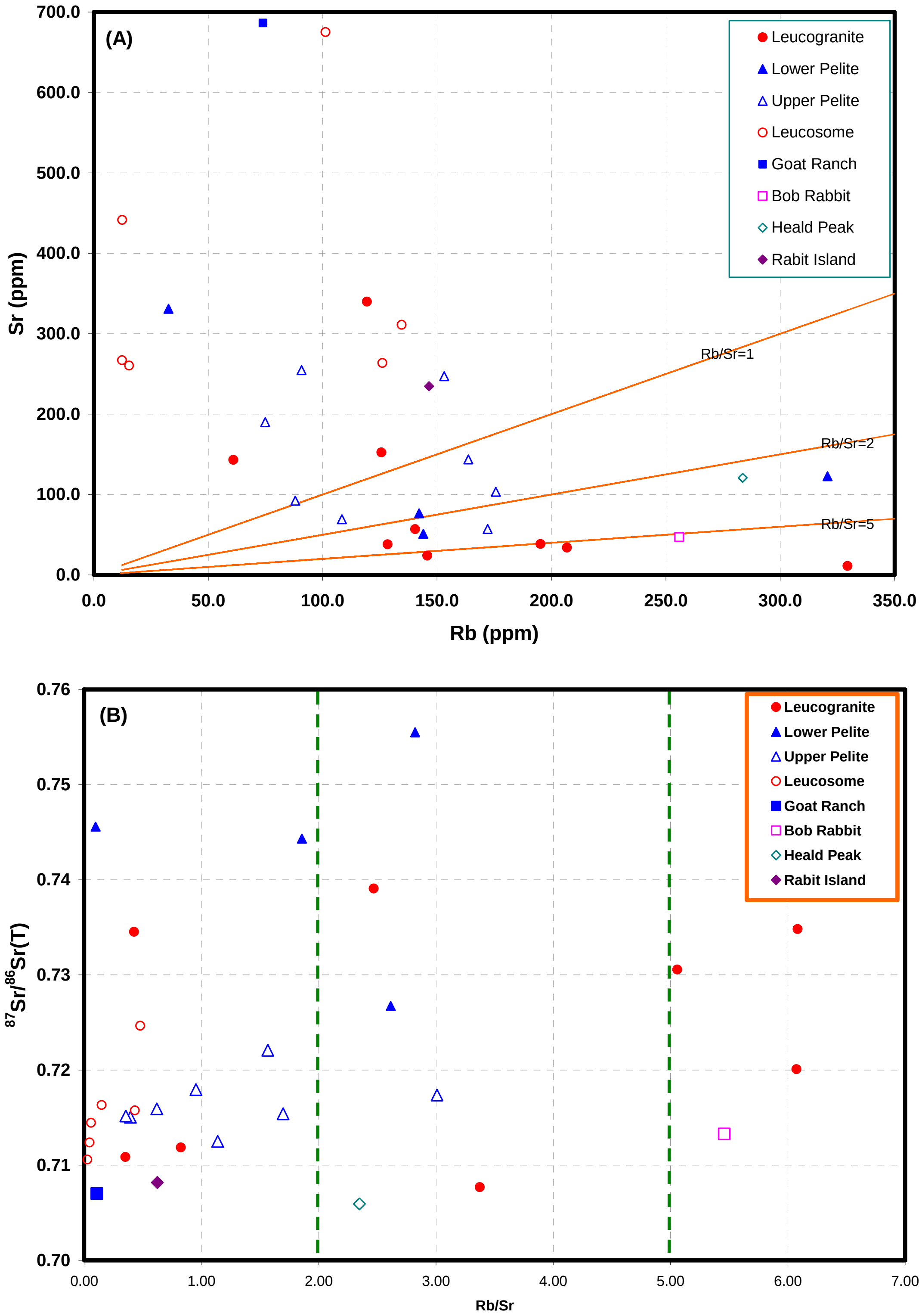(A)
Sr (ppm)
700.0
600.0
500.0
400.0
300.0
200.0
100.0
0.0
Rb (ppm)
0.0
50.0
100.0
150.0
200.0
250.0
300.0
350.0
Rb/Sr=1
Rb/Sr=2
Rb/Sr=5
● Leucogranite
▲ Lower Pelite
△ Upper Pelite
○ Leucosome
■ Goat Ranch
□ Bob Rabbit
◇ Heald Peak
◆ Rabit Island
(B)
$^{87}Sr/^{86}Sr(T)$
0.76
0.75
0.74
0.73
0.72
0.71
0.70
Rb/Sr
0.00
1.00
2.00
3.00
4.00
5.00
6.00
7.00
● Leucogranite
▲ Lower Pelite
△ Upper Pelite
○ Leucosome
■ Goat Ranch
□ Bob Rabbit
◇ Heald Peak
◆ Rabit Island

Figure 5 (A) Plot of $\varepsilon_{Nd}(T)$ values against Sm/Nd ratios of the leucogranite dikes, upper and lower pelite, leucosomes, Rabbit Island, Heald Peak and Bob Rabbit plutons. It also shows the average Nd and Sm compositions of the Goat Ranch pluton. (B) Plot of $\varepsilon_{Nd}(T)$ values against Sm/Nd ratios of Group A and Group B leucogranite dikes, together with leucosomes. They roughly exhibit a common trend that the higher Sm/Nd ratio, the higher is $\varepsilon_{Nd}(T)$ value. Both the leucogranite dikes and leucosomes preserved some degrees of Nd isotopic disequilibrium with respect to their sources, which might be due to extremely low diffusivity of Sm and Nd in silicic melts, and rapid melt extraction assisted by syn-magmatism deformation.

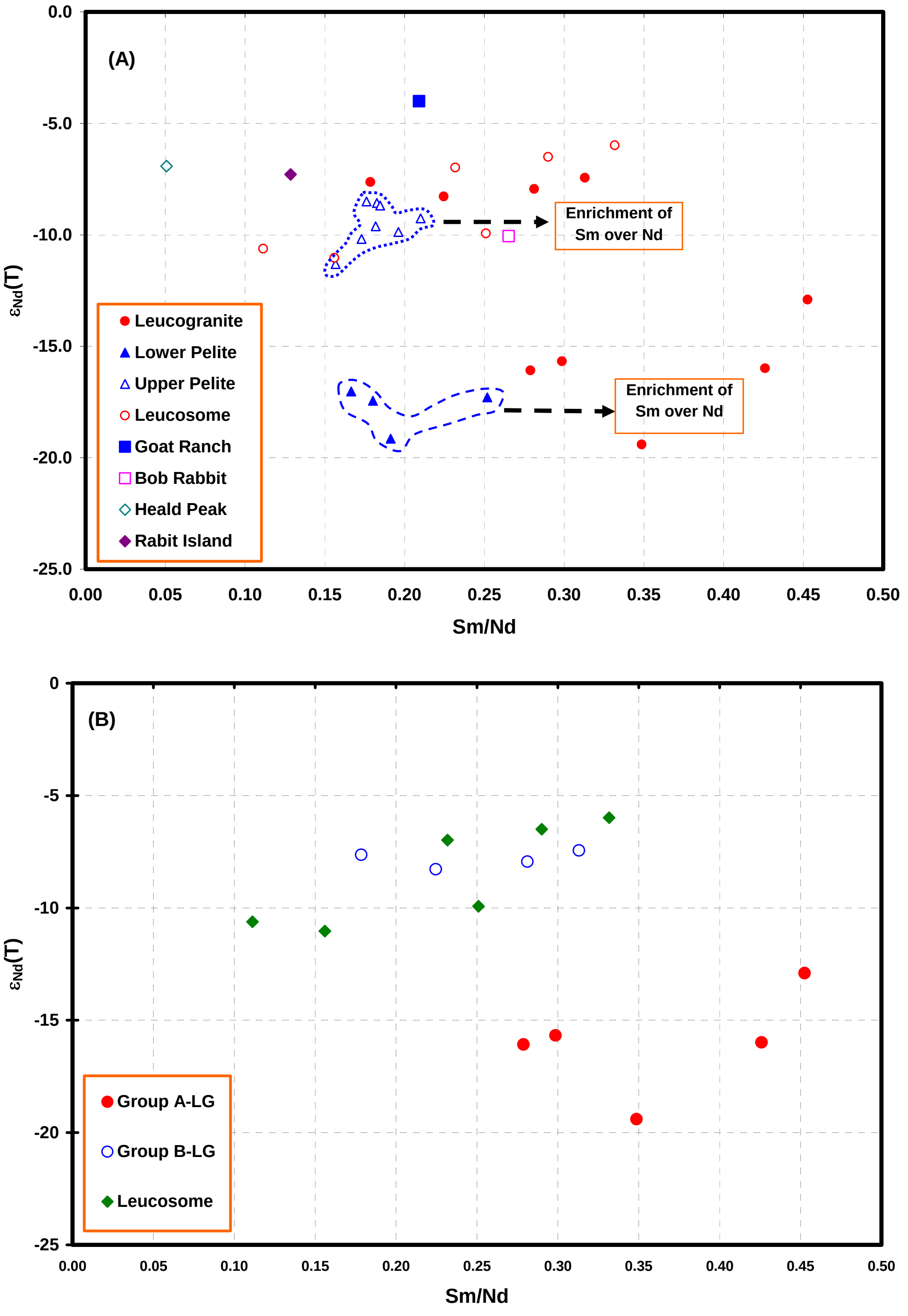
(A)
0.0
-5.0
-10.0
-15.0
-20.0
-25.0
$\varepsilon_{Nd}(T)$
0.00
0.05
0.10
0.15
0.20
0.25
0.30
0.35
0.40
0.45
0.50
Sm/Nd
Enrichment of Sm over Nd
Enrichment of Sm over Nd
● Leucogranite
▲ Lower Pelite
△ Upper Pelite
○ Leucosome
■ Goat Ranch
□ Bob Rabbit
◇ Heald Peak
◆ Rabit Island
(B)
0
-5
-10
-15
-20
-25
$\varepsilon_{Nd}(T)$
0.00
0.05
0.10
0.15
0.20
0.25
0.30
0.35
0.40
0.45
0.50
Sm/Nd
● Group A-LG
○ Group B-LG
◆ Leucosome

Chapter 6

Sr and Nd isotope systematics of anatectic melts: Exploring the role of accessory phases and non-modal partial melting

Lingsen Zeng, Jason B. Saleeby and Paul Asimow

Division of Geological and Planetary Sciences, California Institute of Technology,
Pasadena, CA 91125

Abstract

Advances in experimental petrology and field observations on anatectic products have motivated us to investigate the geochemical consequences of accessory mineral dissolution and non-modal partial melting processes. By incorporation of apatite dissolution into muscovite dehydration melting, we have examined the behavior of Rb-Sr and Sm-Nd isotopic systems in anatectic melts. Modeling results show that (1) the Sm/Nd ratios and Nd isotopic compositions of the melts depend on the amount of apatite dissolved into the melt, and (2) the relative proportion of micas (muscovite and biotite) and feldspars (plagioclase and K-feldspar) that enter the melt is a key parameter determining the Rb/Sr and $^{87}Sr/^{86}Sr$ ratios of the melt. In general, non-modal partial melting of a pelitic source results in melts following two paths in the ε_{Nd}-$^{87}Sr/^{86}Sr$ ratio space. Path 1 represents those partial melting reactions in which muscovite/biotite dehydration and apatite but not monazite dissolution play a significant role; the melt will have elevated Rb/Sr, $^{87}Sr/^{86}Sr$, Sm/Nd, and ε_{Nd} values. In contrast, Path 2 represents those partial melting reactions in which muscovite/biotite dehydration plays an insignificant role, and apatite but not monazite stays as a residue; the melt will have lower Rb/Sr,

$^{87}Sr/^{86}Sr$, Sm/Nd, and ε_{Nd} values than its source. The master variables controlling both accessory phase dissolution (and hence the Sm-Nd system), and melting reaction (and hence the Rb-Sr systematics) are temperature and water content.

Introduction

Most granitoids contain some crustal components derived from assimilation of melts from crustal rocks. Extensive experimental and field observations have shown that an important mechanism for generating large amounts of silicic melt is dehydration partial melting of hydrous mineral-rich metasedimentary rocks at various crustal levels (Wyllie, 1977; Vielzeuf and Holloway, 1988; LeBreton and Thompson, 1988; Rushmer, 1991; Harris and Inger, 1992; Gardien et al., 1995; Thompson, 1996; Patino Douce, 1996; Knesel and Davidson, 2002). Crustal anatexis occurs in tectonic environments in which either: (1) crustal temperature is elevated by intrusion of hot magmas from depth (Bergantz, 1989); (2) the solidus is lowered by addition of water (Harris et al., 1993); or (3) decompression during rapid exhumation of deep seated crustal rocks elevates the geotherm (Harris and Massey, 1994). The trace element and isotopic geochemistry of crustally derived melts is complicated, in part due to non-modal melting and to the disequilibrium nature of crustal anatexis at low temperatures. The geochemical and isotopic characteristics of anatectic melts are determined by mineral phases entering the melt, rather than the bulk source rock (Knesel and Davidson, 2002 & 1999; Tommasini and Davies, 1997; Hammouda et al., 1996). Experimental studies on partial melting of mica-rich metasedimentary rocks are particularly interesting, because it has been demonstrated that not only a wide spectrum of melts and crystalline residues, but also melts with a spectrum of trace element and radiogenic isotopic signatures can be generated from the same source material (Patino Douce, 1996; Patino Douce and Harris, 1998; Knesel and Davidson, 2002). Therefore, the complicated geochemistry of the crust-derived melts that may contaminate an invading granitic magma body can easily bedevil the straightforward interpretation of a granitic batholith by simple mixing of multiple components.

For the last two decades, advances in experimental petrology and field observations have suggested that the behaviour of trace elements hosted dominantly by rock-forming minerals may be quite different from those hosted mainly by accessory minerals such as apatite and monazite (Nabelek, 1999; Bea, 1996; Bea and Montero, 1999; Nabelek and Glascock, 1996; Watson and Harrison, 1984; Miller and Mittlefedldt, 1982; Hogan and Sinha, 1991; Watt and Harley, 1993; Bingen et al., 1996; Pan, 1997). For instance, the behavior of light rare-earth elements (LREE), particularly Sm and Nd, in felsic magma is very different from that which has been inferred for mafic magmas (Miller and Mittlefedldt, 1982). Watson and Harrison (1984) pointed out the possibility that unmelted accessory minerals may carry with them the radiogenic components (Pb, Nd and Hf) of the source region. Hogan and Sinha (1991) presented a model and evaluated the role of accessory minerals in the redistribution of lead isotopes during crustal anatexis. Partitioning of LREE into solid phases rather than liquid in particular has important implications for trace element and Nd-isotopic systematics of the products of crustal anatexis.

In this study, we intend to incorporate accessory mineral dissolution kinetics into crustal anatexis to evaluate the effects of non-modal partial melting in the Rb-Sr and Sm-Nd isotopic systematics of metasediment-derived melts. To meet this end, we will examine muscovite dehydration melting of a hypothetical source system consisting of the rock-forming minerals quartz, plagioclase, muscovite, biotite, and aluminosilicate with one accessory mineral apatite to illustrate (1) how Rb, Sr, Sm and Nd behave and (2) how Sr and Nd isotopic compositions evolve in the melts.

Melting reactions and processes

A number of experiments have determined the melting reactions of metapelites and metabasites. These results show that crustal anatexis in general can be classified as either fluid-present or fluid-absent partial melting, which involves various degrees of breakdown of hydrous minerals such as muscovite, biotite and hornblende. Patiño-Douce and Harris (1998) conducted partial melting experiments on metapelitic rocks from the High Himalayan Crystalline Sequence that are likely sources of the Miocene Himalaya leucogranites. They started with a muscovite schist (MS) and a tourmaline-bearing muscovite-biotite schist (MBS) and conducted experiments at 6, 8 and 10 kbar and 700-900°C, both without added H_2O (dehydration-melting) and with 1-4 wt % added H_2O (H_2O fluxing melting). The melting reactions of this muscovite schist are described by

1. **MS1- Muscovite dehydration melting**

$$22\text{Ms} + 7\text{Pl} + 8\text{Qtz} \rightarrow 25\ \text{Melt} + 5\ \text{Kfs} + 5\text{Sil} + 2\text{Bt}$$

2. **MS2- H_2O-fluxing melting**

$$9\text{Ms} + 15\text{Pl} + 7\text{Qtz} + x\text{H}_2\text{O} \rightarrow 31\ \text{Melt}$$

where x is the stoichiometric coefficient for H_2O added to the experiment, Ms, Pl, Qtz, Kfs, Sil and Bt represent muscovite, plagioclase, quartz, K-feldspar, sillimanite, and biotite, respectively. Mineral abbreviations are after Kretz (1983). The stoichiometry of these melting reactions were determined by the difference between the phase abundances at conditions that just exceed the muscovite-out boundary and those in the starting material (Patiño-Douce and Harris, 1998). Dehydration-melting begins at 750-800°C, and produces melts that are virtually identical in composition to the Himalayan leucogranites. Adding H_2O lowers the solidus by promoting plagioclase + quartz melting. Melts produced from these starting materials at $T = 750°C$ by H_2O-fluxing are trondhjemitic, and different in composition from most Himalayan leucogranites. Because of different proportions of muscovite and plagioclase consumed between these melting reactions, melts produced by these reactions will have different Sr isotopic systematics.

In this study, we only evaluate the two reactions (MS1 and MS2) determined by Patiño-Douce and Harris (1998). For a comprehensive review of experimentally determined partial melting reactions of metasedimentary rocks, please refer to Whittington and Treloar (2002) and references therein. We choose these particular partial melting reactions to evaluate the behavior of the Rb-Sr and Sm-Nd isotope systems during the respective melting reactions because they provided detailed accounts of the residual mode and the melting reactions as functions of melt fraction. These data are essential for us to model the behaviour of Rb, Sr, Sm, and Nd during muscovite dehydration melting.

Dissolution of accessory minerals

Accessory minerals are the predominant hosts of U, Th and rare-earth elements (REE) in silicic rocks (Bea, 1996; Gromet and Silver, 1983). In the majority of crustal rocks, four accessory minerals – apatite, zircon, monazite and xenotime usually contain more than 80-90% of total REE, Zr, Y, U, and Th. Therefore, understanding of the behavior of accessory phases during crustal anatexis is critical to evaluate the magnitude of Sm over Nd parent-daughter fractionation and Nd isotopic composition evolution in the metasediment-derived melts. The behavior of accessory minerals during high-grade metamorphism and crustal anatexis depends primarily on three factors: (1) solubility and dissolution kinetics into the melt; (2) subsolidus stability and involvement in metamorphic reactions; and (3) textural position and hence, availability for both the melt and other solid phases that react with them (Watson et al., 1989; Watt and Harley, 1993).

A series of experiments (Harrison and Watson, 1983; Watson and Harrison, 1983; Watson and Harrison, 1984; Harrison and Watson, 1984; Pichavant et al., 1992; Wolf and London, 1994 and 1995; Rapp and Watson, 1986; Montel, 1993) have been conducted to investigate dissolution kinetics of important accessory phases such as apatite, zircon, monazite and rutile. These results provide a basis from which the effects of accessory phases on the fractionation of LREEs, particularly Sm from Nd, can be understood. Unfortunately, almost all the experimentally determined partial melting reactions have focused on rock-forming minerals, and do not report the kinetic behavior of key accessory phases, even though a number of studies have indicated the importance of accessory minerals in controlling the LREE, trace and some major elements (e. g. phosphorus and titanium) of crustally-derived melts (Watt and Harley, 1993; Watt et al., 1996; Wolf and London, 1995; Sevigny, 1993; Sawyer, 1991; Nabelek and Glascock, 1995). Before we proceed to discuss the effect of accessory phases on the Sm-Nd isotope systematics of the melts, we will briefly review factors that affect the dissolution of accessory phases during crustal anatexis.

1. Zircon solubility

Zirconium is an essential structural component (ESC) of zircon. Experimental dissolution of zircon suggests that Zr saturation levels in an anatectic melt are a function of temperature, water content, and composition of the melt (Harrison and Watson, 1983; Watson and Harrison, 1983; Watson and Harrison, 1984). The equation that describes the dissolution of zircon in a melt is given by

$$\ln D_{Zr}^{Zircon/Melt} = \{-3.8 - [0.85(M-1)]\} + \frac{12900}{T} \tag{1}$$

where $D_{Zr}^{Zircon/Melt}$ is the ratio of Zr concentration in the zircon to that in the melt. T is the absolute temperature, and M is the cation ratio (Na+K+2Ca)/(Al×Si). Since metapelite has very low modal abundance of zircon and zircon has very low Sm and Nd concentrations (a few ppm), the effect of zircon in Sm and Nd isotope compositions of the melts is minor. Therefore, we will not discuss its role in fractionation of Sm over Nd during anatexis of a pelitic source further, even though it is important in determining the Pb and Hf isotope compositions of the melts (Watson and Harrison, 1984; Hogan and Sinha, 1991).

2. Apatite solubility

Phosphorus is an ESC of apatite, thus the concentration of phosphorus in a granitic melt is buffered by apatite solubility, and its saturation levels are a function of temperature and composition of the melt, but are independent of water contents in the melt for a range of 0 to 10 wt% H_2O (Harrison and Watson, 1984; Pichavant et al., 1992; Wolf and London, 1995). The apatite solution reaction is given by

$$Ca_5(PO_4)_3F_{Apatite} + \tfrac{1}{4} O_2 = 5CaO_{melt} + 3/2\ P_2O_{5\ melt} + F_{melt} \tag{2}$$

and apatite dissolution is described by (Harrison and Watson, 1984):

$$\ln D_P^{Ap/Melt} = \frac{8400 + [10^4 \times 2.64(SiO_2 - 0.5)]}{T} - \{3.1 + [12.4 \times (SiO_2 - 0.5)]\} \quad (3)$$

where SiO_2 is the weight fraction of silica in the melt, and T the absolute temperature. This expression appears to be valid between 45% and 75% SiO_2, 0 and 10% water, and for the range of pressures expected in the crust. For apatite solubility in peraluminous felsic melts, Pichavant et al. (1992) have extended the Harrison-Watson model and shown that

$$P_2O_5^{PMR} = P_2O_5^{HW} + P_2O_5^{Per} \quad (4)$$

where $P_2O_5^{HW}$ is given by equation (3), and $P_2O_5^{Per}$ is calculated by

$$P_2O_5^{Per} = \left(\frac{A}{CNK} - 1\right)\exp\left(\frac{-5900}{T} - 3.22SiO_2 + 9.31\right) \quad (5)$$

where SiO_2 is the weight fraction of silica in the melt, T is the absolute temperature and A/CNK is molar ratio of Al/(2Ca+K+Na). This model can account for high P_2O_5 contents observed in peraluminous granites.

3. Monazite solubility

Both LREE and phosphorus are ESCs of monazite. Experimental studies have demonstrated that: (1) monazite plays a significant role in buffering LREE concentration in melts, assuming sufficient phosphorus is available (Rapp and Watson, 1986; Montel, 1993), and (2) LREE saturation levels are a function of melt temperature, composition and water content. Field observations also have shown that monazite plays a dominant role in generation of LREE-depleted granitic melts (Nabelek et al., 1996; Watts and Harvey, 1993; Sawyer, 1991). Monazite dissolution is described by

$$(REE)PO_4^{monazite} \rightarrow \tfrac{1}{2} REE_2O_3^{melt} + \tfrac{1}{2} P_2O_5^{melt} \quad (6)$$

Solubility of monazite in Ca-poor felsic melts is described by equation (Montel, 1993)

$$\ln(REE_t) = 9.50 + 2.34D + 0.3879\sqrt{H_2O} - \frac{13318}{T} \tag{7}$$

Where $REE_t = \sum \frac{REE_i\,(ppm)}{at.weight(gmol^{-1})}$

And $D = \frac{(Na + K + Li + 2Ca)}{Al(Al + Si)}$

Na, K, Li, Ca, Al and Si are in atomic%, H_2O is in wt% and T is the absolute temperature. The REE considered extend from La to Gd, excluding Eu.

Since phosphorus is an ESC common to both apatite and monazite, and apatite generally contains significant amount of LREE, the stability of these two phases may be interrelated during partial melting of a metasedimentary source. For both apatite and monazite, temperature is the most important parameter that determine their dissolution (Fig. 4). But for peraluminous or metaluminous crustal melts with D typically in the range of 0.9 to 1.1, monazite dissolution strongly depends on the water content (Rapp and Watson, 1986; Montel, 1993), which differs from that of apatite (Fig. 4b). For common anatectic conditions, increasing water content will lower the solidus and drive partial melting of a pelitic source toward the MS2 reaction. This will favor dissolution of monazite relative to apatite. At high temperature and low water content conditions, partial melting of a metasedimentary source proceeds following the MS1 reaction, and favors apatite dissolution over monazite dissolution by saturation of phosphorus in the melt released from apatite.

Rb-Sr and Sm-Nd isotopic systems

Sm and Nd are light rare-earth elements (LREE), whereas Rb and Sr are large ion lithophile elements (LILE). In metasedimentary rocks, Sm and Nd reside predominantly in accessory phases, particularly monazite, apatite, zircon and garnet. In their study of Nd isotopic geochemistry of the Himalaya leucogranites, Ayers and Harris (1997) found that LREE concentrations in a melt would be controlled by monazite dissolution, while apatite would contribute ~10% of the LREE, 50% of MREE, and >90% of HREE. Since Sm/Nd ratios are higher in apatite than both in monazite and in the bulk source (Bea et al., 1994; Ayers and Harris, 1997), the liquid will inherit a higher Sm/Nd ratio than its bulk source if the temperature of melting favors apatite dissolution. This result suggests an important role of dissolution of apatite in the Nd isotopic systematics of crustally-derived melts.

In general, monazite has a Sm/Nd ratio slightly less than its hosting rock, but apatite has a Sm/Nd ratio much greater than its hosting rock (Ayers and Harris, 1997; Bea et al., 1994). Given a low Sm/Nd ratio, monazite will evolve over time toward an ε_{Nd} value less than that of the whole rock (Fig. 1a). At the time of anatexis, if significant amount of monazite stays in the residue, the melts will have radiogenic Nd isotopic compositions and higher Sm/Nd ratios than those in their source rocks. In principle, this effect of monazite on the melt is hard to distinguish from the case in which significant amount of apatite dissolve into the melts, if not given other geochemical information. But if monazite stays in the residue, the melt will have a strongly LREE depleted signature. For a typical metapelite, apatite is commonly about an order magnitude more abundant than monazite. Because phosphorus is an ESC common to both minerals, and the concentration of phosphorus in the melt will be dominated by dissolution of apatite, the solubility of monazite in the melt will be limited by apatite dissolution. The correlation of ε_{Nd} values with P_2O_5 contents in the melt can be used as an indicator of apatite dissolution. In a source rock without monazite, apatite dissolution will release both LREE and phosphorus into the melt. If LREE in the melt is oversaturated, monazite crystallization will occur. In their experiments on the dissolution of apatite in peraluminous granitic melts, Wolf and London (1995) found that: (1) apatite has high solubility in strongly peraluminous melts, and in contrast monazite and xenotime have much lower solubility by an order of magnitude; and (2) apatite dissolves incongruently and crystallizes REE-rich monazite on its surface, which results in LREE-depleted melts with elevated Sm/Nd ratios.

In contrast to the Sm-Nd isotopic system, the Rb-Sr system is mainly controlled by rock-forming phases (e.g., plagioclase, K-feldspar, muscovite and biotite). Field and experimental observations have demonstrated the common non-modal nature of partial melting of metasedimentary sources (Knesel and Davidson, 2002; Patiño-Douce and Harris, 1998). In the following, we will discuss the Rb-Sr and Sm-Nd isotopic systematics in partial melting of a hypothetical pelitic source rock. The melting reactions we adopted for this modeling were determined experimentally by Patiño-Douce and Harris (1998). They also have been used by Knesel and Davidson (2002) in their evaluation of Sr isotopic disequilibrium in anatectic melting during collisional orogenesis. For simplicity, we will only consider the effect of apatite, one of the common accessory minerals in metapelites, in regulating the behavior of the Sm-Nd isotopic system during partial melting. We model the behavior of the Rb-Sr isotopic system in a non-modal equilibrium partial melting process, and the Sm-Nd isotope system as a disequilibrium system, because (1) Sm and Nd diffusion are much slower than that of Rb and Sr in a silicic melt; (2) Sm and Nd concentrations in the melt and the residue are dominantly controlled by accessory minerals such as apatite and monazite; (3) large portions of accessory minerals reside as inclusions in major minerals (Watson et al., 1989) such that they are not in good position to be dissolved into the melt readily; (4) the relationship between degree of melting and degree of dissolution of accessory minerals in crustal anatexis is poorly known; and (5) since phosphorous is an ESC in apatite, the behavior of associated LREE in apatite is determined by the dissolution behavior of phosphorus during crustal anatexis. The parameters used in this study are listed in Table 1. The mineral compositions of the hypothetical source rock are slightly different from those used by Patiño-Douce and Harris (1998). We replace garnet with aluminosilicate and lower its proportion by 0.5 wt% to accommodate apatite in our hypothetical source. Both garnet and aluminosilicate are not reactants in the melting reactions that we examined such that this modification will not affect the applicability of the MS1 and MS2 reactions to our trace element modeling.

Melting models

1. Disequilibrium partial melting

Disequilibrium melting refers to any melting event where the liquid phase is not in chemical equilibrium with the restite prior to melt extraction. In disequilibrium melting, the concentration of an element in the melt is kinetically controlled and depends on its concentration in the minerals of the initial solid and on the mineral proportions which dissolve into the melt (Allegre and Minster, 1978). Disequilibrium melting has been observed in the experimental melting of plagioclase in granitic melts (Johannes, 1980), a pelite (Knesel and Davidson, 2002), and a biotite granite (Knesel and Davidson, 1999), and inferred from a number of geochemical observations of anatectic complexes (Sawyer, 1991; Naslund, 1986; Kaczor, 1988; Barbey et al., 1989; Barbero et al., 1995; Ayers and Haris, 1997; Watt and Harley, 1993; Watt et al., 1996). Rubie and Brearley (1990) have performed experiments on incongruent melting of muscovite and quartz, and suggested that disequilibrium can result either from significant temperature oversteps or from fluid infiltration in rocks that are above the fluid-present melting solidus. Both mechanisms will result in rapid melting and achieve significant melt fractions in less than one year. Chemical equilibrium of trace elements will be controlled by the diffusion rates of elements between melt and residue. Chemical disequilibrium between melt and restite can occur if melt is extracted from its source too rapidly to allow complete equilibration between them.

During disequilibrium partial melting, the concentration of element i in the melt (C_L^i) is given by

$$C_L^i = x_1 C_1^i + x_2 C_2^i + \ldots x_n C_n^i \qquad (8)$$

where x_j is the weight proportion of mineral j entering the melt, and C_j^i is the concentration of element i in mineral j (Allegre and Minster, 1978; Prinzhofer and Allegre, 1985, Barbey et al., 1989; Sawyer, 1991).

Using partition coefficients between solids ($d_{n/m}^s$), and assuming subsolidus equilibration of trace element ratios before melting begins, this can be written as

$$C_L^i = C_1^i (x_1 + x_2 d_{2/1}^{si} + \ldots x_n d_{n/1}^{si}), \qquad (9)$$

where $d^{si}_{n/1}$ is the partition coefficient for element i between solid 1 and solid n.

$$C^i_L / C^i_1 = (x_1 + x_2 d^{si}_{2/1} + ... x_n d^{si}_{n/1}) \equiv M^i. \tag{10}$$

The initial concentration of element i in the source rock is given by

$$C^i_0 = C^i_1 (X_1 + X_2 d^{si}_{2/1} + ... X_n d^{si}_{n/1}), \tag{11}$$

where X_j is the weight proportion of mineral j in the source rock.

Let

$$C^i_0 / C^i_1 = (X_1 + X_2 d^{si}_{2/1} + ... X_n d^{si}_{n/1}) \equiv Q^i \tag{12}$$

and hence

$$C^i_L = C^i_0 (M^i / Q^i) \tag{13}$$

Unfortunately solid-solid partition coefficients are not known for most of the rock-forming minerals. It has been suggested that they may be calculated from the solid-melt distribution coefficients (Barbey et al., 1989; Sawyer, 1991) thus

$$d^{si}_{2/1} = d^i_2 / d^i_1 \tag{14}$$

where d^i_j is the partition coefficient of element i between mineral j and the melt.

For Sm-Nd isotope system

$$\left(\frac{C^{Sm}_L}{C^{Nd}_L} \right)_L = \left(\frac{C^{Sm}_0}{C^{Nd}_0} \right)_0 \times \left(\frac{M^{Sm} \times Q^{Nd}}{M^{Nd} \times Q^{Sm}} \right) \text{ or } \left(\frac{Sm}{Nd} \right)_L = \left(\frac{Sm}{Nd} \right)_0 \times \left(\frac{M^{Sm} \times Q^{Nd}}{M^{Nd} \times Q^{Sm}} \right), \tag{15}$$

where $\left(\frac{Sm}{Nd} \right)_L$ and $\left(\frac{Sm}{Nd} \right)_0$ are the Sm/Nd ratios for the melt and initial source rock, respectively. Nd isotopic composition of the melt is calculated by

$$\left(\varepsilon_{Nd} \right)_L = \frac{\sum x_i C^i_{Nd} \varepsilon^i_{Nd}}{\sum x_i C^i_{Nd}} \tag{16}$$

where $\left(\varepsilon_{Nd}\right)_L$ is the Nd isotopic composition of the melt, x_i is proportion of mineral i entering the melt, and C_{Nd}^i and ε_{Nd}^i are Nd concentration and isotopic composition in mineral i, respectively. Whole-rock $(\varepsilon_{Nd})_{wr}$ of the source is given by

$$\left(\varepsilon_{Nd}\right)_{wr} = \frac{\sum X_i C_{Nd}^i \varepsilon_{Nd}^i}{\sum X_i C_{Nd}^i} \tag{17}$$

2. Non-modal equilibrium partial melting

Incongruent or non-modal melting is a melting process where the proportion of reactant phases in the source is different from their proportions entering the melt. Following the expression given by Shaw (1970), the weight concentration of a given element in a melt, C_L^i, relative to the concentration of the element in the parent that is melting, C_0^i, is given by

$$\frac{C_L^i}{C_0^i} = \frac{1}{D_0^i + F(1-P)} \tag{18}$$

where $D_0^i = \sum_j^n X^j d_j^i$

and $P = \sum_j^n x_j d_j^i$

D_0^i is the bulk distribution coefficient of the parent for a given trace element based on the mineral composition at the beginning of melting, X^j is the weight fraction of a given mineral j in the original parent. d_j^i is the mineral/melt distribution coefficient for a given trace element i for mineral j. P is the bulk distribution coefficient of the minerals that are making up the melt in which x_j is the weight normative fraction of mineral j in the melt. For non-modal partial melting reactions, $D_0 \neq P$.

For Rb and Sr isotope system,

$$\frac{C_L^{Rb}}{C_0^{Rb}} = \frac{1}{D_0^{Rb} + F(1 - P^{Rb})}$$

$$\frac{C_L^{Sr}}{C_0^{Sr}} = \frac{1}{D_0^{Sr} + F(1 - P^{Sr})}$$

and

$$\left(\frac{Rb}{Sr}\right)_L = \left(\frac{Rb}{Sr}\right)_0 \times \frac{D_0^{Sr} + F(1 - P^{Sr})}{D_0^{Rb} + F(1 - P^{Rb})} \tag{19}$$

Using an equation analogous to (16), ^{87}Sr/^{86}Sr ratios of the melts can be calculated in a similar fashion, if the proportions of each phase entering the melt are known at each melting step.

Results and Discussion

The profound geochemical consequences of accessory phase dissolution during partial melting of high-grade metapelites are illustrated in Figures 1 and 2. In Figure 1a, it shows that apatite will deviate from the other phases and develop radiogenic Nd isotopic compositions with respect to its host rock, due to its high Sm/Nd ratio. In contrast, monazite will bear nonradiogenic Nd isotopic compositions than it hosting rock. The others phases have low Sm/Nd ratios and evolve into lower ε_{Nd} values than the whole rock. But due to high Nd concentrations in apatite, if apatite dissolves into the melt, it will dominate the Nd isotopic compositions of the melts derived from such a source (Fig. 1b). Figure 1b is a plot of ε_{Nd} values and Sm/Nd ratios of melts derived from the hypothetical source (Table 1) against the fraction of apatite dissolved into the anatectic melts. In construction of this plot, we assume that a partial melting event occurred at 100 Ma after the last isotopic homogenization event (e.g. melting or high-grade metamorphism). All the phases started at the same ε_{Nd}(100Ma) value of -10.0, and evolved with their respective Sm/Nd ratio with time, such that they have different ε_{Nd} values at the time that the hypothetical partial melting occurred. The ε_{Nd} value and Sm/Nd ratio of the melt strongly depend on the amount of apatite dissolved. With about 0.008% apatite dissolved into the melt, the melt has an ε_{Nd} value and Sm/Nd ratio about equal to those of the source rock. The more apatite dissolves into the melt, the higher ε_{Nd} value and Sm/Nd ratio the melt has. Note that since the source rock contains 0.5% apatite, a modal melting model would be far off-scale to the right. The features shown in this modeling may account for observations of Nd isotope disequilibrium, and Sm/Nd parent-daughter fractionation in the Himalaya leucogranites (Deniel et al., 1987; Ayers and Harris, 1997), the migmatites in the Hercynian anatectic complex of Toledo, Spain (Barbero et al., 1995), and the leucogranitic dikes and leucosomes of the Isabella pendant, southern Sierra Nevada (Zeng et al., Chapter 3; Zeng and Saleeby, Chapter 5)

The behavior of the Rb-Sr isotopic system during partial melting of a pelitic source has been studied before. Harris and Inger (1992) applied a non-modal partial melting model to the consequences of muscovite and biotite incongruent dehydration melting for the Rb-Sr-Ba systematics. Unfortunately, they did not model the Sr isotopic composition as a function of degree of melting due to poor knowledge of proportions of reacting phases that enter the melt for each melting reaction. Knesel and Davidson (2002) used the same melting reactions as we used in this study to model the Sr isotopic compositions of the anatectic melts as a function of degree of melting, based on their experimental results. They successfully demonstrated that incongruent melting of muscovite can account for the bi-modal nature of Sr isotopic compositions of the Himalaya leucogranites. Given the details of how the incongruent melting of muscovite proceeds, we can examine how the Sr isotopic composition evolves as a function of degree of melting. To calculate the $^{87}Sr/^{86}Sr$ ratios of the melts from the reaction MS1 and MS2, the Sr concentrations, $^{87}Sr/^{86}Sr$ ratios, and proportions of each phase that contributes to the melt should be known. For each reactant, the Sr concentration and $^{87}Sr/^{86}Sr$ ratio are listed in Table 1. The proportions of each phase entering the melt at each degree of melting are from Patiño-Douce and Harris (1998, Table 2). We only show the results for their experiments at 6 kb both with and without H_2O (Fig. 2). Figure 2a is a plot of Rb/Sr ratio of the melt against degree of melting. It shows that as melting proceeds, Rb/Sr ratios of the melts from either MS1 or MS2 will decrease, which is similar to the results given by Harris and Inger (1992), because Rb is more incompatible than Sr. Melts from MS2 constantly have lower Rb/Sr ratios than those from MS1, because MS2 reaction consumes plagioclase in a greater proportion relative to muscovite. Figure 2c is a plot of $^{87}Sr/^{86}Sr$ ratios of the melts derived from MS1 and MS2 reactions versus degree of melting. For the melts derived from the MS1 reaction, there are several interesting features shown in Figure 2b and c: (1) $^{87}Sr/^{86}Sr$ ratio of the melt increases as melting proceeds until muscovite/plagioclase ratio, which represent the amount of muscovite over plagioclase entering the melt, reaches its maximum(Fig. 2b and c); (2) then it decreases as melting continues until muscovite is completely consumed; (3) after muscovite totally consumed, $^{87}Sr/^{86}Sr$ ratio of the melt increases by a very small fraction due to small amount of biotite entering the melt; and (4) all the melts have higher $^{87}Sr/^{86}Sr$ ratios than the 0.7417 of their source (Fig. 2c). $^{87}Sr/^{86}Sr$ ratios of the melts from the MS2 reaction increase as melting proceeds up to a higher degree (40%), but they are lower than the 0.7417 of the source. Based on these observations, it seems that Sr isotopic compositions of the melts derived from muscovite dehydration melting depend on the relative amount of muscovite and plagioclase entering the melt. In reaction MS2, water plays a dual role. On one hand, it lowers the solidus of quartz + plagioclase. On the other hand, it stabilizes muscovite and thus limits its participation in MS2 melting reaction. Reduced amount of muscovite relative to plagioclase entering the melt results in lower Rb/Sr and $^{87}Sr/^{86}Sr$ ratios of the melts derived from reaction MS2 than those from reaction MS1.

If isotopic differences among constituent minerals at the onset of melting are preserved throughout the melting interval, then non-modal partial melting will produce melts with Sr and Nd isotope compositions significantly different from those in the source. Recent studies of migmatites in the Hercynian anatectic complex of Toledo, Spain (Barbero et al., 1995), and of pelitic gneisses and leucogranite in the Himalaya (George and Bartlett, 1996) show that Sr and Nd isotopic heterogeneity can be preserved on the mineralogic scale before and during anatexis. Barbero et al. (1995) found a broad range of initial Sr and Nd isotopic ratios of leucogranitic leucosomes, suggesting absence of isotopic homogenization in the melts. Ayers and Harris (1997) demonstrated the Nd isotopic disequilibrium as a result of incongruent dissolution of apatite during the formation of Himalaya leucogranites. In our studies on the migmatite zone of the Isabella pendant, southern Sierra Nevada, we found that leucosomes derived from a pelitic source fall into two groups (Fig. 3). Group A leucosomes have higher ε_{Nd}(T) values than those of the metapelite and are of granitic compositions, suggesting they were derived from muscovite dehydration reaction (reaction MS1). Group B leucosomes have similar ε_{Nd} values to those of metapelite, and are of trondhjemitic compositions. They are consistent with melts from H_2O-fluxed melting represented by reaction MS2 (Zeng et al., Chapter 3). We seek here to examine the coupling between accessory mineral dissolution and type of melting reaction in order to explain why ε_{Nd} correlates with trondjemitic vs. granitic character.

Given the implicit complexity of crustal anatexis for the Rb-Sr and Sm-Nd isotopic systematics, it is instructive to examine likely trajectories for melts derived from partial melting of a pelitic source in ε_{Nd}-^{87}Sr/^{86}Sr space. Before we continue our discussion, we will define a ratio, R, describing the relative contribution of Rb-rich over Sr-rich phases to a source and a melt, which is critical for Rb and Sr geochemistry of anatectic melts. R is given by

$$R_m = \frac{x_{Ms} + x_{Bt}}{x_{pl} + x_{Kfs}} \qquad (18)$$

and

$$R_s = \frac{X_{Ms} + X_{Bt}}{X_{Pl} + X_{Kfs}} \qquad (19)$$

where $x_{Ms} + x_{Bt}$ and $X_{Ms} + X_{Bt}$ are the amount of muscovite and biotite entering the melt and in the source, respectively, and $x_{Pl} + x_{Kfs}$ and $X_{Pl} + X_{Kfs}$ are the amount of plagioclase and K-feldspar entering the melt and in the source, respectively. The ratio of R_m describes the relative contribution of Rb-rich minerals over Sr-rich phases to a melt.

In Figure 5, Path A represents melts dominated by muscovite/biotite dehydration melting characterized by high R_m/R_s ratios (>1), while Path B with low R_m/Rs ratios(<1) represents those reactions with minor or no involvement of either muscovite or biotite. Melts following Path A will have more radiogenic Sr isotopic compositions than their source. In contrast, melting following Path B will develop nonradiogenic Sr isotopic compositions with respect to their source. In these circumstances, A and B have no contributions from dissolution of accessory phases and hence no significant variations of ε_{Nd}. However, kinetic experiments on accessory phase dissolution provide a likely basis for coupling between A- and B-type Sr isotopic behavior and characteristic Nd isotopic behavior. Experiments on partial melting of metapelites have shown that type B partial melting usually occurs at a lower temperature but higher water content than those of type A partial melting reactions. As shown by Equations (3) and (7), the lower temperatures and high water contents that favor reaction MS2 will inhibit apatite dissolution relative to monazite dissolution (Fig. 4), which results in more negative ε_{Nd} values in the melt than its source (Path 2 in Fig. 5). At the higher temperatures and dry conditions where muscovite or biotite dehydration melting play a dominant role, dissolution of apatite will increase (Equations (3)-(5)), but monazite dissolution will be relatively inhibited at lower water conditions (Fig. 4b). Melts derived from such partial melting reactions will have more radiogenic Nd isotopic compositions than their source (Path 1 in Fig. 5). Therefore, for melting timescales where kinetics are relevant, the various P-T and water content conditions under which crustal anatexis occurs indicate that the most likely paths for a melt to follow in ε_{Nd}-$^{87}Sr/^{86}Sr$ space will be either Path 1 or Path 2. Path 1 represents those partial melting reactions in which muscovite/biotite dehydration and apatite but not monazite dissolution play a significant role; the melt will have elevated Rb/Sr, ^{87}Sr/^{86}Sr, Sm/Nd, and ε_{Nd} relative to its source. In contrary, Path 2 represents those partial melting reactions in which muscovite/biotite dehydration plays an insignificant role, and apatite but not monazite stays as a residue; the melt will have lower Rb/Sr, ^{87}Sr/^{86}Sr, Sm/Nd, and ε_{Nd} than its source. As discussed in the previous section, we found a strong correlation between ε_{Nd}(T) values and trondhjemitic versus granitic character in the leucosomes from the migmatite zone of the Lake Isabella pendant. In ε_{Nd}-^{87}Sr/^{86}Sr space, leucosomes are distributed along Path 1 (high ε_{Nd} and ^{87}Sr/^{86}Sr), and Path 2 (low ε_{Nd} and ^{87}Sr/^{86}Sr), but their Sr signal is smaller as compared to variations in their Nd isotopic compositions (Zeng et al., Chapter 3). Those leucosomes with high ε_{Nd} values (Group A) also have higher P_2O_5 contents than those with low ε_{Nd} values (Group B) (Fig. 3). At first glance, this correlation seems to be fortuitous, but detailed field and petrographic data, and major element as well as trace element data for these leucosomes indicates that they resulted from partial melting of the hosting pelite unit (Zeng et al., Chapter 3). This correlation can be explained by examining the kinetic equations for apatite and monazite dissolution, which show that conditions associated with dehydration melting also favor dissolution of apatite, whereas conditions associated with hydrous flux melting favor monazite dissolution. Enhancing dissolution of apatite during muscovite dehydration melting is likely to result in the Nd isotopic disequilibrium as observed in the Group A leucosomes (Fig. 3).

Although Sr and Nd isotopic disequilibrium may be a common feature of crustal anatexis in dynamic orogenic environments, there are a number of factors that will complicate or obscure field observations. The primary factors affecting the fate of anatectic melts are their chemistry and physical properties, and the thermal and mechanical state of the crust around and above the zone of melting (Sawyer, 1991; Watt and Harley, 1993; Watt et al., 1996). For those elements concentrated in accessory phases, the melt extraction rate and accessory mineral dissolution rate are critical factors that will determine their partitioning into the melt. If melt extraction rate is greater than accessory phase dissolution rate, the melt will have a disequilibrium signature with respect to its source (Fig. 6). But at higher temperatures, accessory phases dissolve in a rapid enough fashion to exceed the rate of melt extraction (Sawyer, 1991; Watt and Harley, 1993). Therefore, assisted by rapid diffusion, the melts may be in equilibrium with their residue for those elements with high diffusivities. For instance, the leucogranite dikes which formed at relatively higher temperatures than leucosomes in the Isabella pendant have acquired equilibrium Sr isotopic compositions with respect to their protoliths (Zeng and Saleeby, Chapter 5). For anhydrous melting such as MS1, high dilational strain generated by positive volume change of muscovite dehydration melting may encourage rapid melt segregation and extraction, and thus may result in either Sr or Nd isotopic disequilibrium. In contrast, hydrous melting as MS2 may hinder complete extraction of melts from their source due to negative volume change during melting, and thus melts produced by hydrous reactions may have Sr or Nd isotopic equilibrium compositions with respect to their sources.

Summary and Conclusions

We have incorporated accessory mineral dissolution kinetics into non-modal partial melting modeling to examine the geochemical consequences of muscovite dehydration melting of pelitic sources. In particular, assuming a hypothetical source consisting of quartz, plagioclase, muscovite, biotite, aluminosilicate and apatite and following the partial melting reactions MS1 and MS2 determined by Patiño-Douce and Harris (1998), dissolution of apatite into the melt combined with incongruent muscovite melting has profound effects on the Rb-Sr and Sm-Nd isotopic systematics of anatectic melts. Under disequilibrium partial melting conditions which are most suitable for the Sm-Nd isotopic system, Nd isotopic compositions of the melts strongly depend on the amount of apatite dissolved in the melts. The Rb-Sr isotopic system is primarily controlled by rock-forming minerals, especially Rb-rich minerals (e.g. muscovite and biotite) versus Sr-rich minerals (e.g. plagioclase and K-feldspar). When a melting process has Rm/Rs ratio greater than 1.0, the melts will have characteristic high Rb/Sr and $^{87}Sr/^{86}Sr$ ratios. In contrast, the melts produced by a melting process with low Rm/Rs ratios (<1.0) will have low Rb/Sr and $^{87}Sr/^{86}Sr$ ratios. In general, non-modal partial melting of a pelitic source results in melts following two paths in the ε_{Nd}-$^{87}Sr/^{86}Sr$ ratio space. Path 1 represents those partial melting reactions favor muscovite/biotite dehydration and apatite but not monazite dissolution, the melt will have elevated Rb/Sr, $^{87}Sr/^{86}Sr$, Sm/Nd, and ε_{Nd} values. In contrast, Path 2 represents those partial melting reactions in which muscovite/biotite dehydration plays an insignificant role, and favors monazite over apatite dissolution, the melt will have lower Rb/Sr, $^{87}Sr/^{86}Sr$, Sm/Nd, and ε_{Nd} values than its source. The master variables controlling both accessory phase dissolution (and hence the Sm-Nd system), and melting reaction (and hence the Rb-Sr systematics) are temperature and water content. These results can account for either Sr or Nd isotopic disequilibrium which is observed in a number of migmatite complexes and leucogranite plutons. However, disequilibrium signature may be obscured by inefficient melt extraction from its source and rapid diffusion during partial melting, thus equilibrium between melts and their residue are observed in some migmatite zones and leucogranite plutons.

Figure 1 (a) Nd isotope compositions of apatite, plagioclase, K-feldspar, monazite, biotite muscovite, and whole-role metapelite as a function of time and their respective Sm/Nd ratio. For all the phases, we assume they have an initial ε_{Nd} value of -10.0, and Sm/Nd ratios given in Table 1. Due to relatively high Sm/Nd ratio in apatite, it evolves rapidly toward radiogenic ε_{Nd} values over time. (b) Diagram showing effect of apatite dissolution on Nd isotope systematics of the melts formed in a partial melting event occurring 100 my after the last event that homogenized Nd isotope compositions among minerals. We assume all the minerals have the same initial ε_{Nd} value of -10.0, but different Sm/Nd ratio at a time 100 Ma before the melting event. At the time of melting, minerals involved in the melting will have different ε_{Nd} values and Sm/Nd ratios. Both ε_{Nd} value and Sm/Nd ratio of the melt are dominated by the amount of apatite dissolved into the melt. For this specific case, both ε_{Nd} value and Sm/Nd ratio of the melt approach the values in the source rock when the melt contains 0.008% apatite. With higher amount of apatite dissolved, the melt evolves toward higher ε_{Nd} value and Sm/Nd ratio than those in the source.

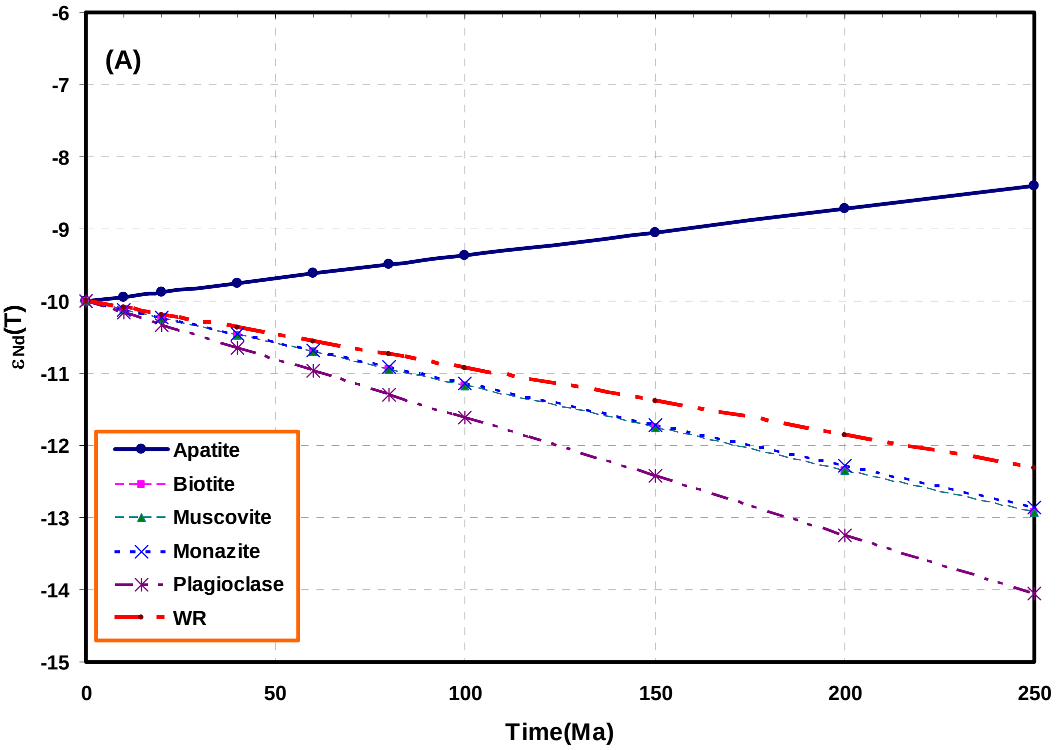
(A)
εNd(T)
-6
-7
-8
-9
-10
-11
-12
-13
-14
-15
0
50
100
150
200
250
Time(Ma)
Apatite
Biotite
Muscovite
Monazite
Plagioclase
WR

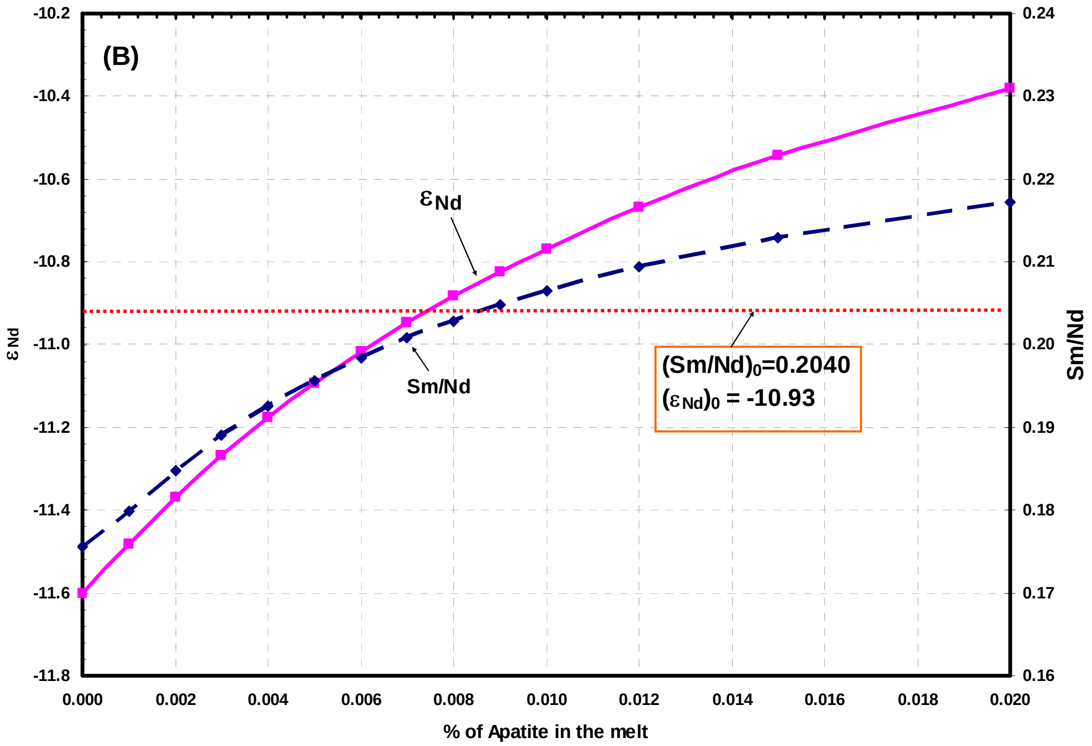
(B)
εNd
Sm/Nd
-10.2
-10.4
-10.6
-10.8
-11.0
-11.2
-11.4
-11.6
-11.8
0.24
0.23
0.22
0.21
0.20
0.19
0.18
0.17
0.16
0.000
0.002
0.004
0.006
0.008
0.010
0.012
0.014
0.016
0.018
0.020
% of Apatite in the melt
εNd
Sm/Nd
(Sm/Nd)0=0.2040
(εNd)0 = -10.93

Figure 2 (A) Diagram illustrating the Rb/Sr ratio in a metasediment-derived melt as a function of degree of melting. Quartz, plagioclase and muscovite are the melting phases. MS1 represents fluid-absent muscovite dehydration melting. MS2 represents H_2O-fluxed muscovite partial melting. Melts derived from MS2 reaction have much lower Rb/Sr ratios than those from MS1, due to reduced amount of muscovite but increasing amount of plagioclase entering the melt. Both reactions suggest a common feature of metasediment-derived melts; i.e., initial melts have higher Rb/Sr ratios than those in the melts derived from higher degrees of melting. (B) Plot of proportions of muscovite and plagioclase entering the melt and their ratios against melt fraction for MS1 reaction. Data are from Patiño-Douce and Harris (1998). The left hand side vertical axis is the proportion of plagioclase or muscovite that enters the melt. The right hand side vertical axis describes the ratio of proportion of muscovite over plagioclase entering the melt. (C) $^{87}Sr/^{86}Sr$ ratios of the melt as a function of degree of melting for MS1 and MS2 reactions at 6 kb. The proportions of reacting phases entering the melt are from Table 2 of Patiño-Douce and Harris (1998). We assign a Sr isotopic composition of each phase involved in the MS1 and MS2 partial melting reactions. The data are listed in Table 1. For the melts derived from the MS1 reaction, their $^{87}Sr/^{86}Sr$ ratios increase as melting proceeds until the proportion of muscovite to plagioclase entering the melt reaches its maximum, and then decrease during continuous melting of muscovite + plagioclase + quartz until muscovite is completely consumed. $^{87}Sr/^{86}Sr$ ratios of the melts from the MS2 reaction increase as melting proceeds up to a higher degree (40%). Addition of water stabilizes muscovite and thus limits its participation in MS2 melting reaction, which results in lower $^{87}Sr/^{86}Sr$ ratios of the melts derived from such a melting reaction than those from MS1 reaction.

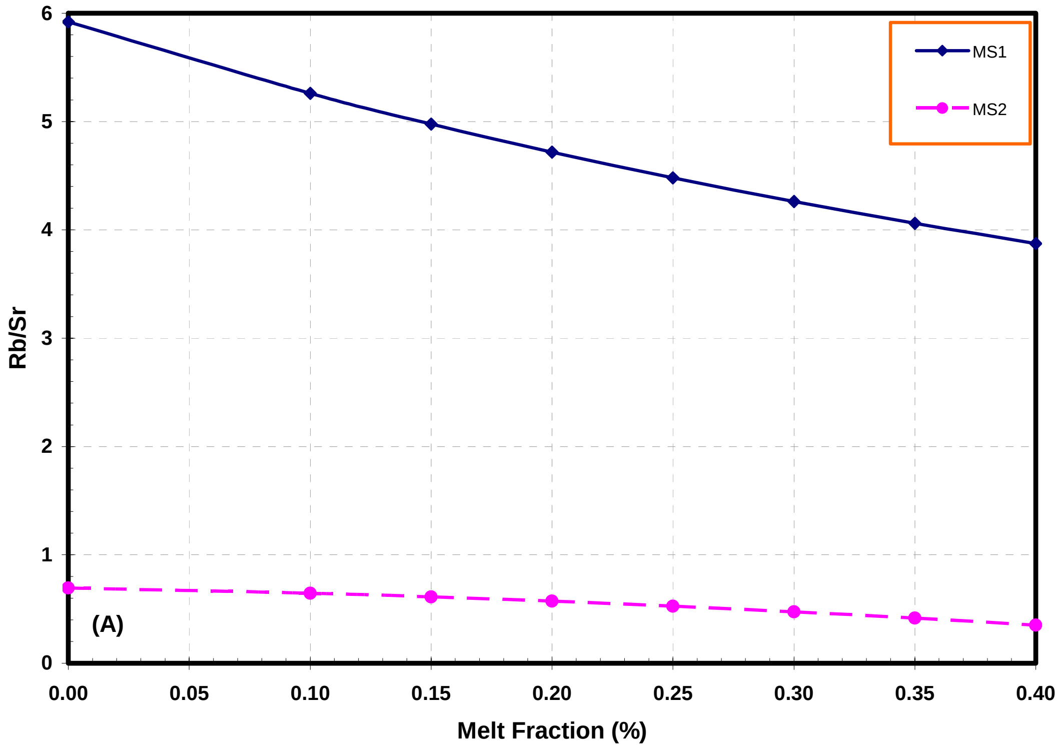
Rb/Sr
6
5
4
3
2
1
0
MS1
MS2
(A)
0.00
0.05
0.10
0.15
0.20
0.25
0.30
0.35
0.40
Melt Fraction (%)

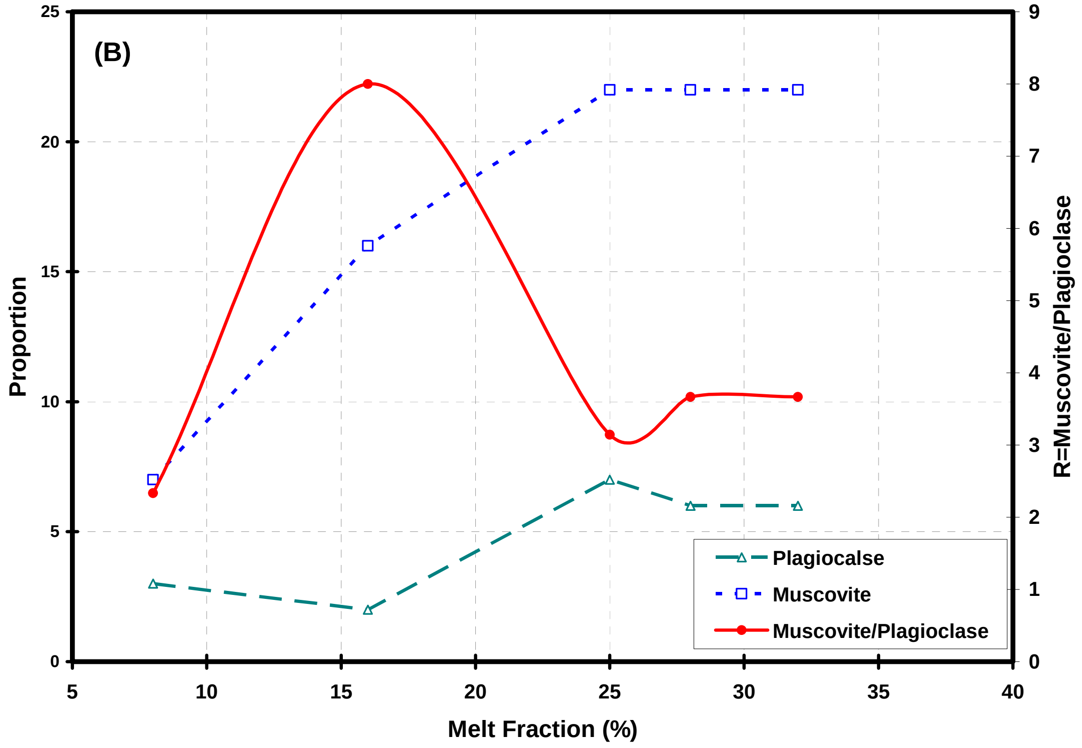
(B)
Proportion
25
20
15
10
5
0
R=Muscovite/Plagioclase
9
8
7
6
5
4
3
2
1
0
Plagiocalse
Muscovite
Muscovite/Plagioclase
5
10
15
20
25
30
35
40
Melt Fraction (%)

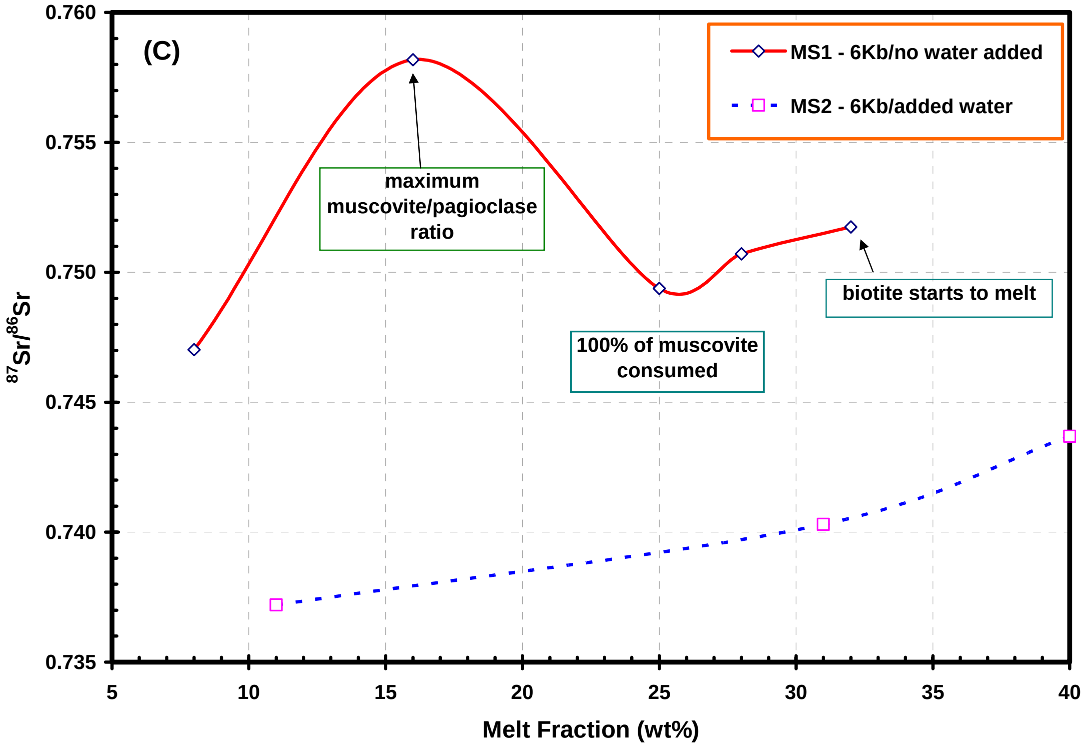
(C)
MS1 - 6Kb/no water added
MS2 - 6Kb/added water
maximum muscovite/pagioclase ratio
100% of muscovite consumed
biotite starts to melt
$^{87}Sr/^{86}Sr$
0.760
0.755
0.750
0.745
0.740
0.735
5
10
15
20
25
30
35
40
Melt Fraction (wt%)

Figure 3 Plot of $\varepsilon_{Nd}(T)$ versus P_2O_5 contents in the leucosomes, metapelites and migmatites from the Goat Ranch migmatite complex, southern Sierra Nevada. Data are from Zeng et al. (2003b).

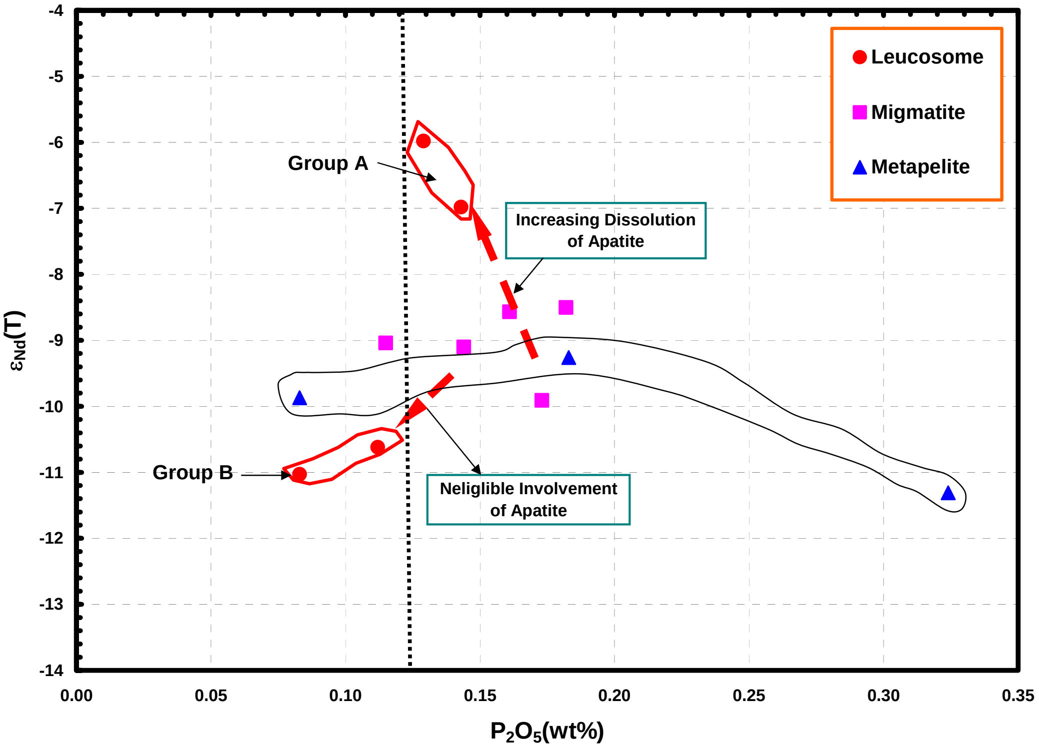

Leucosome
Migmatite
Metapelite
Group A
Group B
Increasing Dissolution of Apatite
Neliglible Involvement of Apatite
$\varepsilon_{Nd}(T)$
P_2O_5(wt%)
-4
-5
-6
-7
-8
-9
-10
-11
-12
-13
-14
0.00
0.05
0.10
0.15
0.20
0.25
0.30
0.35

Figure 4 (A) Dissolution of apatite as functions of temperature and melt compositions (silica content). (B) Dissolution of monazite as functions of temperature and water content in a silicic melt with D = 1.0. D is defined in the text. W is the water content in the melt. At dry conditions, dissolution of monazite is inhibited. The extent of monazite dissolution is represented by the LREE concentrations in the melt. The higher LREE concentration in a melt, the greater amount of monazite is dissolved. It shows that at a same temperature, increasing water content enhances monazite dissolution.

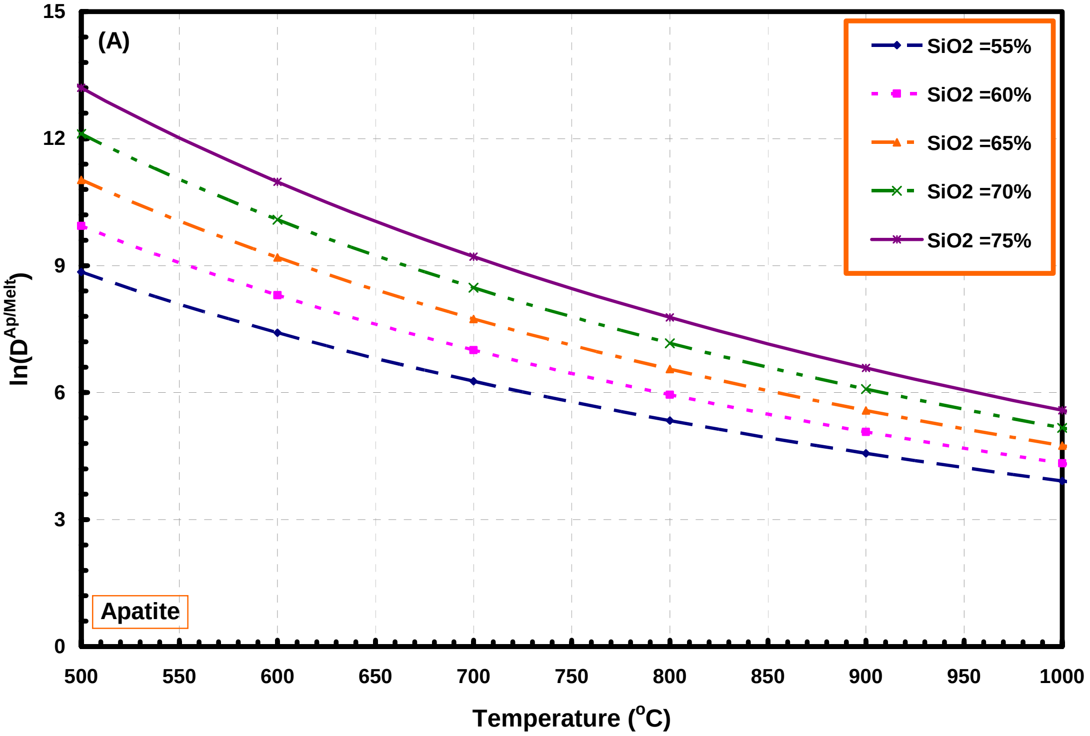
(A)
SiO2 =55%
SiO2 =60%
SiO2 =65%
SiO2 =70%
SiO2 =75%
Apatite
$\ln(D^{Ap/Melt})$
0
3
6
9
12
15
500
550
600
650
700
750
800
850
900
950
1000
Temperature (°C)

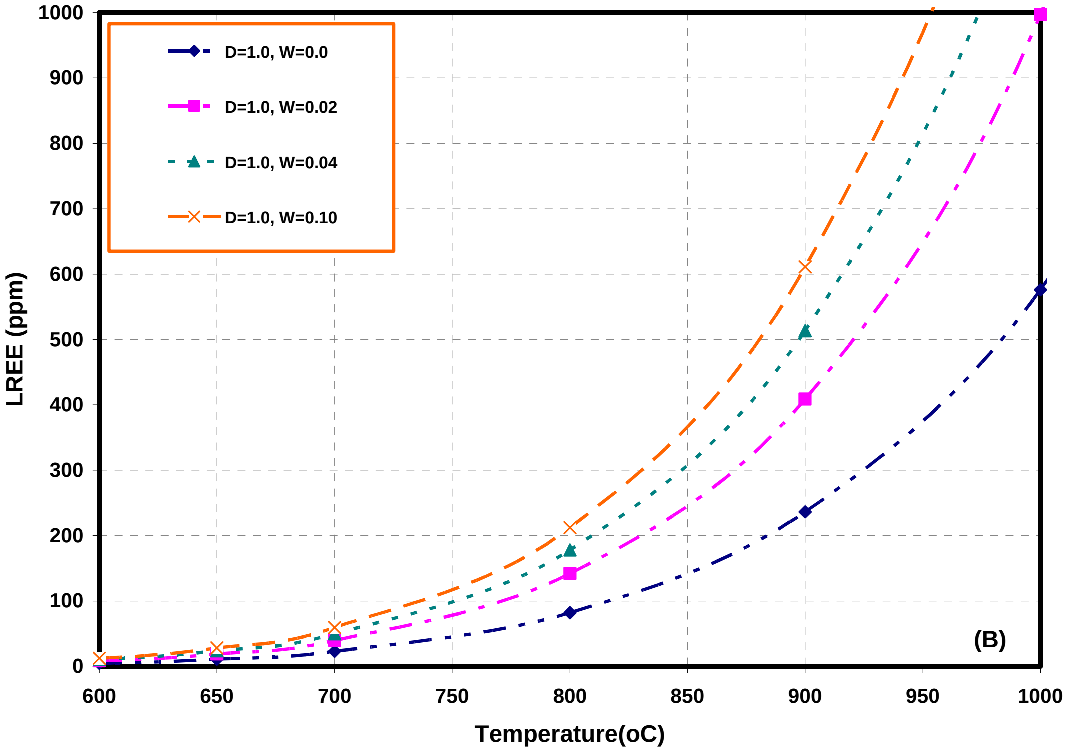
D=1.0, W=0.0
D=1.0, W=0.02
D=1.0, W=0.04
D=1.0, W=0.10
(B)
LREE (ppm)
0
100
200
300
400
500
600
700
800
900
1000
600
650
700
750
800
850
900
950
1000
Temperature(oC)

Figure 5 Schematic diagram showing the effects of non-modal partial melting and dissolution of accessory minerals on the Sr-Nd systematics of metasediments-derived melts. Path A represents melts dominated by muscovite/biotite dehydration melting characterized by high R_m/R_s ratios (>1), while Path B with low R_m/Rs ratios(<1) represents those reactions with minor involvements of either muscovite or biotite. Both A and B have no involvement of accessory phases. Path 1 represents partial melting reactions in which the T and X_{H_2O} environment associated with Type-A melting reactions favor apatite but not monazite dissolution in which the melt will have elevated Rb/Sr, $^{87}Sr/^{86}Sr$, Sm/Nd, and ε_{Nd}. In contrary, Path 2 represents those partial melting reactions in which the T and X_{H_2O} environment associated with Type-B melting reactions favor monazite over apatite dissolution, in which the melt will be have lower Rb/Sr, $^{87}Sr/^{86}Sr$, Sm/Nd, and ε_{Nd} than their source. Rm is the ratio of amount muscovite and biotite over amount of plagioclase and K-feldspar entering the melt. Rs is the ratio of amount of muscovite and biotite over amount of plagioclase and K-feldspar in the source. See text for discussion.

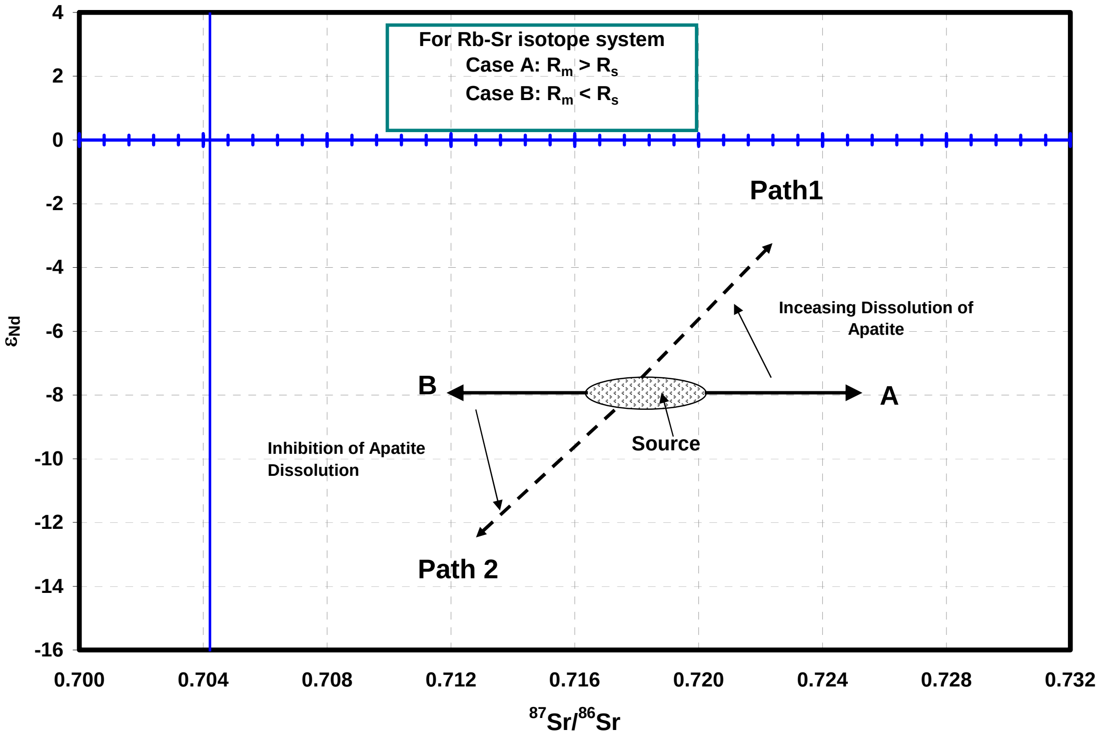
For Rb-Sr isotope system
Case A: $R_m > R_s$
Case B: $R_m < R_s$
Path1
Inceasing Dissolution of Apatite
B
A
Source
Inhibition of Apatite Dissolution
Path 2
ε_{Nd}
4
2
0
-2
-4
-6
-8
-10
-12
-14
-16
0.700
0.704
0.708
0.712
0.716
0.720
0.724
0.728
0.732
$^{87}Sr/^{86}Sr$

Figure 6 Schematic plot showing the competing effects of melt extraction and accessory dissolution on the isotopic geochemistry of the melts derived from partial melting of a metasediment protolith (modified after Sawyer, 1991; Watt and Harley, 1993). The *steep curve* represents the temperature/water content dependent accessory dissolution rate, and the *gentle curve* is the hypothetical temperature/water content dependant melt extraction rate. Melts generated within the hatched area will bear disequilibrium compositions. At lower water content (solid lines), the field of disequilibrium melting can extend to higher temperature. With increasing water contents (dash lines), the field of disequilibrium melting shrinks to lower temperatures, as the rate of accessory mineral dissolution surpasses that of melt extraction.

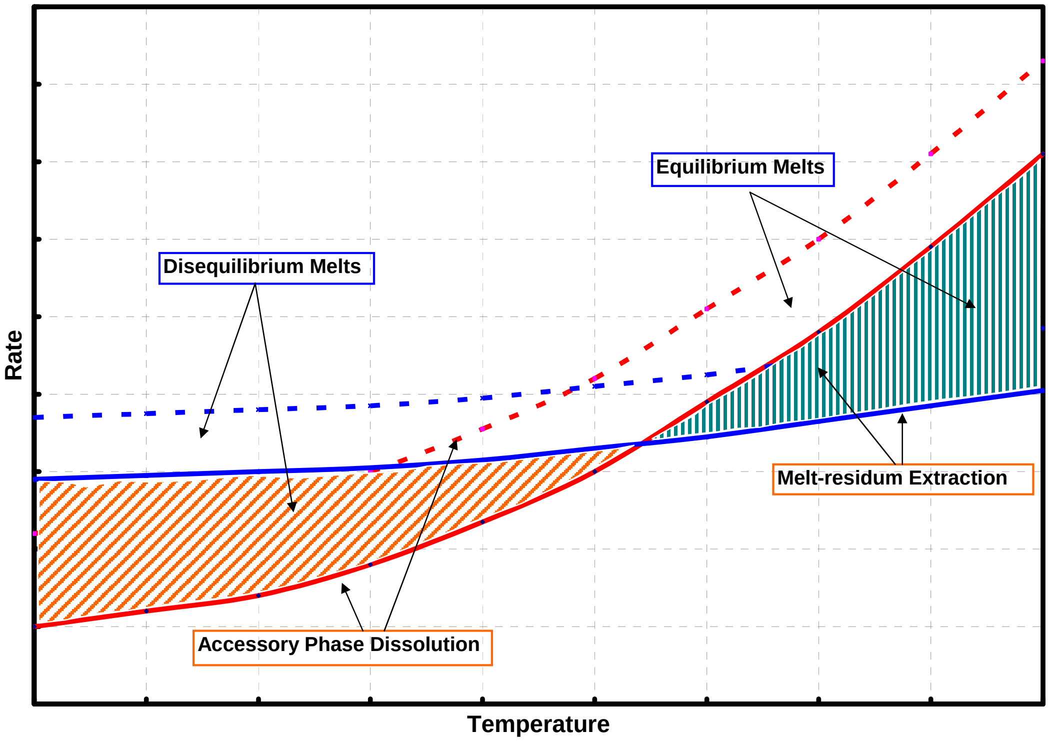
Equilibrium Melts
Disequilibrium Melts
Rate
Melt-residum Extraction
Accessory Phase Dissolution
Temperature

Table 1 Parameters for Rb, Sr, Sm and Nd trace element modeling.

Minerals	**wt%**	**Rb(ppm)**	**Sr(ppm)**	**Rb/Sr**	**Sm(ppm)**	**Nd(ppm)**	**Sm/Nd**	**Drb**	**Dsr**	**Dsm**	**Dnd**	**$^{87}Sr/^{86}Sr(0)$**	**$e_{Nd}(0)$**
Quartz	43	0.0	0.0	0.0000	0.00	0.00	0.0000	0.00	0.00	0.00	0.00	0.0000	0
Plagioclase	28	1.2	288.0	0.0042	2.25	19.53	0.1152	0.06	13.00	0.15	0.19	0.7376	-11.62
Muscovite	22	230.0	41.0	5.6098	0.05	0.29	0.1724	1.60	0.05	1.00	0.90	0.7722	-11.18
Biotite	2	580.0	30.0	19.3333	0.05	0.29	0.1724	3.20	0.52	1.00	0.90	0.8396	-11.18
Aluminosilicate	4.5	0.0	0.0	0.0000	0.00	0.00	0.0000	0.00	0.00	0.00	0.00	0.0000	0
Apatite	0.5	0.0	0.0	0.0000	175.30	432.00	0.4058	0.00	0.00	84.80	57.10	0.0000	-9.36
K-feldspar	0	35.0	135.0	0.2593	0.09	0.40	0.2250	1.80	7.30	0.02	0.04	0.7480	-10.77
Whole-Rock		62.5	90.3	0.6928	1.52	7.70	0.1973					0.7417	-10.93

1. Rb, Sr, Sm and Nd concentraion data are adapted from Bea and Montero (1999), Bea et al. (1994), Ayers and Harris (1997) and Knesel and Daidson (2002).
2. Rb, Sr, Sm and Nd partition coefficients are from Icenhower and London (1995), Nash and Crecraft (1985) and Whittington and Treloar (2002).

References

Ague, J. J. and Brimhall, G. H., 1987, Granites of the batholiths of California: Products of local assimilation and regional-scale crustal contamination. *Geology*, v.15, 63-66.

Ague, J. J, and Brimhall. G. H., 1988a, Regional variations in bulk chemistry, mineralogy, and the composition of mafic and accessory minerals in the batholiths of California, *Geological Society of America Bulletin*, v. 100, 891-911.

Ague, J. J., and Brimhall. G. H., 1988b, Magmatic arc asymmetry and distribution of anomalous plutonic belts in the batholiths of California: Effects of Assimilation, crustal thickness, and depth of crystallization: *Geological Society of America Bulletin*, v. 100, 912-927.

Ague, J. J., 1997, Thermodynamic calculation of emplacement pressures for batholithic rocks, California: implications for the aluminum-in-hornblende barometer, *Geology*, v. 25, 63-566.

Allegre, C. J. and Ben Othman, D., 1980, Nd-Sr isotopic relationship in granitoid rocks and continental crust development: a chemical approach to orogenesis. *Nature*, v. 286, 335-342.

Allegre, C. J. and Minster, J .F., 1978, Quantitative models of trace element behaviour in magmatic processes. *Earth and Planetary Science Letters*, v. 38, 1-25.

Arzi, A. A., 1978, Critical phenomena in the rheology of partially melted rocks. *Tectonophysics*, v. 44, 173-184

Ayres, M and Harris, N., 1997, REE fractionation and Nd-isotope disequilibrium during crustal anatexis: constraints from Himalayan leucogranites. *Chemical Geology*, 139, 249-269.

Ayres, M., Harris, N. & Vance, D., 1997, Possible constraints on anatectic melt residence times from accessory mineral dissolution rates: an example from Himalayan leucogranites. *Mineralogical Magazine*, v. 61, 29-36.

Barbero, L., Villaseca, C., Rogers, G. and Brown, P.E., 1995, Geochemical and isotopic disequilibrium in crustal melting: An insight from the anatectic granitoids from Toledo, Spain. *Journal of Geophysical Research,* v. 100, 15745-15765.

Barbey, P., Bertrand, J-M, Angoua, S. and Dautel, D., 1989, Petrology and U/Pb geochronology of the Telohat migmatites. Aleksod, Central Hoggar, Algeria. *Contrib. Mineral Petrol*., v. 101, 207-219.

Barboza. S. A. and Bergantz, G. W., 1998, Rheological transitions and the progress of melting of crustal rocks. *Earth and Planetary Science Letters*, v. 158, 19-29.

Bateman, P. C. and Eaton, G. P., 1967, Sierra Nevada batholith. *Science*, v. 58, 1407-1417.

Bateman, P. C., 1983, A summary of critical relations in the central part of Sierra Nevada batholith, California, U.S.A., Geological Society America Memoir 159, 241-254.

Bateman, P. C., Clark, L. D., Huber, N. K., Moore, J .G. and Rineheart, C .D., 1963, The Sierra Nevada batholith-A synthesis of recent work across the central part. *USGS Professional Paper*, 414-D, 46p.

Bea, F. and Montero, P., 1999, Behaviour of accessory phases and redistribution of Zr, REE, Y, Th, and U during metamorphism and partial melting of metapelites in the lower crust: An example from the Kinzigite formation of Ivrea-Verbano, NW Italy. *Geochim. Cosmochim. Acta*, 63, 1133-1153.

Bea, F., 1996. Controls on the trace element composition of crustal melts. *Trans. R. Soc. Edinburg: Earth Sci.*, v. 87, 133–141.

Bea, F., 1996. Residence of REE, Y, Th and U in granites and crustal protoliths: Implications for the chemistry of crustal melts. *Journal of Petrology*, v. 37, 521–552.

Bea, F., Pereira, M.D. and Stroh, A., 1994, Mineral/leucosome trace-element partitioning in a peraluminous migmatite (a laser ablation-ICP-MS study). *Chemical Geology*, v. 117, 291-312.

Bell, T. H., 1985, Deformation partitioning and porphyroblasts rotation in metamorphic rocks: a radical reinterpretation. *Journal of Metamorphic Geology*, v. 3, 109-118.

Bergantz, G. W., 1989, Underplating and partial melting: implications for melt generation and extraction. *Science*, v. 254, 1093-1095.

Bingen, B., Demaiffe, D. and Hertogen, J., 1996. Redistribution of rare earth elements, thorium, and uranium over accessory minerals in the course of amphibolite to granulite facies metamorphism: The role of apatite and monazite in orthogneisses from southwestern Norway. *Geochim. Cosmochim. Acta*, v. 60, 1341–1354.

Bottinga and Weill, 1972, The viscosity of magmatic silicate liquids: a model for calculation. *Amer. J. Sci.*, v. 272, pp. 438-475.

Brearly, A.J. and Rubie, D.C., 1990, Effect of H2O on the disequilibrium breakdown of muscovite+quartz, *Journal of Petrology,* v. 31, pp. 925-956.

Brown, M. and Rushmer, T., 1997, The role of deformation in the movement of granitic melt: views from the laboratory and the field. In: Holness M.B. (eds) *Deformation-enhanced fluid transport in the Earth's crust and mantle*. The Mineralogical Society Series, 8. Chapman & Hall, London, 111-144.

Brown, M., 1994, The Generation, segregation, ascent and emplacement of granite magma: The migmatite-to-crustally-derived granite connection in thickened orogens. *Earth-Sci Rev.*, v. 36, 83-130.

Brown, M., Rushmer, T. and Sawyer, E., 1995, Introduction to special section: mechanism and consequences of melt segregation from crustal protoliths. . *Journal of Geophysical Research*, v. 100, 15551-15563.

Chen, J. H. and Moore, J. G., 1982, Uranium-lead isotope ages from the Sierra Nevada batholith, California. *Journal of Geophysical Research*, v. 87, 4761-4784.

Chen, J. H. and Tilton, G. R., 1991, Applications of lead and strontium isotopic relationships to the petrogenesis of granotoid rocks, central Sierra Nevada batholith, California: *Geological Society of America Bulletin.*, v. 101, 439-447.

Clemens, J. D. and Petford, N., 1999, Granitic melt viscosity and silicic magma dynamics in contrasting tectonic settings. *Journal of the Geological Society*, London, v. 156, 1057-1060.

Clemens, J .D. and Vielzeuf, D., 1987, Constraints on melting and magma production in the crust. *Earth and Planetary Science Letters*, v. 86, 287-306.

Clemens-Knott, D., 1992, Geologic and isotopic investigations of the early Cretaceous Sierra Nevada batholith, Tulare, CA, and the Ivrea zone, NW Italian Alps:

Example of interaction between mantle-derived magma and continental crust, PhD Thesis, 345p, California Institute of Technology.

Coleman, D. S. and Glazner, A. F., 1998, The Sierra crest magmatic event: Rapid formation of juvenile crust during the late Cretaceous in California, in Ernst, W.G. and Nelson, C.A., eds., *Integrated Earth and Environmental evution of the Southwestern United Sates,* Geol. Soc. Am. Spec. V.: Columbia, MD, Bellwether, 253-272.

Coleman, D. S., Frost, T., and Glazner, A. F., 1992, Evidence from the Lamarck Granodiorite for rapid late Cretaceous crust formation in California: *Science*, v. 258, 1924-1926.

Connolly, J. A. D., Holness, M. B., Ruble, D. C. and Rushmer, T., 1997, Reaction-induced microcracking: An experimental investigation of a mechanism for enhancing anatectic melt extraction. *Geology*, v. 25, 591-594.

Crawford, M. B. and Windley, B. F., 1990, Leucogranites of the Himalaya/Karakoram: Implications for magmatic evution within collisional belts and the study of collision-related leucogranite petrogenesis. *Journal of Vcanology and Geothermal Research*, v. 44, 1-19.

Dalrymple, G. B., 1963, Potassium-argon dates of some Cenozoic vcanic rocks of the Sierra Nevada, California. *Geological Society of America Bulletin*, v. 74, 379-390.

Dardien, V., Thompson. A. B., Grujic, D. and Ulmer, P., 1995, Experiment melting of biotite + plagioclase + quartz ± muscovite assemblages and implications for crustal melting. *Journal of Geophysical Research*, v. 100, 15581-15591.

Davidson, C., Schmid, S. M. and Hollister, L. S., 1994, Role of melt during deformation in the deep crust, *Terra Nova*, v. 6, 133-142.

Dell'Angelo, L. N. and Tullis, J., 1988, Experimental deformation of partially melted granitic aggregates. *Journal of Metamorphic Geology*, v. 6, 495-515

Deniel, C., Vidal, P., Fernandez, A., Le Fort, P. & Peucat, J. J. (1987). Isotopic study of the Manaslu granite (Himalaya, Nepal): inferences on the age and source of the Himalayan leucogranites. , *Contrib. Mineral. Petrol*., v. 96, 78-92.

DePaolo, D. J. and Wasserburg, G. J., 1976, Nd isotopic variations and petrogenetic models. *Geophysical Research Letters*, v. 3, 249-252.

DePaolo, D. J. and Wasserburg, G. J., 1977, The sources of island arcs as indicated by Nd and Sr isotopic studies. *Geophysical Research Letters*, v. 4, 465-468.

DePaolo, D. J., 1980, Sources of continental crust: Neodymium isotope evidence from the Sierra Nevada and Peninsular Range. *Science*, v. 209, 684-687.

DePaolo, D. J., 1981a, Neodymium isotopes in the Colorado Front Range and crust-mantle evution in the Proterozoic. *Nature*, v. 291, 193-196.

DePaolo, D.J., 1981b, A Neodymium and Strontium isotopic study of the Mesozoic calc-alkaline granitic batholiths of the Sierra Nevada and Peninsular Ranges, California. *Journal of Geophysical Research*, v. 86, 10470-10488.

Dickinson, W. R., 1970, Relation of andersites, granites, and derivative sandstones to arc-trench tectonics. *Review of Geophysics and Space*, v.8, 13-860.

Dixon, E. T., 1995, An evaluation of hornblende barometry, Isabella to Tehachapi region, southern Nevada, California: The University of Michigan, M.S. Thesis, 178p.

Dodge, F., Lockwood, J. and Calk, L., 1988, Fragments of the mantle and crust from beneath the Sierra Nevada batholith: xenoliths in a vcanic pipe near Big Creek, California. *Geological Society of America Bulletin*, v. 100, 938-947

Ducea, M. N. and Saleeby, J. B., 1996, Buoyancy sources for a large, unrooted mountain range, the Sierra Nevada California: evidence from xenolith thermobarometry. *Journal of Geophysical Research*, v. 101, 8229-8244.

Ducea, M. N. and Saleeby, J. B., 1998a, Crustal recycling beneath continental arcs: silica-rich glass inclusions in ultramafic xenoliths from the Sierra Nevada, California. *Earth and Planetary Science Letters*, v.156, 101-116.

Ducea, M. N. and Saleeby, J. B., 1998b, The age and origin of a thick mafic-ultramafic keel from beneath the Sierra Nevada Batholith, *Contrib. Mineral. Petrol.*, v. 113, 169-185.

Ducea, M. N. and Saleeby, J. B., 1998c, A case for delamination of the deep batholithic crust beneath the Sierra Nevada, California. *International Geology Review*. v. 40, 78-93.

Ducea, M. N., 2002, Constraints on the bulk composition and root foundering rates of continental arcs: A California arc perspective: *Journal of Geophysical Research*, v. 107, 2304-2320.

Ebadi, A. and Johannes, W., 1991, Beginning of melting and composition of first melts in the system Qz–Ab–Or–H_2O–CO. *Contrib. Mineral Petrol.,* v. 106, 286-295.

Elan, R., 1986, High grade contact metamorphism at the Lake Isabella North Shore roof pendant, Southern Sierra Nevada, California: PhD thesis, University of Southern California, 202pp.

Everden, J. F. and Kistler, R. W., 1970, Chronology of emplacement of Mesozoic batholithic complexes in California and western Nevada. *U.S. Geological Survey, Professional Paper* 623, 1-42.

Farmer, G. L. and DePaolo, D .J., 1983, Origin of Mesozoic and Tertiary granite in the western United States and implications for pre-Mesozoic crustal structure, 1, Nd and Sr isotopic studies in the geocline of the northern Great Basin, *Journal of Geophysical research*, v. 88, 3379-3401.

Fyfe, W. S., 1973, The granulite facies, partial melting and the Achaean crust. Philosophic *Transactions of the Royal Society of London*, Series A273, 457-461.

George, M. T. and Bertlett, J. M., 1996, Rejuvenation of Rb-Sr mica ages during shearing on the northwestern margin of the Nanga Parbat-Haramosh massif. *Tectonophysics*, v. 260, 167-185.

Goldstein, S. L., 1988, Decoupled evution of Nd and Sr isotopes in the continental crust and the mantle, *Nature*, v. 336, 733-738.

Gromet, L. P. and Silver, L. T., 1983, Rare earth element distribution among minerals in a granodiorite and their petrogenetic implications. *Geochim. Cosmochim. Acta*, v. 47, 925-940.

Guillot, S. & Le Fort, P., 1995, Geochemical constraints on the bimodal origin of High Himalayan leucogranites. *Lithos* **35**, 221-234.

Halliday, A. N., 1983, Crustal melting and the genesis of isotopically and chemically zoned plutons in the Southern Uplands of Scotland, in Atherton, M.P. and Gribble, C.D., eds., "*Migmatites, melting and metamorphism*", Shiva Publishing Ltd., Cheshire, UK., 54-61.

Hamilton, W. and Myers, W. B., 1967, The nature of batholiths. *U.S. Geological Survey Professional Paper* 554-C, 30p.

Hammouda, T., Pichavant, M. and Chaussidon, M., 1996, Isotopic equilibration during partial melting: an experimental test of the behaviour of Sr. *Earth and Planetary Science Letters*, v.144, 109-121.

Handy, M. R., 1990, The solid-state flow of polymineralic rocks. *Journal of Geophysical Research*, v. 95, 8467-8661.

Handy, M. R., 1994, The energetics of steady state heterogenous shear in mylonitic rock. *Materials Science and engineering*, A175, 261-272.

Handy, M. R., Mulch, A., Rosenau, M., and Rosenberg, C. L., 2001, The role of fault zones and melts as agents of weakening, hardening and differentiation of the continental crust: a synthesis. In: Holdsworth, R.E., Strachan, R.A., Magloughlin, J. F. and Knipe, R. J. (eds), *The nature and tectonic significance of fault zone weakening*. Geological society, London, Special Publication 186, pp. 305-332.

Handy, M. R., Wissing, S. and Streit, J. E., 1999, Strength and structure of mylonite with combined frictional-viscous rheology and varied bimineralic composition. *Tectonophysics*, v. 303, 175-192

Harris N. and Massey J., 1994, Decompression and anatexis of himalayan metapelites: *Tectonic*s, v. 13, no. 6, pp. 1537-1546.

Harris N., Inger S. and Massey J., 1993, The role of fluids in the formation of the High Himalayan leucogranites. *in* P. J. T. a. M. P. Searle, ed., *Himalayan Tectonic*s: London, Geol. Soc. Spec. Publ., pp. 391-400.

Harris, N., Ayers, M. & Massey, J., 1995, Geochemistry of granitic melts produced during incongruent melting of muscovite: implications for the extraction of Himalayan leucogranite magmas. *Journal of Geophysical Research*, v. 100, 15767-15777.

Harris, N. B. W. and Inger, S., 1992, Trace element modeling of pelite-derived granites. *Contrib. Mineral Petrol*., v. 110, 46-56.

Harris, N. B. W, Pearce, J.A., and Tindle, A. G., 1986, Geochemical characteristics of collision-zone magmatism. In: Coward, M.P. and Ries, A.C. (eds), *Collision Tectonics*. Geol. Soc. London Spec. Publ., V. 19, 67-81.

Harrison, T. M. and Watson, E. B., 1984. The behavior of apatite during crustal anatexis: Equilibrium and kinetic considerations. *Geochim. Cosmochim. Acta*, v. 48, 1467–1478.

Henderson, P., 1982, Inorganic geochemistry. Pregamon, Oxford.

Henry, D. J. and Dutrow, B. L., 1996, Metamorphic tourmaline and its petrologic applications. In Grew, E.S. and Anovitz, L.M., eds., *Boron: Mineralogy, Petrology and Geochemistry*, Mineralogy Society of America, 503-558..

Hildreth, W. and Moorbath, S., 1988, Crustal contributions to arc magmatism in the Andes of central Chile, Contribution to Mineralogy and Petrology, v. 98, 455-489.

Hill, R., 1965, A self-consistent mechanics of composite materials. *Journal of the Mechanics and Physics of Solids*, v. 13, 213-222.

Hogan, J. P. and Sinha, A. K., 1991, The effect of accessory minerals on the distribution of lead isotopes during crustal anatexis: A model. *Geochim. Cosmochim. Acta*, v. 35, 335-348.

Hollister, L. S. and Crawford, M. L., 1986, Melt enhanced deformation – a major tectonic process. *Geology*, v. 14, 558-561.

Hollister, L. S., 1993, The role of melt in the uplift and exhumation of orogenic belts. *Chemical Geology*, v. 108, 31-48.

Holtz, F., 1989, Importance of melt fraction and source rock composition in crustal genesis-the example of two granitic suites of northern Portugal. *Lithos*, v. 24, 21-25.

Huppert, H. E. & Sparks, R. S. J. 1988, The generation of granitic magmas by intrusion of basalt into continental crust. *Journal of Petrology*. v. 29, 599-642.

Icenhower, J. and London, D., 1995, An experimental study of element partitioning among biotite, muscovite, and coexisting peraluminous silicic melt at 200 MPa (H_2O). *American Mineralogist*, v. 80, 1229-1251.

Icenhower, J. and London, D., 1996, Experimental partitioning of Rb, Cs, Sr, and Ba between alkali feldspar and peraluminous melt. *American Mineralogist*, v. 81, 719-734.

Inger, S. and Harris, N., 1993, Geochemical constrains on leucogranite magmatism in the Langtang Valley, Nepal Himalaya. *Journal of Petrology*, v.34, pp. 345-368.

Johannes, W. and Holtz, F., 1996, Petrogenesis and Experimental Petrology of Granitic Rocks. Springer-Verlag, Heidelberg.

Johannes, W., 1980, Metasstable melting in the granite system Qz-Or-Ab-An-H_2O. *Contrib. Miner. Petrol*. v. 72, 73-80.

Johannes, W., 1988, What controls partial melting in migmatite? *Journal of Metamorphic Geology*, v. 6, 451-465.

Johnson, D. M., Hooper, P. R. and Conrey, R. M., XRF analysis of rocks and minerals for major and trace elements on a single low dilution Li-tectraborate fused bead, *Adv. X-ray Anal*. 41, 843-867.

Kaczor, S. M., Hanson, G.N. and Peterman, Z.E., 1988, Disequilibrium melting of granite at the contact with a basic plug: a geochemical and petrographic study. *J. Geol*., v. 96, 61-78.

King, R. W. and Kerrich, R. W., 1989, Strontium isotope compositions of tourmaline from lode gold deposits of the Archean Albitibi greenstone belt (Ontario-Quebec, Canada); implications for source reservoirs. *Chemical Geology*, v.79, 225-240.

Kistler, R. W. and Peterman, Z. E., 1973, Variations in Sr, Rb, K, Na, and initial 87Sr/86Sr in Mesozoic granitic rocks and intruded wall rocks in central California. *Geological Society of America Bulletin*, v. 84, 3489-3512.

Kistler, R. W. & Peterman, Z. E., 1978. Reconstruction of crustal blocks of California on the basis of initial strontium isotopic compositions of Mesozoic granitic rocks. *U. S. Geological Survey, Professional Paper* 1071, p. 1-17.

Kistler, R. W. and Ross, D.C., 1990, A strontium isotopic study of plutons and associated rocks of the southern Sierra Nevada and vicinity, California. *U.S. Geological Survey Bulletin* 1920, 20 pp.

Kistler, R. W., 1990, Two different lithosphere types in the Sierra Nevada, California. In Anderson, J.L., ed., The nature and origin of Cordilleran magmatism: Boulder, Colorado, *Geological Society of America Memoir*, 174, p. 271-281.

Kistler, R.W., Chappell, B.W., Peck, D.L., and Bateman, P.C., 1986, Isotopic variation in the Toulumne Intrusive Suite, central Sierra Nevada. *Contrib. Mineral Petrol.*, v. 94, 205-220.

Kistler, R. W., Evernden, J .F. and Shaw, H. R., 1971, Sierra Nevada plutonic cycle-Part 1, origin of composite granitic batholith. *Geological Society of America Bulletin*, v. 82, 853-868.

Knesel, K. M. and Davidson, J. P., 1999, Sr isotope systematics during melt generation by intrusion of basalt into continental crust. *Contrib. Mineral Petrol.*, v. 136, 285-295.

Knesel, K. M. and Davidson, J. P., 2002, Insight into collisional magmatism from isotopic fingerprints of melting reactions. *Science,* v. 296, 2206-2208.

Kretz, R., 1983, Symbols for rock-forming minerals. *American Mineralogist*, v. 68, 277-279.

Lackey, J. M., Valley, J. W. and Saleeby, J. B., 2003, Evidence from zircon for high-δO^{18} contamination of magmas in the deep Sierra Nevada batholith, California. *Geology,* in press.

Le Breton, N. and Thompson, A. B., 1988, Fluid-absent (dehydration) melting of biotite in metapelite in the early stages of crustal anatexis. *Contrib. Mineral. Petrol.*, v. 99, 226-237.

Le Fort, P., 1981, Manaslu leucogranite: a collision signature of the Himalaya, a model for its genesis and emplacement. *Journal of Geophysical Research* v. 86, 10545-10568.

Leeman, W. P. and Sisson, V. B., 1996, Geochemistry of boron and its implications for crustal and mantle processes. In Grew, E.S. and Anovitz, L.M., eds., *Boron: Mineralogy, Petrology and Geochemistry*, Mineralogy Society of America, pp. 645-708.

Lisle, R. J., Rondeel, H. E., Doorn, D., Brugge, J., and van der Gaag, P., 1983, Estimation of viscosity contrast and finite strain from deformed elliptical inclusions. *Journal of Structural Geology*, v. 5, 603-609.

Martin, H., 1994, The Archean gray gneisses and genesis of continental crust, in Condie, K., ed., *Archean crustal evution*, p. 205-259, Elsevier, Amsterdam.

Masi, U., O'Neil, J. R. and Kistler, R. W., 1981, Stable isotope systematics in Mesozoic granites of Central and Northern California and Southwestern Oregon. *Contrib. Mineral. Petrol.*, v. 76, 116-126.

McDermott, F., Harris, N. B. and Hawkesworth, C .J., 1996, Geochemical constraints on crustal anatexis: a case study from the Pan-African Damara granitoids of Namibia. *Contrib. Mineral. Petrol.*, v. 123, 406-423.

McKenzie, D. P., 1987, The compaction of igneous and sedimentary rocks. *Journal of Geological Society*, London, v. 144, 299-307.

Miller, C. F. and Mittlefehldt, D. W., 1982, Depletion of LREE in felsic magma. *Geology*, v. 10, 129-133.

Montel, J. M., 1993. A model for monazite/melt equilibrium and the application to the generation of granitic magmas. *Chemical Geology,* v. 110, 127–146.

Moore, J. G. & Dodge, F. C. W., 1980. Late Cenozoic vcanic rocks of the southern Sierra Nevada, California: I geology and petrology. *Geological Society of America Bulletin*, v. 91(Part 2), 1995-2038.

Mukhopadhyay, B. and Manton, W. I., 1994, Upper-mantle fragments from beneath the Sierra Nevada batholith: partial fusion, fractional crystallization, and metasomatism in a subduction-related ancient lithosphere. *Journal of Petrology* v. 35, 1417-1450.

Murrell, S. A. F., 1985, Aspects of relationships between deformation and prograde metamorphism that causes evution of water. In: Thompson, A.B. and Rubie, D.C. (eds), *Metamorphic reactions, kinetics, textures, and deformation*. Springer-Verlag, New York, pp. 211-241.

Nabelek, P. I., 1999, Trace element distribution among rock-forming minerals in Black Hills migmatites, South Dakota: A case for soild-state equilibrium. *American Mineralogist,* v. 84, 1256-1269.

Nabelek, P. T. and Glascock, M. D., 1995, REE-depleted leucogranites, Black Hills South Dakota: a concequence of disequilibrium melting of monazite-bearing schist. *Journal of Petrology*, v. 36, 1055-1071.

Nash, W. P. and Crecraft, H. R., 1985, Partition coefficients for trace elements in silicic magmas. *Geochim. Cosmochim. Acta*, v. 49, 2309-2322.

Naslund, H. R., 1986, Disequilibrium partial melting and rheomorphic layer formation in the contact aureole of the Basistoppen sill, East Greenland. *Contrib. Miner. Petrol*. v. 93, 359-367.

Pan, Y. M., 1997, Zircon- and monazite-forming metamorphic reactions at Manitouwadge, Ontario. *Can. Mineral.,* v. 35, 105–118.

Patiño Douce A. E. and Beard J. S., 1995, Dehydration-melting of biotite gneiss and quartz amphibolite from 3 to 15 kbar. *Journal of Petrology*, v. 36, 707-738.

Patiño Douce A. E. and Beard J. S., 1996, Effects of P, f(O2) and Mg/Fe ratio on dehydration-melting of model metagreywakes. *Journal of Petrology*, v. 37, 999-1024.

Patiño Douce A. E. and Harris N., 1998, Experimental constraints on Himalayan Anatexis: *Journal of Petrolog*y, v. 39, 689-710.

Patiño Douce A. E. and Johnston, A. D., 1991, Phase equilibria and melt productivity in the pelitic system: Implications for the origin of peraluminous granitoids and aluminous granulites. *Contrib. Mineral Petrol*., v. 107, 202-218.

Patiño Douce, A. E., Humphreys, E. D. and Johnston, A. D., 1990, Anatexis and metamorphism in tectonically thickened continental crust exemplified by the Sevier hinterland, western North America. *Earth and Planetary Science Letters* v. 97, 290–315.

Patiño-Douce, A. E., 1996. Effects of pressure and H_2O content on the compositions of primary crustal melts. *Trans. R. Soc. Edinburg: Earth Sci.* v. 87, 11–21.

Peucat, J. J., 1986, Behavior of Rb-Sr whole rock and U-Pb zircon system during partial melting as shown in migmatitic gneisses from the St Malo Massif, NE Brittany, France. *Journal of the Geological Society, London,* v. 143, 875-885.

Pichavant, M., Montel, J. M. and Richard, L. R., 1992. Apatite solubility in peraluminous liquids: Experimental data and an extension of the Harrison-Watson model. *Geochim. Cosmochim. Acta*, v. 56, 3855–3861.

Pickett, D. A. and Saleeby, J. B., 1993, Thermobarometry of Cretaceous rocks of the Tehachapi Mountains, California: Plutonism and metamorphism in deep levels of the Sierra Nevada batholith. *Journal of Geophysical Research*, v. 98, 609-629.

Pickett, D. A. and Saleeby, J. B., 1994, Nd, Sr and Pb isotopic characteristics of Cretaceous intrusive rocks from deep levels of the Sierra Nevada batholith, Tehachapi Mountains, California. *Contrib. Mineral Petrol.*, v. 118, 98-215.

Pitcher, W. S., 1993, The nature and origin of granite, Blackdie Acad. & Prof., London, 321p.

Prinzhofer, A. and Allegre, C. J., 1985, Residue peridotites and the mechanisms of partial melting. *Earth and Planetary Science Letters*, v. 74, 251-265.

Rapp, R. P. and Watson, E. B., 1986, Monazite solubility and dissolution kinetics: Implications for the Th and light rare-earth chemistry of felsic magmas. *Contrib. Mineral Petrol.*, v. 94, 304-316.

Renner, J., Evans, B. and Hirth, G., 2000, On the rheologically critical melt fraction. *Earth and Planetary Science Letters*, v. 181, 585-594.

Rosenberg, C. L. and Riller, U., 2000, Partial-melt topology in statically and dynamically recrystallized granite. *Geology,* v. 28, 7-10.

Rosenberg, C. L., 2001, Deformation of partially molten granite: a review and comparison of experimental and natural case studies. *Int. J. Earth Sci.,*v. *90, 60-76,* DOI: 10.1007/s005310000164

Rubie, D. C. and Brearly, A. J., 1990, A model for rates of disequilibrium melting during metamorphism. In Ashworth, J.R. and Brown, M. eds., *High-temperature metamorphism and crustal anatexis*. Unwin Hyman, Boston, Mass. pp. 57-86.

Rushmer, T., 1991, Partial melting of two amphibolites: contrasting experimental results under fluid-absent conditions. *Contrib. Mineral. Petrol.*, v. 107, 41-59.

Rushmer, T., 2001, Vume change during partial melting reactions: implications for melt extraction, melt geochemistry and crustal rheology. *Tectonophysics*, v.342, pp. 389-405

Saleeby, J. B and Bushy, C., 1993, Paleogeographic and tectonic setting of axial and western metamorphic framework rocks of the southern Sierra Nevada, California, In Dunn, G., and MacDougall, k., eds., *Mesozoic Paleogeography of Western United States-II*, Pacific Section SEPM, Book 71, pp. 197-226.

Saleeby, J. B. and Zeng, L., 2003, Structure and geochronology of plutonic and high-grade metamorphic rocks of the Lake Isabella area, southern Sierra Nevada, CA. In preparation.

Saleeby, J. B., 1990, Progress in tectonic and petrogenetic studies in an exposed cross-section of young (~100 Ma) continental crust, southern Sierra Nevada, California, In Salisbury, M.H., ed., *Exposed Cross-Section of the continental Crust*, NATO Advanced Studies Institute.

Saleeby, J. B., Ducea, M. N. and Clemens-Knott, D., 2003, Production and loss of high-density batholithic root - southern Sierra Nevada, California. *Tectonics*, in press

Saleeby, J. B., Sams, D. B. and Kistler, R .W., 1987, U/Pb zircon, strontium, and oxygen isotopic and geochronological study of the southernmost Sierra Nevada batholith, California. *Journal of Geophysical Research*, v. 92, 10443-10466.

Sawyer, E. W., 1991. Disequilibrium melting and the rate of melt-residuum separation during migmatization of mafic rocks from the Grenville Front, Quebec. *Journal of Petrology,* v. 32, 701–738.

Sawyer, E. W., 1994, Melt segregation in the continental crust. *Geology*, v. 22, 1019-1022.

Sawyer, E. W., 1998, Formation and evution of granite magmas during crustal reworking: the significance of diatexites. *Journal of Petrology*, v. 39, 1147-1167.

Scaillet, B., Holtz. F., and Pichavant, M., 1997, Rheological properties of granitic magmas in their crystallization range. In: Bouchez, JL, Hutton DHW, Stephens WE (eds) *Granite: from segregation of melt to emplacenment fabrics*. pp 11-29

Searle, M. P., Parrish, R. R., Hodges, K. V., Hurford, A. J., Ayres, M. W. & Whitehouse, M. J. (1997). Shisha Pangma leucogranite, South Tibetan Himalaya: field relations, geochemistry, age, origin, and emplacement. *J. Geol.*, v. 105, 295-317.

Sederholm, J. J., 1967, Selected works: Granites and migmatites, John Wiley and Sons Inc., New York, 608p.

Sevigny, J. H., 1993, Monazite controlled Sm/Nd fractionation in leucogranite: An ion microprobe study of garnet phenocrysts. *Geochim. Cosmochim. Acta*, v. 57, 4095-4102.

Shaw, H. R., 1972, Viscosities of magmatic silicate liquids: A empirical method of prediction. *Am. J. Sci*., v. 272, 870-893.

Shaw, D. M., 1970, Trace element fractionation during anatexis. *Geochim. Cosmochim. Acta*, v. 42, 933-943.

Shaw, H. R., 1965, Comments on viscosity, crystal settling and convection in granitic magmas. *Am. J. Sci*. v. 265, 120-152.

Shaw, H. R., 1980, Fracture mechanisms of magma transport from the mantle to the surface, in *Physics of magmatic process*, ed. R.B. Hargraves, Priceton University Press, Princeton, New Jersey, 201-264.

Silver, L.T. and Chappell, B.W., 1988, The Peninsular Ranges batholith: an insight into the evution of the Cordilleran batholith of southwestern North America. *Trans. Royal Soc. Edinburgh, Earth Sci.*, v. 79, 105-121.

Solomon, G. C. and Taylor, H. P., Jr., 1986, Isotopic evidence for the origin of Mesozoic and Cenozoic granitic plutons in the northern Great Basin. *Geology*, v. 17, 591-594.

Stevens, G., Clemens, J. D. and Droop, G. T. R., 1997, Melt production during granulite-facies anatexis: Experimental data from "primitive" metasedimentary protoliths. *Contrib. Mineral Petrol*., v. 128, 352-370.

Sun, S-S. and McDonough, W. F., 1989, Chemical and isotopic systematics of oceanic basalts: implication for mantle composition and processes. In: Saunders, A. & Norry, M. (eds) *Magatism in the Ocean Basins*. Geological society, London, Special Publication 42, pp. 313-345.

Taylor, H. P. and Silver, L. T., 1978, Oxygen isotope relationships in plutonic igneous rocks of the Peninsular Ranges batholith, southern and Baja California, *U.S. Geological Survey Open File Report*, 78-701, 423-426.

Thompson, A. B., 1996, Fertility of crustal rocks during anatexis. *Transactions of Royal Society of Edinburgh, Earth Sciences*, v. 87, 1–10.

Thompson, A. B., 1982, Dehydration melting of pelitic rocks and the generation of H_2O-undersaturated granitic liquids. *Am. J. Sci*., v. 282, 1567-1595.

Tomomasini, S. and Davies, G. R., 1997, Isotope disequilibrium during anatexis: a case study of contact melting, Sierra Nevada, California. *Earth and Planetary Science Letters*, v.148, 273-285.

Treagus, S. H. and Treagus, J. E., 2002, Studies of strain and rheology of conglomerates. *Journal of Structural Geology*, v. 24, 1541-1567.

Treagus, S. H., 2002, Modelling the bulk viscosity of two-phase mixtures in terms of clast shape. *Journal of Structural Geology*, v. 24, 57-76.

Truschel, J. T., 1996, Petrogenesis of the Fine Gold Intrusive Suite, Sierra Nevada batholith [M.S. thesis]: Northridge, California State University, 137 pp.

van der Molen I. and Paterson, M. S., 1979, Experimental deformation of partially-melted granite. *Contrib Mineral Petrol*., v. 70, 299-318

Vanderhaeghe, O. and Teyssier, C., 2001, Partial melting and flow of orogens**,** *Tectonophysics*, v. 342, 451-472

Vielzeuf, D. and Montel J. M., 1994, Partial melting of metagreywackes; Part 1, Fluid-absent experiments and phase relationships. *Contrib Mineral Petrol*., v. 117, 375-393.

Vielzeuf, D. and Holloway, J. R., 1988. Experimental determination of the fluid-absent melting relations in the pelitic system. *Contrib Mineral Petrol*., v. 98, 257–276.

Vigneresse, J. L., Barbey, P. and Cuney, M., 1996, Rheological transitions during partial melting and crystallization with application to felsic magma segregation and transfer. *J Petrol*., v. 37, 1579-1600

Watson, E. B. and Harrison, T. M., 1983. Zircon saturation revisited: temperature and composition effects in a variety of crustal magma types. *Earth Planetary Sciences Letters*. v. 64, 295–304.

Watson, E. B. and Harrison, T. M., 1984, Accessory minerals and the geochemical evution of crustal magmatic system: a summary and prospectus of experimental approaches. *Physics of the Earth and Planetary Interiors*, v. 35, 19-30.

Watson, E. B., 1979a. Apatite saturation in basic intermediate magmas. *Geophys. Res. Lett.* v. 6, 937–940.

Watson, E. B., 1979b. Zircon saturation in felsic liquids: Experimental results and applications to trace element geochemistry. *Contrib. Mineral. Petrol.* v. 70, 407–419.

Watson, E. B., 1996. Dissolution, growth and survival of zircons during crustal fusion: Kinetic principles, geological models and implications for isotopic inheritance. *Trans. R. Soc. Edinburg: Earth Sci.* v. 87, 43–56.

Watson, E. B., Vicenzi, E. P. and Rapp, R. P., 1989. Inclusion/host relations involving accessory minerals in high-grade metamorphic and anatectic rocks. *Contrib. Mineral. Petrol.* v.101, 220–231.

Watt, G. R. and Harley, S. L., 1993. Accesory phase controls on the geochemistry of crustal melts and restites produced during water-undersaturated partial melting. *Contrib. Mineral. Petrol.* v. 114, 550–556.

Watt, G. R., Burns, I. M. and Graham, G. A., 1996. Chemical characteristics of migmatites: Accessory phase distribution and evidence for fast melt segregation rates. *Contrib. Mineral. Petrol.,* v. 125, 100–111

Weaver, B. L. and Tarney, J., 1980, Continental crust composition and nature of the lower crust: constraints from mantle Nd-Sr isotope correlation. *Nature*, v. 286, 342-346.

Whittington, A. G. and Treloar, P. J., 2002, Crustal anatexis and its relation to the exhumation of collisional orogenic belts, with particular reference to the Himalaya. *Mineralogical Magazine*, v. 66, 53-91.

Wickham, S. M., 1987, The segregation and emplacement of granitic magmas. Journal of the Geological Society, London, v. 144, 281-297.

Wolf, M. B. and London, D., 1994, Apatite dissolution into peraluminous haplogranitic melts: An experimental study of solubilities and mechanisms. *Geochim. Cosmochim. Acta*, v**.** 58, 4127–4146.

Wolf, M. B. and London, D., 1995, Incongruent dissolution of REE- and Sr-rich apatite in peraluminous granitic liquids: Differential apatite, monazite, and xenotime solubilities during anatexis. *Am. Mineral.,* v. 80, 765–775.

Wyllie, P. J., 1977, Crustal anatexis: an experimental review. *Tectonophysics* **43**, 41–71.

Wyllie, P. J., 1984, Constraints imposed by experimental petrology on possible and impossible magma sources and products. *Phil. Trans. R. Soc. Lond*., v. A310, 439-456.

Zeng, L., Lee, C-T. and Saleeby, J. B., 2001, Nd-Sr-Os systematics of mantle xenoliths from the Sierra Nevada Batholith: Structural and geochemical evolution of a subcontinental lithospheric mantle. *GSA Abstracts with Programs*, 33 (6), A-396.

Zeng, L. and Saleeby, J. B., 2003, Partial melting of roof pendant rocks and the formation of migmatite at the southern Sierra Nevada, California: Major and trace element studies. In preparation.

Zeng, L., Saleeby, J. B. and Ducea, M.N., 2003, The origin of within-pluton isotopic heterogeneity in the southern Sierra Nevada batholith (SNB): Constraints from Sr and Nd isotope studies. (Chapter 2)

Zeng, L., Saleeby, J. B. and Ducea, M. N., 2003, Non-modal crustal anatexis during the formation of migmatite at the Southern Sierra Nevada, California. (Chapter 3)

Zeng, L., Saleeby, J. B. and Ducea, M. N., 2003b, Melting of metasedimentary wallrocks and its effects on the strain partitioning: An example from the southern Sierra Nevada batholith, California. (Chapter 4).

Zhao, P. and Ji, S., 1997, Refinements of shear-lag model and its applications. *Tectonophysics*, v. 279, 37-53.

Appendix 1

Samples for petrography, geochemical and radiogenic isotopic analysis.

Number	Station Number	Petrology	Longitude	Latitude
1	**OOSS01-X**	Enclave	118°21'47"	35°36'17"
2	**OOSS01-G**	Granodiorite	118°21'47"	35°36'17"
3	**OOSS02-X**	Enclave	118°21'54"	35°36'20"
4	**OOSS02-G**	Granodiorite	118°21'54"	35°36'20"
5	**OOSS03-X**	Enclave	118°22'03"	35°36'22"
6	**OOSS03-G**	Granodiorite	118°22'03"	35°36'22"
7	**OOSS04-G**	Granodiorite	118°22'12"	35°36'25"
8	**Li99/01**	Granodiorite	118°21'59"	35°35'41"
9	**Li99/02**	Granodiorite	118°21'53"	35°35'44"
10	**Li99/03**	Granodiorite	118°21'45"	35°35'47"
11	**Li99/04**	Granodiorite	118°21'44"	35°35'50"
12	**Li99/06-a**	Granodiorite	118°21'40"	35°35'53"
13	**Li99/06-b**	Enclave	118°21'40"	35°35'53"
14	**Li99/07-a**	Granodiorite	118°21'31"	35°35'54"
15	**Li99/07-b**	Enclave	118°21'31"	35°35'54"
16	**Li99/08**	Granodiorite	118°21'28"	35°35'55"
17	**Li99/09**	Granodiorite	118°21'27"	35°35'57"
18	**Li98/0**	Granodiorite	118°21'20"	35°35'54"
19	**Li98/2**	Granodiorite	118°21'21"	35°35'52"
20	**Li98/12**	Leucogranite Dike	118°20'28"	35°36'24"
21	**PP0101**	Metapelite	118°20'52"	35°37'01"
22	**PS0101**	Metapelite	118°20'50"	35°37'00"
23	**Li9805**	Migmatite	118°21'24"	35°36'03"
24	**Li9808**	Migmatite	118°21'20"	35°36'14"
25	**Li9810**	Metapelite	118°20'58"	35°36'11"
26	**Li9813**	Metapelite	118°20'57"	35°36'13"
27	**Li9815**	Metapelite	118°20'50"	35°37'03"
28	**Li9816**	Metapelite	118°20'42"	35°36'28"
29	**L0404**	Leucosome	118°21'36"	35°36'04"
30	**L0405**	Leucosome	118°21'28"	35°36'08"
31	**L0406**	Leucosome	118°21'20"	35°35'54"
32	**L0407**	Leucosome	118°21'15"	35°35'44"
33	**L0408**	Leucosome	118°21'22"	35°36'18"
34	**L0410**	Leucosome	118°21'12"	35°36'26"
35	**TPLG01**	Leucogranite Dike	118°21'46"	35°37'11"
36	**TPLG02**	Leucogranite Dike	118°21'47"	35°37'08"
37	**1027LG01**	Leucogranite Dike	118°21'03"	35°36'54"
38	**1027LG02**	Leucogranite Dike	118°21'08"	35°36'59"
39	**1027LG03**	Leucogranite Dike	118°21'12"	35°36'59"

40	**051101-LG**	Leucogranite Dike	118^{o}20'28"	35^{o}36'29"
41	**051203-LG**	Leucogranite Dike	118^{o}22'06"	35^{o}37'12"
42	**051303-LG**	Leucogranite Dike	118^{o}21'27"	35^{o}36'30"
43	**1154b**	Leucogranite Dike	118^{o}21'09"	35^{o}37'06"
44	**051203-P**	Metapelite	118^{o}22'06"	35^{o}37'12"
45	**PNGt01**	Metapelite	118^{o}22'21"	35^{o}40'41"
46	**TP01**	Metapelite	118^{o}21'43"	35^{o}37'11"
47	**TP02**	Metapelite	118^{o}21'41"	35^{o}37'03"
48	**97SS4B**	Leucogranite	118^{o}18'27"	35^{o}34'18"
49	**00SS5**	Granite	118^{o}18'57"	35^{o}36'03"
50	**03SS7**	Granodiorite	118^{o}16'36"	35^{o}37'38"
51	**M051803**	Matble	118^{o}21'44"	35^{o}36'14"
52	**Li9806**	Granodiorite	118^{o}21'01"	35^{o}35'46"
53	**Li9809**	Granodiorite	118^{o}21'34"	35^{o}35'58"
54	**S9902**	Migmatite	118^{o}21'02"	35^{o}35'52"
55	**S9903**	Migmatite	118^{o}21'33"	35^{o}36'00"
56	**S9904**	Migmatite	118^{o}21'30"	35^{o}36'00"
57	**S9905**	Metapelite	118^{o}21'06"	35^{o}36'03"
58	**S9906**	Metapelite	118^{o}21'08"	35^{o}36'03"
59	**S9907**	Metapelite	118^{o}21'23"	35^{o}37'13"
60	**S9909**	Granodiorite	118^{o}20'33"	35^{o}35'15"
61	**S9910**	Migmatite	118^{o}20'31"	35^{o}35'20"
62	**S9911**	Migmatite	118^{o}20'28"	35^{o}35'22"
63	**S9912**	Metapelite	118^{o}20'30"	35^{o}35'30"
64	**S9913**	Metapelite	118^{o}20'33"	35^{o}36'21"
65	**M-02**	Marble	118^{o}21'14"	35^{o}36'44"

Appendix 2

Trace element geochemistry data of the leucosomes, migmatites, and upper pelites.

Sample ID	**L0404**	**L0405**	**L0407**	**L0410**	**R0404**	**R0407**	**R0410**	**Li9805**	**Li9808**	**PP-01-01**	**PS-01-01**	**Li9815**
La	13.88	39.01	20.15	32.17	34.91	48.01	47.88	40.88	48.54	50.52	49.46	45.31
Ce	26.46	72.88	38.31	61.17	65.83	92.42	90.53	78.17	92.82	93.57	88.23	83.83
Pr	3.01	8.06	4.33	6.90	7.38	10.37	10.12	8.77	10.18	10.70	10.19	9.42
Nd	11.92	30.68	16.74	26.67	29.75	40.43	39.81	34.84	39.63	41.42	38.81	36.63
Sm	3.07	6.70	4.22	6.26	6.93	8.95	8.74	7.77	8.78	9.03	8.10	7.98
Eu	0.60	1.80	2.58	2.48	1.41	1.81	2.50	1.16	1.74	1.79	1.61	1.50
Gd	3.20	5.79	4.24	5.67	6.50	7.59	7.36	6.73	7.36	7.51	6.29	6.96
Tb	0.57	0.96	0.88	1.01	1.02	1.21	1.16	1.11	1.17	1.20	1.01	1.15
Dy	3.58	5.83	6.02	6.37	5.66	7.11	6.72	6.73	6.84	7.13	6.13	6.80
Ho	0.73	1.19	1.35	1.34	1.08	1.43	1.32	1.34	1.39	1.43	1.27	1.36
Er	2.12	3.31	4.03	3.81	2.83	3.94	3.60	3.73	3.69	3.84	3.49	3.68
Tm	0.35	0.50	0.63	0.59	0.40	0.58	0.51	0.55	0.55	0.58	0.52	0.54
Yb	2.28	3.06	4.14	3.67	2.47	3.68	3.26	3.42	3.53	3.62	3.35	3.42
Lu	0.37	0.49	0.66	0.58	0.38	0.58	0.51	0.54	0.55	0.58	0.53	0.53
Ba	128.00	190.00	1134.00	872.00	377.00	654.00	800.00	554.00	1026.00	473.00	501.00	528.00
Th	9.19	20.60	14.31	15.19	14.03	20.27	17.15	14.70	17.30	17.76	19.06	17.47
Nb	2.45	7.49	2.04	12.19	14.58	25.03	20.98	18.24	17.06	19.83	19.66	19.27
Y	20.69	32.84	38.88	37.61	29.42	38.69	35.63	36.50	37.48	38.97	33.68	36.01
Hf	2.72	4.72	3.42	3.76	5.32	6.42	5.39	6.13	7.02	5.48	4.77	4.89
Ta	1.66	2.00	1.25	1.67	2.10	2.27	2.12	2.17	1.99	1.94	1.94	2.03
U	6.42	3.52	4.60	4.62	6.08	3.90	3.41	3.95	3.64	3.98	3.88	3.36
Pb	18.59	34.29	50.31	49.55	38.07	28.85	41.12	19.97	30.10	18.39	23.92	14.33
Rb	13.00	17.10	146.90	134.30	122.30	195.50	173.90	128.40	96.50	194.60	112.70	162.20
Cs	1.58	1.43	2.19	8.25	11.36	9.65	12.84	11.75	6.64	13.86	6.72	13.14
Sr	236.00	274.00	322.00	243.00	461.00	200.00	233.00	167.00	155.00	106.00	65.00	122.00
Sc	3.40	3.10	1.50	12.00	14.00	26.80	21.30	23.10	14.50	23.50	21.30	20.20
Zr	64.00	171.00	80.00	116.00	184.00	223.00	188.00	219.00	254.00	191.00	162.00	164.00
W	663.00	662.00	441.00	282.00	320.00	225.00	258.00	405.00	348.00	222.00	219.00	270.00

Appendix 3

Plate 1 Geologic map of the Goat Ranch area, south Lake Isabella area, California